Subunit composition, assembly and regulation of human TIP48 and TIP49 complexes

by Andrew Niewiarowski

Thesis submitted to University College London for the degree of Doctor of Philosophy 2009

Declaration

I, Andrew Niewiarowski, confirm that the work carried out for the production of this thesis is my own. Work carried out by other parties is acknowledged accordingly.

Signed…….....

Abstract

The two closely related eukaryotic AAA^+ proteins, TIP48 and TIP49, are essential components of large multi-protein complexes that are involved in diverse cellular processes. Specific mechanisms for their activity in transcriptional regulation, chromatin remodelling, DNA repair and apoptosis have not yet been characterised; however, different oligomeric forms, sub-cellular localisation and post translational modification of TIP48 and TIP49 may be important in co-ordinating these functions.

The assembly of the human TIP48 and TIP49 into different oligomers was studied. Both proteins were mainly monomeric in the absence of nucleotide cofactors. Incubation with ATP or ADP in the presence of Mg^{2+} modified the distribution of TIP48 oligomers to favour hexamers, but this did not occur with TIP49. The double hexameric complex of TIP48/TIP49 was also analysed and indicated a heterodisperse population of species, which provided clues about assembly pathways.

TIP48 and TIP49 are structurally homologous to the bacterial branch migration motor RuvB. TIP48 and TIP49 do not incorporate the DNA binding domain present in RuvB, and instead have acquired a novel domain (Domain II) inserted between the Walker A and B ATPase motifs. Using mutants, we demonstrated that TIP48 Domain II is critical for regulating nucleotide dependent hexamerisation of TIP48. Furthermore, TIP48/TIP49 complexes lacking Domain II indicated that hexamer-hexamer interactions are not exclusively mediated by Domain II; this domain may regulate the assembly of different forms of the heteromeric complex.

Interactions between TIP48 and TIP49 and several putative binding partners were tested *in vitro*. The ATPase activity and oligomerisation of TIP48 and TIP49 were assayed in the presence of Hint1, which was reported to disrupt the homotypic and heterotypic interactions within the TIP48/TIP49 complex.

Finally, the sub-cellular localisation and post translational modification of TIP48 and TIP49 were analysed. Using immunofluorescence and GFP-tagged TIP49, we confirmed that TIP48 and TIP49 associate with the mitotic spindle; however, TIP48 accumulates at the midbody during cytokinesis, while TIP49 does not. Furthermore, we investigated potential modifications of TIP48 and TIP49 by 2-D polyacrylamide gel electrophoresis, which may account for the regulation of these distinct functions.

Acknowledgements

First and foremost, I would like to extend my gratitude to Irina Tsaneva, who gave me the opportunity to work on this project, and provided limitless experience, encouragement and enthusiasm. I would also like to thank the other members of the academic staff in our department in University College London, especially Finn Werner and Ivan Gout, who maintained constant interest in the project, as well as well timed heated debates about experiments and interpretations.

For social and scientific support, I am grateful to the graduate students and post doctoral researchers in the department, who collectively offer an excellent support network for the bemused Ph. D. student. This is especially true of the members of the 4th floor, of the Darwin Building exemplified by Lindsey Houseman, to whom I will always be much obliged.

I am also grateful to several people for help with work carried out in this thesis. Previous members of the Tsaneva group, Barbara Sigala and Teena Puri, were instrumental in the initial support needed to begin such a project, and helped with initial recombinant protein work and immunofluorescence. I am also grateful to Mina Edwards, who maintained HeLa cell cultures and somehow managed to brighten even the most overcast gloomy day.

I am also appreciative of Jayesh Gor, who assisted with data collection for analytical ultracentrifugation, and Steve Perkins, for his interest in the project and unlimited enthusiasm for AUC.

I wish to thank my family and friends, who were always excited about my progress, even when I bombarded them with incomprehensible science. Finally, I thank my partner in crime, Alison Bradley, who was with me every step of the way.

Contents

Figures and Tables

Abbreviations

@	at
~	approximately
1º	primary
2-D	two dimensional
2-ME	2-mercaptoethanol or β-mercaptoethanol
2º	secondary
3-D	three dimensional
Å	Angstrom (10^{-10})
a	archaeal
AAA^+	ATPases associated with various cellular activities +
Ac	acetyl group
ADP	Adenosine 5'-diphosphate
Amp	Ampicillin
AMPS	Ammonium persulfate
Arp(s)	Actin related protein(s)
ATF2	Activating transcription factor 2
ATM	Ataxia telangiectasia mutated
ATP	Adenosine 5'-triphosphate
ATR	ATM related
AUC	Analytical Ultracentrifugation
BAF53	BRG/BRM associated factor 53 kDa
bp	base pair(s)
BSA	Bovine serum albumin
$CaCl_2$	Calcium Chloride
Cam	Chloramphenicol
CDS	Coding Sequence
CHAPS	3-[(3-Cholamidopropyl)dimethylammonio]-1-propanesulfonate
CIP	Calf intestinal (alkaline) phosphatase
cp	centipoise
C-terminal	carboxy-terminal
d	*Drosophila*
Da	Dalton
DMEM	Dulbecco's modified Eagle's medium
DNA	Deoxyribonucleic Acid
dNTP	Deoxyribonucleotide triphosphate
DSB(s)	DNA double-strand break(s)
dsDNA	double-stranded DNA
DTT	Dithiothreitol
E(Pc)	enhancer of polycomb
eAUC	Equilibrium Analytical Ultracentrifugation
EDTA	Ethylenediaminetetraacetic acid
EM	Electron microscopy
f/f_0	frictional ratio

F/T	flowthrough
FPLC	Fast protein liquid chromatography
g	g-force/relative centrifugal force (RCF)
g	gram
g/ml	grams per mililitre
h	human
HAT(s)	histone acetyltransferase
HCl	Hydrochloric acid
HDAC	histone de-acetylase
Hint1	histidine triad nucleotide binding protein 1
His_6-	amino-terminal hexa-histidine tag
-His_6	carboxy-terminal hexa-histidine tag
HOX	homeobox
HR	homologous recombination
hrs	hours
Ies4	INO eighty subunit 4
IF	immunofluorescence
ILK	Integrin linked kinase
INO80	inositol auxotroph 80 kDa
IPTG	Isopropyl-1-thio-β-D-galactopyranoside
IR	ionizing radiation
k	kilo (10^3)
Kan	kanamycin
KCl	Potassium chloride
KP_i	Potassium phosphate
l	litre
LB	Luria Broth
lik	*liebeskummer* mutation
m	milli (10^{-3})
M	molar
M	mega (10^6)
m	meter(s)
MC	monoclonal
MCM	mini-chromosome maintenance
$MgCl_2$	Magnesium Chloride
min	minute(s)
MM	molecular markers
MMS	methyl methanesulphonate
Mol	mole(s)
MOPS	3-[N-Morpholino] propane sulphonoic acid
mRNA	messenger RNA
n	nano (10^{-9})
NaCl	Sodium Chloride
NaOH	Sodium hydroxide
NFκB	Nuclear Factor kappa-light-chain-enhancer of activated B cells
NHEJ	non-homologous end joining

NMR	nuclear magnetic resonance
NP40	Nonidet P40
NSF	N-ethylmaleimide sensitive factor
N-terminal	amino-terminal
ºC	degrees Celsius
OD	optical density
ORF	Open reading frame
p	Pico (10^{-12})
P	phosphate group
PAGE	Polyacrylamide gel electrophoresis
PBS	Phosphate buffered saline
PC	polyclonal
PcG	polycomb group
PCR	Polymerase chain reaction
PDB	protein data bank
pH	potenz hydrogen
P_i	inorganic phosphate
pI	isoelectric point
PMA	phorbol 12-myristate 13-acetate
PMSF	phenyl methyl sulphonyl fluoride
PPIα	protein phosphatase Iα
PRC1	protein regulator of cytokinesis 1
PTM	post-translational modification
r	rat
^{r}	resistant
r.p.m.	revolutions per minute
Rb	retinoblastoma protein
RbCl	Rubidium chloride
RNA	Ribonucleic acid
RNAi	RNA interference
RNAP	RNA polymerase
RNP	Ribonucleoprotein
rRNA	Ribosomal RNA
Ruv	Resistant to ultraviolet light
s	seconds(s)
S	Svedberg
SDM	site directed mutagenesis
SDS	Sodium dodecyl sulphate
SEC	Size Exclusion Chromatography (or Gel filtration)
siRNA	small interfering RNA
snoRNA	small nucleolar ribonucleic acid
snoRNP	small nucleolar ribonuclearprotein
SRCAP	Snf2-related CBP activator protein
ssDNA	single-stranded DNA
SUMO	small ubiquitin like modifier
SWI2/SNF2	Switch 2/Sucrose non-fermentable 2

Swr1	SWI2/SNF2 related ATPase 1
TAE	Tris - Acetic acid - EDTA
TB	Tris borate
TBP	TATA box binding protein
TBS	Tris buffered saline
TE	Tris - EDTA
TEMED	N,N,N',N'-Tetra-methyl-ethylenediamine
TERC	telomerase RNA component
TERT	telomerase reverse transcriptase
Tet	Tetracyclin
TIP48	TBP/Transactivation Domain interacting protein 48 kDa
TIP49	TBP/Transactivation Domain interacting protein 49 kDa
TIP60	HIV-Tat interacting protein 60 kDa
Tm	Melting temperature
TRIS	Tris (hydroxymethyl) aminoethane
Triton X-100	polyethylene glycol p-(1,1,3,3-tetramethylbutyl)-phenyl ether
TRRAP	Transformation/transcription domain-associated protein
TrxG	Trithorax Group
Tween 20	Poloxyethylene Sorbitan Monolaurate
U	unit(s)
URI	unconventional prefoldin RNP3 interacting protein
UV	Ultraviolet light
UV_{280}	280 nanometre Ultraviolet light
V/cm	volts per centimetre
v/v	volume to volume
V_0	void volume
vAUC	Velocity Analytical Ultracentrifugation
WCE	whole cell extract(s)
w	nematode worm
w/v	weight to volume
x	Xenopus *laevis*
X-gal	5-brom-4-chloro-3-indolyl-beta-D-galactopyranoside
y	yeast
YY1	Yin Yang 1
z	Zebrafish
γ	gamma (i.e. phosphorylated)
Δ	Domain II deletion mutant
µ	Micro (10^{-6})

Chapter 1

General Introduction

1.1 AAA$^+$ Proteins

1.1.1 Structure and Function of AAA$^+$

An important and diverse family of proteins present in all forms of life are the AAA$^+$ (ATPases associated with various cellular activities) proteins. The range of functions of different AAA$^+$ proteins varies considerably; some examples include DNA replication and repair (e.g. MCM (Minichromosome maintenance) proteins, RuvB), proteolysis and protein turnover (e.g. Clp proteases) and cell structure and motility (dynein motor proteins). For reviews of AAA$^+$ proteins and their varied functions, see (Hanson and Whiteheart, 2005; Lupas and Martin, 2002; White and Lauring, 2007). The mechanism of action of AAA$^+$ proteins can generally be attributed to ATP binding and hydrolysis and the subsequent changes in protein structure. The interplay between different conformations of the proteins translates into actions on nucleic acids, proteins or other cellular components. Typical examples include protein unfolding by ClpA and ClpX before proteolysis (Ishikawa et al., 2001); disassembly of large protein aggregates by Hsp104 (Glover and Lindquist, 1998); unwinding of membrane bound SNARE complexes by NSF (Lenzen et al., 1998); unidirectional motion along microtubules by dynein (Burgess et al., 2003); helicase activity by MCM proteins (Chong et al., 2000) and Holliday junction branch migration by RuvB (Yamada et al., 2002), which is discussed below. Taken together, AAA$^+$ proteins seem to have a propensity for modulating protein folding, protein-protein or protein-substrate interactions and do this using a highly conserved ATPase domain to harness energy and carry out their various functions.

One common structural theme of AAA$^+$ proteins is organisation into single or double hexameric ring structures with a central pore; this event is often dependent on ATP or substrates. Thus, hexamerisation seems to coincide with assembly into the 'functional form' of the AAA$^+$ protein. This is probably due to the complex conformational changes needed to convert chemical energy to

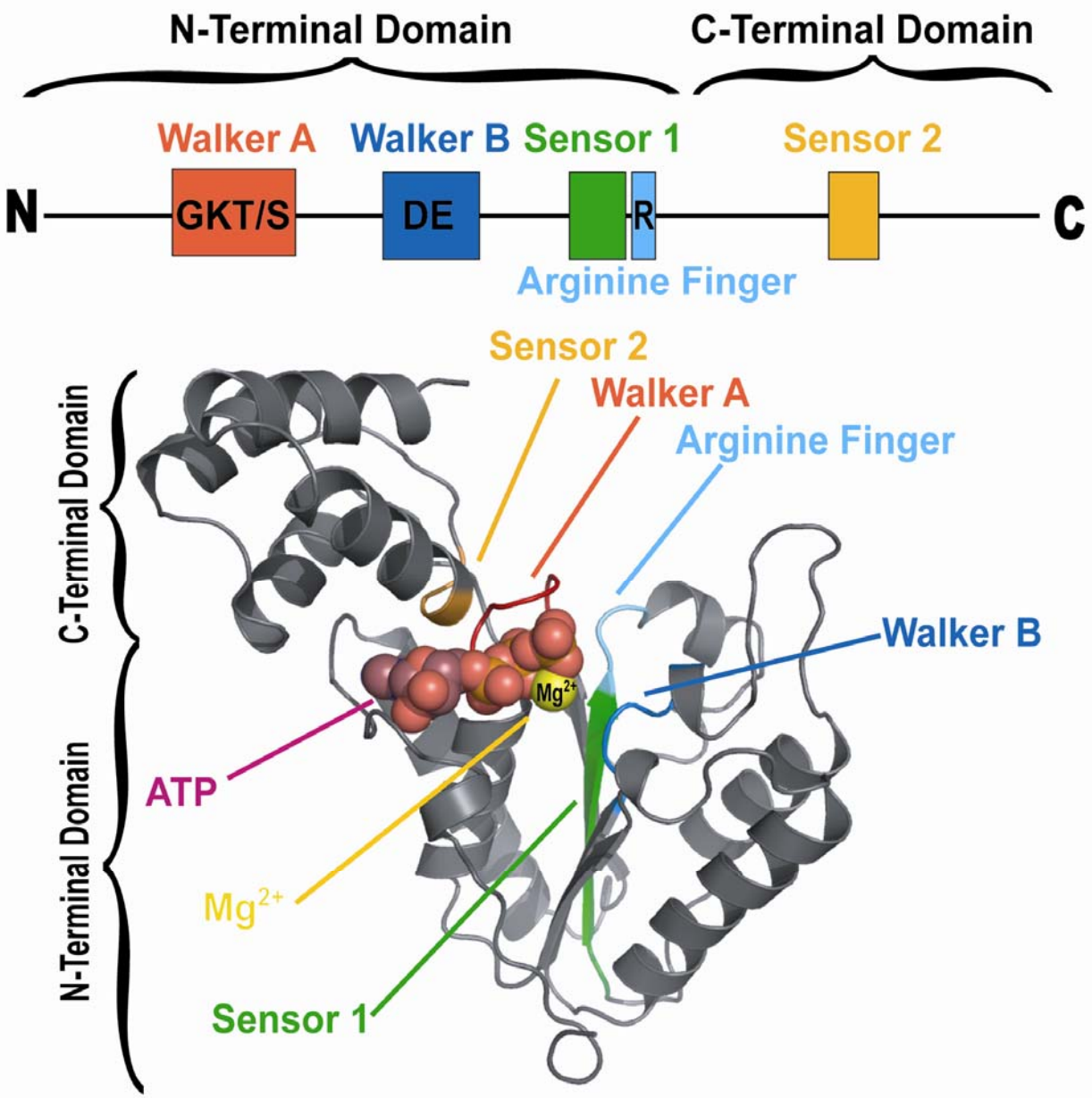

Figure 1.1. A typical protein fold of AAA$^+$ proteins. A schematic representation of conserved domains of AAA$^+$ proteins is shown above. Conserved residues are depicted in coloured boxes, which represent the five conserved motifs typically found within AAA$^+$ family members. The colour scheme for conserved motifs is also employed below. The cartoon represents the crystal structure of a *Cricetulus griseus* NSF monomer (PDB number 1NSF), demonstrating the positions of conserved Walker A, Walker B, sensor 1, sensor 2 and arginine finger motifs. ATP is represented as purple and brown space fill, magnesium is shown in yellow.

mechanical functions, and the ability (in some cases) to have different conformations of the individual monomers within the oligomeric rings (Hishida et al., 2004; Putnam et al., 2001).

AAA^+ proteins are characterised by a specific structural organisation with two conserved sub-domains: an N-terminal α/β Rossman fold and an α-helical C-terminal domain (Figure 1.1). The N-terminal domain adopts a wedge-shaped configuration and contains important Walker-A and Walker-B motifs, which are crucial for ATP binding and hydrolysis; the C-terminal domain forms a partial lid over the wide end of the N-terminal wedge-shaped nucleotide binding site. Within the two domains are several remarkably conserved sequences. The Walker A and Walker B motifs are essential for nucleotide binding and hydrolysis respectively. The sensor 1 and sensor 2 regions are involved in nucleotide recognition, positioning and hydrolysis. Additionally, an arginine finger is important in nucleotide hydrolysis, and is a key player in transducing conformational changes through the protein, subunit interaction and oligomerisation.

1.1.2 The bacterial AAA^+ RuvB protein

Recombination is a crucial process in all organisms. Recombination gives rise to genetic diversity, and in addition, provides a means of faithfully repairing DNA after damage. Late intermediates of recombination are cruciform structures known as Holliday junctions. In order to complete recombination, the Holliday junction must be cleaved to form two double stranded daughter duplexes. Holliday junction branch migration and resolution is carried out by the RuvABC complex in bacteria (Figure 2.1); for a review, see (West, 1997). Within this RuvABC system, the AAA^+ ATPase protein RuvB - a DNA helicase - serves as a motor, coupling the hydrolysis of ATP to DNA translocation, resulting in efficient branch migration (Tsaneva et al., 1992). RuvB forms hexameric rings which assemble on two diametrically opposite arms of the Holliday junction. These rings are recruited and stabilised onto the junction via interactions with

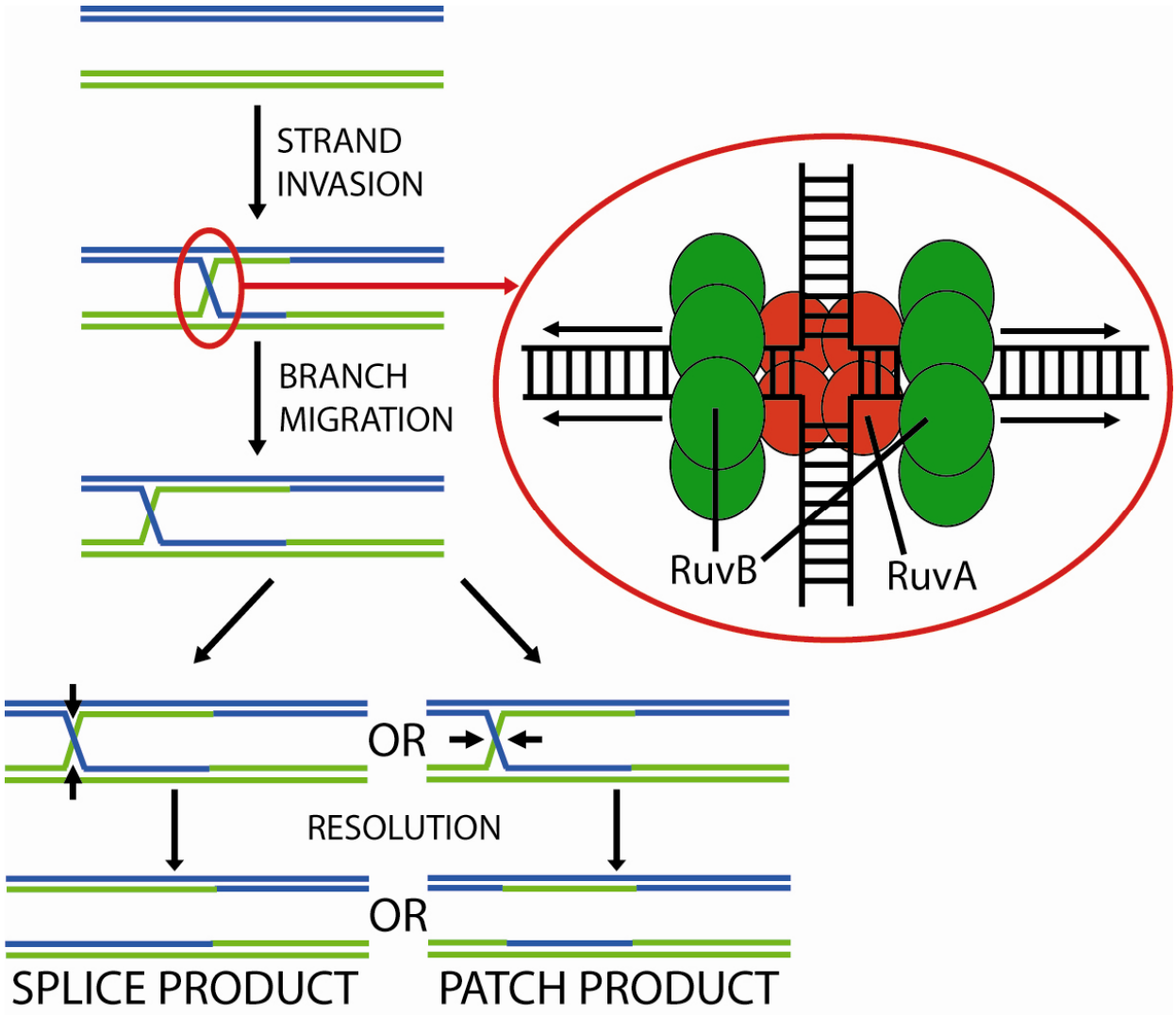

Figure 1.2. Schematic representation of Holliday junction branch migration by RuvAB. A simplified representation of homologous recombination between two homologous DNA sequences is depicted on the left. After branch migration, cleavage of the junction results in either a patch or splice product, depending on the orientation of cleavage. RuvAB bound to a Holliday junction is schematically represented on the right. One or two RuvA tetramers bind the cruciform DNA structure and load RuvB hexamers on opposite arms of the DNA. RuvB can then couple ATP hydrolysis to efficient uni-directional branch migration.

RuvA: a DNA binding protein with an affinity for Holliday junctions (Hiom and West, 1995). RuvA binds the Holliday junction as a tetramer; whether one or two RuvA tetramers bind the junction is still unknown, although recent evidence suggests stable double tetramers are required for branch migration (Baharoglu et al., 2008; Bradley, 2009).

Crystal structures of RuvAB demonstrated the molecular mechanism of branch migration (Figure 1.2). The RuvA tetramer acts as a stator and keeps the position of the RuvB hexamers static, causing DNA rotation and translocation through the RuvAB complex (Yamada et al., 2002). RuvA has positively charged surface residues that bind DNA and negatively charged 'pins', which separate duplex DNA and allow it to move freely (Rafferty et al., 1996). RuvB hydrolyses ATP, causing specific changes in protein structure and pumps duplex DNA through the centre of the hexameric ring towards RuvA. The monomers in the RuvB hexameric ring are non-equivalent, both in their ATP bound state and subsequent configuration (Hishida et al., 2004; Putnam et al., 2001). This allows efficient unidirectional helicase activity. Branch migration is terminated when a dimer of RuvC cleaves the junction, leaving two DNA duplex strands (Connolly et al., 1991). RuvC can cleave the junction resulting in a 'patch' or 'splice' product (see Figure 1.2). RuvC binds the opposite side of the junction to the RuvA tetramer via interactions with RuvA. Whether RuvC is bound to the junction during RuvAB mediated branch migration, or replaces one RuvA tetramer before scission is an ongoing un-answered question. This elegant RuvABC system has no known functional equivalent in eukaryotes, although a number of RuvB 'like' proteins have been identified. TIP48 and TIP49 are two such homologues of RuvB and will be the focus of this project

1.2 Initial discovery of TIP48 and TIP49

A homologue of the AAA^+ bacterial DNA helicase RuvB was identified in animal cells and characterised by several different groups (Bauer et al., 1998; Holzmann

et al., 1998; Kanemaki et al., 1997; Kikuchi et al., 1999; Qiu et al., 1998). Initially this protein was named TATA Binding Protein Interacting Protein 49 kDa - TIP49 - due to its *in vivo* interaction with TATA binding protein (Kanemaki et al., 1997). Since then it has accumulated a multitude of names in the literature. During this report, this protein will be called TIP49 regardless of species; other groups have referred to it as p50, p55, NMP238, TIP49a, RuvBL1, Rvb1, ECP-54, Pontin52, TAP54α or TIH1p. Northern blot analysis demonstrated that TIP49 is ubiquitously expressed in all human tissues (Holzmann et al., 1998; Makino et al., 2000). As well as having conserved homologues in other mammals, *in silico* and *in vivo* analysis of TIP49 revealed closely related homologues in humans (hTIP49*), *Drosophila melanogaster* (dTIP49*), *Caenorhabditis elegans* (wTIP49*), yeast *Saccharomyces cerevisiae* and *Schizosaccharomyces pombe* (yTIP49*) and the Archaea *Archaeoglobus fulgidus* and *Pyrococcus horikoshii* (aTIP49*) (Holzmann et al., 1998; Kurokawa et al., 1999; Salzer et al., 1999). Early characterisation of the protein showed that TIP49 was essential for viability and growth in both lower and higher eukaryotes (Qiu et al., 1998).

A protein that strongly interacted with TIP49 was isolated from mammalian cells (Gohshi et al., 1999; Kanemaki et al., 1999; Salzer et al., 1999). This protein, also a nuclear matrix protein, was identified as a RuvB homologue and highly similar to TIP49 in sequence. This protein will be referred to herein as TIP48 irrespective of species; it goes by a plethora of names in the literature: p47, TIP49b, RuvBL2, Rvb2, ECP-51, Reptin52, TAP54β and TIH2p). Human TIP48 (hTIP48) is ubiquitously expressed in all human tissues (Salzer et al., 1999). Like TIP49, TIP48 is also essential for growth and viability (Kanemaki et al., 1999). Further investigation demonstrated that TIP49 and TIP48 are distinct proteins and are both present in all eukaryotic species (Qiu et al., 1998). Crenarchaeota and some Euryarchaeota, however, do not have both TIP48 and TIP49; they possess a single homologue (Kurokawa et al., 1999). aTIP49 shares 45-49 % identity with hTIP48 and hTIP49. Moreover, *in silico* analysis demonstrated that the archaeal homologue is more related to TIP48 in sequence than TIP49

*The names in parentheses will be used in this thesis.

(Kurokawa et al., 1999). For that reason, it is likely that a gene duplication event occurred in an early eukaryotic ancestor, which led to eukaryotic TIP48 and TIP49 and the divergence of their sequences.

1.3 Structural studies of TIP48 and TIP49

1.3.1 TIP48 and TIP49 primary sequence and comparison to RuvB

Both hTIP48 and hTIP49, as well as being related themselves, have highly conserved homologous proteins throughout the eukaryotic domain (Kurokawa et al., 1999). Archaeal TIP49 also shows striking similarity to both proteins (Salzer et al., 1999). Several groups have catalogued the sequence identity between human TIP48, TIP49 and their eukaryotic and archaeal counterparts (summarised in Figure 1.3A).

hTIP49 differs from its homologue in rat (rTIP49) by a single amino acid: Ile^{291} in hTIP49, Val^{291} in rTIP49. This exemplifies the remarkable conservation of this protein between mammals. yTIP49 (yeast) and dTIP49 (*Drosophila*) both display ~ 70 % identity with hTIP49, while wTIP49 displays 60 % identity. TIP48, like TIP49, is highly conserved between eukaryotic species (Figure 1.3a). Primary sequence comparison shows that hTIP48 shares 99 % identity with rat and mouse TIP48. hTIP48 exhibits ~ 70 % identity to yTIP48, 78 % identity to dTIP48 and 58 % identity to wTIP48.

Calculation of molecular masses from amino acid sequences predicts ~ 52 kDa and 51 kDa for hTIP48 and hTIP49 respectively. Further study of the primary sequences provided key insights into their homology and functions. TIP48 and TIP49 bear significant sequence similarity to the bacterial RuvB protein. TIP48 and TIP49 in all species share the specific motifs characteristic of AAA^+ ATPases, which align well with the respective motifs on RuvB (Figure 1.3B). Primary sequence alignment with RuvB shows high conservation in the Walker A and B

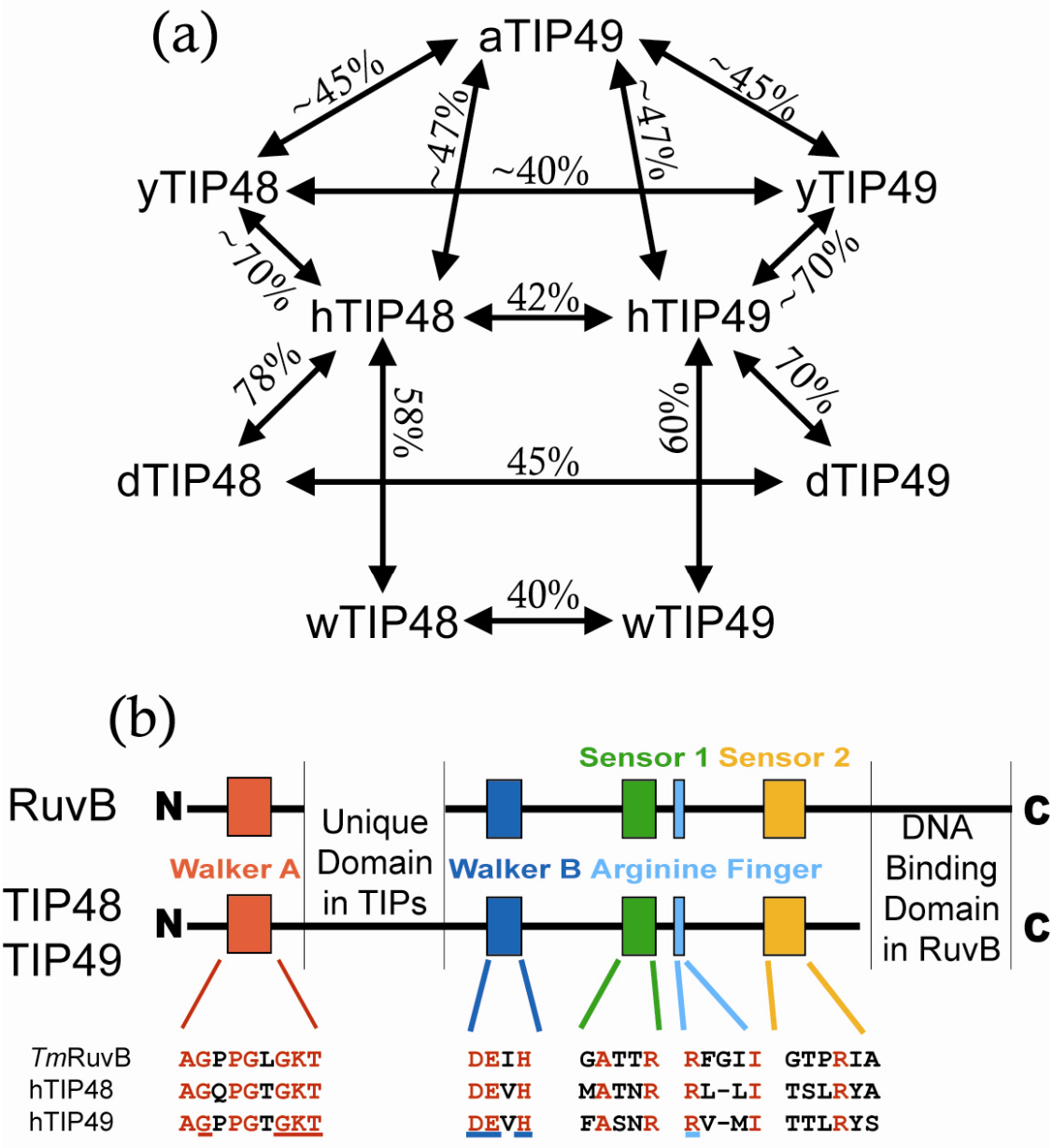

Figure 1.3. Homology between TIP48, TIP49 and RuvB. (a) A summary of the sequence identity between TIP48 and TIP49 across different species. The percentage sequence identity between human (h), yeast (y), *Drosophila* (d) and nematode worm (w) TIP48 and TIP49, and archaeal (a) TIP49 is shown. (b) Alignment of the AAA$^+$ motifs of *Thermotoga maritima* RuvB and human TIP48 and TIP49. The colour scheme from Figure 1.1 is used for the five conserved motifs. Identical residues between the three proteins are shown in red.

motifs as well as the sensor 1, sensor 2 and arginine finger regions. This information suggested that TIP48 and TIP49 are putative AAA^+ ATPases. Due to sequence homology with RuvB, some groups also proposed that TIP48 and TIP49 are DNA helicases (see section 1.4.4). However, TIP48 and TIP49 lack the C-terminal DNA binding domain of RuvB. This C-terminal domain in RuvB includes a winged helix motif common in non-specific DNA binding proteins, and is essential for efficient branch migration by RuvB (Putnam et al., 2001). Finally, TIP48 and TIP49 have a unique and conserved ~ 200 amino acid insertion between the Walker A and Walker B motifs of Domain I (Matias et al., 2006). This 'insertion' constitutes a novel domain: Domain II. The function of this unique domain is still unclear, although it was proposed that it is a substitute for the missing C-terminal DNA binding domain present in RuvB (Matias et al., 2006); however, the loss of the DNA binding domain in RuvB and acquisition of a unique domain in TIP48 and TIP49 may indicate the acquisition of a novel function.

The sequence identity between TIP48 and TIP49 within the same species is approximately 40 % (Figure 1.3a). This again implies that both TIP48 and TIP49 are functionally important due to their conservation. The conservation of identical residues between hTIP48 and hTIP49 is 195 out of 463 (42%) throughout the sequence, with Domain I (equivalent to RuvB Domain I) showing 54% identity, Domain II (the novel insertion domain) showing 36% identity and Domain III (equivalent to RuvB Domain II) showing 27% identity. Of the thirteen extra residues in TIP49 compared to TIP48, twelve are at three sites in Domain II. Almost all the secondary structure of TIP49 coincided well with regions that were well conserved between the two proteins (Matias et al., 2006; Putnam et al., 2001). This shows that TIP48 and TIP49 are expected to have similar protein folding and solution structures, and that many structural differences between the two proteins occur in the novel 'insertion' Domain II.

1.3.2 Oligomerisation of TIP48 and TIP49

One important feature of TIP48 and TIP49 is their homo-typic and hetero-typic interactions. Early characterisation involved studying the oligomeric properties of mammalian TIP48 and TIP49. TIP48 and TIP49 were isolated from rat nuclei in high salt and analysed in the absence of $MgCl_2$; both TIP48 and TIP49 were monomers with molecular masses of ~50 kDa (Gohshi et al., 1999; Kikuchi et al., 1999). Sedimentation coefficients for monomeric TIP48 and TIP49 were both calculated to be ~3.2 S from these data.

Several groups have also analysed recombinant proteins by size exclusion chromatography. hTIP49 eluted as a monomer under all conditions in each independent study (Ikura et al., 2000; Puri et al., 2007; Puri, 2006). However, hTIP48 eluted as an oligomer consistent with a dimer or trimer (Ikura et al., 2000), or as a ~70 kDa species, which was interpreted as a monomer-dimer equilibrium or an elongated monomer (Puri et al., 2007). Significantly, hTIP48 formed oligomers of around 400 kDa when incubated with ATP and ADP; $MgCl_2$ enhanced this nucleotide dependent oligomerisation; however, $MgCl_2$ alone was not capable of regulating the oligomerisation of hTIP48 (Puri et al., 2007). It was therefore proposed that hTIP48 forms hexameric rings when incubated with nucleotide cofactors, whereas hTIP49 does not *in vitro*. This implied a clear difference in the structural properties of the two proteins. These data are in contrast to the yeast proteins, where yTIP48 and yTIP49 are individually monomeric at low concentrations and form oligomers consistent with hexamers at high concentrations (Gribun et al., 2008). Furthermore, nucleotides did not modulate the oligomerisation of TIP48 and TIP49 in yeast. This implies a difference between the regulation of TIP48 and TIP49 oligomers between yeast and mammals.

TIP48 and TIP49 interact *in vivo* and *in vitro*. Interestingly, when TIP48 and TIP49 from rat nuclear extracts were analysed in the presence of $MgCl_2$, they

were associated with complexes of ~700 kDa, with TIP48 and TIP49 being the predominant components within this complex (Gohshi et al., 1999; Kanemaki et al., 1999; Kikuchi et al., 1999). The most likely explanation for this was a double hexameric configuration of TIP48 and TIP49, which is consistent with the molecular shapes of canonical AAA^+ proteins. As with the rat nuclear extracts, analysis of TIP48 and TIP49 from other species demonstrated that they exist in several large protein complexes where they are both major components (Gohshi et al., 1999; Ikura et al., 2000; Shen et al., 2000). Significantly, TIP48 and TIP49 were present in a 6:1 ratio with other components of yeast INO80 complex; this argues that TIP48 and TIP49 form hexamers *in vivo* (Shen et al., 2000). In most studies, the proportion of TIP48 and TIP49 monomers was above that of the other components of multi-subunit complexes (Ikura et al., 2000; Ruhl et al., 2006). However, to date, only the stoichiometries of TIP48 and TIP49 in the INO80 complex have been accurately calculated, highlighting the possibility of different TIP48/TIP49 oligomers working in different multi-subunit complexes. Nevertheless, these multisubunit complexes are likely to be the functional forms of TIP48 and TIP49. Furthermore, mixing of recombinant TIP48 and TIP49 *in vitro* then further purification by size exclusion chromatography yielded a complex of ~500 kDa with equal proportions of TIP48 and TIP49 (Ikura et al., 2000). Interestingly, when HeLa cell extracts were fractionated by size exclusion chromatography, the majority of hTIP48 and hTIP49 eluted in a 1:1 stoichiometry in fractions corresponding from 500 to 2000 kDa (Gstaiger et al., 2003). Furthermore, a 1:1 ratio of hTIP48 and hTIP49 was seen in the fraction corresponding to 300 kDa, which could signify individual homo-hexameric rings, hetero-hexameric (single) rings, or a mixture of both. Interestingly, only hTIP48 was detected in the lower fractions which corresponded to monomers or dimers, although the significance of this was not explored (Gstaiger et al., 2003).

Further insights into their structural properties were gained from electron microscopy studies of the human TIP48/TIP49 complex (Puri et al., 2007), and later, the yeast complex (Gribun et al., 2008; Torreira et al., 2008). The X-ray

crystal structure of hexameric hTIP49 was also solved (Matias et al., 2006); however, no structures of full length TIP48 have been published to date.

1.3.3 High resolution structures of TIP48 and TIP49

An X-ray crystal structure of hTIP49 was published (PDB number 2C90), showing TIP49 hexamers with ADP bound (Matias et al., 2006). The hexameric configuration of TIP49 is consistent with other AAA^+ proteins that have hexameric rings as their active forms (Gorynia et al., 2006; Matias et al., 2006). The TIP49 monomer comprises of three distinct domains. Domain I (residues 1-120 & 296-365) is a mixed α-helical and β-sheet domain, which contains the conserved Walker A and B, sensor 1 and arginine finger ATP binding and hydrolysis motifs. Between the Walker A and Walker B motifs is Domain II: the novel domain not present in RuvB. Domain II (residues 121-295) consists mainly of β-sheets and is linked to Domain I by two anti-parallel β-strands. Domain II was found to be unique to TIP49 (and TIP48) when screened against a primary structure database. However, screening against a structural library showed Domain II to be related to the DNA binding domains of DNA processing enzymes, including the highly conserved protein, RPA (Replication protein A) (Matias et al., 2006). Domain III (residues 366-456) is an α-helical domain, which includes the conserved sensor 2 motif. ADP is bound to a monomer of TIP49 at the interface between Domains I and III. Comparison with the crystal structure of RuvB shows remarkable similarity, both in the overall fold of the proteins, and the ADP binding site (Figure 1.4).

The hTIP49 crystals showed two different tessellating hexameric arrangements, giving rise to three independent monomers (A, B and C) in the asymmetric subunit. Monomer A was repeated six times giving rise to a hexameric ring with C6 symmetry (Hexamer 1); the other two monomers (B and C) were repeated three times to give an asymmetric hexameric ring (Hexamer 2) (Figure 1.4), see (Gorynia et al., 2006). Hexamer 1 was proposed to be the biologically relevant structure (Matias et al., 2006). hTIP49 Hexamer 1 contained six ADP molecules,

with one ADP bound between the TIP49 subunit-subunit interaction surfaces (Matias et al., 2006). Consequently, ADP is restrained in this binding pocket in the hexameric configuration of hTIP49. This may be one reason for the low ATP turnover of TIP49 observed *in vitro* (see section 1.4.2) - conversely nucleotide binding may be important for hexamerisation, as has been shown for TIP48 (Puri et al., 2007). The hexameric ring of TIP49 also forms a central pore of around 18 Å, which could accommodate ssDNA but not dsDNA.

In addition to the crystal structure of hTIP49, a NMR solution structure of K^{132} to R^{213} of Domain II of hTIP48 has been deposited in the PDB (accession number 2CQA). This structure shows a predominant β-sheet arrangement for Domain II with a single α-helix. Comparison with the X-ray structure of TIP49 indicated high conservation between the structures of Domain II of hTIP49 and hTIP48 (Figure 1.4b). As Domain II is less conserved than Domain I between TIP48 and TIP49, this suggests that the proteins have a highly conserved structure overall.

1.3.4 Electron Microscopy of TIP48 and TIP49

Although TIP48 and TIP49 may have functions independent of each other *in vivo*, they have been found together in several complexes. To further investigate this, hTIP48 and hTIP49 in the absence of co-factors, were assembled into a complex consisting of stoichiometrically equal proportions of TIP48 and TIP49; this complex was then examined by EM (electron microscopy). The TIP48/TIP49 complex was analysed by negatively staining, followed by a 3-D (three dimensional) reconstruction at 20 Å resolution. Consistent with other AAA^+ proteins, the 3-D reconstruction of the TIP48/TIP49 complex displayed two stacked rings with six-fold rotational (C6) symmetry, and a 26 Å central pore (Puri et al., 2007). The dimensions of the particle, C6 symmetry and stoichiometrically equal proportions of TIP48 and TIP49 firmly pointed to a double hexameric configuration of the TIP48/TIP49 complex (Puri et al., 2007).

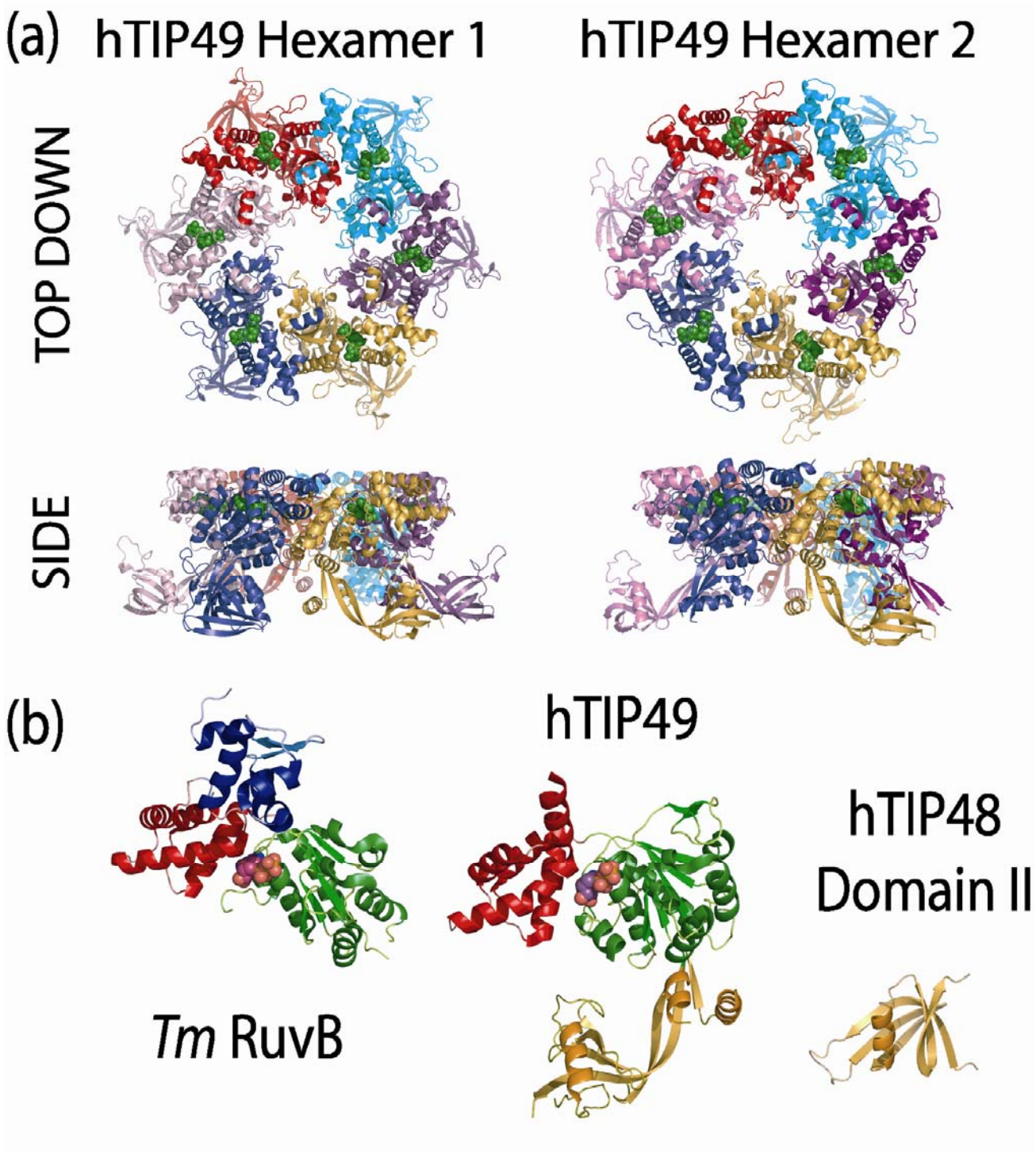

Figure 1.4. High resolution structures of hTIP48 and hTIP49. (a) Top down and side views of the two different hexamers derived from the hTIP49 crystal structure (PDB number 2C9O) (Matias et. al., 2006). Monomers are shown in different colours, while ADP is shown as green spheres. (b) Crystal structures of monomers of *T. maritima* RuvB (PDB number 1IN4) (Putnam et. al., 2001), hTIP49, and the NMR structure of residues 132-213 of hTIP48 (2CQA). Equivalent domains are shown in the same colours, ADP is shown as spheres.

The resolution of the final reconstruction was not high enough to confirm whether the TIP48/TIP49 complex comprised of a TIP48 homo-hexamer stacked on a TIP49 homo-hexamer, or whether the two rings were composed of TIP48/TIP49 hetero-hexamers. Notably, the top and bottom rings of the reconstructed TIP48/TIP49 complex were non-equivalent (Figure 1.5). The substantial structural differences between the top and bottom rings may favour TIP48 and TIP49 homo-hexamers within the double hexamer; alternatively, if the rings are heteromeric, the top and bottom rings seem to be in different conformational states. One important observation was that the crystal structure of TIP49 could not be easily incorporated into the top or bottom ring of the EM reconstruction, suggesting that some conformational change had occurred due to protein-protein interactions, or the absence of nucleotide co-factors (Puri et al., 2007). Furthermore, the authors also suggested a head-to-tail or tail-to-tail (head - Domains I and III; tail - Domain II) arrangement of hexameric rings within this structure, as these orientations agreed best with the EM reconstruction (Puri et al., 2007).

As work was being carried out for the production of this thesis, two further studies were published which utilised EM to analyse the architecture of yeast TIP48/TIP49 complexes. Analysis of yeast TIP48 and TIP49 using equilibrium analytical ultracentrifugation and size exclusion chromatography suggested that the yeast proteins form a single hetero-hexamer, with three yTIP48 and three yTIP49 monomers (Gribun et al., 2008). However, the analytical centrifugation studies of the yeast complex were performed in the presence of ADP; as the observed intensities above 1.5 may be saturated, the molecular mass may have been underestimated (Cole et al., 2008).

More recently, a high resolution reconstruction of the yeast TIP48 and TIP49 complex was generated using cryo-electron microscopy, and clearly showed a double hexameric configuration of yTIP48/TIP49 (Torreira et al., 2008). This structure showed a more elongated organisation of the double hexamer compared with the more spherical human TIP48/TIP49 complex (Figure 1.5). The

top and bottom rings were also more symmetrical than in the human complex, although the rings still seemed to be in an unequivalent conformation. After alteration of Domain II relative to the other domains of TIP49, the crystal structure could be accommodated into the top and bottom rings. This gave an orientation of the complex with the rings stacked head-to-head: Domain II of the rings were facing inwards, making up the equatorial region, with Domains I and III making up hexamers on the top and bottom (Torreira et al., 2008). This suggested that interactions between the top and bottom rings were exclusively mediated by Domain II. Although the structure was not of sufficient resolution to determine the composition of the rings, antibodies used to visualise Myc tagged TIP49 within the complex suggested that the rings were made of homo-hexamers of TIP48 stacked on TIP49 (Torreira et al., 2008). In agreement with the human TIP48/TIP49 EM study, the central pore of the complex was determined to be 25 Å wide (Torreira et al., 2008).

There are clear differences between the two electron microscopy studies on the yeast TIP48 and TIP49 complex, including the globular shape, orientation of the rings and symmetry. For this reason, it has been proposed that TIP48 and TIP49 may form several distinct complexes, each with a specialised function (Torreira et al., 2008). Furthermore, the differences between reconstructions of yeast and human TIP48/TIP49 complexes may point to differences between the organisation of TIP48/TIP49 complexes in lower eukaryotes and mammals; this is supported by the observation that TIP48 in yeast cannot be substituted by mammalian TIP48 (Lim et al., 2000).

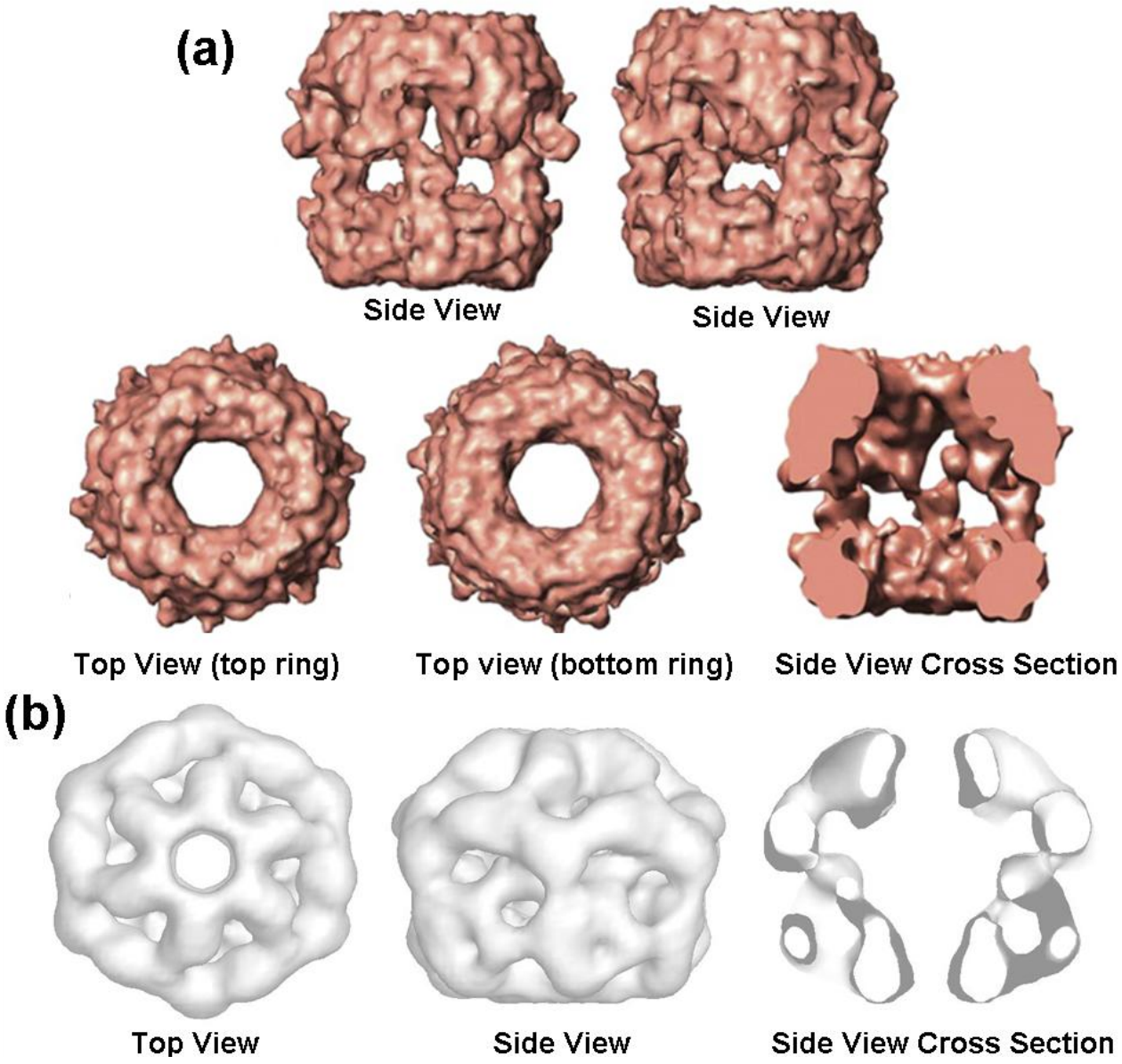

Figure 1.5. Electron Microscopy (EM) reconstructions of TIP48/TIP49 complexes. (a) *S. cerevisiae* TIP48/TIP49 double hexamer cryo-EM structure at 13 Å resolution in different orientations (Torreira et al., 2008). (b) Several orientations of the reconstructed human TIP48/TIP49 double hexamer at 20 Å resolution (Puri et. al, 2007). The reconstruction was derived from negative staining followed by EM.

1.4 Biochemical Studies of TIP48 and TIP49

1.4.1 Gene locus, tissue distribution & sub-cellular localisation

Investigations into the *in vivo* expression of TIP48 and TIP49 gave insights into their respective functions. After discovery, TIP49 was mapped to 3q21 and TIP48 to 19q13.2 in the human genome (Makino et al., 2000). The human Altsplice database (http://www.ebi.ac.uk/asd/altsplice/) shows hTIP49 consists of 11 exons and 10 introns, whereas the TIP48 gene contains 14 exons and 13 introns. Several groups have studied the tissue distribution of TIP48 and TIP49 in mammals; both proteins show ubiquitous expression in all cells with increased expression in testes tissue (Bauer et al., 1998; Etard et al., 2000; Holzmann et al., 1998; Kanemaki et al., 1999; Makino et al., 2000; Salzer et al., 1999). These findings indicate essential functions for TIP48 and TIP49, and increased expression in testes tissue suggests involvement in DNA recombination and repair. Studies in yeast showed that TIP48 and TIP49 genes are self-regulated, as endogenous expression of either gene was reduced by over 80% when the respective protein was episomally overexpressed (Radovic et al., 2007). Knockout mutations of TIP48 and TIP49 showed they are individually essential for growth in *S. cerevisiae* (Kanemaki et al., 1999; King et al., 2001; Lim et al., 2000; Qiu et al., 1998). These data imply that TIP48 and TIP49 have a more fundamental role than simply in DNA repair pathways, which are normally non-essential. Indeed, TIP48 and TIP49 are involved in the regulation of transcription and chromatin remodelling, as well as several other essential pathways in yeast (Jonsson et al., 2001; Lim et al., 2000). These data are consistent with evidence that TIP48 and TIP49 are individually essential for the viability of all eukaryotes, including yeast, nematode worms, insects and mammals (Bellosta et al., 2005; Etard et al., 2005; Rottbauer et al., 2002).

TIP48 or TIP49 were shown to be consistently expressed throughout the cell cycle (Qiu et al., 1998; Sigala et al., 2005). TIP48 and TIP49 both have putative

nuclear localisation signals: ^{229}HKKK and ^{264}KPKK for TIP49 (both in Domain II) and ^{413}RKRK in TIP48 (in Domain III). This is consistent with *in vivo* data, as hTIP48 was shown to be a mainly nuclear matrix protein during interphase (Sigala et al., 2005). hTIP48 dissociated from condensing chromatin during mitosis, and could then be seen localised in the midbody during cytokinesis, indicating a role in late mitosis (Sigala et al., 2005). hTIP48 was also observed at the mitotic spindle (Sigala et al., 2005).

As with hTIP48, hTIP49 was observed mainly in the nuclear matrix during interphase and dissociated from chromatin during mitosis, and co-localised with the mitotic spindle (Gartner et al., 2003). Interactions with the mitotic spindle were corroborated by pulldown assays showing interaction of hTIP49 with α-tubulin and γ-tubulin. In contrast with hTIP48, hTIP49 did not localise at the midzone or midbody during cytokinesis (Gartner et al., 2003). These data indicate distinct roles of TIP48 and TIP49 during mitosis, but further investigation will conclude if the proteins are acting alone, or as part of TIP48 and TIP49 containing complexes.

The signals for nuclear localisation of TIP48 and TIP49 were later studied in more detail. TIP48 and TIP49 co-purified with enzymes responsible for conjugating and cleaving SUMO (small ubiquitin like modifier) groups (Kim et al., 2006; Kim et al., 2007). Significantly, it was demonstrated that N-terminally SUMO conjugated TIP48 and TIP49 localised exclusively in the nucleus, while proteins which could not be SUMOylated (TIP48^{K456R} or TIP49^{K225R}) were exclusively cytoplasmic (Kim et al., 2006; Kim et al., 2007). Interestingly, it was noted that only 5 % of the endogenous pool of TIP48 or TIP49 are SUMOylated, while over a third of the respective proteins localise in the nucleoplasm (Gallant, 2007). This discrepancy could be explained by a highly dynamic balance between SUMOylation and SUMO cleavage; alternatively, other post-translational modifications or mechanisms could contribute to the sub-cellular localisation of TIP48 and TIP49.

Characterisation of TIP48 and TIP49 as part of snoRNP complexes (see section 1.5.7) indicated that they both localised in the nucleoplasm, but not in the nucleolus (Watkins et al., 2004). However, later studies identified TIP48 and TIP49 as nucleolar components in a proteomic analysis (Leung et al., 2006). Subsequently, it was confirmed by confocal microscopy that TIP49 localises in the nucleolus (Cvackova et al., 2008). Furthermore, electron microscopy was used to show that TIP49 associated with the fibrillar centres, which are sites of rRNA transcription by RNA Polymerase I, and this accumulation was enhanced in S phase (Cvackova et al., 2008).

In summary, it is evident that the sub-cellular localisation of both TIP48 and TIP49 is rather complicated. It would be important to further delineate the molecular cues and stimuli resulting in the movement and distribution of TIP48 and TIP49.

1.4.2 ATPase activity of TIP48 and TIP49

Several groups have shown *in vitro* ATPase activity for both hTIP48 and hTIP49, consistent with them being members of the AAA^+ ATPase family. The individual rates of ATPase activity were observed to be less than 0.1 mole of ATP hydrolysed / mole of monomer / minute (Ikura et al., 2000; Puri et al., 2007). Interestingly, the individual ATPase activities of hTIP48 and hTIP49 were significantly higher in the first minute, with little or no activity thereafter. This low rate of ATP turnover is consistent with observations in the TIP49 crystal structure that ADP release is blocked by hexamer formation (Matias et al., 2006). More significantly, the TIP48/TIP49 double hexamer shows a synergistic increase in ATPase activity *in vitro*, suggesting this is the catalytically active form of the proteins *in vivo*. The activity of the complex was up to 1 mole of ATP hydrolysed / monomer of protein / minute - around ten fold that of the individual proteins (Ikura et al., 2000; Puri et al., 2007). Both TIP48 and TIP49 have been shown to bind and hydrolyse ATP as part of this complex, and the formation of this complex may be necessary for ADP release and subsequent rounds of ATP hydrolysis

(Puri et al., 2007). It is likely that either post-translational modifications of TIP48 and TIP49 or interactions with other proteins or substrates may increase ATPase activities of the individual proteins or the TIP48/TIP49 complex.

1.4.3 Catalytic activity of TIP48 and TIP49 *in vivo*

In addition to the *in vitro* nucleotide hydrolysis activity of TIP48 and TIP49, *in vivo* studies of mutants have shed light on how their enzymatic activity and functions are linked. Several groups have generated TIP48 and TIP49 mutants which have mutations in the Walker A or Walker B motifs, where analogous mutations in RuvB result in defective ATP binding and hydrolysis respectively (Mezard et al., 1997).

In yeast, mutations in the Walker A motif (yTIP48^{G75A}, yTIP48^{K81D}, yTIP48^{K81R} and yTIP49^{K85D}) caused a lethal phenotype (Jonsson et al., 2001; King et al., 2001; Lim et al., 2000). Similarly, Walker B mutations (yTIP48^{D296N} and yTIP49^{D302N}) also resulted in lethality in yeast (Jonsson et al., 2001; King et al., 2001; Wood et al., 2000). These data indicate the individual requirement of ATP binding and hydrolysis by yTIP48 and yTIP49 for vegetative growth. Interestingly, a Walker B mutant yTIP48^{E297G}, which was defective in ATP hydrolysis but not binding, could promote the correct assembly of the yINO80 complex (Jonsson et al., 2004) (see section 1.5.3). This indicates that ATP binding, but not hydrolysis, is required for this particular activity of yTIP48, in concert with wild type yTIP49, while ATP hydrolysis may be required to dissociate TIP48 and TIP49 from the fully formed yINO80 complex.

In metazoans, several catalytically compromised TIP48 and TIP49 proteins have been studied. Interestingly, a Walker B mutant of hTIP48^{D296N} is able to interact with ATF2 (activating transcription factor 2) (Cho et al., 2001) (see section 1.7.6). Over-expression of TIP48^{D295N} Walker B mutant in *Drosophila* caused a lethal phenotype in developing larvae, while the equivalent mutation, dTIP49^{D302N}, resulted in viable larvae with developmental defects (Diop et al., 2008). Likewise, over-expression of hTIP49^{D302N} in human cells conferred a dominant negative

phenotype for several TIP49 activities, including c-Myc dependent gene regulation and apoptosis, and TIP60 dependent histone H4 acetylation (Dugan et al., 2002; Feng et al., 2003; Wood et al., 2000) (see sections 1.5.5) Surprisingly, over-expression of TIP49^{D302N} did not affect cell viability. Significantly, replacing endogenous hTIP49 with hTIP49^{D302N} in human cells reduced telomerase activity (Venteicher et al., 2008) (see section 1.7.6), confirming that the catalytic activity of TIP49 is required for this process.

One striking study into mutations of TIP48 was carried out in Zebrafish. A fish exhibiting a heart hyperplasia phenotype after 72 hours of development, was due to a mutation within zTIP48: a three amino acid insertion (FCR after G^{191}) within 'ATPase insertion' Domain II (Rottbauer et al., 2002). The mutation in TIP48 was called *liebeskummer* ('lover's grief' in German), abbreviated to *lik*TIP48. As the mutated region in TIP48 is well conserved between species, the *lik* mutation was introduced into yeast TIP48 to assess the effect on the TIP48 protein. Yeast chromosomal TIP48 was deleted and *lik*TIP48 was ectopically expressed; however, ectopic expression of *lik*TIP48 did not support viability, suggesting that the mutation affected an essential function of TIP48 (Rottbauer et al., 2002). Recombinant Zebrafish *lik*TIP48 was purified from an insect cell expression system, and formed aggregates and displayed abnormally high ATPase activity. Significantly, the increased activity could have been due to contaminants, as it did not peak with the eluted *lik*TIP48, and the authors could purify the activity away from the recombinant protein (Rottbauer et al., 2002).

In summary, ATP binding and hydrolysis by TIP48 and TIP49 are critical for their activities *in vivo*. The data discussed above have also provided clues about how the activities of TIP48 and TIP49 are linked to their functions; however, a more conclusive mechanism has not yet been described, but would greatly increase our understanding of TIP48 and TIP49.

1.4.4 DNA processing activity of TIP48 and TIP49

Yeast TIP48 and TIP49 as a complex have been shown to have ssDNA stimulated ATPase activity and helicase activity *in vitro* (Gribun et al., 2008), although the 5'-3' directionality of the complex was opposite to the TIP60 and INO80 complexes (of which they are components), and several other groups have disputed TIP48 and TIP49 as active helicases (Jonsson et al., 2004). Furthermore, in several studies, human TIP48 and TIP49 have not been found to have DNA dependent helicase activity *in vitro* (Matias et al., 2006; Puri et al., 2007; Puri, 2006; Qiu et al., 1998). In contrast, rTIP48 and rTIP49 were individually demonstrated to have ssDNA stimulated ATPase activity and helicase activity of opposite polarities *in vitro* (Kanemaki et al., 1999; Makino et al., 1999). It has been suggested that contaminants, which were carried over during protein purifications, may have been responsible for some observations of DNA stimulated ATPase activity and helicase activity (Puri et al., 2007; Puri, 2006; Qiu et al., 1998).

The ATPase activity of TIP48 and TIP49 in all species is not in dispute; however, the helicase activity is still controversial. The different results by different groups (particularly the assorted directionalities of helicase activity that have been reported) make it difficult to form conclusions about the *in vivo* activities of TIP48 and TIP49.

1.5 TIP48 and TIP49 in multi-subunit complexes

1.5.1 Chromatin and the need for remodelling

Generally, eukaryotic genomes are more complex than their bacterial counterparts, in terms of total open reading frames, gene complexity and DNA length. In eukaryotes, this poses a problem: these enormous molecules of DNA (over 1 meter in length for each human cell) must be tightly packaged into a nucleus which is ~100,000 fold shorter in length. This problem is solved in the form of chromatin: ~147 bp of DNA is wound around a core octamer of histones H2A, H2B, H3 and H4 (Arents and Moudrianakis, 1993). These core histone-

DNA units are then compacted further into tight chromatin structures and eventually, with the help of other scaffold proteins, condenses into individual chromosomes. Unfortunately, this elegant packaging system poses a further problem: the transcription machinery must access DNA promoters in order to transcribe genes; however, the DNA is now packaged into unyielding chromosome structures. This is also the case for any other process which requires ready access to DNA, including DNA replication and repair. Nature has solved this problem in the form of chromatin remodelling, whereby specialised proteins alter the position, structure and composition of core histones to allow orchestrated access to DNA processing enzymes. The link between TIP48, TIP49 and chromatin remodelling will be discussed in the following sections.

1.5.2 TIP48 and TIP49 containing complexes

Many functions of TIP48 and TIP49 are linked with their inclusion in several large multi-protein complexes, predominantly in the nucleus. Many of these complexes function in transcriptional regulation, with an emphasis on chromatin remodelling. To date TIP48 and TIP49 have both been found in complex with the INO80 complex; the mammalian TIP60 complex; the yeast Swr1 complex and its mammalian counterpart SRCAP; the URI complex; and snoRNP complexes; as well as interacting with the RNAP II holoenzyme. Interestingly, a number of transcriptional regulation complexes have been reportedly purified with either, but not both, TIP48 or TIP49; polycomb group (PcG) and trithorax group (TrxG) complexes are noted examples. A proteomics based analysis of probabilistic multi-protein complex modules demonstrated at least four discrete complexes in which hTIP48 and hTIP49 are core components: hINO80, hSWR, hTIP60 and hURI (Figure 1.6) (Sardiu et al., 2008). Interestingly, the number of TIP49 proteins in yeast is too small for them to be permanently associated with each complex they are components of, indicating a transient function (possibly by modulating protein-protein interactions) in these complexes, rather than direct catalytic activity (Gallant, 2007; Ghaemmaghami et al., 2003). These complexes and the roles of TIP48 and TIP49 within them will be discussed below.

Figure 1.6. Interaction map of TIP48 and TIP49. Using a proteomics approach, the interactions between four TIP48/TIP49 containing complexes were depicted in this Venn diagram (Sardiu et al., 2008). Underlined proteins were used as bait in the analysis. Proteins with asterisks are novel complex components. Components shared between the complexes are coloured in orange. Proteins depicted in circles with dashed lines interacted with components of the respective complexes, but were not considered core components. Figure adapted from (Sardiu et al., 2008)

1.5.3 The yeast and mammalian INO80 chromatin remodelling complexes

The INO80 complex was first identified in yeast cells, and consisted of ~ 12 proteins built around the SWI2/SNF2 family ATPase INO80 (inositol auxotroph 80 kDa) (Ebbert et al., 1999; Shen et al., 2000). Subsequently, the INO80 complex was shown to unwind DNA in a 3' to 5' direction, and to remodel chromatin *in vitro* (Shen et al., 2000). This chromatin remodelling activity was linked to transcriptional regulation and DNA damage repair *in vivo* (Shen et al., 2000). A complex built around a catalytically deficient mutant of INO80 (K737A) had minimal ATPase activity and no helicase activity, implying that INO80 was the *bona fide* catalytic subunit within the complex (Shen et al., 2000). The INO80 complex also displayed ATP dependent nucleosome mobilization *in vitro* (Shen et al., 2003), exemplifying its expected activity *in vivo*.

A more direct link between DNA damage and INO80 has been established in the model organisms *S. cerevisiae* and *A. thaliana*. In yeast, the INO80 complex was shown to bind to phosphorylated histone H2A (known as γH2A) (Morrison et al., 2004). γH2A is a marker for DNA double-strand breaks (DSBs) in yeast and recruits repair proteins to sites of DNA damage (Downs et al., 2000). Yeast γH2A is equivalent to γH2AX in higher eukaryotes: a phosphorylated histone variant which marks DSBs. The recruitment of the INO80 complex to DSBs correlates with chromatin remodelling, allowing the damaged DNA to be processed by the non-homologous end joining (NHEJ) repair pathway (van Attikum et al., 2004). Moreover, INO80 was shown to regulate the transcription of some genes involved in NHEJ, providing a further link between INO80 and DNA repair (van Attikum et al., 2004). In *A. thaliana*, the INO80 complex was required for homologous recombination (HR) mediated DNA repair of DSBs (Fritsch et al., 2004); the yeast INO80 complex was also implicated in HR (van Attikum et al., 2004). Importantly, the human INO80 complex was shown to be necessary for transcription (Cai et al., 2007) and HR dependent DNA repair (Wu et al., 2007) in conjunction with the YY1 ubiquitous transcription factor. Interestingly, YY1

showed similarity to the bacterial branch migration co-factor RuvA (see section 1.1.2) by binding to synthetic Holliday junctions *in vitro* and, like RuvA, was tetrameric in solution; however, the significance of these findings remains to be elucidated.

More recently it was shown that the different roles of the yINO80 (yeast INO80) complex in transcription and DNA damage repair may be regulated by post translational modifications. Ies4, a component of the INO80 complex, was phosphorylated in response to DNA damage, and phosphorylation was required for correct DNA damage checkpoint responses (Morrison et al., 2007). Together, these data provided a direct link between chromatin remodelling, DNA repair and the INO80 complex. It is likely that the involvement of INO80 in HR and NHEJ DNA repair is conserved throughout eukaryotes.

Further characterisation of the yINO80 complex showed that actin, as well as actin related proteins yArp4 (homologous to human BAF53), yArp5 and yArp8 were essential components of the INO80 complex (Shen et al., 2003). Actin and actin related proteins (Arps) are common to several chromatin remodelling complexes, including TIP60 and SWR (see sections 1.5.3 to 1.5.5). Nucleotide binding of Arps does not seem to affect their *in vivo* functions; however, yeast mutants lacking Arps are either non-viable or have severe transcriptional or chromatin remodelling defects (Galarneau et al., 2000; Shen et al., 2003). Consistent with this, Arp4 was shown to bind core histones *in vitro* (Galarneau et al., 2000; Harata et al., 1999), Arp8 was required for histone binding by INO80 *in vitro*, and for recruiting actin and Arp4 to the INO80 complex (Shen et al., 2003). Arp5 and Arp8 were also shown to be recruited to the INO80 complex by interactions with the N terminal region of yINO80. These data indicate that Arps and actin assemble in a hierarchal fashion and provide a histone binding or chaperone function in the INO80 complex.

TIP48 and TIP49 were both identified as components of yeast and human INO80 complexes. Moreover, they are both present in a 6:1 stoichiometry with the other

components, indicating they function as a double hexamer within the INO80 complex (Shen et al., 2000). Yeast strains expressing degron tagged TIP48 or TIP49 (resulting in proteins which are rapidly degraded following galactose-induction and temperature shift to 38 ºC), coupled with micro-array analyses, were used to demonstrate that yTIP48 and yTIP49 regulate the transcription of around 5 % of yeast genes (Jonsson et al., 2001). Interestingly there was a strong correlation between transcription of genes by TIP48 and TIP49, indicating that they co-operate. The expression of these genes also significantly, but not completely, correlated with yINO80 regulated transcription; however, chromatin immunoprecipitation showed the localisation of INO80, but not TIP48 or TIP49, at the promoters of these genes (Jonsson et al., 2004). Yeast strains with degron-tagged TIP48 or TIP49 were further used to probe interactions within the INO80 complex. Significantly, reduction in yTIP48 or yTIP49 levels resulted in INO80 complexes being inactive and reduced the association of Arp5 with INO80 (Jonsson et al., 2004). Thus, yTIP48 and yTIP49 may function to recruit the actin related protein yArp5 into the INO80 complex (Jonsson et al., 2004). Interestingly, a Walker B mutant TIP48^{E297G} still facilitated in the recruitment of Arp5 (Jonsson et al., 2004). This indicates that ATP hydrolysis by TIP48 is not required for this process, at least when functional TIP49 is present. This provided the first indication of a molecular function of TIP48 and TIP49 within the nucleus: yTIP48 and yTIP49 may recruit proteins for the correct assembly of multi-subunit complexes. Significantly, when yTIP48 was immunoprecipitated, the other components of the yINO80 complex co-immunoprecipitated, as well as various other proteins (Shen et al., 2000). This was a strong indication that TIP48 and TIP49 are components of several distinct nuclear complexes in yeast, and explains why TIP48 and TIP49 deletion mutants in yeast are individually lethal (Kanemaki et al., 1999; Qiu et al., 1998), but INO80 deletion mutants are not always lethal (Shen et al., 2000).

1.5.4 H2A variant H2A.Z and the SWR complex

Histone variant H2A.Z (a.k.a. Htz1 in yeast) is a highly conserved protein with ~ 90 % sequence identity between species (Iouzalen et al., 1996). H2A.Z has conserved functions between species that are distinct to those of H2A (Jackson and Gorovsky, 2000), and is essential for correct embryonic development in metazoans (Faast et al., 2001). To date, the functions of H2A.Z have not been fully elucidated, and seem to be contradictory, although H2A.Z has now been established as an important marker in processes such as chromatin remodelling around promoters, DNA repair, chromosome segregation, heterochromatin regulation and cell cycle progression; reviewed in (Zlatanova and Thakar, 2008). More recently, it was demonstrated that H2A.Z marks the -1 nucleosome position of promoters, and these H2A.Z containing nucleosomes are removed when promoters are activated, presumably to allow the transcription machinery to bind (Schones et al., 2008). Histone H2A is exchanged for H2A.Z by the chromatin remodelling complex TIP60 (discussed below) in mammals; the related SWR complex also carries out this function, in an ATP dependent manner, in yeast (Kobor et al., 2004; Krogan et al., 2003; Mizuguchi et al., 2004) and in metazoans (Cai et al., 2005; Ruhl et al., 2006). Yeast SWR complexes consist of ~ 12 proteins and are built around the Swr1 (Swi2/Snf2-related 1) protein. In metazoans, the SWR complex is built around SRCAP (Snf2-related CBP activator protein).

In addition to its other putative functions, it was shown that H2A.Z is required for maintaining the correct regulation of transcription of a subset of genes by limiting the spread of 'transcriptionally silent' heterochromatin, particularly around telomeres (Meneghini et al., 2003). ySwr1 deletion mutants displayed a similar gene transcription profile to mutants lacking H2A.Z, implicating the ySwr1 complex in the deposition of H2A.Z into histones as a transcription marker (Kobor et al., 2004). The ySWR complex was subsequently shown to catalyse H2A.Z exchange *in vitro* in an ATP dependent manner, while a complex built around a catalytically dead mutant of ySwr1 (K727G) did not (Mizuguchi et al., 2004).

Interestingly, the H2A.Z yeast mutants were also sensitive to UV damage, indicating H2A.Z, and thus the ySWR complex, is required during DNA damage repair processes (Mizuguchi et al., 2004). Consistent with this, the ySWR complex was shown to localise to DNA double-strand breaks (DSBs) and was required for recruitment of yKu80, a key protein in facilitating NHEJ (Non-homologous end joining) repair proteins to DNA double strand ends (van Attikum et al., 2007).

The functions of H2A.Z between yeast and metazoans are thought to be conserved (Jackson and Gorovsky, 2000), although reports suggest different roles for yeast and metazoan H2A.Z in transcriptional regulation (Bruce et al., 2005). The human SWR complex was purified from HeLa cells, and was mostly comprised of close homologues of the yeast SWR complex (Cai et al., 2005), and demonstrated ATP dependent *in vitro* H2A.Z exchange (Ruhl et al., 2006). Further analysis of the hSWR complex showed it was responsible for H2A.Z exchange *in viv*o and localised at active promoters (Wong et al., 2007), highlighting a conserved role in transcriptional regulation across species.

Yeast TIP48 and yTIP49 were identified as genuine components of the SWR complex, which was also true for metazoan SWR complexes. Yeast Swr1 also co-purified with Arp4 and Actin, which are common components of yINO80 and yTIP60 complexes (Krogan et al., 2003); the same was also true for the human SWR complex, as BAF53 (homologue of Arp4) and Actin were also detected (Cai et al., 2005). This TIP48/TIP49/BAF53/Actin complex is common to many chromatin remodelling complexes, and may form an important core sub-complex. Clearly, the presence of TIP48 and TIP49 in nuclear chromatin remodelling complexes with links to transcription and DNA repair is a common theme; however, the precise mechanisms of TIP48 and TIP49 within these complexes remains an intriguing question.

1.5.5 The metazoan TIP60 Histone acetyltransferase complex

Histone acetyltransferases (or HATs) catalyse the addition of acetyl groups to conserved lysine residues on histones. A subset of chromatin remodelling complexes modify chromatin by HAT (histone acetyl transferase) activity, resulting in reduced stability of histone-DNA interactions, allowing the access of DNA processing enzymes to DNA. The metazoan TIP60 complex, which is built around the catalytic subunit TIP60 (HIV-Tat interacting protein, 60 kDa), displays HAT activity. The homologous yeast TIP60 complex (a.k.a. the yNuA4 complex) is built around Esa1 - Esa1 will be termed yTIP60 hereafter for clarity. The TIP60 complex also incorporates the p400 and TRRAP subunits. p400 is a homologue of SWR1, and may allow TIP60 complexes to incorporate nucleosome switching functions (Auger et al., 2008). TRRAP (Transformation–transactivation domain-associated protein) is a catalytically inactive member of the phosphatidylinositol 3-kinase-related protein kinase family, and seems to act as a protein scaffold within the TIP60 complex (McMahon et al., 1998). yTIP60 complexes do not purify with TIP48 and TIP49 as components (Cai et al., 2003; Doyon et al., 2004); however, in metazoan TIP60 complexes, TIP48 and TIP49 are *bona fide* components (Doyon et al., 2004; Ikura et al., 2000). Furthermore, metazoan TIP60 complexes seem to be well conserved between species (Kusch et al., 2004).

Although TIP48 and TIP49 are not components of the yeast TIP60 complex, to aid understanding of the mammalian TIP60 complex, the isolation and characterisation of yTIP60 will be summarised. yTIP60 was identified as essential for cell cycle progression (Clarke et al., 1999) and transcriptional regulation (Reid et al., 2000). yTIP60 was identified as a HAT which catalysed the acetylation of histone H2A and H4 tails (Kimura and Horikoshi, 1998; Yamamoto and Horikoshi, 1997). yTIP60 was then identified as part of a large nuclear complex of ~ 13 subunits (Allard et al., 1999), which was also implicated in direct response to DNA DSBs by remodelling chromatin (Bird et al., 2002; Downs et al., 2004). Interestingly, the catalytic activity of yTIP60 can be demonstrated *in vitro* using

only three core subunits (yTIP60, Epl1 and Yng2), and this complex was shown to exist *in vivo* (Boudreault et al., 2003). This led to the conclusion that the core complex (named the piccolo yTIP60 complex) is responsible for global histone acetylation, whereas the full yTIP60 complex is targeted to specific promoters and sites of DNA damage by the other subunits of the complex (Boudreault et al., 2003). It is also thought that these sub-complexes are conserved in metazoans.

Significantly, 12 of the subunits of the yeast TIP60 complex were also present in the human TIP60 complex, including the eponymous catalytic subunit TIP60 (Doyon et al., 2004). This demonstrated good conservation between the yeast and human complexes. The hTIP60 subunit was responsible for the HAT activity directed at histones H2A and H4, again showing correlation with yeast (Doyon et al., 2004). Notably, the hTIP60 complex was made up of ~ 16 subunits, and included hTIP48 and hTIP49 (Doyon et al., 2004; Ikura et al., 2000). The additional subunits present in the human complex were homologous to components of the yeast and human SWR complexes which display chromatin remodelling in the form of nucleosome switching of histone H2A for H2A.Z (discussed above). This observation was used to hypothesise that the mammalian TIP60 complex is a fusion of the yeast TIP60 and SWR complexes (Auger et al., 2008; Doyon and Cote, 2004). Indeed, the TIP60 and SWR mutants were synthetically lethal in yeast, indicating that their activities are coordinated (Auger et al., 2008). Moreover, p400 (which is not a component of the yeast TIP60 complex) is homologous to ySwr1: which catalyses histone switching (Doyon et al., 2004). Indeed, it is feasible that the p400 subunit evolved as a fusion of yeast Swr1 and yeast Eaf1 (the putative scaffolding subunit of yTIP60 complex), bringing together the TIP60 HAT and SWR histone switching activities (Figure 1.7) (Auger et al., 2008). In support of this, the human TIP60 complex displays both histone acetylation and nucleosome switching activities (Martinato et al., 2008). This ‘nuclear complex evolution’ is made more convincing, as hTIP48 and hTIP49 are recruited to the hTIP60 complex by interaction with p400 (Fuchs et al., 2001): the putative bridge between TIP60 and SWR complexes in metazoans.

Figure 1.7. Hypothetical evolution of human TIP60 and SRCAP complexes. Adapted from (Auger et al., 2008). Human TIP60 complexes may have evolved from a physical merge of TIP60 and SWR as depicted above. The human SWR complex is equivalent to that of yeast. TIP48/TIP49 are called RuvBL1/2 in this Figure.

The mammalian TIP60 complex has been shown to regulate the expression of specific genes. This activity is likely to be via the histone or protein acetyltransferase activity of the complex, activating transcription factors and remodelling chromatin around promoters. Furthermore, TIP60 and some of the subunits within its complex interact with transcription factors such as NFκB, p53, c-Myc and E2F (see below and sections 1.7.2 to 1.7.4) to activate target genes.

As well as being an important regulator of gene expression, the mammalian TIP60 complex has been linked to DNA repair and apoptosis (Bird et al., 2002; Cheng et al., 2008; Gorrini et al., 2007; Ikura et al., 2000; Ikura et al., 2007). Both yeast and human TIP60 complexes have numerous shared subunits, including actin and actin related proteins (Arps). Actin and Arps frequently appear in nuclear chromatin remodelling complexes, including INO80 and SWR complexes (discussed in 1.5.3 and 1.5.5 above). The hBAF53 homologue yArp4 was shown to recruit the yTIP60 complex to γH2A: a marker for DSBs (Downs et al., 2004). This provides a direct mechanism by which TIP60 is recruited to sites of DSBs to remodel chromatin and facilitate repair. γH2A in yeast is equivalent to γH2AX in higher eukaryotes, and it is thought that hBAF53 targets the TIP60 complex to sites of DNA damage; however, this has yet to be formally demonstrated.

hTIP60 has also been shown to modulate the activities of ATM (Ataxia telangiectasia mutated) and p53. In response to DSBs, ATM phosphorylates target proteins (including p53 and histone H2AX), resulting in expression and activation of genes involved in the DNA damage repair pathways, check point activation or apoptosis; for a review of DNA double-strand break cellular responses see (Cann and Hicks, 2007). Similarly, p53 is a transcription factor which regulates the expression of genes that govern cell cycle arrest and apoptosis (Okorokov et al., 2006). p53 switches gene transcription to favour either cell cycle arrest or apoptosis depending on the type and extent of damage caused, although the molecular mechanisms of this regulation by p53 are still poorly understood. It has been reported that the hTIP60 acetylation of ATM activates ATM dependent phosphorylation of targets in response to DNA damage

(Sun et al., 2005; Sun et al., 2007). It was also demonstrated that TIP60 is a co-activator of p53 and is required for p53 dependent transcription and cell cycle arrest (Legube et al., 2004). Interestingly, p400 and TIP60 were shown to antagonistically regulate p53 pathways: p400 induced cell cycle arrest while TIP60 was required for apoptosis (Tyteca et al., 2006). The authors concluded that p400 was a regulatory subunit of the TIP60 complex, or that specific sub-complexes of the TIP60 complex exist to channel p53 gene expression towards different cell fates. More recently, it was demonstrated that TIP60 acetylates p53 after DNA damage, resulting in p53 dependent transcription of pro-apoptotic genes (Sykes et al., 2006; Tang et al., 2006). Indeed, UV irradiation dependent SUMOylation of TIP60 was recently shown to regulate its nuclear localisation and ability to activate p53 (Cheng et al., 2008). These data suggest an important mechanism by which TIP60 regulates the cellular response to DNA damage, and highlights the intricacy of TIP60 regulated transcription.

The activity of TIP48 and TIP49 within the human TIP60 complex has been investigated. The hTIP60 complex displayed DNA dependent ATPase activity and 5'-3' helicase activity *in vitro* (Ikura et al., 2000). In the same study, recombinant TIP48 and TIP49 individually showed little ATPase activity, and a complex of recombinant human TIP48 and TIP49 displayed ATPase activity roughly half that of the purified TIP60 complex. However, the TIP48/TIP49 complex did not bind DNA or display any helicase activity, making it unlikely that they were responsible for the TIP60 complex helicase activity (Ikura et al., 2000).

Together, these data provide clues about the roles of TIP48 and TIP49 within the TIP60 complex. TIP48 and TIP49 do not seem to be essential for the HAT activity of TIP60, as they are not present in the analogous yeast complex, and the piccolo hTIP60 complex displays HAT activity *in vitro* (Doyon et al., 2004). They may, however, be important for targeting the TIP60 complex to regions of DNA under different cellular conditions. Alternatively, TIP48 and TIP49 could be critical for the putative H2A.Z switching ability of the hTIP60 complex, as in the homologous SWR complexes in yeast and mammals. The mechanisms by which

TIP48 and TIP49 act within these complexes is unclear; however, TIP48 and TIP49 facilitated the correct assembly of INO80 complex (see section 1.5.3), and this may also be the case for SWR related complexes. Indeed, recently it was shown that TIP49 is required for DNA damage response mediated by hTIP60 (Gospodinov et al., 2009; Jha et al., 2008), strengthening this hypothesis.

1.5.6 The yeast and mammalian URI nutrient sensing complex

Prefoldins are a conserved small molecular mass family of proteins which assemble into molecular chaperone complexes; including chaperones that assist the folding of cyto-skeletal proteins, actin and tubulin (Vainberg et al., 1998). Prefoldins are characterised by their N- and C-terminal α-helical coiled coil regions which are connected by one or two β-hairpins (Siegert et al., 2000). A novel prefoldin was isolated from yeast and human cells and named URI (Unconventional prefoldin RBP5 Interactor) due to its large molecular mass and its reported interaction with RBP5 (Gstaiger et al., 2003); interestingly, RBP5 is a subunit of all three eukaryotic RNA Polymerase holoenzymes (Woychik et al., 1990), which implies URI has a transcriptional role. URI was found to be a component of a large mega-Dalton complex (around 2 MDa) which comprised of several proteins, including TIP48 and TIP49 (Gstaiger et al., 2003). Characterisation of the URI complex demonstrated a conserved function between yeast and metazoans: the URI complex is involved in transcriptional regulation of nutrient metabolising proteins in response to nutrient sensing and signalling by the mTOR pathway (Gstaiger et al., 2003). Further characterisation of URI complexes in metazoans revealed that URI is required in *C. elegans* for maintaining endogenous genomic integrity and correct cell cycle progression (Parusel et al., 2006). URI in *D. melanogaster* was shown to bind specifically to protein phosphatase Iα (PPIα) and was required for genome stability and efficient transcription (Kirchner et al., 2008). The significance of TIP48 and TIP49 within the URI complex has not yet been elucidated; it is, however, another example of a highly conserved eukaryotic complex that regulates transcription with TIP48 and TIP49 proteins as components.

1.5.7 Small nucleolar ribonucleoprotein (snoRNP) facilitate ribosomal RNA biogenesis

Before the incorporation of ribosomal RNA (rRNA) into ribosomes, rRNA must undergo a series of specific modifications, including cleavage, methylation and pseudouridylation. The modification of rRNA is guided by small nucleolar RNAs (snoRNAs), which combine with proteins in complexes called snoRNPs, or small nucleolar ribonucleoproteins. Two major classes of snoRNPs have been demonstrated: box C/D snoRNPs and box H/ACA snoRNPs; for a review, see (Granneman and Baserga, 2004). This process is conserved between yeast and mammals, and a number of archaeal species also have both C/D and H/ACA class snoRNPs (Omer et al., 2000). The core complex of mammalian box C/D snoRNPs contains snoRNA in addition to at least four conserved proteins: 15.5K, NOP46, NOP58 and Fibrillarin. However, the factors regulating biogenesis of snoRNPs are not limited to these core proteins, and it has been shown that a number of proteins guide maturation and sub-nuclear localisation of snoRNPs, probably as part of a large nuclear complex. One such maturation step is the localisation of core box C/D snoRNPs from the nucleoplasm to the nucleolus. It was discovered that a complex of several proteins associates with immature nucleoplasmic snoRNPs, but is not associated with mature nucleolar snoRNPs (King et al., 2001; Newman et al., 2000; Watkins et al., 1998). Moreover, the stability of the core complex was much greater in the nucleolus than in the nucleoplasm. This led to the hypotheis that a large multi-protein nuclear complex guides the core snoRNP to the nucleolus. During or after this localisation, a restructuring event may occur, resulting in maturation of the snoRNP. TIP48 and TIP49 were identified as proteins essential for this maturation step (King et al., 2001). The fact that TIP48 and TIP49 are the only components of this complex with ATPase activity and are members of the AAA^+ family suggested that TIP48 and TIP49 take an active role in restructuring core Box C/D snoRNPs (Watkins et al., 2002; Watkins et al., 2004). This model was strengthened by the observation that a catalytically dead mutant of TIP48 reduced both Box C/D and Box H/ACA

snoRNP maturation in yeast (King et al., 2001). Moreover, nucleotide binding, particularly TIP48 bound to ATP, increased the binding affinity of TIP48 and TIP49 to other components of the snoRNP maturation complex (McKeegan et al., 2007). It is evident from analysis of snoRNA containing complexes that the maturation of snoRNPs involves a number of dynamic complexes before nucleolar localisation and restructuring. Taken together, it was concluded that TIP48 and TIP49 are important in modulating protein-protein or protein-RNA interactions during the maturation of snoRNPs. Moreover, it has recently been shown that TIP48 and TIP49 are required for the correct assembly of the telomerase complex, which also contains an H/ACA motif RNA component: TERC (Venteicher et al., 2008) (see section 1.7.6). Accordingly, restructuring RNA containing complexes is a common function of TIP48 and TIP49.

1.5.8 Interactions with the RNA polymerase II holoenzyme and other transcription machinery

TIP49 was originally identified as an interacting protein of TBP in rat cells (Kanemaki et al., 1997). TBP binds to conserved 'TATA Box' regions of DNA at gene promoters and recruits the transcription machinery in a stepwise fashion. Both TIP48 and TIP49 were subsequently shown to interact with TBP in yeast *in vitro* and *in vivo* (Ohdate et al., 2003), the same was also demonstrated for metazoan TIP48 and TIP49 (Bauer et al., 2000; Bauer et al., 1998). Furthermore, hTIP49 was identified as an interacting partner of RPA3 in yeast two-hybrid assays (Qiu et al., 1998) and hTIP48 was shown to interact with RPAP3 (Jeronimo et al., 2007; Ni et al., 2009). Both RPA3 and RPAP3 are components of the RNAP II holoenzyme complex, responsible for the transcription of genes. Interestingly, RPAP3 is tightly associated with RNAP II, was reported to mediate interactions between the RNAP II holoenzyme and regulators of protein complex formation, during active transcription (Jeronimo et al., 2007). This interaction with TBP and components of the RNA Polymerase II holoenzyme led to the hypothesis that TIP48 and TIP49 worked in conjunction with the transcription machinery. Indeed, in yeast, TIP48 and TIP49 were shown to regulate the

transcription of over 5 % of genes (Jonsson et al., 2001); however, this regulation is likely to be as part of the chromatin remodelling complexes they are essential components of (see relevant sub-sections in section 1.5). Supporting this observation, only 1 % of yTBP was associated with yTIP48 as judged by pull down assays, indicating a transient or promoter specific interaction of TIP48 with TBP (Ohdate et al., 2003). TIP48 and TIP49 may function to target TBP to specific promoters, or TIP48/TIP49 containing chromatin remodelling complexes may modify histones to allow TBP to bind the unmasked TATA Box and allow transcription.

A further link with transcription machinery was provided by observations that TIP49 interacted with RNAP I, which is responsible for the transcription of rRNA (ribosomal RNA). TIP49 and RNAP I co-localised in fibrillar centres of the nucleolus; however, in this case, TIP49 was suggested to reduce RNAP I dependent rRNA production in conjunction with the transcription factor c-Myc (Cvackova et al., 2008). TIP48 and TIP49 are progressively being linked to the basal transcription machinery, and their mechanism of action within this system is rapidly developing into an important area of research.

1.5.9 Antagonistic regulation of transcription by TIP48 or TIP49 complexes with β–catenin

The Wnt signalling pathway plays a major role in development by regulating gene expression. β–catenin is normally present at the cell surface bound to cadherin, and is involved in the regulation of cell-cell contacts. In the presence of a Wnt signal, β–catenin is transported to the nucleus and associates with transcription factors (such as TCF4 or LEF1) to regulate the transcription of Wnt target genes; for reviews on β–catenin dependent Wnt signalling see (Brembeck et al., 2006; Huang and He, 2008). The molecular details of β–catenin dependent transcription are still poorly understood. However, in humans and *Drosophila*, TIP48 and TIP49 antagonistically regulate expression of genes in response to a Wnt signal, via β–catenin dependent transcription. In this system, TIP48 is a co-

repressor, while TIP49 is a co-activator (Bauer et al., 2000). In Zebrafish, TIP48 mutants were found to deregulate the transcription of β–catenin dependent genes, causing heart hyperplasia during development (Rottbauer et al., 2002). It was suggested that TIP48 and TIP49 antagonistically regulate β–catenin dependent genes during heart development, although this was not conclusively demonstrated (see 1.4.3) (Rottbauer et al., 2002). Interestingly, hTIP49 was shown to co-activate genes with β–catenin by recruiting subunits of the TIP60 HAT complex (Feng et al., 2003). Indeed, over-expression of hTIP49^{D302N} (a dominant negative Walker B mutant) resulted in reduced Histone H4 acetylation at the promoter of ITF1: a target of β–catenin (Feng et al., 2003). This was later corroborated by elucidating the regulation of the KAI1 metastasis suppressor gene.

KAI1 is a tetraspannin protein, and repression of KAI1 is an important step in the metastatic progression of tumours (Baek et al., 2002; Kim et al., 2005). The KAI1 promoter is normally repressed by HDAC (histone deacetylase) complex of N-CoR/TAB2/HDAC3 (Baek et al., 2002). Interleukin-1β stimulation of cells causes nuclear export of this N-CoR complex and subsequent activation of the KAI1 gene by TIP60 (Baek et al., 2002). When the promoter of KAI1 was analysed in metastatic cells, in response to interleukin-1β, a repressive complex of β–catenin/TIP48/HDAC1 was recruited, while in non-metastatic cells, the TIP60 co-activator complex was recruited. Both β–catenin and the TIP60 complex were directly recruited to the promoter by interactions with the p50 NFκB transcription factor, thus the recruitment of both complexes was mutually exclusive (Kim et al., 2005). The authors concluded that relative levels of TIP60 and β–catenin complexes modified the acetylation state of chromatin at the KAI1 promoter, regulating the transcription of the gene, and influencing metastasis (Kim et al., 2005). Surprisingly, only TIP49 was detected within the TIP60 complex in these experiments (Kim et al., 2005): TIP48 and TIP49 are normally found in equal stoichiometry within the TIP60 complex (see section 1.5.5). These observations could be explained by a limitation of the detection technique, meaning only TIP49 was observed, or by reduced protein expression within the cell lines. Furthermore,

reducing TIP49 levels did not affect the expression KAI1, while reducing TIP60 did; however, these issues were not addressed by the authors.

In a more recent study, it was shown that KAI1 transcription can be induced by PMA (phorbol 12-myristate 13-acetate) in a metastatic cell line, and that this was mediated by classical Protein Kinase C signalling via MEK/ERK (Rowe et al., 2008). These authors also found that TIP48/β–catenin complexes were recruited to repress the promoter, but again, did not rule out that TIP48 was also in the TIP60 complex. Surprisingly, they also saw that TIP48 and TIP60, but not β–catenin or TIP49, left the promoter after 6 hours of PMA activation, which corresponded with maximal expression of KAI1 (Rowe et al., 2008); however, the authors did not comment on this discrepancy. The KAI1 gene serves as a marker for the progression of tumours. TIP48 and TIP49 are clearly important co-factors in the regulation of KAI1 expression, and further work defining their roles within this system would be of great interest.

1.5.10 Antagonistic HOX gene regulation by *Drosophila* TIP48-Polycomb Group and TIP49-Trithorax Group complexes

Gene regulation at the level of transcription can be carried out by chromatin remodelling (discussed in section 1.5.1). Two antagonistic mediators of HOX gene expression via remodelling chromatin are Polycomb group (PcG) and Trithorax group (TrxG) complexes in *Drosophila melanogaster*; for reviews see (Ringrose and Paro, 2004; Simon and Tamkun, 2002). PcG complexes silence HOX gene expression by preventing chromatin remodelling by SWI/SNF; the mechanism of this silencing is currently unknown, although it could be due to PcG complexes physically preventing remodelling factors and transcription machinery having access to nucleosomes. TrxG complexes (SWI/SNF homologues) decompact the chromatin, using an ATP dependent chromatin remodelling activity, allowing transcription of HOX genes. One major *Drosophila* PcG complex, the PRC1 complex, was purified and the components identified by mass spectroscopic analysis. dTIP48 but not dTIP49 was identified as part of this

complex (Saurin et al., 2001). Oddly, the stoichiometry of dTIP48 in this complex was ~ 0.7:1 with other components, which would mean dTIP48 does not act as a hexamer within this complex (Saurin et al., 2001), although this could signify that hexameric TIP48 only associates with a subset of complexes.

The identification of dTIP48 with the PRC1 PcG complex is supported by genetic interactions between TIP48 and several PcG complexes in *Drosophila*, not limited to just PRC1 (Qi et al., 2006). However, in the same study, it was suggested that TIP48 mediates its repression of HOX genes via the TIP60 HAT complex, as TIP60 components Domino (the homologue of Swr1), and E(Pc) (Enhancer of Polycomb) also demonstrated genetic interaction with PcG complexes (Qi et al., 2006). The authors also noted that the biochemical activity of chromatin silencing of genes can be carried out by the core components of PRC1, which does not include dTIP48, arguing that dTIP48 is not necessary for PRC1 dependent HOX gene silencing. This was later contradicted by another group, who demonstrated that dTIP48 was indeed necessary for PRC1 PcG complex dependent silencing of HOX genes (Diop et al., 2008). Significantly, they identified dTIP49 as a co-activator of these genes with TrxG complexes, indicating that dTIP48 and dTIP49 form distinct complexes which antagonistically regulate HOX gene transcription (Diop et al., 2008). Furthermore, they showed that dTIP48 but not dTIP49 co-purified with the core proteins of PRC1 PcG complex. Strikingly, the group also identified dTIP49, but not dTIP48, as a component in Brahma (*Drosophila* SWI2/SNF2 homologue) TrxG chromatin remodelling complexes, and dTIP49 in this complex ran as a 170 kDa species on denaturing gels (Diop et al., 2008). The authors suggested that TIP49 in this complex was a denaturation resistant oligomer, although heavily post-translationally modified forms of TIP49 could also account for this size on SDS PAGE. Indeed, modifications may be a mechanism by which TIP48 and TIP49 are assembled into distinct complexes for antagonistic transcriptional regulation.

1.6 TIP48 and TIP49 interact with cytoskeletal components

1.6.1 TIP48 and TIP49 are implicated in mitotic spindle assembly

Both hTIP48 and hTIP49 have been individually shown to associate with the centrosomes and mitotic spindle, using immunofluorescence microscopy (Gartner et al., 2003; Sigala et al., 2005). TIP49 co-immunoprecipitated with α- and γ-tubulin in U937 cells, indicating an interaction of TIP49 and microtubules (Gartner et al., 2003). An RNAi screen in S2 *Drosophila* cells identified dTIP49 as essential in the regulation of mitotic spindles and centrosomes (Ducat et al., 2008). Further analysis using knockdown of dTIP49 and visualisation of the mitotic spindle apparatus showed defects in spindle formation, including abnormal spindles and splayed spindle poles. Centrosomal defects were also observed, including low centrosome numbers and centrosome position defects (Ducat et al., 2008). Similar experiments in human derived cell lines indicated that hTIP49 was also essential for mitotic spindle and centrosome organisation. *in vitro* Xenopus egg extracts were used to demonstrate that both TIP48 and TIP49 interacted with the γ-tubulin ring complex, which facilitates the correct orientation and nucleation of microtubules. Furthermore, immunodepletion of endogenous TIP49 (which also depleted TIP48) from the extracts caused abnormal spindle assembly, which was rescued by addition of γ-tubulin ring complex together with recombinant hTIP48/hTIP49 complex (Ducat et al., 2008). These data indicated that TIP48 and TIP49 may modulate protein-protein interactions involving tubulin and the γ-tubulin ring complex.

Further insights into the mitotic functions of TIP48 and TIP49 came from studies characterising interacting partners of ILK (Integrin Linked Kinase). ILK is a scaffold protein and a serine/threonine kinase (Qian et al., 2005). TIP48 and TIP49 were identified in a screen for functional interactions with ILK in HEK293 cells (Dobreva et al., 2008; Fielding et al., 2008). TIP49 seemed to be included in

a sub-complex with α-tubulin and ILK (Dobreva et al., 2008), and this complex localised at centrosomes during interphase and mitosis (Fielding et al., 2008). Even though TIP48 also associated with ILK, the co-localisation and presence of TIP48 in this complex was not investigated. As ILK has also been shown to induce stabilisation and nuclear localisation of β-catenin, the authors noted that TIP49 with β-catenin may be shuttled to the nucleus by ILK, which may in turn affect the transcription of specific genes (Dobreva et al., 2008).

1.6.2 Links to cilium formation

Evidence for the involvement of TIP48 and TIP49 in cilium formation came from studies that identified interactions between TIP48, TIP49 and OFD1 (Giorgio et al., 2007). OFD1 (named after Orofaciodigital syndrome type 1) localises at the base of the primary cilium and is required for primary cilium formation and correct left-right axis specification. Interestingly, OFD1 was also shown to be nuclear and associated with subunits of the TIP60 HAT complex. How TIP48, TIP49 and OFD1 are linked during cilium formation, as well as their mutual presence in the TIP60 complex is still open to investigation; however, evidence suggests that TIP49 is essential for cilium formation. A proteomics study linked TIP49, as well as TIP48, with the photoreceptor sensory cilium complex in mice (Liu et al., 2007). Furthermore, a microarray analysis demonstrated that both TIP48 and TIP49 mRNA levels were up-regulated during flagellar regeneration in the algal species *Chlamydomonas reinhardtii* (Stolc et al., 2005). Mutations in TIP49 also cause cystic kidneys in Zebrafish (Sun et al., 2004); cystic kidneys have been linked with ciliary dysfunction (Pazour and Witman, 2003). The most likely explanation for these data is that TIP48 and TIP49 co-regulate transcription in response to cilium based signaling events (Stolc et al., 2005; Sun et al., 2004), possibly via β-catenin related transcriptional regulation (see sections 1.5.9 & 1.7.2). Alternatively, as cilia contain tubulin, TIP48 and TIP49 may directly act on the tubulin components of cilia emulating their activities during mitotic spindle formation.

1.7 TIP48 and TIP49 have been implicated in cancer

1.7.1 Expression and incidence in cancers

The TIP49 gene locus is in 3q21 and TIP48 is in 19q13.2 in the human genome (Makino et al., 2000). 3q21 is a gene rich region which is frequently rearranged in leukaemias (Rynditch et al., 1997). Moreover, this region was found to be duplicated in human non small cell lung cancer samples, and TIP49 mRNA levels were around 4 fold higher than in wild type samples (Dehan et al., 2007). 19q13.2 is a region where rearrangements are associated with breast cancer (Parfait et al., 2000). However, when mRNA levels of TIP48 in breast cancer tissues were tested, no up-regulation of TIP48 was detected (Parfait et al., 2000), suggesting TIP48 levels were not critical for cancer progression in those cases.

Expression of TIP48 and TIP49 was shown to be deregulated in several clinical cases of cancer. When hepatocarcinoma cells from a patient were compared with wild type liver cells from the same patient, expression of TIP48 and TIP49 was shown to be elevated (Blanc et al., 2005; Huber et al., 2008; Rousseau et al., 2007). Moreover, an increase in TIP49 expression correlated with a poorer prognosis in hepatocarcinoma patients (Rousseau et al., 2007). Interestingly, increased expression of TIP49 in a hepatocarcinoma cell line correlated with a more aggressive phenotype, while knockdown of TIP49 correlated with less cell growth and more apoptosis, indicating that TIP49 was necessary for the viability and metastasis of these cells (Rousseau et al., 2007). The oncomine database (www.oncomine.org), which contains extensive microarray analysis of protein expression in clinical cases of cancer, also indicated up-regulation of TIP48 and TIP49 in several cases of cancer, including bladder tumours and melanomas (Huber et al., 2008). Consistent with this, TIP49 was found to be up-regulated in some colon cancers (Carlson et al., 2003); the authors linked the increase in TIP49 to an increase of the colon cancer marker COX-2, via the Wnt/β-catenin signalling pathway. Finally, the sub-cellular localisation of TIP49 also seemed to

be modulated in cancer cells, as TIP49 seemed to have greater nuclear localisation in hepatocarcinoma cells (Lauscher et al., 2007).

As well as their involvement in clinical cases of cancer, TIP48 and TIP49 are key players in signalling pathways and transcription mechanisms which are frequently involved in oncogenic transformation. This makes them good candidates for cancer therapy targets, particularly as they have an enzymatic ATPase activity that could be specifically targeted. The involvement of TIP48 and TIP49 in these processes will be summarised below.

1.7.2 The Wnt pathway: β–catenin and Hint1

The Wnt signalling pathway is instrumental for the regulation of gene transcription in response to developmental and proliferation signals (discussed in section 1.5.9). Crucially, Wnt signalling is often de-regulated during the development of human cancers (Polakis, 2007). β–catenin is a pivotal factor which regulates the transcription of Wnt target genes in response to signalling cues. TIP48 and TIP49 have already been linked with cancer metastasis by modulating β–catenin dependent regulation of the KAI1 metastasis suppressor gene (see section 1.5.9). Further studies into the role of TIP48 and TIP49 in regulating β–catenin dependent transcription will be detailed below.

Hint1 (Histidine triad nucleotide binding protein 1, a.k.a. Protein Kinase C interacting protein) is a haplo-insufficient mammalian tumour suppressor (Li et al., 2006; Zhang et al., 2009). A crystal structure demonstrated that Hint1 binds Zinc via a conserved histidine triad motif (His-X-His-X-His-X-X, where X is a hydrophobic residue) (Lima et al., 1996). Although this analysis provided much information on the structure of Hint1, the impact and mechanism of Hint1 during cancer progression is still poorly understood. Several lines of investigation have implicated Hint1 in cell cycle control, transcriptional regulation and apoptotic induction. Overexpression of Hint1 was shown to induce p53 dependent apoptosis (Weiske and Huber, 2006), although the molecular mechanisms of this effect remain to be tested. Recent evidence also points to the role of Hint1 in

regulating Cyclin dependent kinase inhibitor 1B (a.k.a $p27^{KIP1}$) protein levels and thus blocking progression into S phase (Cen et al., 2009). These effects of Hint1 were attributed to transcriptional regulation of Src, and transcription independent inhibition of SCF^{SKP2} (Cen et al., 2009), as Src and SCF^{SKP2} are negative inhibitors of $p27^{KIP1}$. Hint1 was also required for efficient ATM and γH2AX acetylation (presumably by TIP60) in response to DNA damage (Li et al., 2008). Taken together, these data provide a strong link between Hint1 and the involvement of the TIP60 complex in DNA damage responses (see sections 1.5.5).

Hint1 was shown to bind TIP48 and TIP49 *in vitro* and *in vivo*, while no interaction between Hint1 and β–catenin and LEF1 was detected *in vitro* (Weiske and Huber, 2005). Pull down assays using truncated forms of TIP48, TIP49 and Hint1 demonstrated that TIP48 and TIP49 interact with the N-terminal domain of Hint1. Furthermore, Hint1 interacted with residues 214-295 and 218-289 of TIP48 and TIP49 respectively (Weiske and Huber, 2005). It should, however, be noted that removing these regions of the proteins could have affected their structural integrity, as judged by analysis of the crystal structure of TIP49 and our work carried out in Chapter 4.2. Hint1 over-expression repressed β–catenin mediated transcription in reporter assays, and repression was also seen when cells were co-transfected with TIP48 or TIP49 (Wang et al., 2009; Weiske and Huber, 2005). The authors speculated that Hint1 disrupts interactions between TIP48 and TIP49 oligomers to exert this effect, although this was not demonstrated (Weiske and Huber, 2005).

Hint1 is clearly important in regulating the DNA damage response and transcription, possibly by modulating TIP60. The finding that Hint1 interacts with TIP48 and TIP49 is one of interest, and elucidating the significance of this interaction *in vivo* will provide clues into the tumour suppressor properties of Hint1.

1.7.3 Role of TIP48 and TIP49 in c-Myc transformation

c-Myc is a focal transcription factor and responsible for the regulation of over 10 % of genes in metazoans (Fernandez et al., 2003). c-Myc is one of the most frequently mutated proteins in human cancers, and many of its transcription targets are required for cellular transformation; for appropriate reviews, see (Henriksson and Luscher, 1996) and (Amati et al., 2001). In this context, transcriptional regulation by c-Myc impacts on cell growth, proliferation, and apoptosis, although the molecular signals which direct c-Myc dependent transcription into specific pathways are still being characterised. In addition, c-Myc was recently identified as one of the four critical genes that, when co-expressed, can reprogram somatic cells to become pluripotent stem cells in mice and man (Takahashi et al., 2007; Takahashi and Yamanaka, 2006).

Several components of the TIP60 complex have been identified as interacting partners of c-Myc. hTRRAP, was immunoprecipitated from HeLa cells ectopically expressing an epitope-tagged N-terminal domain of c-Myc (McMahon et al., 1998); subsequently, it was shown that TRRAP was required for c-Myc dependent transcriptional regulation by recruiting the hGCN5/PCAF HAT complex (Frank et al., 2001; McMahon et al., 2000; Park et al., 2001). As well as being a component of the hGCN5 complex, TRRAP is also in the TIP60 HAT complex (see section 1.5.5). Significantly, BAF53, p400, TIP48 and TIP49 – all components of the TIP60 complex – were also shown to interact with c-Myc and be required for c-Myc dependent oncogenic transformation (Park et al., 2002; Wood et al., 2000). Indeed, it has been shown that the entire TIP60 complex is recruited to promoters by c-Myc, in order to regulate a subset of genes by histone acetylation and histone switching (Frank et al., 2003; Martinato et al., 2008).

TIP48 and TIP49 were revealed as essential cofactors for c-Myc dependent transformation in human cell lines (Wood et al., 2000). Although it is now evident that the entire TIP60 complex is recruited to promoters by c-Myc, this early report elucidated interactions between hTIP48, hTIP49 and c-Myc. TIP48 and TIP49

were shown to interact with the N-terminal domain of c-Myc; this interaction (at least for TIP49) was mediated by Domain II: the novel ATPase insert domain (Wood et al., 2000). Interestingly, cells ectopically expressing a hTIP49^{D302N} Walker B mutant protein were unaffected for growth and apoptosis, but displayed a dominant negative phenotype for c-Myc dependent transformation. The same mutation was lethal when it replaced wild type TIP49 in yeast, supporting the idea that the mutation compromised the catalytic activity of TIP49 (Wood et al., 2000). In another study using hTIP49^{D302N}, TIP49 was shown to be required for c-Myc dependent apoptosis, under serum starved conditions (Dugan et al., 2002). Thus, TIP49 promotes c-Myc dependent transformation or suppresses c-Myc dependent apoptosis under different cellular conditions. These data supported the argument that the activity of TIP49 is critical for transformation, is under tight control, and could therefore be important for developing cancer therapies.

Studies in metazoan model organisms revealed further insights into the relationship between TIP48, TIP49 and c-Myc. In early development of *X. laevis*, c-Myc and Miz-1 form a transcription repressor complex, which in turn, increases cell proliferation (Staller et al., 2001). Individual over-expression of xTIP48 and xTIP49 caused a hyperproliferation phenotype in developing embryos, an effect which was dependent on c-Myc and Miz-1 (Etard et al., 2005). Significantly, these effects were independent of the Wnt signalling pathway. Moreover, N-terminal truncation mutants of xTIP48 and xTIP49, which could not bind c-Myc but did bind β–catenin (and themselves), resulted in a proliferation phenotype similar to reducing endogenous xTIP48 and xTIP49 levels (Etard et al., 2005). Taken together, these data indicate that, with c-Myc and Miz-1, xTIP48 and xTIP49 are co-repressors of proliferation-inhibiting genes.

Studies in *D. melanogaster* revealed that dTIP48, dTIP49 and c-Myc interacted genetically (Bellosta et al., 2005). Like in *X. laevis*, *Drosophila* TIP48, TIP49 and c-Myc were required for proliferation. Interestingly, dTIP49 showed stronger interaction with c-Myc than dTIP48 with c-Myc, although it was unclear whether this was biologically significant. Moreover, c-Myc mutants with heterozygous

TIP48 mutants showed no phenotype, while TIP49 heterozygous mutants did, indicating that the relative levels of TIP48 and TIP49 are important for regulating c-Myc dependent proliferation (Bellosta et al., 2005). Indeed, the authors interpreted that TIP48 exists in complexes both with and without TIP49 (e.g. INO80 complexes contain TIP48 and TIP49, while PcG complexes only contain TIP48 (see relevant sub-sections in section 1.5); ergo, altering the levels of TIP49 alters the balance of TIP48 complexes, resulting in different transcriptional regulation. RNAi screens were used to conclude that gene regulation correlated well between dTIP48 and dTIP49, although regulation of only 11 genes was shared between dTIP48/dTIP49 and c-Myc; the *mfas* promoter was bound by TIP49 and c-Myc to regulate transcription in this system (Bellosta et al., 2005).

It is evident that the cellular roles of c-Myc, TIP48 and TIP49 are tightly linked. However, the effects described above may all be attributed to the recruitment of the TIP60 complex to promoters by c-Myc and its interacting partners. Nevertheless, it is important to delineate the necessity of TIP48 and TIP49 for the correct functioning of c-Myc dependent pathways, and their roles within the TIP60 complex, as elucidating these details could have implications for clinical research.

1.7.4 TIP48 and TIP49 are required for E2F transcriptional activity

Adenovirus protein E1A is an oncogene that operates by de-regulating proliferation and apoptosis (Moran, 1993). E1A drives proliferation or apoptosis by modulating the transcriptional activity of its target proteins, which include the E2F transcription activators: E2F1, E2F2 and E2F3. There is a large overlap between the effects of c-Myc (see above) and E1A oncoproteins. Significantly, E2F1 mRNA transcription is also regulated by c-Myc, which further implies that the oncogenic activities of c-Myc and E1A are linked (Leone et al., 2001). Transcription of E2F target genes is a requirement for progression through the G1/S checkpoint, and thus, proliferation (Wu et al., 2001). The tumour

suppressor protein, Rb (retinoblastoma protein), regulates the transcription of E2F1 dependent genes by binding and suppressing E2F1; E1A deregulates this repression by sequestering Rb (Moran, 1993). Importantly, E1A can also induce apoptosis via E2F1, p53 and other pathways (Moran, 1993).

Human TIP49 was shown to associate with E2F1 *in vivo* (Dugan et al., 2002). As with c-Myc (see above), over-expression of a dominant negative mutant, hTIP49^{D302N}, reduced oncogenic potential of E1A and, under serum starvation conditions, increased E2F1 dependent apoptosis (Dugan et al., 2002). More recently, it was shown that E2F transcription activators recruit the TIP60 HAT complex (including TIP48 and TIP49) to promoters, and that this recruitment is necessary for acetylation of Histone H4 (and partially for H3). This recruitment of HAT complexes to promoters led to an increase in transcription of E2F target genes and was necessary for E2F dependent cell cycle progression (Taubert et al., 2004). Interestingly, TIP48 and TIP49 were also detected at E2F target promoters independent of the TIP60 complex (Taubert et al., 2004), implying that they regulate E2F target genes as part of various distinct chromatin remodelling complexes. It would be interesting to investigate the composition of these TIP48 and TIP49 containing complexes, and the interactions required to target distinct chromatin remodelling complexes to E2F target promoters under specific cellular stimuli.

1.7.5 Interactions of TIP48 with ATF2

Activating transcription factor 2 (ATF2) is a transcription factor and HAT which regulates the cellular response to stress (Kawasaki et al., 2000). ATF2 forms homodimers and heterodimers (predominantly with c-Jun), which regulate genes involved in transformation and DNA damage dependent apoptosis (Kawasaki et al., 2000). The C-terminal domain of hTIP48 was shown to interact with hATF2 in a yeast two hybrid screen (Cho et al., 2001). Consequently, TIP48 was shown to repress the transcriptional activity of ATF2 in a c-Myc and β-catenin independent manner, presumably by direct association with ATF2. ATF2 phosphorylation

regulates its transcriptional activation, and phosphorylated ATF2 bound TIP48 more strongly, which correlated with TIP48 mediated repression of ATF2 activity (Cho et al., 2001). The authors proposed a mechanism where TIP48 either alters the HAT activity of ATF2, or blocks interactions between ATF2 and co-activators of ATF transcription. This interaction of TIP48 with ATF2 would therefore function as an extra level of control of ATF2 dependent transcription, and could potentially channel the cell stress response towards different pathways. Strikingly, TIP49 did not bind to ATF2, nor did it elicit any regulation of ATF2 dependent transcription *in vivo* (Cho et al., 2001). Thus, the relative levels of ATF2 and TIP48, but not TIP49, serve to control the response of cells to stress. This mechanism may define an important step in the progression of cancer, although further investigation into the molecular role of TIP48, in this system, needs to be elucidated.

1.7.6 TIP48 and TIP49 are necessary for Telomerase activity

An unexpected recent insight into how TIP48 and TIP49 may be important for cancer progression and metastasis was revealed when TIP48 and TIP49 were shown to be essential for telomerase activity. Mature telomerase is essential for the extension of telomeres *in vivo*, which are synthesised to protect the ends of chromosomes and are critical in cell senescence, longevity, and cancer progression. Telomerase complexes comprise of TERT, the reverse transcriptase component; TERC, the RNA component; and Dyskerin, which specifically binds the H/ACA motif found in TERC. Recently, hTIP48 and hTIP49 were shown to directly interact with TERT and Dyskerin, but not TERC (Venteicher et al., 2008). Interestingly, TIP48 and TIP49 were shown to be essential for mature telomerase accumulation and associated with TERC during S phase (Venteicher et al., 2008). Moreover, the ATPase activity of TIP49 was required for telomerase activity. Most significantly, TIP48 and TIP49 were also shown to associate with a pool of telomerase complexes which did not display high activity *in vitro*; this led the authors to conclude that TIP48 and TIP49 are required for restructuring a pre-telomerase complex into a mature telomerase complex by recruiting TERT or

other factors to Dyskerin/TERC or by remodelling the complex (Baek, 2008; Venteicher et al., 2008). Alternatively, TIP48 and TIP49 could be associated with mature telomerase which does not display activity *in vitro*. Another alternative explanation is that TIP48 and TIP49 synergistically repress the activity of the telomerase complex, until it is in its mature configuration. These findings suggest TIP48 and TIP49 could be targets for cancer therapy as they are necessary for the activity of the telomerase complex.

1.7.7 Post Translational Modification of TIP48 and TIP49

Post translational modification (PTM) of proteins is a major method of regulating their activity, sub-cellular localisation and interactions with other cellular factors. Modifications of TIP48 and TIP49 have been demonstrated *in vivo* and the significance of these will be outlined below (also see Figure 1.8).

TIP48 and TIP49 are SUMOylated by Ubc9 *in vivo* (see section 1.4.1). TIP48 is SUMOylated on lysine K456 (Kim et al., 2006), while SUMO is conjugated to K225 of TIP49 (Kim et al., 2007). It is interesting that the SUMO modification is at the periphery of Domain III in TIP48, but in a random coil region of Domain II for TIP49. This suggests that the SUMO modification has separate functions in TIP48 and TIP49. For both TIP48 and TIP49, SUMO modification resulted in nuclear localisation. Interestingly, the N-terminally SUMO tagged TIP48 or TIP49 was sufficient for nuclear localisation, indicating that localisation was due to the presence of the modification, and not its location of it on the protein. Intriguingly only 5 % of endogenous TIP48 and TIP49 are SUMOylated *in vivo*, while over a third of the proteins localise in the nucleus (discussed in section 1.4.1). The SUMOylation of TIP48 may increase its interactions with HDAC1, and result in transcriptional repression (as seen with KAI1). SUMOylation of TIP49 did not affect interactions with TIP48, but may increase interactions with β-catenin. In either case, ablating the SUMOylation of TIP48 or TIP49 greatly reduced the metastatic potential of cancer cell lines, which are likely due to modulated transcriptional regulation (Kim et al., 2006; Kim et al., 2007).

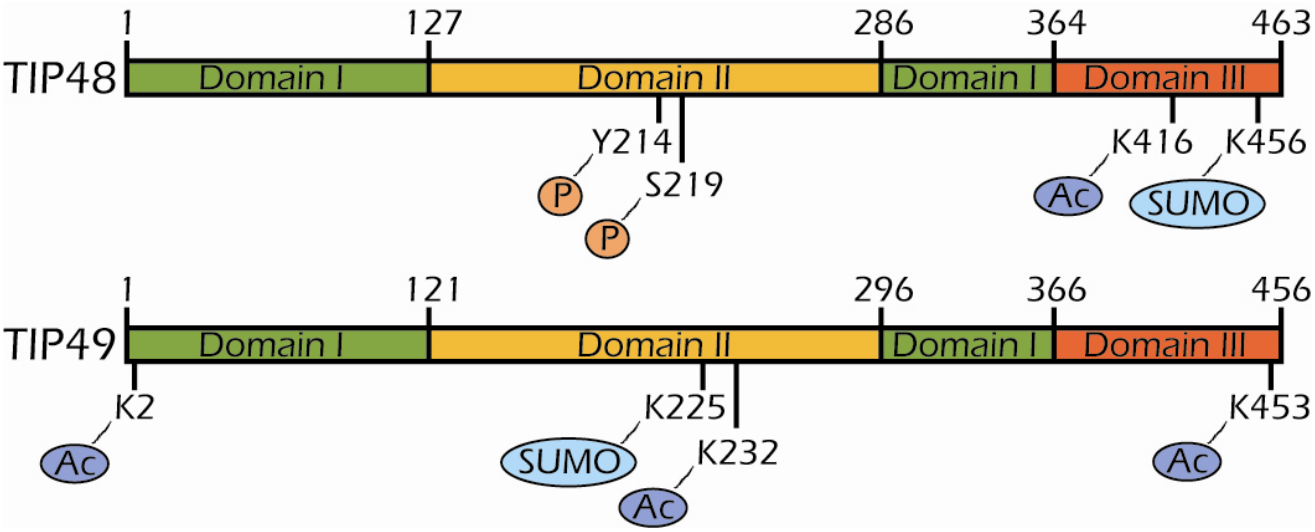

Figure 1.8. Post translational modification (PTM) of hTIP48 and hTIP49. A schematic depicting the domain structure of human TIP48 and TIP49 is shown. Sites which are reportedly modified are annotated. Modifications include phosphorylation (P), acetylation (Ac) and SUMOylation (SUMO).

In a global analysis of proteins phosphorylated by ATM and ATR, TIP48, but not TIP49, was identified as a substrate. TIP48 is phosphorylated on serine S219 (in Domain II) in response to DNA damage (Matsuoka et al., 2007). It would be interesting to investigate the significance of this modification, how it relates to the function of TIP48 and the connotations of detecting phosphorylated TIP48, but not TIP49. The Phosphosite PTM database (www.phosphosite.org), in which data on global PTM studies is deposited, contains information on further modifications of TIP48 and TIP49. TIP48 was reportedly acetylated on lysine K416, and phosphorylated on tyrosine Y214 .TIP49 was reportedly acetylated on lysines K2, K232 & K453. Of particular interest is that acetylation sites K416 of TIP48 and K232 of TIP49 correspond with putative nuclear localisation signals: ^{413}RKRK and ^{229}HKKK respectively. In addition to the previously described SUMOylation of TIP48 and TIP49, acetylation at these sites may provide a further mechanism by which sub-cellular localisation is modulated by PTM.

Evidently, the modification of TIP48 and TIP49 is a complex and temporal process. It would be interesting to study the management of different modifications and how they impact on the structure and function of TIP48 and TIP49.

1.7.8 Links with DNA damage repair

The onset of cancer is tightly linked with DNA damage and its subsequent repair, or channelling cells into apoptotic pathways. Various lines of evidence have converged to implicate TIP48 and TIP49 as important co-factors in the DNA damage response.

Direct evidence for the involvement of TIP48 and TIP49 in the DNA damage response is their inclusion in several chromatin remodelling complexes (see the relevant sections in Chapter 1.5 for more details). INO80 and TIP60 protein complexes have both been implicated in non-homologous end joining (NHEJ) and homologous recombination (HR) dependent repair of DNA double strand

breaks (DSBs). In addition, transcriptional regulation by these protein complexes is also likely to impact on the DNA damage response.

The role of TIP48 and TIP49 in DSB repair was further studied in PC-3 human prostate cancer cells. TIP49 levels were depleted using RNAi and the accumulation of Rad51 was monitored at DSB loci (Gospodinov et al., 2009). Rad51 is involved in HR by facilitating strand invasion, and accumulates in DNA repair loci after IR (Ionising Radiation) or MMS (methyl methanesulfonate) treatment of cells. Depletion of TIP49 reduced the number of Rad51 foci 50 % compared with control experiments (Gospodinov et al., 2009); this was also the case when TIP48 was depleted. HDAC inhibitors rescued this phenotype, suggesting that TIP48 and TIP49 are critical for the correct functioning of HATs (presumably TIP60) in the DNA damage repair (Gospodinov et al., 2009). This is supported by evidence that siRNA against either TIP48, TIP49 or TIP60 resulted in the abnormal accumulation of γH2AX in human cancer derived cell lined (Jha et al., 2008; Ni et al., 2009). This was attributed to a defect in histone H4 acetylation at sites of DNA damage, resulting in reduced de-phosphorylation of γH2AX, rather than a transcriptional or DNA damage signalling defect (Jha et al., 2008). It was also suggested that RPAP3 negatively regulates TIP48 in this pathway, although this has yet to be demonstrated (Ni et al., 2009).

Interestingly, TIP48 but not TIP49, was phosphorylated by the ATM/ATR kinases in response to DNA damage (Matsuoka et al., 2007). This implies that some property of TIP48 is regulated in response to DSBs. Discerning what particular attribute of TIP48 is modulated by phosphorylation could give important insights into its molecular functions and cellular roles.

1.8 Proposed functions for TIP48 and TIP49 *in vivo*

There is conflicting evidence about the biological roles of TIP48 and TIP49 in the literature; both in the nature of how TIP48 and TIP49 are involved in disparate fundamental processes (transcriptional regulation, chromatin remodelling,

telomere extension, rRNA biogenesis and cyto-skeletal dynamics) and whether they carry out different functions in different eukaryotic species. TIP48 and TIP49 also work either synergistically or antagonistically depending on the molecular process. Taking together all of the evidence and observations from primary research, one can deduce several possibilities for the molecular mechanisms of TIP48 and TIP49 *in vivo*, which are not necessarily mutually exclusive:

- TIP48 and TIP49 are *bona fide* DNA or RNA helicases, and function during processes such as transcription, rRNA biogenesis and telomerase activity
- TIP48 and TIP49 modulate protein-DNA or protein-RNA interactions, potentially during the assembly of chromatin remodelling complexes, snoRNPs and the telomerase complex
- TIP48 and TIP49 may recruit protein complexes to DNA, RNA or nucleosomes in a concerted fashion. Protein complexes may include the transcription machinery, chromatin remodelling complexes, snoRNPs and the telomerase complex
- TIP48 and TIP49 could remodel protein-protein interactions within complexes or recruit specific proteins to their respective complexes under the correct conditions. Candidate complexes are all of those already mentioned above, as well as components of the mitotic spindle and primary cilium
- TIP48 and TIP49 could synergistically repress the activities of certain protein complexes until they are correctly assembled. These observations are supported by work carried out with INO80, the telomerase complex and snoRNPs.

1.9 Project Outline

After consideration of all of the research on the various homologues of TIP48 and TIP49, the aims of this thesis were to investigate the aspects of hTIP48 and hTIP49 as follows:

I. To purify recombinant TIP48, TIP49 and their complex for *in vitro* characterisation of their biophysical properties and ATPase activity

II. To study the oligomerisation of TIP48, TIP49 and their complex and how the oligomers are regulated, including formation of sub-complexes

III. To generate mutants of TIP48 and TIP49 in order to address how the novel Walker A – Walker B insertion Domain II affects the ATPase activity and oligomerisation of the individual proteins and heteromeric complexes

IV. To study the ATPase activity of TIP48 and TIP49 in the presence of some of their core interacting partners, to better understand the molecular mechanisms of their activity

V. To study the *in vivo* sub-cellular localisation of TIP48 and TIP49, and establish whether they work together or have separate roles at different stages of the cell cycle

VI. To study the possibility of post-translational modification of TIP48 or TIP49 as means of regulating their activity or oligomerisation

Chapter 2

Materials & Methods

2.1 Chemicals, Materials & Reagents

All chemicals and reagents were supplied by BD Biosciences, Bio-Rad, Fisher Scientific, Sigma-Aldrich or VWR International unless stated otherwise.

2.2 Enzymes

Restriction and other DNA modifying enzymes were provided by New England Biolaboratories. Enzymes for polymerase chain reactions were supplied along with kits: Phusion SDM Kit (Finnzymes), pGEM T-Easy Easy Kit (Promega), or ExTaq (TaKaRa Bio).

2.3 Tools for Protein Purification

Resins and pre-packed columns used for protein chromatography were as follows:

Hi-Trap DEAE Heparin columns (GE Healthcare),
Hi-Trap Heparin columns (GE Healthcare),
Hi-Trap Protein A columns (GE Healthcare),
Hi-Trap Q Sepharose Heparin columns (GE Healthcare),
Hi-Trap SP Sepharose Heparin columns (GE Healthcare),
Hydroxylapatite resin (Bio-Rad),
Mono Q 1ml FPLC (GE Healthcare),
NHS activated columns (GE Healthcare),
ssDNA cellulose (Sigma-Aldrich),
Superdex 200 HR FPLC (GE Healthcare),
Superose 6 HR FPLC (GE Healthcare),
Talon resin (Clontech).

2.4 Plasmid DNA techniques

2.4.1 Isolation of Plasmid DNA from Bacteria

Isolation of plasmid DNA was performed using QIAGen Plasmid Miniprep or Midiprep kits according to the manufacturer's instructions. DNA was eluted with TE buffer (10 mM Tris pH 7.5, 1 mM EDTA) or water.

2.4.2 Determination of DNA Concentration

DNA concentration was measured on a Nanodrop ND-1000 (Thermo Scientific), TE Buffer was used as a blank measurement. 2 µl of blank or sample was loaded onto the pedestal; the absorbance at 260 nm was measured and used to calculate the DNA concentration.

2.4.3 Restriction digest analysis of plasmid DNA

Restriction digests were carried out with enzymes from NEB (New England Biolabs). Digestion reactions were performed as recommended by NEB, using 50 – 100 µg of DNA in 10 µl reactions (10 enzyme units/reaction, 1 x NEBuffer, 0.1 mg/ml BSA) with totals made to 10 µl with water. Reactions were incubated for 1 hr at 37 ˚C then analysed by 1 % agarose gel electrophoresis to confirm the size of fragments.

2.4.4 Agarose gel electrophoresis and gel extraction of plasmid DNA

1 % agarose solutions were made in TAE Buffer (40 mM Tris, 20 mM glacial acetic acid, 1 mM EDTA) with 0.5 µg/ml ethidium bromide, heated in a microwave, then cast in horizontal tanks. Gels were placed in electrophoresis tanks, then submerged in TAE Buffer. Samples were loaded into wells after mixing 4:1 with DNA Loading buffer (50 mM EDTA, 45 % glycerol, 0.25 %

bromophenol blue; bromophenol blue was omitted when fluorescently labelled DNA was used). O-Gene 1000 bp markers (Helena Biosciences) were loaded into one or more lanes and the gel was run at 7 V/cm for 45 - 90 minutes. DNA in the gels was visualised in a Gene Genius imaging system using low wavelength UV light.

DNA was electrophoresed in 1% agarose gels supplemented with 0.5 µg/ml ethidium bromide and the sizes of required bands were estimated using molecular standards. Low wavelength UV light was used to observe the DNA and a section containing DNA of the correct length was excised from the gel, using a clean scalpel. The DNA was purified from the gel and other contaminants using a gel purification kit (QIAGen mini spin columns), following the manufacturer's instructions.

2.4.5 CIP treatment and ligation of plasmid DNA

CIP was added to reactions to a final concentration of 0.5 units per µg DNA and the reaction incubated for 30 mins at 37 °C.

Ligations were performed with 10 – 50 µg of insert DNA. Vector DNA was added so that the insert:vector ratio was 3:1 in 10 µl reactions using T4 DNA ligase (2 units/µl) in 1 x T4 DNA ligation buffer. Reactions were incubated overnight at 4 ˚C or for 1 hour at room temperature.

2.5 Plasmid Construct Generation

2.5.1 Standard plasmids

The standard plasmids used for cloning and recombinant protein expression were pGEM T-Easy (Promega), pET15b+ and pET21b+ (Novagen). After amplification by polymerase chain reaction (PCR), coding sequences (CDSs), were cloned into pGEM T-Easy, then subcloned into pET15b or pET21b expression plasmids. The CDS was cloned into pET15b+ to produce

recombinant proteins with an N-terminal hexa-Histidine (His_6-) tag in *E. coli* expression strains. The CDS was cloned into pET21b+ to express non-tagged (with a stop codon) or C-Terminal hexa-Histidine taged (-His_6) protein in *E. coli* expression strains.

2.5.2 Initial Expression Plasmids

A list of plasmids provided by Dr. Tsaneva, which were used for recombinant protein expression or as templates to generate mutant protein expression plasmids, is shown in Table 2.1.

2.5.3 Polymerase Chain Reaction

PCR were performed in 50 µl volumes in 0.5 ml eppendorf tubes. Reactions consisted of template DNA (10 - 500 pg), forward and reverse primers (normally 0.5 µM), deoxynucleotide triphosphates (dNTPs), DNA polymerase and the buffer conditions recommended by the manufacturers. Reactions were mixed then placed in a Techne Progene PCR machine and subjected to rounds of amplification, which generally include a detaturation stage, primer annealing stage and extension stage. Individual primers and PCR conditions are described in Table 2.2.

2.5.4 Mutagenesis of TIP48 and TIP49 expression plasmids

A list of mutations introduced into the amino acid sequences of TIP48 and TIP49 is given in Table 2.3. Expression plasmids for mutants of TIP48 and TIP49 were obtained by using a Phusion SDM Kit (Finnzymes). PCR amplification was carried out according to the manufacturer's instructions using primers with 5' Phosphate modifications. Conditions and primers for individual PCR amplification are detailed in Table 2.2. Successful amplification by PCR was confirmed by analysis of products using 1 % agarose electrophoresis the product was then ligated into the plasmid vector and transformed into competent DH5α *E. coli*.

#	Plasmid	Tag	Selection	Expression Strain	Restriction Digest	Source
(1)	**pET21-TIP48**	C-Term His_6	Amp^r	BL21-Gold (DE3)	*Nde* I and *Xho* I	Dr. Tsaneva [#214]
(2)	**pET15-TIP49**	N-Term His_6	Amp^r	BL21-Gold (DE3)	*Nde* I and *Xho* I	Dr. Tsaneva [#261]
(3)	**pET21-TIP49**	C-Term His_6	Amp^r	BL21-Gold (DE3)	*Nde* I and *Kpn* I	Dr. Tsaneva [#263]
(4)	**pET21-BAF53**	C-Term His_6	Amp^r	BL21-Gold (DE3) or Origami (DE3)	*Nde* I and *Xho* I	Dr. Tsaneva [#298]
(5)	**pET30-β-catenin**	C-Term His_6	Kan^r	BL21-Gold (DE3)	unknown	Prof. Pearl [#320]

Table 2.1. A list of the initial plasmids used in this study. In the first column, the numbers in round brackets refer to the plasmid annotation in this thesis. The numbers in square brackets refer to the location of the plasmid in the laboratory's glycerol stock collection at -80 ºC.

Template	Product (· = Stop codon)	#	(5' – 3') Primer Sequences (★ = phosphate)	Anneal Temp. (°C)	Ext. Time (min)	Cycles
(1) pET21-TIP48-His_6	**(6)** pET21-Δ^1TIP48-His_6	IT503 IT504	★CCTGGAGTGCTGTTCATCGAC ★CTGGATCTCCACCTCCC	67	7	25
(1) pET21-TIP48-His_6	**(7)** pET21-Δ^2TIP48-His_6	IT513 IT514	★GTGCAGTGCACACCGTGTCCCT ★CTGCCTTGATGCGAACGCCGATG	67	10	30
(1) pET21-TIP48-His_6	TIP48·	IP522 [*sic*] IT523	ctggtcatccagcggatagttaatg tggtggatcctcaggatccTCAGGAGGTGTCAATG	67	5	30
(7) pET21-Δ^2TIP48-His_6	Δ^2TIP48·	IP522 [*sic*] IT523	ctggtcatccagcggatagttaatg tggtggatcctcaggatccTCAGGAGGTGTCAATG	67	5	35
(1) pET21-TIP48-His_6	**(16)** pET21-***lik***TIP48-His_6	lik48F lik48R	★GCAGAGACGTGATCACCATCGACAAGG ★AGAACCCGGCCTGGACCTTGTC	n/a	n/a	n/a
(3) pET21-TIP49-His_6	**(15)** pET21-Δ^2TIP49-His_6	IT509 IT510	★GTGCGATCCAAGATGTGACCTTGCAT ★CCGCCTTTCGCAGCCCAATG	67	7	30
(2) pET15-His_6-TIP49	**(8)** pET15-$\Delta^1$$His_6$-TIP49	IT505 IT506	★GGTGTGCTGTTTGTTGATGAGGTC ★CGGAGTTAGCTCTGTGACTTCACC	65	10	25
(2) pET15-His_6-TIP49	**(9)** pET15-$\Delta^2$$His_6$-TIP49	IT509 IT510	★GTGCGATCCAAGATGTGACCTTGCAT ★CCGCCTTTCGCAGCCCAATG	67	7	30
(2) pET15-His_6-TIP49	**(10)** pET15-$\Delta^3$$His_6$-TIP49	IT509 IT512	★GTGCGATCCAAGATGTGACCTTGCAT ★CCGCCTTGGTCTCCTTTATTCGCA	67	7	30
(2) pET15-His_6-TIP49	**(11)** pET15-$\Delta^4$$His_6$-TIP49	IT510 IT511	★CCGCCTTTCGCAGCCCAATG ★GTGCGAAAGAAATCATCCAAGATGTGACC	67	7	30
(2) pET15-His_6-TIP49	**(12)** pET15-$\Delta^5$$His_6$-TIP49	IT511 IT512	★GTGCGAAAGAAATCATCCAAGATGTGACC ★CCGCCTTGGTCTCCTTTATTCGCA	67	7	30
(2) pET15-His_6-TIP49	**(17)** pET15-***lik***His_6-TIP49	lik49F lik49R	★GCAGAGATGTGATTTACATTGAAGCCAACAGTG ★AGAATCCAGCTTCTACTCGCTCTTTCTGC	67	9	30
Human cDNA	Hint1 CdS	IT501 IT502	gagatcatATGGGCAGATGAGATTGCC gagaggatccTTAACCAGGAGGCCATTGC	65	1	30

Table 2.2. Primers and PCR conditions used for mutagenesis and cloning. The numbers in parentheses refer to the plasmid annotation in this thesis. Primer numbers (#) and sequences are shown. Non coding regions are shown in lower case letters; coding sequences are shown in upper case letters. Mutations introduced by PCR are shown in light green. Restriction enzyme sites are shown in red. Stop codons are shown in dark blue. Start codons are highlighted in dark green. Primers with 5' phosphate modifications are also depicted (★).

Protein	Mutation
Δ^{1}TIP48	Deleted I^{147} – I^{293}
Δ^{2}TIP48	Replaced E^{133} – V^{238} with AGA
*lik*TIP48	Inserted FCR after G^{193}
Δ^{1}TIP49	Deleted C^{141} – P^{296}
Δ^{2}TIP49	Replaced E^{126} – I^{234} with AGA
Δ^{3}TIP49	Replaced E^{129} – I^{234} with AGA
Δ^{4}TIP49	Replaced E^{126} – K^{231} with AGA
Δ^{5}TIP49	Replaced E^{129} – K^{231} with AGA
*lik*TIP49	Inserted FCR after G^{191}

Table 2.3. A list of mutated recombinant proteins generated for this thesis.

For the *lik*TIP48 mutation, PCR amplification using the Phusion SDM kit was attempted under various conditions, but was unsuccessful. Mutagenic primers (lik48F and lik48R – see Table 2.2) were used in conjunction with the full length primers (IT115 with likTIP48R and IT119 with likTIP48F – see below). These were designed to amplify two sections of the CDS in two separate PCR reactions, while introducing the *lik* mutation. The primers were designed to incorporate a 9 bp insertion at the 5' ends that corresponded to the *lik* mutation. Phusion DNA polymerase was used to amplify the two regions as outlined below:

start

IT115 - 5' ATATCTCGAGCATATGGCAACCGTTACAGCC-3'

***Xho* I** ***Nde* I**

IT119 - 5' ATATGAATCTCGAGGGAGGTGTCCATGGTCTCGCC-3'

Anneal. Temp. 67 °C Extension Time 2 mins, 30 cycles

The two products were ligated with T4 DNA ligase, then purified with a PCR purification kit (QIAGen mini spin columns). A final PCR step, using primers for full length TIP48 (IT115 and IT119), using ExTaq DNA polymerase (Takara) under the conditions above, resulted in a full length *lik*TIP48 PCR product. This was electrophoresed on a 1 % agarose gel, the 1.5 kbp fragment was excised and gel purified, then ligated into a pGEM vector. DH5α *E. coli* were transformed with the ligation product and colonies selected using blue-white screening, (ampicillin) antibiotic selection and restriction analysis. After verifying the sequence of the *lik*TIP48 CDS in pGEM, it was digested using *Nde* I and *Sac* I and ligated into pET21-TIP48-His_6 **(1)** which had been digested with *Nde* I and *Sac* I and CIP treated prior to the ligation. This resulted in a pET21-*lik*TIP48-His_6 **(16)** expression plasmid.

2.5.5 Generation of the dual pET21-TIP48/TIP49-His$_6$ expression plasmid

The pET21-TIP48/TIP49-His$_6$ **(18)** plasmid was engineered so that expression of each of the two sequences was controlled by separate T7 promoters (Figure 2.1). To generate the construct, pET21-TIP48-His$_6$ **(1)** was amplified using primers which would introduce a stop codon and a *Bam* HI site at the end of the CDS (Table 2.2). This resulted in a CDS where TIP48 would be expressed without a tag. The PCR product was then analysed by 1 % agarose electrophoresis, then cleaved in a double restriction digest with *Mlu* I and *Bam* HI, then further purified using a PCR purification kit (QIAGen). At the same time, pET21-TIP49-His$_6$ **(3)** was double digested with *Bgl* II and *Mlu* I, then digested with CIP, and finally, purified using the PCR purification kit. The resulting DNA fragments were ligated and transformed into DH5α *E. coli*, then screened for the correct inserts using *Kpn* I and *Nde* I. DNA sequencing using internal primers (Table 2.4) was used to confirm the correct coding sequences were present.

2.5.6 Generation of Δ^2 mutants of dual pET21-TIP48/TIP49-His$_6$ expression plasmid

The cloning strategy used for generating the pET21-TIP48/TIP49-His$_6$ **(18)** expression plasmid was repeated with plasmids **(1), (3)**, **(7),** and **(15)** (see Table 2.5) in the correct combinations to obtain expression constructs pET21-Δ^2TIP48/TIP49-His$_6$ **(19)**, pET21-TIP48/Δ^2TIP49-His$_6$ **(20)** and pET21-Δ^2TIP48/Δ^2TIP49-His$_6$ **(21)**.

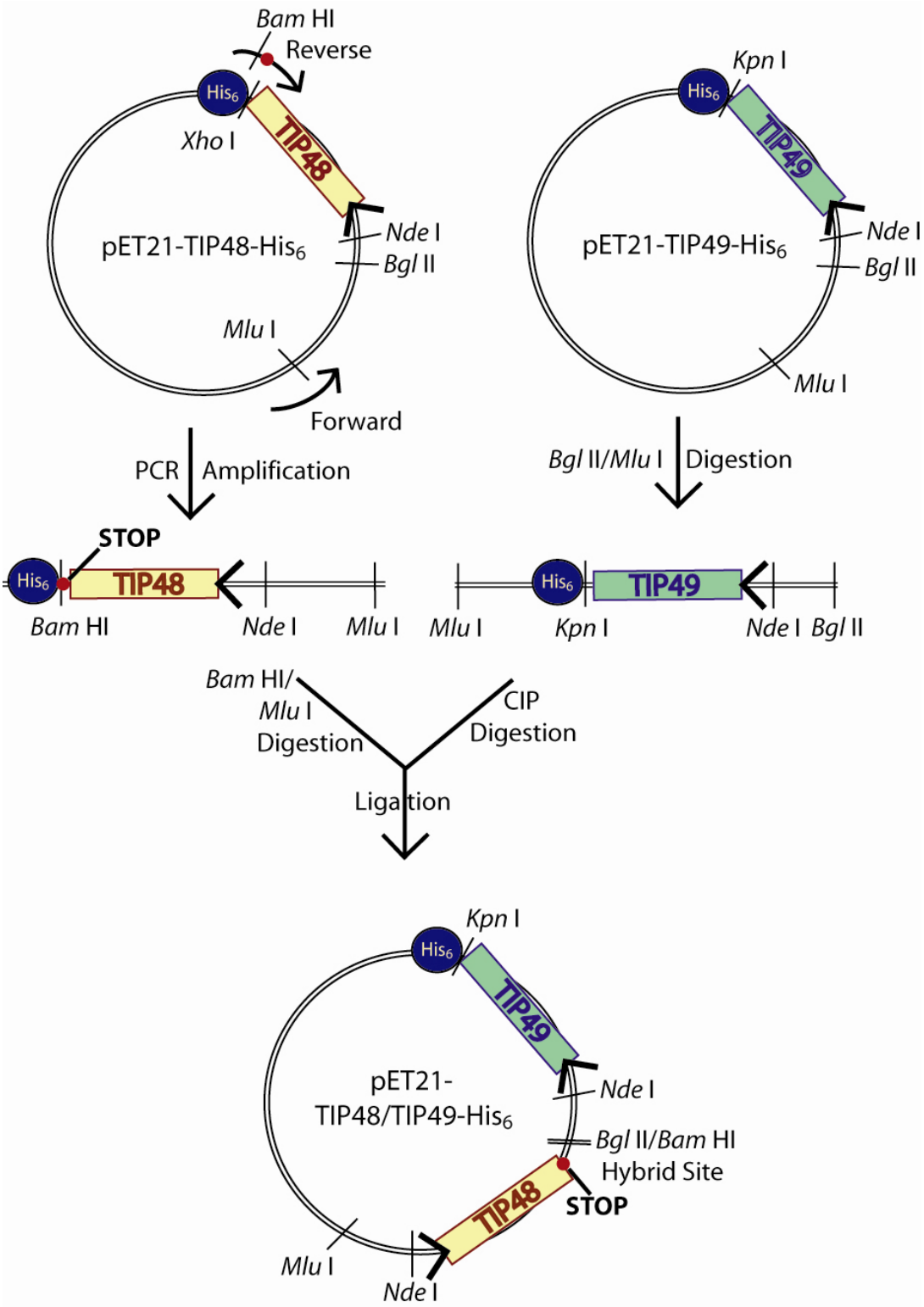

Figure 2.1. A schematic representation of the cloning strategy used to generate the pET21-TIP48/TIP49-His$_6$ dual expression plasmid, and related plasmids.

2.5.7 Generation of pET15-His$_6$-Hint1

The human Hint1 CDS was PCR amplified from a human testis cDNA library using a Failsafe PCR kit (Epicentre Biotechnologies) according to the manufacturer's instructions (1 µM of each primer and 0.1 µl of testis cDNA were used per reaction). Primers were designed to introduce *Nde* I and *Bam* HI restriction sites into the 5' and 3' ends respectively. (For primers and PCR conditions, see Table 2.2). 5 µl of the Hint1 PCR product was electrophoresed on a 1 % agarose gel to assess the size (~ 380 bp). A PCR purification kit (QIAGen mini spin columns) was used to obtain purified PCR product from the reaction, which was ligated into a pGEM T-Easy vector using T4 DNA ligase. The ligation reaction was transformed into DH5α *E. coli*. Blue-white screening, (ampicillin) antibiotic selection and restriction analysis were used to select a pGEM plasmid with an insert of the correct size. The Hint1 sequence was confirmed by sequence analysis, then double restriction digested with *Nde* I and *Bam* HI and ligated into the pET21b+ and pET15b+ T7 expression vectors (double restriction digested with *Nde* I and *Bam* HI) using T4 DNA ligase.

2.5.8 Sequencing

All sequencing was performed by the sequencing service in Wolfson Institute for Biomedical Research (UCL, London) or EuroFins MWG Operon (in Germany, formerly MWG Biotech). DNA was sent in water or Tris-HCl pH8 at the required concentration. As well as standard T7, SP6 or T7 Terminator primers, internal primers were also used for sequencing (Table 2.4)

2.5.9 List of Expression Plasmids used

The final list of expression plasmids used for subsequent recombinant protein expression is given in Table 2.5.

Template	Sequence from	#	(5' – 3') Primer Sequences
TIP48	~500 bp Forward	IT275	CACAGAGATGGAGACCAT
TIP48	~100 bp Forward	IT525	CTGGACGATGCCTTGGAG
TIP48	~800 bp Forward	IT265A	GGAGATCAAGTCAGAAGTCCG
TIP48	~900 bp Reverse	IT277	GATGAACAGCACTCCAGG
TIP48	~1000 bp Reverse	IT276	ACGGTTGGTGGCCATGAT
TIP48	~600 bp Reverse	IT266	CCTTGTCGATGGTGATCA
TIP49	~400 bp Forward	IT261A	GGTGAAGTCACAGAGCTAACTC
TIP49	~800 bp Reverse	IT262A	CAAAGAAGACAGAAATCACAGAC
TIP49	~600 bp Reverse	IT263	TCACATCTCCAGCTTCTA
TIP49	~250 bp Forward	IT524	GTGGCGTCATAGTAGAATTAATC
TIP49	~1100 bp Reverse	IT526	GTCCTCAGTGCCTCTGATG

Table 2.4. A list of primers used for internal sequencing of TIP48 and TIP49.

#	Plasmid	Tag	Selection	Expression Strain	Restriction Digest	Source [# Glycerol Stock]
(1)	**pET21-TIP48**	C-Term His_6	Amp^r	BL21-Gold (DE3)	*Nde* I and *Xho* I	Dr. Tsaneva [#214]
(2)	**pET15-TIP49**	N-Term His_6	Amp^r	BL21-Gold (DE3)	*Nde* I and *Xho* I	Dr. Tsaneva [#261]
(3)	**pET21-TIP49**	C-Term His_6	Amp^r	BL21-Gold (DE3)	*Nde* I and *Kpn* I	Dr. Tsaneva [#263]
(4)	**pET21-BAF53**	C-Term His_6	Amp^r	BL21-Gold (DE3) or Origami (DE3)	*Nde* I and *Xho* I	Dr. Tsaneva [#286]
(5)	**pET30-β-catenin**	C-Term His_6	Kan^r	BL21-Gold (DE3)		Prof. Pearl [#320]
(6)	**pET21-Δ^1TIP48**	C-Term His_6	Amp^r	BL21-Gold (DE3)	*Nde* I and *Xho* I	PCR of **(1)**
(7)	**pET21-Δ^2TIP48**	C-Term His_6	Amp^r	BL21-Gold (DE3)	*Nde* I and *Xho* I	PCR of **(1)** [#472]
(8)	**pET21-Δ^1TIP49**	N-Term His_6	Amp^r	BL21-Gold (DE3)	*Nde* I and *Xho* I	PCR of **(2)**
(9)	**pET21-Δ^2TIP49**	N-Term His_6	Amp^r	BL21-Gold (DE3)	*Nde* I and *Xho* I	PCR of **(2)** [#473]
(10)	**pET21-Δ^3TIP49**	N-Term His_6	Amp^r	BL21-Gold (DE3)	*Nde* I and *Xho* I	PCR of **(2)**
(11)	**pET21-Δ^4TIP49**	N-Term His_6	Amp^r	BL21-Gold (DE3)	*Nde* I and *Xho* I	PCR of **(2)**
(12)	**pET21-Δ^5TIP49**	N-Term His_6	Amp^r	BL21-Gold (DE3)	*Nde* I and *Xho* I	PCR of **(2)**
(13)	**pET21-TIP48**	No Tag	Amp^r	BL21-Gold (DE3)	*Nde* I and *Bam* HI	PCR of **(1)**
(14)	**pET21-Δ^2TIP48**	No Tag	Amp^r	BL21-Gold (DE3)	*Nde* I and *Bam* HI	PCR of **(7)**
(15)	**pET21- Δ^2TIP49**	C-Term His_6	Amp^r	BL21-Gold (DE3)	*Nde* I and *Kpn* I	PCR of **(3)**
(16)	**pET21-*lik*TIP48**	C-Term His_6	Amp^r	Rosetta II (DE3)	*Nde* I and *Xho* I	PCR of **(1)** [#471]
(17)	**pET15-*lik*TIP49**	N-Term His_6	Amp^r	Rosetta II (DE3)	*Nde* I and *Xho* I	PCR of **(2)** [#402]
(18)	**pET21-TIP48/TIP49**	TIP48 No Tag TIP49 C His_6	Amp^r	Rosetta II (DE3)	*Nde* I, *Bam* HI and *Kpn* I	Using **(13)** and **(3)** [#492]
(19)	**pET21- Δ^2TIP48/TIP49**	TIP48 No Tag TIP49 C His_6	Amp^r	Rosetta II (DE3)	*Nde* I, *Bam* HI and *Kpn* I	Using **(14)** and **(3)** [#494]
(20)	**pET21-TIP48/ Δ^2TIP49**	TIP48 No Tag TIP49 C His_6	Amp^r	Rosetta II (DE3)	*Nde* I, *Bam* HI and *Kpn* I	Using **(13)** and **(15)** [#493]
(21)	**pET21- Δ^2TIP48/ Δ^2TIP49**	TIP48 No Tag TIP49 C His_6	Amp^r	Rosetta II (DE3)	*Nde* I, *Bam* HI and *Kpn* I	Using **(14)** and **(15)** [#495]

Table 2.5. Final list of plasmids used in this thesis. The numbers in round brackets refer to the plasmid annotation in this thesis. Numbers in square brackets denote the position of the resulting plasmid in the laboratory's glycerol stock collection, stored at -80 ºC

2.6 Bacterial Techniques

2.6.1 Overnight cultures

Overnight cultures for protein induction or harvesting plasmid DNA were carried out in Luria Broth (LB) (1 % Bacto-Tryptone, 0.5 % Yeast Extract, 1 % NaCl) supplemented with the appropriate antibiotics and 1 % glucose where necessary. Inoculations were performed using sterile plastic culture loops. Cultures were then incubated at 37 °C for 16-20 hours in a shaking incubator.

2.6.2 Generation of competent *E. coli*

For generating competent *E. coli*, bacteria were grown overnight in LB with antibiotic selection where necessary. 1.6 ml of overnight culture was added to 100 ml of fresh LB media and grown for 3 hrs at 37 ˚C to an optical density of 0.6 at 600 nm. The procedure was carried out at 4 ˚C from this point on. Cells were pelleted for 15 mins at 2000 g, re-suspended in 34 ml of chilled Buffer CA (0.1 M MOPS pH 7, 0.1 M RbCl) and pelleted for 2 mins at 2000 g. The pellet was re-suspended in 34 ml of Buffer CB (0.1 M MOPS pH 6.5, 0.1 M RbCl, 0.1 M $CaCl_2$) and incubated for 90 mins, then pelleted for 2 mins at 2000 g. The cells were finally re-suspended in 10 ml of Buffer CB with 10 % glycerol, aliquoted, and stored at -80 ˚C until needed.

2.6.3 Bacterial transformation with plasmid DNA

To transform competent bacteria, 1-100 ng of plasmid DNA was added to 100 µl of competent bacterial cells and incubated on ice for 30 mins. Cells were heat shocked for 25 s at 42 ˚C and incubated on ice for 2 mins. 0.9 ml of warm LB media was added, and the cells were allowed to recover at 37 ˚C for 1 hr in a shaking incubator. 100 µl of cells were then spread onto LB agar plates (1 % Bacto-Tryptone, 0.5 % yeast extract, 0.5 % NaCl, 2 % agar) with appropriate antibiotic selection (and 1 % glucose for *E. coli* expression strains) and incubated at 37 ˚C overnight.

2.6.4 Blue White Screening

For blue-white colony screening, 0.5 mM IPTG was added to the LB agar plates and 100 µl of 10 mg/ml X-Gal was spread on top and air dried for 20 mins before the cells were plated.

2.7 Expression and Purification of Recombinant Proteins

2.7.1 Antibiotic Selection

Amp^r – Ampicillin resistant; used 100 µg/ml for selection.
Tet^r – Tetracycline resistant; used 20 µg/ml for selection.
Cam^r – Chloramphenicol resistant; used 33 µg/ml for selection.
Kan^r – Kanamycin resistant; used 20 µg/ml for selection.

2.7.2 *E. Coli* Strains

E. coli strains used for storage of plasmids and expression of recombinant proteins are outlined in Table 2.6.

	Function	Plasmid	Selection	Company
DH5α	Storage	none	none	Invitrogen
XL1-Blue	Storage	none	Tet^r	Stratagene
BL21-Gold (DE3)	Expression	none	Tet^r	Stratagene
Rosetta II (DE3)	Expression	pRARE	Cam^r	Novagen
Origami (DE3)	Expression	none	Kan^r; Tet^r	Novagen

Table 2.6. A list of strains used for bacterial expression of recombinant proteins.

2.7.3 Over-expression of recombinant proteins in *E. coli*

A single colony of *E. coli* bacteria with the appropriate T7 expression construct was grown in LB Glucose (Luria Broth with 1% Glucose), with the appropriate antibiotic selection. After growth overnight at 37 ˚C, 10 ml of overnight culture was added per 500 ml LB media in a 2 litre conical flask. For individual proteins, the suspension was incubated for ~ 2 ½ hrs, in a shaking incubator (at 37 ˚C, 250 r.p.m.), and grown to an optical density of 0.6 - 0.8 at OD_{600}. IPTG was added to a final concentration of 1 mM, and the suspension was then incubated at 30 ˚C for a further 4 hours. For complexes of TIP48/TIP49-His_6, the above procedure was followed with the following modifications: cell cultures were grown at 30 ˚C to an optical density of 0.6 - 0.8 at $OD_{600,}$ then 0.5 mM IPTG was added; the cultures were then incubated at 20 ˚C for 20-24 hours. In all cases, after induction, the cells were pelleted at 4000 r.p.m. for 15 mins in a SLA - 3000 rotor . The pellets were stored at -20 ˚C for up to one month.

2.7.4 Cell lysis and solubilisation

Cells were thawed on ice and re-suspended in 10 ml of Lysis Buffer per 500 ml of induced cells, supplemented with one EDTA-free protease inhibitor tablet (Roache) per 30 ml of Lysis Buffer (See Table 2.7 for individual Lysis Buffers and conditions). 2 mM $MgCl_2$ was added to the lysis buffer where necessary. Lysozyme was added to the appropriate concentration, and the cells were incubated for 20 minutes on ice; Nonidet P40 was added and the lysate was incubated for a further 10 minutes. The cell lysate was sonicated on power 10, for 15 seconds, thrice. The lysate was clarified in a Ti-70 Rotor for 45 minutes at 42,000 r.p.m. at 4 ˚C, to separate the soluble supernatant and an insoluble pellet. Proteins were monitored throughout the purification using Coomassie stained 12 or 15 % SDS PAGE analysis.

	Lysis Buffer	Lysozyme (mg/ml)	Nonidet P40 (%)
TIP48-His_6	Talon Buffer	0.75	0.5
His_6-TIP49	Talon Buffer	0.75	0.5
TIP48/TIP49-His_6	Talon Buffer	1	0.75
His_6-BAF53	Talon Buffer	1	0.75
His_6-β-catenin	Talon Buffer	0.75	0.25
Hint1 & His_6-Hint1	Talon Buffer with 1 mM $ZnCl_2$	0.75	0.5

Table 2.7. Conditions used for cell lysis of strains expressing recombinant proteins. Talon buffer is 20 mM Tris pH 8, 300 mM NaCl, 10 % Glycerol, 1 mM 2-mercaptoethanol and 1 mM PMSF.

2.7.5 Purification of TIP48-His_6

After cell lysis, the supernatant was loaded onto a 5 - 10 ml Talon metal affinity column (resin from Clontech) equilibrated in Talon Buffer (20 mM Tris pH8, 300 mM NaCl, 10 % Glycerol, 1 mM PMSF, 1 mM 2-Mercaptoethanol). Non-specifically bound protein was washed off with 50 ml Talon Buffer, then 30 ml of Talon Buffer with 20 mM imidazole. The protein was eluted with a 20 - 500 mM imidazole gradient in Talon Buffer, collecting 10 ml fractions over 100 ml.

Fractions containing protein were dialysed against 2 litres of R Buffer (20 mM Tris-HCl pH 8, 100 mM NaCl, 1 mM EDTA, 10 % Glycerol, 1 mM DTT, 1 mM PMSF) overnight at 4 °C. For proteins used in biochemical assays, the dialysed protein was first passed through a ssDNA (single stranded DNA) cellulose column in R Buffer to remove bacterial contaminants. In all cases, for the final purification and concentration step, the protein was loaded onto a 1 ml Mono Q column. The column was washed with 20 ml of R Buffer, then protein was eluted with a 0.1 - 1 M NaCl gradient in R Buffer in ten fractions of 1 ml.

2.7.6 Purification of His_6-TIP49

For TIP49 expression, cell lysis, Talon column chromatography, and ssDNA purification were performed as described above (sections 2.7.3 – 2.7.6). Fractions containing protein were dialysed against Buffer H (20 mM potassium phosphate pH 6.8, 100 mM KCl, 10 % glycerol, 1 mM DTT, 1 mM PMSF) overnight. TIP49 was then loaded onto a 5 ml hydroxylapatite column equilibrated in Buffer H, washed with 50 ml of Buffer H, then eluted with a 10 – 500 mM potassium phosphate gradient in Buffer H collecting ten fractions of 5 ml.

2.7.7 Purification of TIP48/TIP49-His_6 complexes and TIP49-His_6

Expression, lysis and solubilisation were carried out in Talon Buffer as described above (sections 2.7.3 – 2.7.4). Soluble lysate was loaded onto a 5 - 10 ml Talon column. The column was washed extensively with Talon Buffer, then with 30 ml

of 10 mM imidazole in Talon Buffer. TIP48 and TIP49-His_6 co-eluted from the column in a 10-250 mM imidazole gradient in Talon Buffer over ten fractions of 5 ml. Fractions containing protein were dialysed against R Buffer at 4 °C overnight. After dialysis, proteins were passed through an ssDNA cellulose column, then the flow-through fractions were concentrated to 0.5 ml using Amicon Ultra centrifugal filters (Millipore) and loaded onto a Superose 6 HR 10/30 size exclusion chromatography column. 0.5 ml of protein was injected onto the column through a 0.2 µm syringe filter (Millipore) then eluted from the column in R Buffer in 24 fractions of 1 ml. Fraction 1 corresponds to an elution volume of 0.5 - 1.5 ml etc. A complex of TIP48 and TIP49-His_6 with stoichiometrically equal proportions of both proteins eluted in fractions 12 to 15.

Excess TIP49-His_6 monomers eluted in fractions 17 and 18, and were used for experiments which required a C-terminally hexa-Histidine tagged TIP49.

2.7.8 Purification of mutant TIP48, TIP49 and complexes

Expression, solubilisation and purification of Δ^2TIP48-His_6 and His_6-Δ^2TIP49 were as described for the wild type proteins in sections 2.7.3 to 2.7.6. Mutant complexes of TIP48/TIP49-His_6 lacking Domain II were purified as the wild type complex in sections 2.7.3 to 2.7.7.

2.7.9 Purification of His_6-BAF53 under denaturing conditions

BAF53 was expressed in BL21-Gold (DE3) *E. coli* as described in section 2.7.3 and the bacteria were lysed as described in section 2.7.4; the cell lysate was clarified by centrifugation at 15,000 r.p.m. in an SS-34 rotor for 30 mins at 4 °C. The resulting pellet after centrifugation contained all of the recombinant BAF53.

All subsequent procedures using 6 M urea or above were carried out at room temperature; procedures using less than 6 M urea were carried out at 4 °C. The pellet was re-suspended in 20 ml of Talon buffer, supplemented with 8 M urea per litre of original cell culture, using a glass homogeniser. The suspension was

centrifuged in an SS-34 rotor at 15,000 r.p.m. at room temperature. With the resulting pellet, the re-suspension and centrifugation steps were repeated. The two supernatants were pooled and loaded onto a Talon column equilibrated with Talon buffer supplemented with 8 M urea. The purification was completed in one of two ways: 1) The column was washed in decreasing concentrations of urea in Talon buffer (6 M, 4 M, 2 M and 0 M – 5 column volumes of each), then the column was washed with ten column volumes of Talon buffer, and BAF53 was eluted using a 0-500 mM imidazole gradient in ten fractions of 10 ml each. 2) The column was washed in ten column volumes of 8M urea in Talon buffer, then BAF53 was eluted using a 0-500 mM imidazole gradient in Talon buffer with 8 M urea in ten fractions of 5 ml each. Finally BAF53 was dialysed against Talon buffer with successively decreasing concentrations of urea (6 M, 4 M, 2 M, 0 M) for at least 8 hours each.

2.7.10 Purification of His_6-β-catenin

Expression, cell lysis and purification of His_6-β-catenin was carried out using the procedure for TIP48-His_6 (see sections 2.7.3 to 2.7.5 and Table 2.7). However, only 10 mM imidazole in Talon Buffer was used for the Talon column wash, with a 10-500 mM imidazole gradient for elution.

2.7.11 Purification of Hint1 and His_6-Hint1

Lysis and solubilisation of His_6-Hint1 or non-tagged Hint1 was carried out in Talon Buffer as described above (Section 2.7.3 and 2.7.4; 1 mM $ZnCl_2$ was included in the lysis buffer – see Table 2.7). For His_6-Hint1, purification was carried out as with TIP48-His_6 (Section 2.7.5). However, Hint1 flowed through the MonoQ column, and this was used as the final purification step.

For non tagged Hint1, the soluble lysate was passed through a Talon column and the flow-through was collected. Flow-through that contained Hint1 was dialysed into TEGD Buffer (20 mM Tris-HCl pH 7.5, 1 mM EDTA, 10 % Glycerol, 1 mM DTT) overnight. Hint1 was then applied to a 5 ml DEAE column then a 5 ml

Heparin column both equilibrated in TEGD Buffer; however, Hint1 flowed through both columns. Hint1 was then applied to stacked 5 ml Q Sepharose and SP Sepharose columns in TEGD, and again flowed through both columns.

2.8 Antibody Production

2.8.1 Generation of Polyclonal and monoclonal antibodies

Polyclonal antibodies against TIP48 or TIP49 were raised in rabbits using recombinant proteins produced by prior members of Dr. Tsaneva's group and are described in (Sigala et al., 2005). Culture medium containing monoclonal antibodies against TIP49 were kindly provided by Dr. Wagner's group and are described in (Gartner et al., 2003).

2.8.2 Affinity purification of antibodies

Serum containing polyclonal antibodies was purified at 4 °C on a 1 ml HiTrap NHS column (GE Healthcare) conjugated with the corresponding recombinant protein (according to the manufacturer's instructions). The column was washed in 6 ml of Buffer AB1 (500 mM triethanolamine-HCl pH 8.3, 500 mM NaCl), followed by 6 ml of Buffer AB2 (100 mM sodium acetate pH 4, 500 mM NaCl), then a further 6 ml of Buffer AB1. The column was incubated with Buffer AB1 for 30 mins at room temperature. The column was then washed in 6 ml of Buffer AB2, Buffer AB1, and Buffer AB2 then 10 ml of Buffer AB3 (1 M MOPS pH7). Ice-cold serum containing antibodies was passed through the column and re-circulated through the column overnight at 4 ˚C. The column was washed in 10 ml of Buffer AB3 then eluted in ten 1 ml fractions by washing the column with Buffer AB4 (100 mM Glycine-HCl pH 2, 150 mM NaCl). The fractions were neutralised with 200 µl of 1 M Tris-HCl pH 8; for long-term storage, sodium azide was added to a final concentration of 0.2 %.

For purification of mouse monoclonal antibodies, 10 ml of solution containing antibodies was diluted 1:4 in Buffer AB5 (100 mM Tris-HCl pH9, 1 M NaCl). This

was then loaded onto a HiTrap 1 ml Protein A column (GE Healthcare) at 4 °C and continually re-applied to the column for 4 hours at a flow rate of 1 ml/min. The column was washed with Buffer AB5, then the antibodies were eluted using Buffer AB6 (0.1 M Sodium Citrate pH3). The eluted fractions were neutralised by making them to 100 mM Tris-HCl pH8; 0.3% sodium azide was added for long term storage.

2.8.3 Antibody Dilutions

Antibody dilutions used for each technique are summarised in Table 2.8.

	Antigen	Raised In	Tag	Technique	Dilution
1°	**hTIP48**	Rabbit (PC)	n/a	Western IF	1:1,000 1:200
1°	**hTIP49**	Rabbit (PC)	n/a	Western	1:1,000
1°	**hTIP49**	Mouse (MC)	n/a	Western	1:500
1°	**human α-Tubulin**	Mouse (MC)	n/a	Western IF	1:1,000 1:400
2°	**Rabbit IgG**	Goat	IRD 800	Western	1:10,000
2°	**Rabbit IgG**	Goat	AlexaFlour 488	IF	1:500
2°	**Mouse IgG**	Goat	AlexaFlour 680	Western	1:10,000
2°	**Mouse IgG**	Goat	TRITCH	IF	1:400

Table 2.8. Antibodies dilutions used in this thesis. IF – Immunofluorescence, 1º – primary antibody, 2º – secondary antibody, h – human, MC – monoclonal, PC – polyclonal.

2.9 Protein Techniques

2.9.1 Protein concentration determination

Protein concentrations were assessed using the Bradford assay. 20 µl samples of seven different concentrations of BSA (bovine serum albumin) were prepared as standards: 1, 0.8, 0.6, 0.4, 0.2, 0.1 and 0 mg/ml. 20 µl of the protein to be assayed was also prepared to a suitable concentration (0.1 – 1 mg/ml). Bradford's reagent (Biorad) was diluted 1:5 with water and 0.98 ml was added to each 20 µl sample, incubated at room temperature for 10 mins and the absorbance at 595 nm was measured for each sample in a spectrophotometer. Concentrations of protein samples were estimated by comparison with the standard curve obtained for BSA.

Protein concentrations were also assessed by measuring the absorbance of the sample at 280 nm on a Nanodrop ND-1000 spectrophotometer. Extinction coefficients for proteins were used for the calculation of protein concentrations.

2.9.2 1-D SDS PAGE Analysis

12 or 15 % SDS PAGE gels were cast using the Mini Protean II system (Biorad), with 0.7 mm spacers and 10-well combs. Gels consisted of a resolving gel (0.375 mM Tris-HCl pH 8.8, 12 or 15 % 29:1 polyacrylamide, 0.1 % SDS, 0.1 % AMPS and 0.005 % TEMED), and a stacking gel (0.2875 mM Tris-HCl pH 6.8, 5 % 29:1 polyacrylamide, 0.1 % SDS, 0.1 % AMPS and 0.01 % TEMED). The gels were placed in tanks and submerged in SDS Running Buffer (25 mM Tris pH 8.8, 190 mM glycine, 0.1 % SDS). Samples were mixed 1:1 with SDS PAGE loading buffer (125 mM Tris-HCl pH 6.8, 2 % SDS, 10 % glycerol, 10 % 2-ME, 0.01 % bromophenol blue) and boiled for 3 minutes at 100 ˚C, then loaded into the wells of the gel. 20 µl of broad range pre-stained markers (NEB) or 5 of µl broad range pre-stained markers (Fermentas) were loaded into the appropriate wells. Gels were run at a 20 - 28 V/cm for 1-2 hours, stained with warm Coomassie brilliant blue (10 % isopropanol, 10 % glacial acetic acid, 0.25 % Coomassie brilliant

blue) for 1 hr, then placed in destaining solution (10 % isopropanol, 10 % glacial acetic acid). A silver staining kit (Biorad) was used where necessary, by following the manufacturer's instructions.

2.9.3 2-D SDS PAGE Analysis

For preparation of HeLa cell extracts, see Chapter 2.12.4. Samples were made up to 0.2 ml with 2-D Rehydration Buffer (8 M urea, 2 % CHAPS, 20 mM DTT, 0.01 % bromophenol blue). Each sample was pipetted across the entire length of a focusing chamber in a 7 cm focusing tray. A 7 cm pH 3-10 ReadyStrip IPG strip (Biorad) was placed face down onto each sample in the chamber and the strips were covered in 1.5 ml of mineral oil. The tray was placed into a Protean IEF Cell (Biorad) and actively rehydrated overnight at 50 mV using the machine's default settings. After rehydration, wicks were placed between the strip and the electrodes and the isoelectric focusing was performed using the machine's default settings (fast focusing). The strips were then washed in water and placed in an equilibration tray. If required, the strips could be stored at -80 °C at this point. The strips were equilibrated in 2-D Equilibration Buffer (6 M urea, 20 % Glycerol, 2 % SDS, 50 mM Tris-HCl pH 8.8) supplemented with 1 % DTT. After 15 mins, the buffer was removed and 2-D Equilibration Buffer with 2.5 % iodoacetamide was added for 15 mins. The strips were then placed on a 12 % Acrylamide SDS PAGE Gel (4 ml resolving gel, no stacking gel) and set in place with molten 1 % agarose in SDS Running Buffer. The gel was run at 15 V/cm for 2 hours. Proteins were visualised by Coomassie staining or Western blotting.

2.9.4 Western Blotting

Protein samples were run on SDS PAGE gels as above, but not stained with Coomassie; gels were instead washed in chilled Transfer Buffer (48 mM Tris, 39 mM glycine, 0.037 % SDS, 20 % methanol) for 10 mins. Proteins were transferred onto a nitrocellulose membrane using a semi-dry transfer kit (BIORAD) in Transfer Buffer (the order of addition was one extra thick blot paper,

two filter papers, one nitrocellulose membrane, one SDS PAGE gel, two filter papers and one extra thick blot paper, all soaked in Transfer Buffer) for 25 mins at a constant voltage of 15 mV. The membrane was washed in TBS-T Buffer (20 mM Tris-HCl pH 7.5, 137 mM NaCl, 0.05 % Tween-20) with 5 % skimmed milk powder (Marvel) for 30 mins at room temperature, then washed in TBS-T Buffer for 5 mins twice, then for a further 15 mins. The membrane was incubated with primary antibody (Table 2.8) at the appropriate concentration in TBS-T Buffer with 5 % skimmed milk powder overnight at 4 ˚C (or for 1 hour at room temperature). After primary antibody incubation, membranes were washed in TBS-T Buffer for 10 mins thrice, then incubated with the secondary antibody (Table 2.8) for 40 mins at room temperature. Membranes were washed in TBS-T Buffer for 30 mins twice, then visualised on a Li-Cor infrared imaging system.

2.10 Biochemical Assays

2.10.1 Size Exclusion Chromatography (SEC)

A Superose 6 HR or Superdex 200 HR column was used for SEC. Proteins dialysed against R Buffer with 1 mM EDTA or 2 mM $MgCl_2$ were incubated for 20 min on ice with 1 mM ATP if required. The samples (0.1 – 0.5 mg of protein in up to 500 µl) were filtered through 0.2 µm syringe filters (Millipore) then loaded onto the column, and eluted in R Buffer (with 1 mM EDTA or 2 mM $MgCl_2$ with 0.1 mM ATP when required) in 24 fractions of 1 ml each. The protein composition of each fraction was determined by 12 % SDS PAGE analysis using Coomassie brilliant blue to visualise proteins. Monitoring using 280 nm absorbance was used to estimate the elution volume of each species. Protein molecular masses were estimated by comparison with five standards (Biorad) and Dextran blue was used to determine the column void volume, both of which were monitored in the column using R Buffer:

$$K_{av} = (V_e - V_o) / (V_t - V_o) \qquad \textbf{Equation 2.1}$$

Where K_{av} is the partition coefficient for each protein; V_e is the elution volume of the protein (ml); V_o is the void volume of the column (ml); V_t is the total volume of the column (Superdex 200 HR and Superose 6 HR = 24 ml)

For the capture of single hexamers on Talon resin, fraction 15 that eluted as part of the purification of TIP48/TIP49 was further separated on a Superose 6 column in R buffer with no EDTA. Fractions 14-16, which eluted from the column were incubated with 200 µl of Talon resin for 30 mins at 4 ºC with mild agitation. The resin was washed twice with Talon buffer and the supernatant discarded. Protein was eluted by incubating the resin with 500 µl of Talon buffer supplemented with 200 mM imidazole for 10 mins at 4 ºC.

2.10.2 ATPase assays

Assays were carried out using the P_i ColorLock ALS colourimetric kit (Innova Biosciences). Reactions were carried out in a final volume of 200 µl and incubated at 37 ºC for 30 minutes in ATPase Buffer (50 mM Tris pH 8, 100 mM NaCl, 0.1 mg/ml Bovine Serum Albumin, 2 mM $MgCl_2$, 0.5 mM ATP). To start the reactions, 20 µl protein samples or material from SEC fractions was added. At several time points (including 0 mins), 20 µl from each reaction was added to 5 µl of 0.5 M EDTA pH 8.5 in 96 well round bottomed tissue culture test plates (Techno Plastic Products) in triplicate. 125 µl of ALS malachite green solution was added to each well, the colour was left to develop for 30 mins, and then the absorbance at 635 nm was measured using a Tecan Sunrise microplate absorbance reader. 20 µl of different concentrations of KP_i were also measured as above to generate a standard curve.

2.10.3 Gradient Centrifugation

Glycerol or sucrose gradients were made manually in 3.5 ml glass centrifugation tubes. 600 µl of five concentrations of glycerol (40, 35, 30, 25 and 20 %) or sucrose (25, 20, 15, 10 and 5 %) in the appropriate buffer were layered from the bottom to top of the tube and left to equilibrate for 2 hours at 4 ˚C. Up to 200 µl of

sample was loaded onto the glycerol gradient, and it was placed in a MLS-50 swinging rotor and centrifuged at 40,000 r.p.m. for 24 hrs at 4 ˚C. Fractions of 100-200 µl were collected manually from top to bottom and the composition of each fraction was analysed using electrophoresis and the appropriate detection method.

2.10.4 Helicase assays

For generating substrates for helicase assays, 5' IRD700-labelled oligonucleotides were annealed to ΦX174 virion ssDNA (NEB):

IT.300	5'-ATCGAGCTGCGCAAGGATAGGTCGAA-3'	+ ΦX174 = H26
IT316	5'-CTCGAGCTGCGCAAGG-3'	+ ΦX174 = H16

For the annealing reaction 20 pmol of IRD-700-labelled IT.300 was added to 20 pmol ΦX174 virion ssDNA in 10 mM Tris-HCl pH 7.5, 10 mM $MgCl_2$, 50 mM NaCl. The mixture was denatured at 95 °C for 3 min, incubated at 68 °C for 30 min and slowly cooled down at room temperature. Fractionation was performed on a 5–25 % sucrose gradient in 10 mM Tris pH 7.5, 1 M NaCl and 10 mM EDTA. Peak fractions were dialysed into Storage Buffer (10 mM Tris pH 7.5, 100 mM NaCl, 1 mM EDTA) overnight at 4°C.

For the helicase assays, ~5 ng of labelled substrate was incubated with 1 µM protein in Helicase Buffer (40 mM Tris pH 7.5, 3 mM $MgCl_2$, 10 % glycerol, 50 mM NaCl) to a final volume of 80 µl. 1 mM ATP was added to start the reaction, and 10 µl of reaction was removed at several time points and mixed with 2 µl Stop Buffer (5 % SDS, 125 mM EDTA, 250 µg/ml Proteinase K) to stop the reaction. 5 µl of 80 % glycerol was added to each sample, which was then analysed by 1 % agarose gel electrophoresis in TAE Buffer (40 mM Tris, 20 mM glacial acetic acid, 1 mM EDTA). Labelled oligonucleotides were visualized on a Li-Cor infrared imaging system. RuvA (200 nM) with RuvB (1 µM) were provided

by Dr. Tsaneva and used as positive controls in this assay; 15 mM $MgCl_2$ was used in the Helicase Buffer for RuvAB.

2.11 Biophysical Analysis

2.11.1 Velocity Analytical Ultracentrifugation (vAUC)

TIP48, TIP49 and the TIP48/TIP49 complex were dialysed extensively against one of four different AUC buffers supplemented with cofactors as required. (i) the EDTA buffer comprised of 20 mM Tris-HCl pH 8, 200 mM NaCl, 0.1 mM dithiothreitol, 0.1 mM EDTA. (ii) the magnesium buffer was 20 mM Tris-HCl pH 8, 200 mM NaCl, 0.1 mM dithiothreitol, 2 mM $MgCl_2$, to which was added either (iii) 0.5 mM ATP or (iv) 0.5 mM ADP when preparing the ATP and ADP buffers respectively. Buffer densities and viscosities were determined using the program SEDNTERP (Laue et al., 1992). These were 1.0072 g/ml and 0.01027 cp respectively for the four buffers. ADP and ATP were added after sample dialysis.

Sedimentation velocity runs were performed using a Beckman Optima XL-I analytical centrifuge at 20 °C using an AnTi50 rotor. Absorbance and interference data sets were collected at rotor speeds of 25,000, 30,000, 35,000 and 42,000 r.p.m. for TIP48 and TIP49, and 25,000 and 30,000 r.p.m. for the TIP48/TIP49 complex in two sector cells with column heights of 12 mm. The different rotor speeds established the absence of diffusion effects on the sedimentation coefficient. Scans were recorded at 8 min intervals until all the species had fully sedimented. Protein molecular masses and partial specific volumes of 52.1 kDa and 0.743 ml/g for TIP48, 52.4 kDa and 0.747 ml/g for TIP49 and 102.5 kDa and 0.745 ml/g for the TIP48/TIP49 complex were calculated from their amino acid compositions. The *g(s*)* time-derivative analyses of 4 to 12 absorbance or interference scans were analysed using DCDT+ (version 2.06) (Philo, 2006) from which the sedimentation coefficients were determined from the peak position. The number of scans selected for the DCDT+ analyses ensured that peak broadening effects were negligible. Sedimentation analysis was also performed

using direct boundary Lamm fits of 70 to 110 absorbance or interference scans using SEDFIT (version 9.4b) (Schuck, 2000). SEDFIT resulted in size distribution *c(s)* analyses that assumed that all species have the same frictional ratio *(f/f_0)*. These were used to establish the oligomeric species that were present. The final SEDFIT *c(s)* fit was optimised by floating the meniscus, frictional ratio, and baseline one by one until the overall root mean square deviations and visual appearance of the fits were satisfactory. Figures depicting vAUC analyses show one in five scans for clarity.

2.11.2 Equilibrium Analytical Ultracentrifugation (eAUC)

For sedimentation equilibrium experiments, TIP48 was dialysed extensively against magnesium buffer (ii), then ATP or ADP were added to each sample and reference buffer to obtain a 20 fold molar excess of nucleotides over the protein concentration. Sedimentation equilibrium data were acquired during centrifugation for up to 150 h at 20 ºC using six-sector cells with solution column heights of 2 mm at rotor speeds of 7,000 r.p.m., 9,000 r.p.m., 11,000 r.p.m., 14,000 r.p.m., 17,000 r.p.m. and 20,000 r.p.m. until equilibrium had been reached at each speed (confirmed by the perfect overlay of runs measured at 3 h intervals). The middle four speeds were used for final global fits. The molecular mass for TIP48 was initially determined on the assumption of a single species using SEDPHAT (version 4.3) (Schuck, 2003):

$$c_r = c_{ro} \exp [(\omega^2/2RT) MW (1- \bar{\nu} \rho) (r^2 - r_o^2)] \qquad \textbf{Equation 2.2}$$

where c_r is the concentration at radius r, c_{ro} is the concentration of the protein at the reference radius r_o, ω is the angular velocity, MW is the molecular mass, R is the gas constant, T is the temperature (Kelvin), and ρ is the solvent density of the buffer. Final molecular masses were obtained using global fits of up to 24 curves in SEDPHAT in the “single species of interacting system” model with both the “M and s” and Marquardt-Levenberg fitting routines, while floating the molecular mass, molar extinction coefficient, the baseline and the bottom of the cell. The

best-fit solutions were determined using the reduced χ^2 value as a monitor. Fits in figures depicting eAUC show one in four scans for clarity.

2.11.3 Hydrodynamic modelling of sedimentation coefficients

The modelling of TIP48 and TIP49 oligomers was based on the crystal structure of the human TIP49-ADP complex which contained three independent monomers A, B and C (PDB code 2c9o) (Matias et al., 2006). To generate Hexamer 1, monomer A in the PDB file was used to build the hexameric form of TIP49 in spacegroup P6, using the Protein Quaternary Structure website at http://pqs.ebi.ac.uk/. The resulting Hexamer 1 showed that an accessible surface area of 4102 Å^3 (15.8% of the total) was lost on hexamer formation, and all six monomers were in the same symmetric orientation around the hexameric ring. Up to 10 salt bridges between each monomer with its two neighbours occurred between Arg14-Asp353, Lys107-Glu105, Arg339-Asp343 and Arg404-Asp356. The symmetry operators for the six monomers were defined by X, Y, Z; Y,-X+Y, Z; X-Y, X, Z; -X+Y,-X, Z; -Y, X-Y, Z; and -X, -Y, Z. Hexamer 2 was generated by alternating orientations of monomers B and C around the ring. Sedimentation coefficients $s^0_{20,w}$ were calculated directly from the atomic coordinates in the HYDROPRO shell modelling program using the default value of 0.31 nm for the atomic element radius for all atoms to represent the hydration shell (Garcia De La Torre et al., 2000; Garcia de la Torre et al., 2001).

The structure of the TIP48/TIP49 complex was based on its electron microscopy model at 20 Å resolution. This was downloaded from the 3-D-EM electron microscopy database (deposition code 1317) at http://www.ebi.ac.uk/msd/projects/IIMS.html and converted into SPIDER format using the IMAGIC em2em utility at http://www.imagescience.de/em2em/. A pixel size of 3.3 Å and a density cut-off threshold of 0.547 generated a volume of 728,000 Å^3 which is close to the sequence-derived volume of 751,000 Å^3 for the TIP48/TIP49 complex. Sedimentation coefficients $s^0_{20,w}$ were calculated from the electron microscopy model using the HYDROMIC shell modelling program using

the default value of 0.31 nm for the atomic element radius for all atoms to represent the hydration shell (Garcia De La Torre et al., 2000; Garcia de la Torre et al., 2001).

2.12 HeLa cell culture

2.12.1 Synchronization in mitosis

HeLa cells were grown on cover slips in 24 well plates or grown in 75 cm^2 flasks. To obtain an asynchronous population, HeLa cells were grown in DMEM growth medium (DMEM supplemented with 5 % fetal bovine serum, 100 U/ml streptomycin/penicillin mix (Gibco) and 1 % L-glutamine) at 37 ºC with 5 % CO_2. To encourage a mitotic cell population, cells were grown in DMEM growth medium at 37 ˚C, then synchronised at G2/M checkpoint by incubating the cells in DMEM growth medium supplemented with 9 µM RO-3306 for 20 hrs. Cells were released from the G2/M checkpoint by washing twice in DMEM growth medium, then incubating in fresh growth medium for 30 - 120 mins.

2.12.2 Cell fixing and immunostaining

HeLa cells were seeded onto cover slips in 24 well plates and treated as above, then grown to ~ 50 % confluence. Cells were washed twice in PBS (140 mM NaCl pH 7.3, 2.7 mM KCl, 10 mM Na_2HPO_4, 1.8 mM KH_2PO_4), then fixed with PFA Buffer (2 % PFA in PBS) for 3 mins. Cells were washed with PBS-T Buffer (0.2 % Tween-20 in PBS) twice for 10 minutes. Cells were rinsed in ice cold-methanol for 1 min then air dried before adding Blocking Buffer (2 % goat serum & 0.3 % BSA in PBS) for 30 mins. Primary antibodies were added to the Blocking Buffer (for antibody dilutions see Table 2.8 page 96) and incubated at 4 ˚C overnight on a shaker. After removal of the primary antibodies, the cover slips were washed twice in Blocking Buffer, the secondary antibodies were then added in Blocking Buffer for 1 hour at room temperature (Table 2.8). Cover slips were washed in Blocking Buffer for 10 mins twice, then mounted onto glass slides in

Vectashield (Vector Laboratories) containing DAPI stain and sealed with clear nail varnish. The immunostained cells were visualised under a Zeiss Axio Skop 2 plus microscope and images were processed using Openlab 4.0.4 and Adobe Photoshop.

2.12.3 Transfection and TIP49-GFP fluorescence microscopy

TIP49 CDS, cloned into a pEGFP plasmid was constructed in Dr. I Tsaneva's laboratory, and used to ectopically express a TIP49-GFP fusion protein *in vivo*. HeLa cells were grown on cover slips in 24 well plates in DMEM growth medium, as above, to 80 % confluence. 0.8 µg of pEGFP-TIP49-GFP plasmid DNA was diluted in 50 µl of OptiPro SFM (Invitrogen) and 2 µl of Lipofectamine 2000 CD (Invitrogen) was diluted to 50 µl with OptiPro SFM. The DNA and Lipofectamine were then mixed and incubated for 30 mins at room temperature, then added to the growth medium (0.5 ml) in each well. Cells were grown with the Lipofectamine in the medium, after 5 hrs, the medium was replaced with fresh DMEM growth medium without Lipofectamine. Mock transfections were set up by replacing the DNA with distilled water.

Cells were seeded onto cover slips in 24-well plates and transfected with pEGFP-TIP49-GFP as described above. Cell were then synchronised in G2/M and released into mitosis (as described in 2.12.1). For an asynchronous population, the cells were grown for 48 hours after transfection. The cells were washed twice in PBS, then fixed with PFA Buffer for 3 minutes. Cells were washed with PBS-T Buffer (0.2 % Tween-20 in PBS) twice for 10 mins, rinsed in ice cold-methanol for 1 min then air-dried. The cells were washed with PBS twice for 10 mins, then mounted onto glass slides in Vectashield and sealed with clear nail varnish. The GFP-TIP49 expressing cells were visualised under a Zeiss Axio Skop 2 plus microscope and images were processed using Openlab 4.0.4 and Adobe Photoshop.

2.12.4 Cytoplasmic and nuclear fractionation and whole cell extracts of HeLa

HeLa cell pellets were prepared by growing monolayers in tissue culture flasks until confluent (see 2.12.1 for conditions). Cells were then washed in PBS, then scraped with a sterile scraper until the majority of cells had detached. The cells were collected and centrifuged at 500 *g* for two minutes, resuspended in fresh PBS, then pelleted again. The PBS was removed, and the resulting HeLa cell pellet was then stored at -80 ºC until needed.

A pellet of 1 x 10^7 cells was used to obtain whole cell extracts (WCE) of HeLa. The cells were suspended in HeLa lysis buffer (7 M urea, 2 M thiourea, 4 % CHAPS, 20 mM spermidine, 20 mM DTT, 1 mM PMSF) on ice for 1-2 hours. The lysate was then spun at maximum speed on a bench-top centrifuge for 30 mins at 4 ºC. The insoluble protein in the resulting pellet was discarded. The protein concentration of the soluble fraction was estimated by the method of Bradford. The lysate was used for 1-D and 2-D SDS PAGE analysis of TIP48 and TIP49. Approximately 100 µg of lysate was used for 2-D PAGE.

Cytoplasmic and nuclear fractionation of a HeLa cell pellet containing 1 x 10^7 cells was carried out using the ProteoJET cytoplasmic nuclear extraction kit (Fermentas Life Sciences). For generating fractions for 1-D PAGE analysis, the manufacturers instructions were followed, and a suitable amount of complete EDTA free protease inhibitor cocktail (ROCHE) and phosphatase inhibitor cocktail II (Sigma-Aldrich) were added to the buffers, as recommended. For generating fractions for 2-D PAGE analysis, washed nuclei were suspended directly into 2-D Rehydration Buffer (8 M urea, 2 % CHAPS, 20 mM DTT, 0.01 % bromophenol blue). For better analysis of cytoplasmic fractions by 2-D PAGE, immediately prior to rehydration, urea was added directly into the cytoplasmic fraction to a final concentration of 8 M, followed by the other components of the 2-D Rehydration Buffer.

Chapter 3

Investigating the Oligomeric Properties of TIP48 and TIP49 and the Assembly of their Heteromeric Complex

3.1 Introduction

To date, TIP48 and TIP49 have been implicated in a broad range of cellular functions; however, no information about how the ATPase activity of TIP48 and TIP49 is linked to mechanical function has so far been described. Moreover, the regulation of this activity still remains unclear. Interestingly, TIP48 and TIP49 have functions which are either synergistic, e.g. chromatin remodelling (Jonsson et al., 2001); antagonistic, e.g. β-catenin signalling (Rottbauer et al., 2002); as well as roles where they act independently, e.g. mid-body localisation (Sigala et al., 2005). One way of regulating these different roles is by assembly into different oligomers, exemplified by the requirement of the TIP48/TIP49 double hexamer for optimal ATPase activity. Thus, better understanding of the oligomers formed by TIP48 and TIP49 could lead to a superior comprehension of their mechanism of action. In order to address some of these questions, we used SEC (Size exclusion chromatography) and AUC (Analytical Ultracentrifugation) to study the oligomerisation of TIP48 and TIP49 and how this is affected by nucleotide cofactors. We also used biophysical techniques to understand the assembly, regulation and composition of TIP48/TIP49 complexes. We modelled published structures of TIP49 and the TIP48/TIP49 complex to strengthen our interpretation of oligomerisation of TIP48, TIP49 and their complex.

3.2 Expression and purification of TIP48-His_6, His_6-TIP49 and the TIP48/TIP49-His_6 complex

Recombinant TIP48-His_6 and His_6-TIP49 (hereafter referred to as TIP48 and TIP49) were expressed and purified using a bacterial expression system (see Chapter 2.7) and judged to be 95 % pure by SDS PAGE analysis with Coomassie brilliant blue staining (Figure 3.1a). The complex of TIP48/TIP49-His_6 (hereafter referred to as TIP48/TIP49) was cloned by using a $pET21b^+$ TIP48 (no tag) and $pET21b^+$ TIP49-His_6 (see Chapter 2.7) so that the expression of each

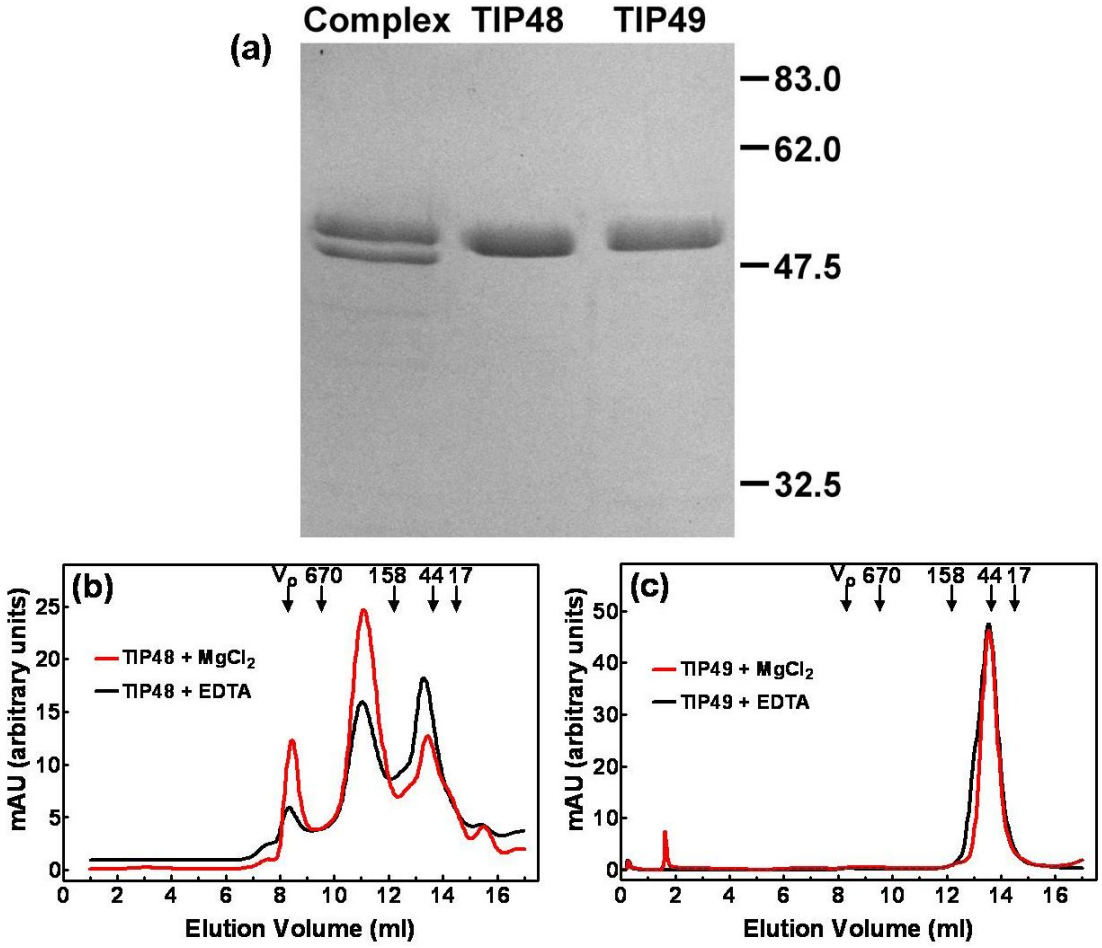

Figure 3.1. SDS-PAGE and SEC analysis of TIP48 and TIP49. Purified recombinant proteins were examined using 15 % polyacrylamide SDS-PAGE (a). The lanes from left to right show the complex of TIP48/TIP49-His_6, TIP48-His_6 and His_6-TIP49. The positions of the molecular weight standards in kDa are indicated at the right. Superdex 200 HR SEC elution profiles show TIP48 purified in $MgCl_2$, which was dialysed against $MgCl_2$ or EDTA containing buffer (b). SEC elution profiles show His_6-TIP49 purified in $MgCl_2$, which was dialysed against $MgCl_2$ or EDTA containing buffer (c). Arrows indicate the elution volumes of protein standards (in kDa) and the void volume (V_o).

coding sequence was controlled by an individual T7 promoter. Rosetta II (DE3) *E. coli* were transformed with the plasmid. Bacterial cultures were grown and recombinant protein production was induced with 0.5 mM IPTG. Bacterial cells were lysed and the soluble lysate was loaded onto a Talon metal affinity column. The column was washed with 5 mM imidazole, and then a gradient of 5 – 250 mM imidazole was applied to the column. Untagged TIP48 eluted with TIP49-His_6 at 50-200 mM imidazole. The complex was then dialysed and passed through an ssDNA column, concentrated to 0.5 ml, then separated according to size using a Superose 6 HR 10/30 SEC column (Figure 3.2a and b).

3.3 Size exclusion chromatography (SEC) of TIP48, TIP49 and their complex

3.3.1 TIP48 and TIP49 have different oligomeric properties by SEC

Recombinant TIP48 and TIP49 were analysed by SEC using a Superdex 200 HR SEC column. TIP48 has been shown to undergo ATP and ADP dependent oligomerisation, which is enhanced in the presence of divalent magnesium (Puri et al., 2007). We purified TIP48-His_6 from *E. coli* BL21-Gold (DE3) in the presence of $MgCl_2$ to identify if this would be sufficient to induce oligomerisation of TIP48. Indeed, inclusion of $MgCl_2$ in the buffers during purification of TIP48 resulted in samples with several oligomers. TIP48 purified in $MgCl_2$ was analysed by SEC and eluted at 11.1 ml, consistent with an oligomer of ~ 400 kDa. Smaller species also eluted at 13.4 ml, calculated to be ~ 70 kDa. Intermediates were visible between these peaks, but molecular masses could not be assigned as the peaks were not sufficiently resolved (Figure 3.1b). When this sample was dialysed against buffer containing EDTA, there was a reduction in the proportion of the 400 kDa species, and an increase in the proportion of the 70 kDa species, confirming that Mg^{2+} is necessary for oligomerisation of TIP48; however, oligomerisation under these conditions is likely due to TIP48 co-purifying with

ADP from the bacterial lysate when Mg^{2+} is present. Using these data, it was difficult to predict the number of subunits of TIP48 contained in each oligomer. As size and shape both affect the volume of elution from a SEC column, the 70 kDa peak could be interpreted as either a monomer-dimer equilibrium, or a monomer with an elongated shape; the 400 kDa peak could be interpreted as anything between a pentamer and an octamer of TIP48. To rule out any effect of the histidine$_6$ tag in mediating this oligomerisation, TIP48 purified in $MgCl_2$ was also analysed by SEC in the presence of 250 mM imidazole, as imidazole destabilises interactions between histidine groups. The 400 kDa peak of TIP48 was observed with and without imidazole, indicating that the histidine groups do not promote oligomerisation of TIP48 (data not shown).

TIP49 was also analysed by SEC after being purified from *E. coli* BL21-Gold (DE3) cells in the presence of $MgCl_2$. In correlation with previous observations, TIP49 eluted as a monomer of 55 kDa under these conditions (Figure 3.1c) (Puri et al., 2007). To confirm that the N-terminal histidine$_6$ tag did not affect oligomerisation, C-terminally tagged TIP49-His$_6$ was analysed by SEC in EDTA, or with ATP in the presence of $MgCl_2$. Again, TIP49-His$_6$ eluted as a monomer under all conditions tested, suggesting that the histidine$_6$ tag does not interfere with oligomerisation of TIP49 (data not shown).

3.3.2 TIP48 and TIP49-His$_6$ form an active dodecameric complex by SEC

TIP48 and TIP49 form a dodecameric complex which displays a synergistic increase in ATP hydrolysis, compared with the individual proteins. To confirm that the above method of co-purifying TIP48/TIP49 from bacteria gave active complex in the correct conformation, we analysed the complex by SEC on a Superose 6 HR SEC column and measured the ATPase activity of the fractions collected (Figures 3.2a, b and c). The complex eluted at 13.1 ml, equating to approximately 617 kDa. This is in good agreement with the predicted molecular mass of a

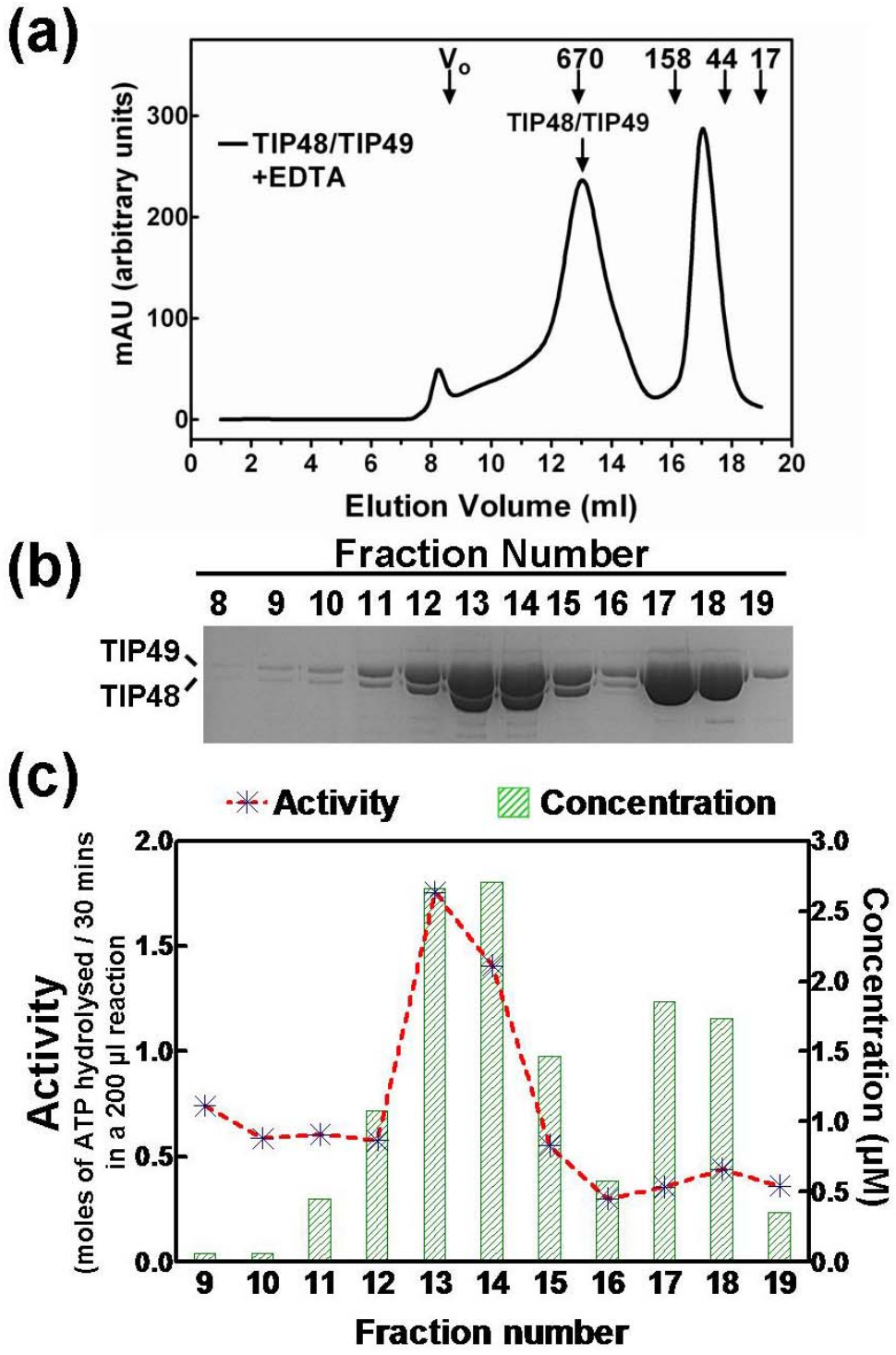

Figure 3.2. Oligomerisation and activity of the TIP48/TIP49-His$_6$ complex. Separation of TIP48/TIP49-His$_6$ oligomers using a Superose 6 HR SEC column is shown as a UV_{280} absorbance trace (a). 1 ml fractions were collected (Fraction 1 is from 0.5 – 1.5 ml etc), which were analysed by 12 % SDS PAGE stained with Coomassie (b). The ATPase activity and protein content of each fraction was measured by a colourimetric assay that quantifies the release of inorganic phosphate (P_i) upon ATP hydrolysis and Bradford's assay respectively (c). ATPase activity is defined as the moles of ATP hydrolysed after 30 minutes incubation at 37 ºC.

dodecamer of TIP48/TIP49-His_6 of 622 kDa. The ATPase activity peaked in fractions 13 and 14; these fractions are where the dodecamer is expected to elute, and also coincided with a peak in protein concentration. Moreover, monomeric TIP49 in fractions 17 and 18 has very little ATPase activity compared with the dodecameric complex, confirming that assembly into a double hexamer results in a synergistic increase in ATPase activity (Figure 3.2c).

The SEC profile of the TIP48/TIP49 complex showed a relatively discrete peak corresponding with a dodecamer; however, TIP48 and TIP49 were seen eluting between 8 ml (the void volume) and 11 ml (Figures 3.2a, b and 3.3a). This may indicate that oligomers higher than a dodecamer are part of the sample. To investigate the stability of the double hexamer, fractions 13 and 14, where the dodecamer eluted, were pooled and re-applied to the column after being diluted to different concentrations (Figure 3.3b). At all protein concentrations tested, the complex eluted at the same volume, with little or no monomeric protein present. This indicates that the complex is stable and does not undergo dissociation or self-association at these protein concentrations. Sample loaded on the column in Figure 3.3a was in excess of 10 mg/ml. It is therefore likely that much higher protein concentrations than those in Figure 3.3b are needed to observe species higher than a dodecamer by SEC.

We wanted to observe if there were any changes in the oligomeric state of the TIP48/TIP49 complex in the presence of ATP and $MgCl_2$. TIP48/TIP49 complex that eluted in fractions 12 and 13 in Figure 3.3A was dialysed against buffer containing 0.5 mM EDTA or 2 mM $MgCl_2$, then the sample with $MgCl_2$ was incubated with 0.5 mM ATP. Both samples were then analysed by SEC. In EDTA, the TIP48/TIP49 complex eluted predominantly as a dodecamer, with a small proportion of 70 kDa TIP48 and 55 kDa TIP49. When incubated with ATP, the dodecameric species remained unchanged, and the 70 kDa TIP48 peak shifted to a hexameric peak (Figure 3.3c) consistent with previous observations. The 55 kDa TIP49 peak remained unchanged. The presence of the hexameric peak

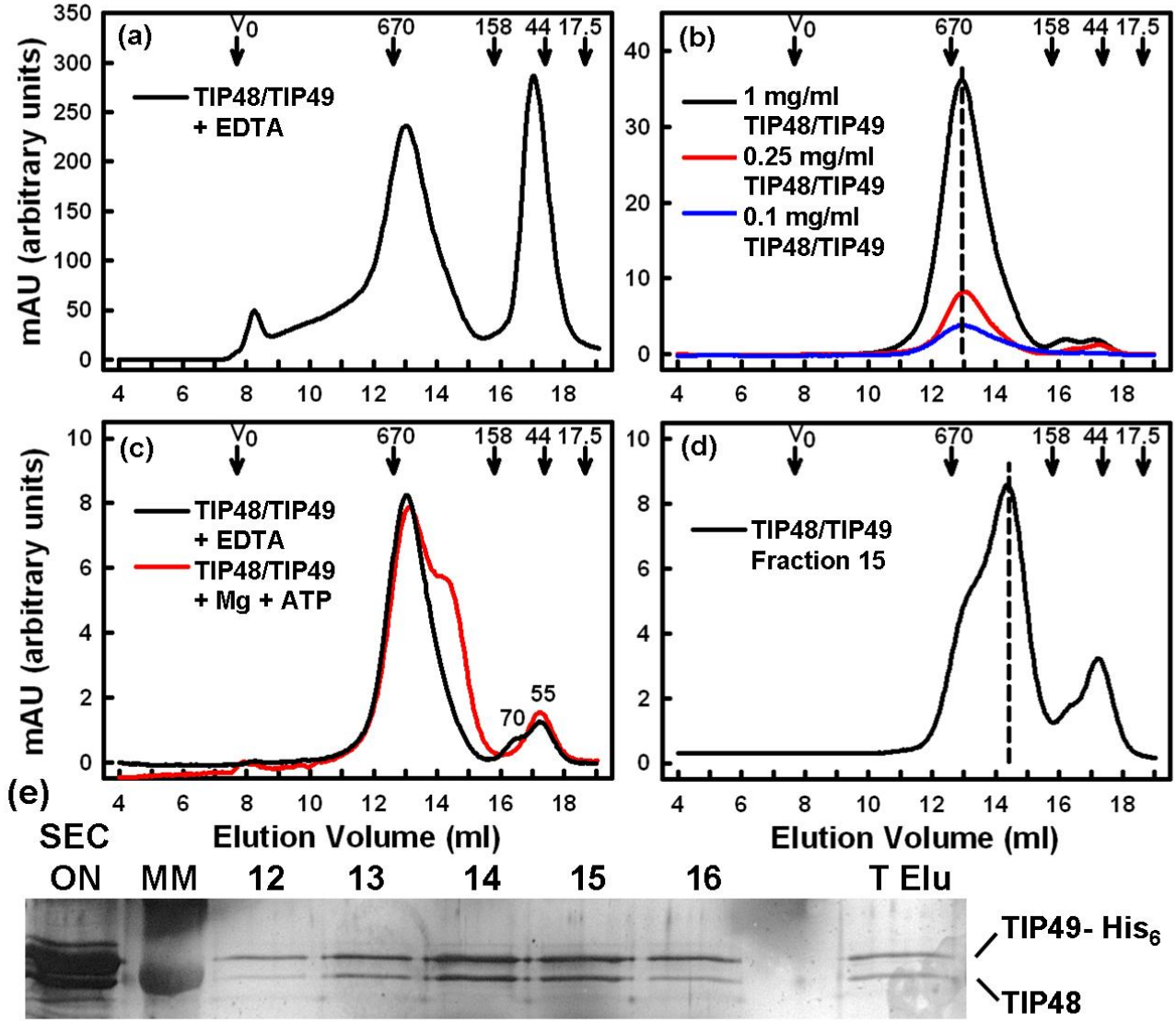

Figure 3.3. Oligomerisation of the TIP48/TIP49-His$_6$ complex by SEC. TIP48 and TIP49-His$_6$ that co-eluted from a Talon column were further purified on a Superose 6 SEC column (a). Fractions 13 and 14 from (a) were re-applied to the column at different protein concentrations (b). The dotted line represents the expected elution volume of a dodecamer of TIP48/TIP49. The complex was incubated with EDTA or with ATP in $MgCl_2$ then analysed by SEC (c). The hexameric complex (from fraction 15 in (a)) was re-applied to the column and again eluted as a hexamer (d); the dotted line indicates the expected elution volume of a single hexamer of TIP48/TIP49. Fractions 14, 15 and 16 from (d), which contained single hexamers of TIP48/TIP49 were captured on Talon resin and eluted with imidazole. SEC fractions 12 to 16 from (d) and the eluant from the Talon resin (T Elu) were analysed by 12 % SDS PAGE stained with silver (e); MM indicates molecular markers of ~70 and ~55 kDa. The numbered arrows show the elution volumes of four molecular size standards in kDa and the void volume (V_0).

upon incubation with ATP in $MgCl_2$ suggested there may also have been some dissociation of the dodecameric complex into hexamers, although this was difficult to judge using this technique.

3.3.3 A small proportion of TIP48/TIP49-His_6 forms a single hexameric complex by SEC

Interestingly, both TIP48 and TIP49 were present in fraction 15, which corresponds to the elution volume for a hexamer. When fraction 15 (from Figure 3a) was re-applied to the column, it still eluted at the position of a hexamer and contained stoichiometrically equal proportions of TIP48 and TIP49 (Figures 3d and e). Fractions 14 to 16 were applied to Talon resin and eluted with imidazole. Both TIP49-His_6 and the untagged TIP48 were captured on the Talon column (T Elu in Figure 3.3e). These results confirm that fraction 15 contained a mixed TIP48/TIP49 oligomer, which is most likely to be a heterohexamer comprised of three monomers of TIP48 and three of TIP49. This presumed hexamer seemed to be a discreet species independent of the TIP48/TIP49 double hexamer. Nevertheless, the double hexamer of TIP48/TIP49 was the predominant species, displayed the highest ATPase activity (see Figure 3.2), and is therefore likely to be the form of the TIP48/TIP49 complex with the optimal enzymatic activity.

3.4 Analysis of TIP48 and TIP49 oligomers by velocity and equilibrium analytical ultracentrifugation

TIP48 and TIP49 clearly demonstrate different properties during SEC analysis, and TIP48 with TIP49 assemble into a dodecameric complex when co-expressed in bacteria. However, it is difficult to accurately assign specific oligomers to those observed by SEC for TIP48, and there seem to be several intermediates in the oligomerisation of TIP48 and the TIP48/TIP49 complex which could not be resolved by SEC. To investigate the oligomeric species of TIP48 further, and to elucidate the assembly of the TIP48/TIP49 complex, we analysed the

recombinant proteins by velocity and equilibrium analytical ultracentrifugation (vAUC and eAUC).

3.4.1 DCDT+ analysis of TIP48 and TIP49 vAUC data

AUC data were collected for TIP48 and TIP49 in EDTA at protein concentrations between 0.1 – 2.0 mg/ml and 0.1 – 1.5 mg/ml respectively at four rotor speeds. Data were initially analysed using the program DCDT+ (Philo, 2006), which uses 5-10 pairs of absorbance or interference scans to compute the *g(s*)* curves. The TIP48 data showed a broad peak at a sedimentation coefficient $s^0_{20,w}$ value of 3.9 S (Figure 3.4a). Better residuals for the *g(s*)* fits for TIP48-His_6 were occasionally obtained if a small amount of a higher sedimentation species was included (Figure 3.4a). This indicated that the data corresponded to a mixed population of TIP48 oligomers, which was consistent with the SEC data. Similar *g(s*)* curves were obtained for the TIP49 data, and the $s^0_{20,w}$ value was again determined as 3.9 S (Figure 3.4b). Again, the fit for TIP49 was occasionally better when a faster sedimentation species was included in the fits. The $s^0_{20,w}$ values were not affected by protein concentrations or rotor speeds (Figures 3.8a and b). In order to study the TIP48 oligomeric species, TIP48 was incubated with 0.5 mM ATP and 2 mM $MgCl_2$. This time, the AUC data analyses gave two distinct peaks. The main species sedimented at 11.0 S, while the smaller peak occurred at 3.9 S coinciding with the peak observed in the absence of nucleotides (Figure 3.4c). In contrast to this, but in agreement with the SEC data, the oligomeric state of TIP49 remained unchanged when incubated with adenine nucleotides and $MgCl_2$ (data not shown). Of particular interest is that both TIP48 and TIP49 in EDTA gave the same $s^0_{20,w}$ value for the predominantly monomeric species. In contrast, SEC gave an apparent molecular mass of 70 kDa for TIP48 while TIP49 showed a mass of 55 kDa.

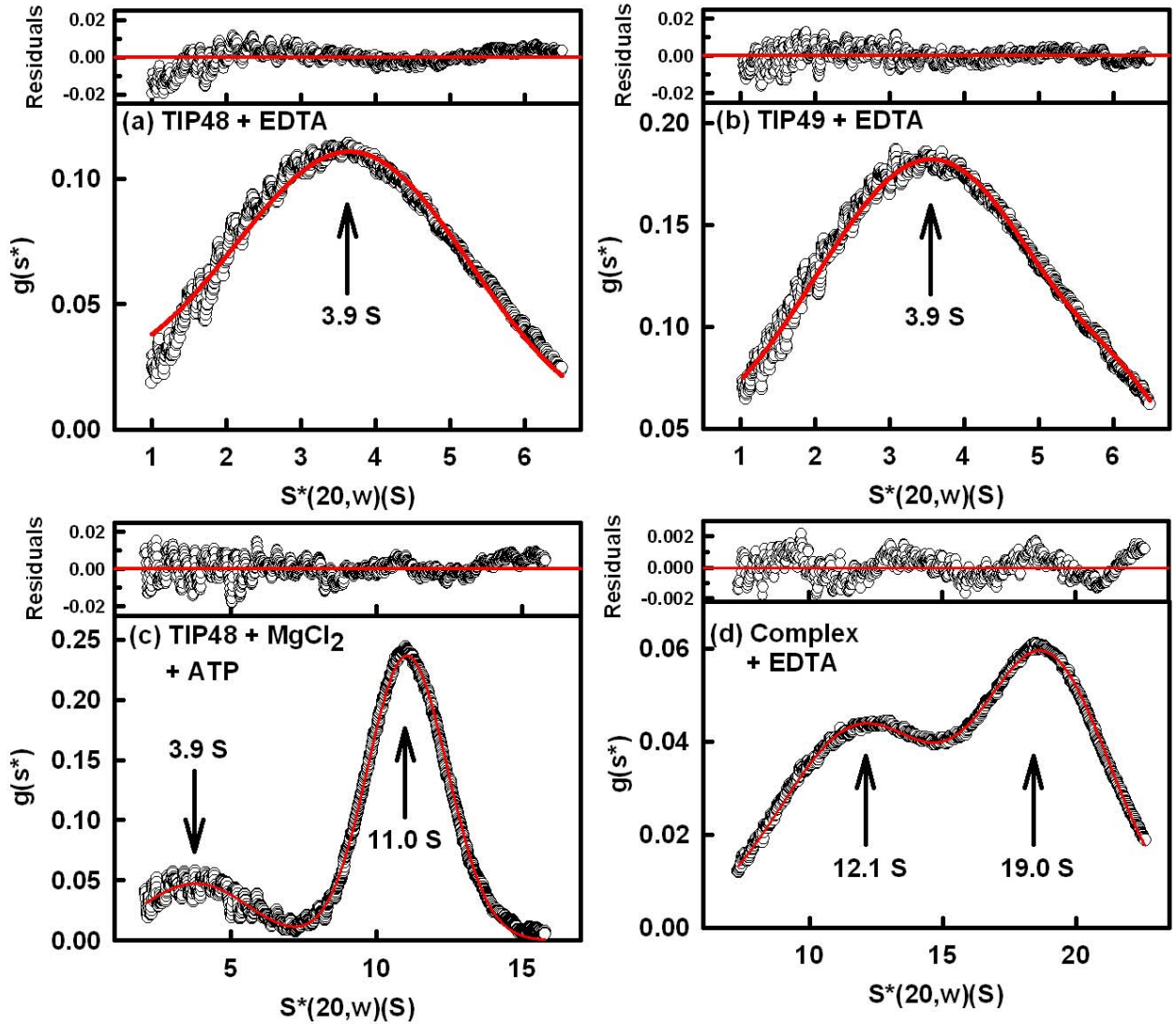

Figure 3.4. Time-derivative sedimentation velocity analyses of TIP48, TIP49 and their complex using DCDT+. All the data sets were based on interference optics. The arrows indicate the $s^*_{20,w}$ values determined for each fit. (a,b) The data for TIP48-His_6 at 0.65 mg/ml and His_6-TIP49 at 1.1 mg/ml, both in 0.1 mM EDTA, were obtained at 30,000 r.p.m. (c) The data for TIP48-His_6 at 0.80 mg/ml in the presence of 2 mM $MgCl_2$ and 0.5 mM ATP were obtained at 30,000 r.p.m. (d) Data for the TIP48/TIP49-His_6 complex at 0.4 mg/ml were acquired in the presence of 0.1 mM EDTA at 25,000 r.p.m..

3.4.2 SEDFIT analysis of TIP48 and TIP49 vAUC data

The SEDFIT analyses of the sedimentation velocity data fit the complete set of scans to derive the size distribution function *c(s)* (Schuck, 2000). From the interference data for TIP48 in EDTA, the *c(s)* plots indicated the existence of at least four discrete species. In 31 experiments, the major peak was consistently observed at 2.9 – 3.1 S, and further peaks at 4.5 – 5.0 S, 6.5 – 7.0 S and 10.0 – 10.5 S, which successively decreased in intensities (Figure 3.5a). The conversion of the *c(s)* curves to *c(M)* curves identified these species as monomers, dimers, trimers and hexamers, respectively, showing good agreement within error between the molecular mass associated with each peak and that calculated from the sequence (Table 3.1). Smaller peaks with sedimentation coefficients higher than 10 S were also evident, and a peak at 14.8 ± 0.5 S could be reproducibly detected (Table 3.1), although these were generally more difficult to identify. Significantly, when TIP48 was pre-incubated with either 0.5 mM ADP or ATP in 2 mM $MgCl_2$, the hexamer peak at 10.0 – 10.5 S became the predominant species, and the intensity of the monomer, dimer and trimer peaks decreased significantly (Figures 3.5b and c). This showed that ADP or ATP in the presence of $MgCl_2$ both induced TIP48 to form hexamers. In retrospect, the 70 and 400 kDa peaks in SEC experiments (Figure 3.1b) can now be assigned as monomer-dimers and hexamers respectively.

Analyses of the interference data for TIP49 collected in 0.1 mM EDTA under identical conditions, revealed similar sedimenting species as observed for TIP48. In 11 experiments, the 2.9 – 3.1 S peak was the principal species and minor peaks were observed at 4.5 – 5.0 S, 6.5 – 7.0 S and 10.0 – 10.5 S (Figure 3.5d). These species were also determined to be monomers, dimers, trimers and hexamers from the *c(M)* plots (Table 3.1). As with TIP48, a small peak was sometimes observed at 14.2 ± 0.5 S, which was calculated to be a nonamer. Unlike TIP48, however, there was no significant change in the proportions of these species when TIP49 was incubated with 0.5 mM ADP or ATP in the

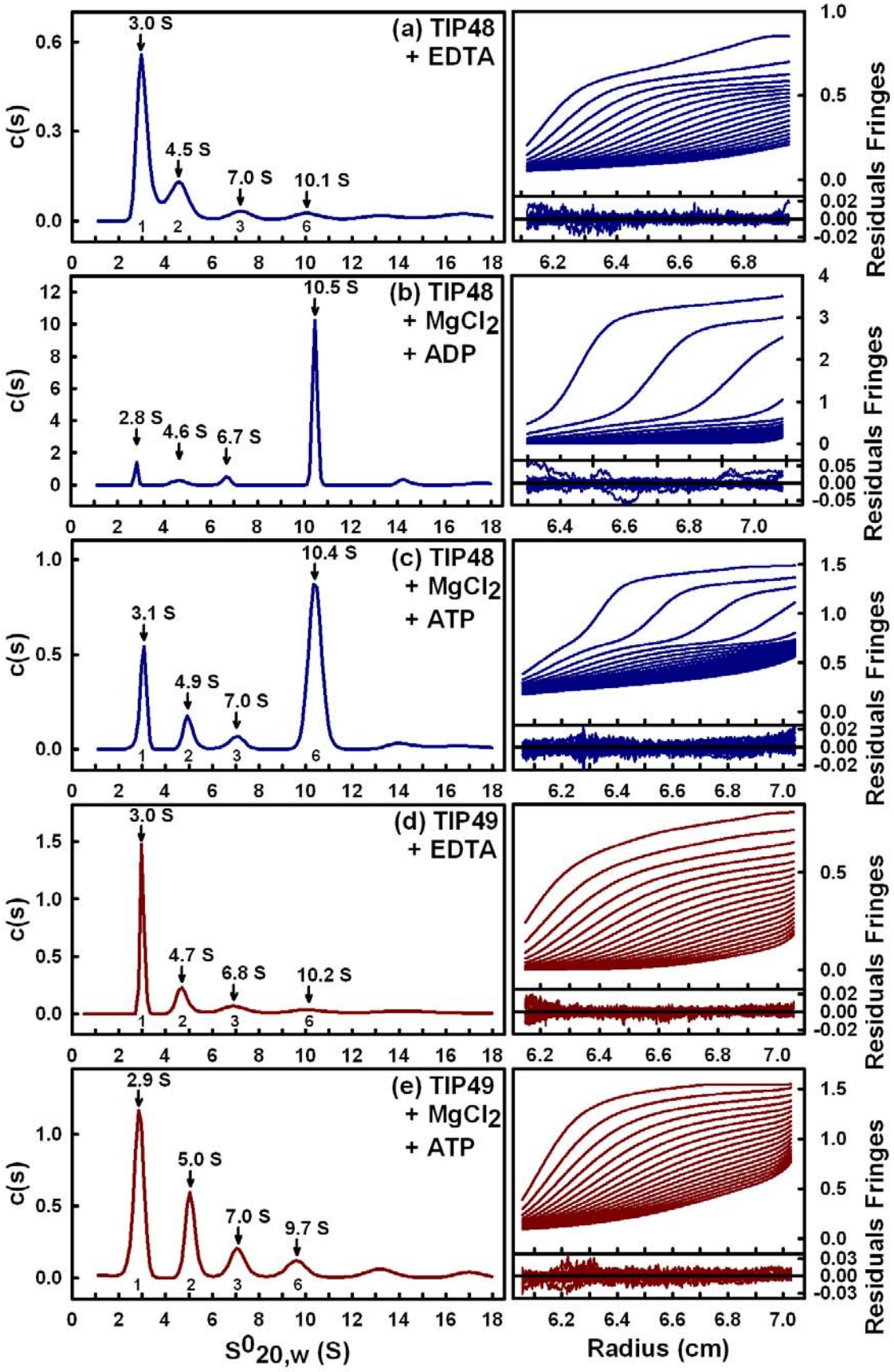
(a) TIP48
+ EDTA
3.0 S
4.5 S
7.0 S
10.1 S
(b) TIP48
+ MgCl2
+ ADP
10.5 S
2.8 S
4.6 S
6.7 S
(c) TIP48
+ MgCl2
+ ATP
10.4 S
3.1 S
4.9 S
7.0 S
(d) TIP49
+ EDTA
3.0 S
4.7 S
6.8 S
10.2 S
(e) TIP49
+ MgCl2
+ ATP
2.9 S
5.0 S
7.0 S
9.7 S
c(s)
Residuals Fringes
S0 20,w (S)
Radius (cm)

Figure 3.5. *c(s)* distribution analyses of sedimentation velocity data for TIP48 and TIP49. The figures demonstrate representative interference optics data sets at rotor speeds of 30,000 r.p.m. Arrows indicate the $s^0_{20,w}$ value for each discrete peak calculated using SEDFIT. (a) TIP48-His_6 at 1.2 mg/ml in 0.1 mM EDTA. (b) TIP48-His_6 at 1.2 mg/ml in 2 mM $MgCl_2$ and 0.5 mM ADP. (c) TIP48-His_6 at 0.8 mg/ml in 2 mM $MgCl_2$ and 0.5 mM ATP. (d) His_6-TIP49 at 0.8 mg/ml in 0.1 mM EDTA. (e) His_6-TIP49 at 1.5 mg/ml in 2 mM $MgCl_2$ and 0.5 mM ATP.

Oligomer	Monomer	Dimer	Trimer	Hexamer	Intermediate	Dodecamer
Number of experiments	31	29	27	29	16	
TIP48-His_6 sequence mass (kDa)	52	104	156	313	469	616
TIP48-His_6 *c(M)* mass (kDa)	47 ± 14	92 ± 24	160 ± 39	303 ± 76	500 ± 104	n.o.
TIP48-His_6 *c(s)* (S)	3.0 ± 0.2	4.7 ± 0.3	6.9 ± 0.4	10.3 ± 0.4	14.8 ± 0.5	n.o.
Number of experiments	11	11	11	10	9	
His_6-TIP49 sequence mass (kDa)	52	105	157	314	471	628
His_6-TIP49 *c(M)* mass (kDa)	49 ± 8	97 ± 20	169 ± 36	299 ± 30	491 ± 79	n.o.
His_6-TIP49 *c(s)* (S)	3.0 ± 0.1	4.7 ± 0.4	6.8 ± 0.5	10.1 ± 0.4	14.2 ± 0.5	n.o.
Number of experiments	11	11	11	11	11	11
TIP49 / TIP48-His_6 sequence mass (kDa)	51	102	153	307	460	614
TIP49 / TIP48-His_6 *c(M)* mass (kDa)	72 ± 9	154 ± 14	265 ± 35	406 ± 78	594 ± 133	975 ± 196
TIP49 / TIP48-His_6 *c(s)* (S)	3.2 ± 0.2	5.2 ± 0.2	7.3 ± 0.3	10.3 ± 0.2	13.0 ± 0.5	18.4 ± 0.4
Modelled sedimentation coefficient Hexamer 1 (S)	3.3	5.2	6.8	10.6	9mer = 14.7	18.4
Modelled sedimentation coefficient Hexamer 2 (S)	3.3, 3.7	5.6	7.2	11.5	n.o.	n.o.

Table 3.1. Summary of AUC interference data analyses by SEDFIT. n.o. – not observed

presence of 2 mM $MgCl_2$ (Figure 3.5e; ADP data not shown). The occurrence of dimers, trimers and hexamers of TIP49 revealed by the AUC data clearly shows that TIP48 and TIP49 have similar oligomeric forms in the absence of cofactors. Even though the AUC data show similar sedimentation profiles for TIP48 and TIP49 in the absence of cofactors, they also differed, as only TIP48 forms hexamers in the presence of ATP or ADP and Mg^{2+}.

3.4.3 SEDPHAT analysis of TIP48 eAUC data

To extend the sedimentation velocity analyses, sedimentation equilibrium experiments were carried out to determine the molecular mass of the nucleotide dependent oligomer of TIP48. Individual SEDPHAT fits of the interference data were initially calculated. Fits were generated on the assumption of a single species model using concentrations between 0.3 mg/ml and 1.3 mg/ml and four rotor speeds. Global fits for each of the ADP or ATP data sets were performed using models based on a single species and others based on various equilibria between the species observed by sedimentation velocity. The fits with the best reduced χ^2 values were obtained with a single species fit (Figure 3.6). Mass values of 321 kDa with ADP present and 310 kDa with ATP present were obtained, which correspond well with masses of 313 kDa calculated from the composition of the hexamer (Table 3.1). Even with this, a slight tendency towards higher oligomers was indicated by the small deviation of the residuals at the larger radius values (McRorie and Voelker, 1993).

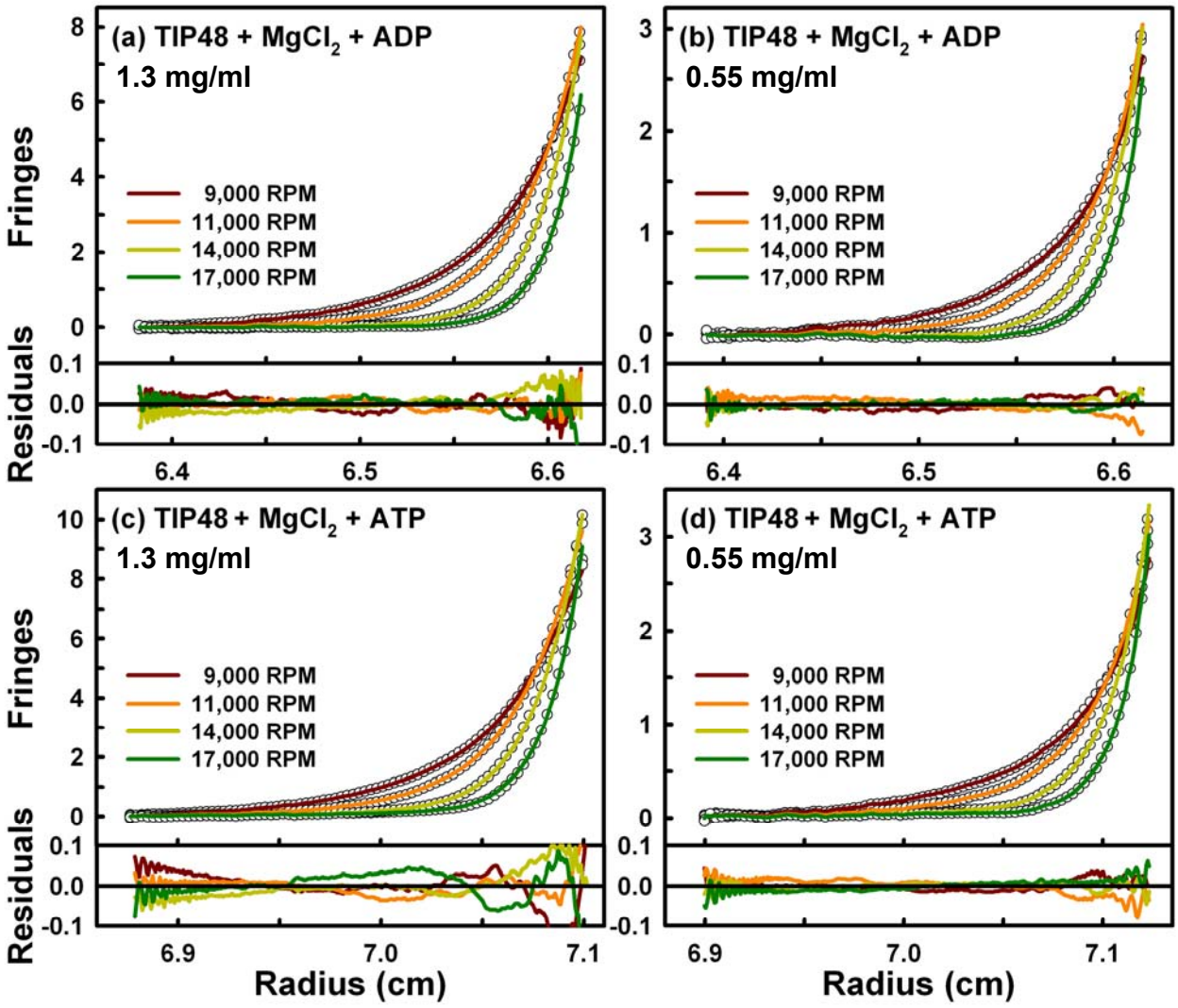

Figure 3.6. Sedimentation equilibrium analyses of TIP48 with ADP and ATP. Global fits of TIP48 in Mg^{2+} and either ADP or ATP at 20 ^{o}C were performed in a concentration series from 0.3 mg/ml to 1.3 mg/ml using rotor speeds of 9k r.p.m., 11k r.p.m., 14k r.p.m. and 17k r.p.m. (a,b) The concentrations of 1.3 mg/ml and 0.55 mg/ml respectively in the presence of ADP are shown, and led to a molecular mass of 321 kDa. (c,d) The concentrations of 1.3 mg/ml and 0.55 mg/ml respectively in the presence of ATP are shown, and led to a molecular mass of 310 kDa.

3.5 Analysis of the TIP48/TIP49 complex by velocity analytical ultracentrifugation (vAUC)

The TIP48/TIP49 complex was analysed by AUC after isolation of high molecular mass fractions (between 12.5 ml to 14.5 ml - fractions 13 and 14 - in Figure 3.3a) using a Superose 6 HR SEC column. Data were collected at protein concentrations ranging from 0.1 – 0.8 mg/ml. When analysed by DCDT+, the complex comprised of at least two major species: one with an average sedimentation coefficient of 11.2 S and one of 19.1 S (Figure 3.4d). The 11.2 S species is likely to be a hexamer, while the 19 S species is most likely to be a dodecamer. The peaks were not affected by change in concentration or rotor speed used (Figure 3.8c).

When the interference data for the preformed TIP48/TIP49 complex were analysed by SEDFIT, a series of oligomeric species were observed (Figure 3.7). In the presence of EDTA, a 3.0 – 3.3 S peak was attributed to the monomer of either TIP48 or TIP49. Prominent peaks at 4.5 – 5.0 S, 6.5 – 7.0 S and 10.0 – 10.5 S were again observed, consistent with dimers, trimers and hexamers seen with the individual proteins (Table 3.1). A major peak was observed at 18 – 19S, which corresponded to a high molecular mass form of the TIP48/TIP49 complex (Figure 7a). Intermediates between this form and the hexameric peak were observed, but difficult to accurately measure, due to their heterogeneity. Since the pre-formed TIP48/49 complex was a high molecular mass fraction isolated by SEC, the range of oligomeric species observed is likely to reflect the dissociation of the complex.

As with SEC experiments, the presence of 0.5 mM ADP or ATP in 2 mM $MgCl_2$ increased the proportion of the hexameric peak relative to the other species, although the 18 – 19 S peak was still prominent (Figures 7b and 7c). This is probably due to hexamerisation of free TIP48 in the presence of ADP or ATP, but

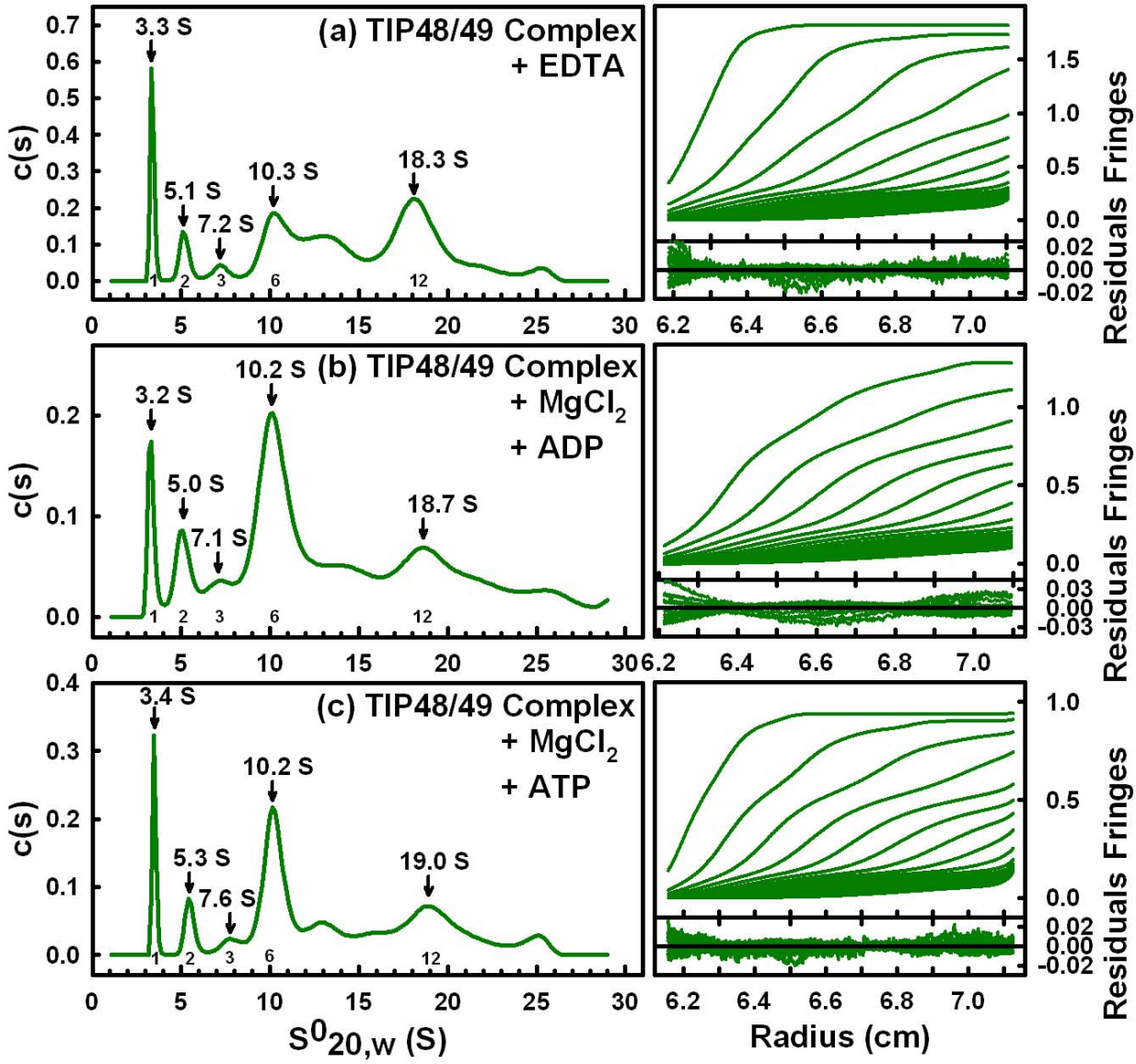

Figure 3.7. *c(s)* distribution analyses of sedimentation velocity data for the TIP48/TIP49-His$_6$ complex. Arrows indicate the $s^0_{20,w}$ value for each discrete peak calculated using SEDFIT and observed in representative interference optics data sets at rotor speeds of 25,000 r.p.m.. (a) The TIP48/TIP49 complex at 0.8 mg/ml in 0.1 mM EDTA. (b) The TIP48/TIP49 complex at 0.5 mg/ml in 2 mM $MgCl_2$ and 0.5 mM ADP. (c) The TIP48/TIP49 complex at 0.5 mg/ml in 2 mM $MgCl_2$ and 0.5 mM ATP.

could also be due to some dissociation of dodecameric TIP48/TIP49 complex into individual hexamers.

The *c(M)* plots for the 18 - 19 S species showed masses considerably higher than that predicted for a double hexamer (Table 3.1). However, the *c(M)* plots were generated with a single frictional ratio (f/f_0) applied to all species in the observed S range, which does not allow correct calculation of mass if several species are present. Therefore, masses obtained from *c(M)* plots are not accurate enough to attribute specific oligomeric states to the complex without predicting sedimentation coefficients from published structures. As shown in our modelling below (Figure 3.10), this 18 – 19 S species is consistent with a dodecamer of TIP48/TIP49 (predicted mass of 614 kDa). As with SEC, small amounts of higher molecular mass species of the complex were also seen. In addition, the weaker resolution of the peaks in the *c(s)* plots between hexamers and dodecamers indicated that several intermediate forms of the TIP48/TIP49 complex exist.

3.6 Oligomeric species of TIP48, TIP49 and their complex show no concentration dependence

In order to summarise the three AUC studies of TIP48, TIP49 and their complex, the sedimentation coefficients were plotted against protein concentrations (Figure 3.8). All five distinct species observed using SEDFIT for both TIP48 and TIP49 showed no concentration dependence (Figures 3.8d and e). The TIP48/TIP49 complex comprised of six peaks which were not affected by concentration (Figure 3.8f). The averaged sedimentation coefficients for each species from Figure 3.8 are summarised in Table 3.1.

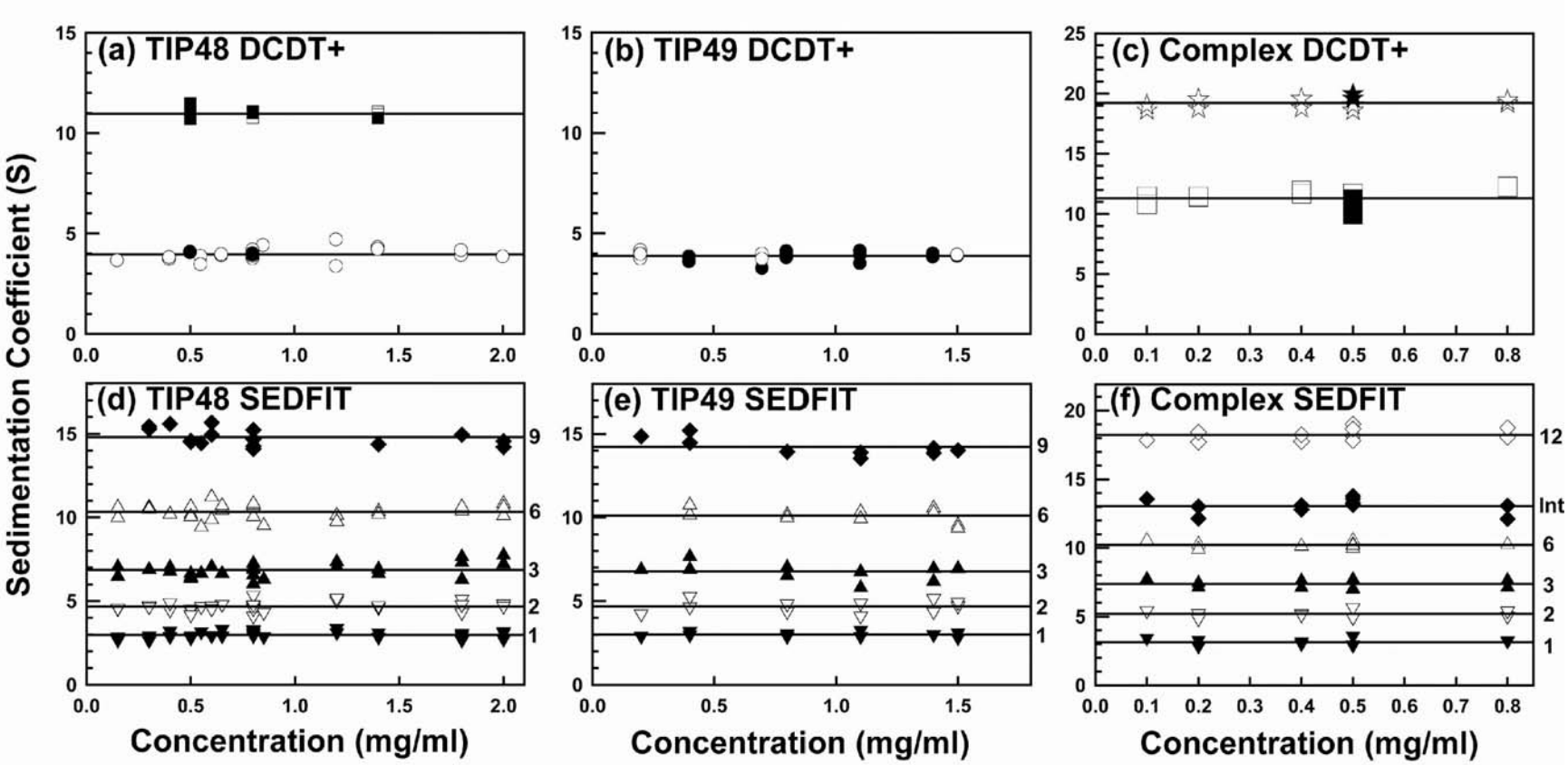

Figure 3.8. Concentration dependence of the sedimentation coefficients for TIP48, TIP49 and their complex by DCDT+ and SEDFIT. The three upper panels (a,b,c) summarise the DCDT+ analyses, while the lower three panels (d,e,f) summarise the corresponding SEDFIT analyses. The fitted regression lines summarise the sedimentation coefficients for each observed species.

(a,b,c) For each of the species, the *g(s*)* data with no nucleotide co-factors are denoted by ○ (monomers), □ (hexamers) or ✩ (double hexamers) , while the *g(s*)* data in the presence of ADP or ATP are denoted by ●, ■ or ★.

(d,e,f,) The corresponding c(s) analyses resulted in the resolved peaks of Figures 3.5 and 3.7. The symbols in alternation (▼;▽;▲;△;◆;◇) show the distinct oligomeric species that were clearly resolved in each *c(s)* plot. The number of monomers assigned to each peak is shown at the right (either 1, 2, 3, 6, 9, 12 or unassigned intermediate, Int).

3.7 vAUC absorbance data for TIP48, TIP49 and their complex

As a control for the interference data sets, the absorbance data sets for TIP48 and TIP49 and the complex were also analysed. These were limited in their scope because ADP and ATP have high absorbance coefficients at the 280 nm wavelengths, which would interfere with protein detection at the same wavelength. The absorbance analyses for TIP48 and TIP49 in EDTA individually displayed monomers, dimers, trimers and hexamers as successively smaller peaks (Figures 3.9a and b). The absorbance analyses for the TIP48/TIP49 complex in EDTA also showed monomers, dimers and trimers. Furthermore, the hexameric peak was prominent compared with analyses of the individual proteins, and a large peak was observed at 18.5 S, consistent with a double hexamer of TIP48/TIP49 (Figure 3.9c). Thus, AUC absorbance data agree well with the corresponding interference analyses, although the resolution of the *c(s)* plots for absorbance data was reduced compared with data sets from interference optics (Figure 3.9).

3.8 Calculation of sedimentation coefficients from structures of TIP49 and the TIP48/TIP49 complex

To confirm that the oligomeric species of TIP48 and TIP49 had been determined correctly, the crystal structure of TIP49 and the EM reconstruction of the TIP48/TIP49 complex were used to calculate sedimentation coefficients using HYDROPRO and HYDROMIC (Figure 3.10). The calculations assumed that the structures of TIP48 and TIP49 were similar to each other, based on the sequence and secondary structure comparison; see Appendix Figure A1 and (Putnam et al., 2001). Two hexameric rings of TIP49 were generated from the crystal structure of TIP49 (See Chapter 1.3.3 and Figure 1.4): one corresponded to a hexamer of

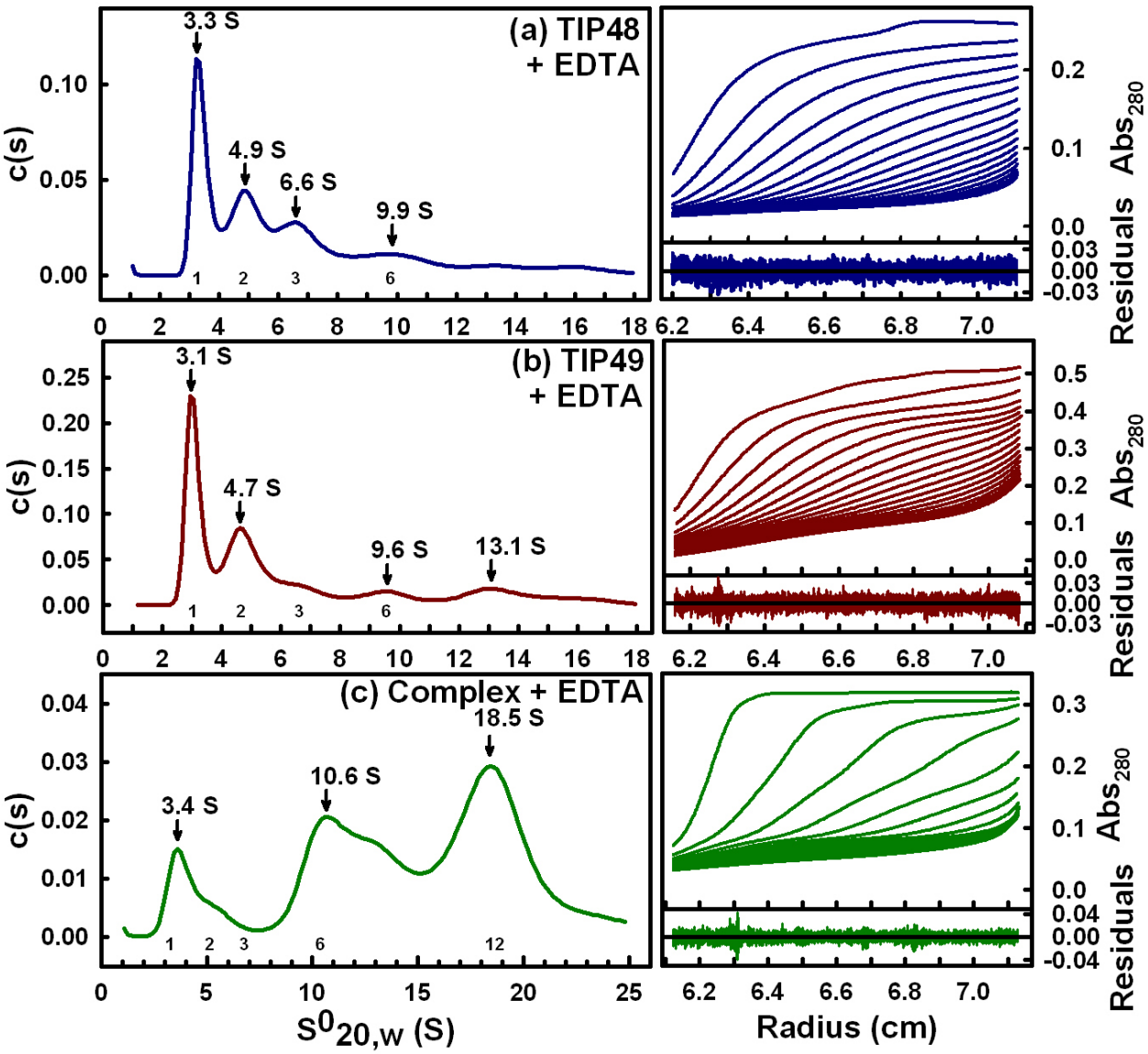

Figure 3.9. *c(s)* distribution analyses of sedimentation velocity data for TIP48-His$_6$, His$_6$-TIP49 and the TIP48/TIP49-His$_6$ complex. Arrows indicate the $s^0_{20,w}$ value for each discrete peak calculated using SEDFIT and observed in representative absorbance optics data sets. (a) TIP48 at 0.3 mg/ml in 0.1 mM EDTA at a rotor speed of 30,000 r.p.m. (b) TIP49 at 0.4 mg/ml in 0.1 mM EDTA at a rotor speed of 30,000 r.p.m. (c) The TIP48/TIP49-His$_6$ complex at 0.8 mg/ml in 0.1 mM EDTA at a rotor speed of 25,000 r.p.m.

monomer A (Hexamer 1), the other was a 3-fold repetition of monomers B and C (Hexamer 2) (Gorynia et al., 2006; Matias et al., 2006). The predicted sedimentation coefficients from Hexamer 1 gave 3.3 S, 5.2 S, 6.8 S and 10.6 S for the monomer, dimer, trimer and hexamer forms of TIP49 respectively (Table 3.1). These predicted sedimentation coefficients agree well with the observed sedimentation coefficients for TIP48 and TIP49 and were better than predictions for Hexamer 2, which showed slightly higher values (Table 3.1).

Further calculations using Hexamer 1 showed that a double hexamer would have a sedimentation coefficient of 18.4 S. This was formed by the most compact arrangement of two hexameric structures placed in a head-to-tail arrangement. This arrangement would permit the growth of further oligomers such as an 18-mer. The sedimentation coefficient of the TIP48/TIP49 dodecamer was calculated from its electron microscopy map, and this gave 19.0 S in good agreement with the observed value of 18.4 S. Thus, the sedimentation coefficients of the oligomeric forms of the TIP48/TIP49 complex could be replicated by the modelling based on the crystal structure of TIP49.

3.9 Discussion

The sedimentation velocity studies of TIP48, TIP49 and their complex provide new insights into the oligomeric forms of these proteins, most notably the oligomeric intermediates of the TIP48/TIP49 complex. The similarities in sedimentation profiles of TIP48 and TIP49 indicate that the two proteins have similar solution structures in the absence of cofactors.

Although monomers were the predominant form in the absence of co-factors, the AUC data showed that both TIP48 and TIP49 also formed dimers, trimers and hexamers as minor species. While DCDT+ analysis of TIP48 and TIP49 gave sedimentation coefficients of 3.9 S for both proteins, the SEC results showed that TIP49 eluted only as a monomer of 55 kDa while TIP48 eluted as a 70 kDa peak with higher oligomers. SEC observations may result from different kinetic rates

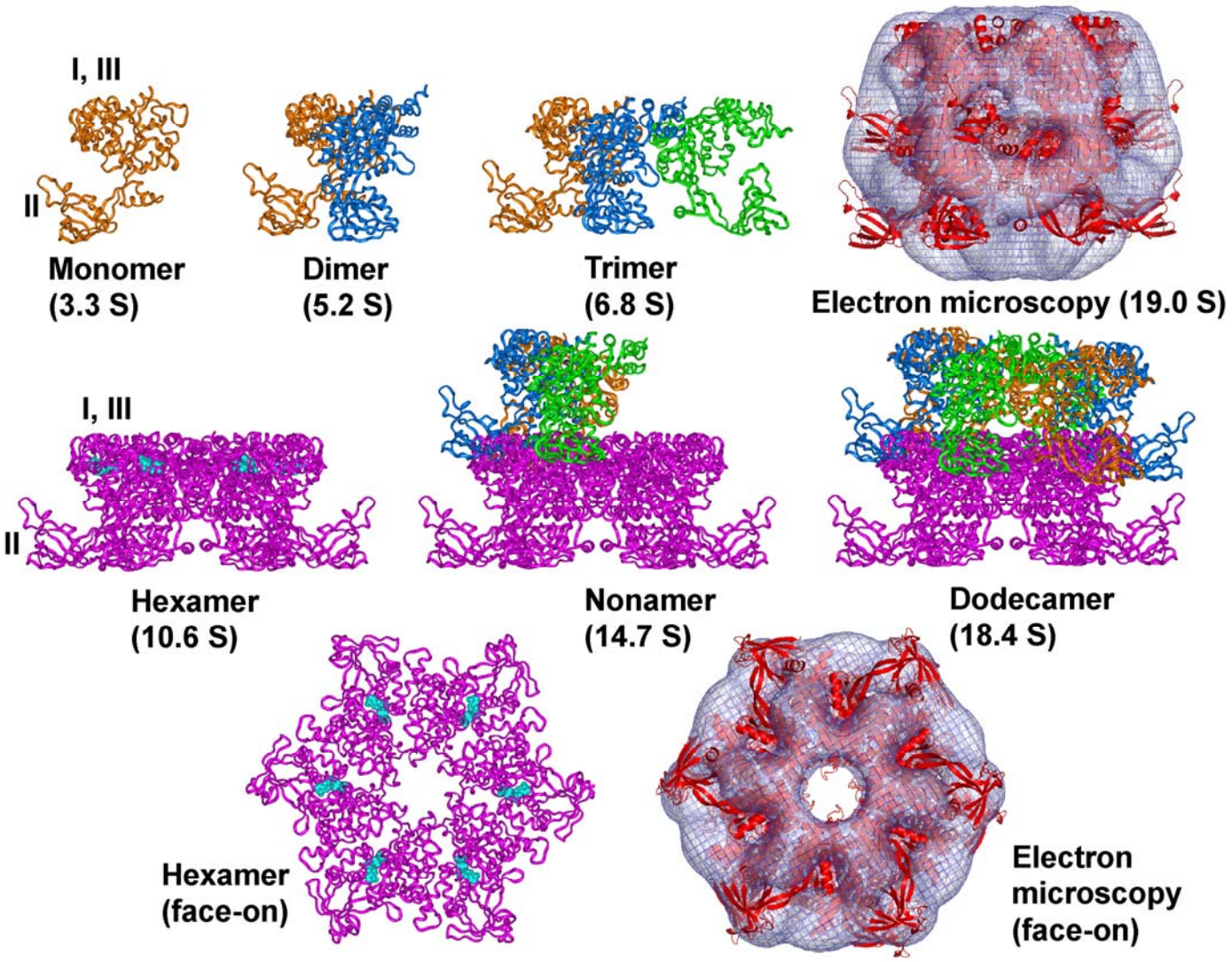

Figure 3.10. Oligomeric forms of TIP48 and TIP49 used for modelling predictions of the sedimentation coefficients. The crystal structure of TIP49 was used to predict sedimentation coefficients of different oligomers. Sedimentation coefficients are shown in brackets below each structure. In the top row, the monomers in the dimer and trimer forms are shown as orange, blue and green ribbon traces. In the middle row, the hexamer is shown in magenta with the six bound ADP molecules in blue, and the two trimers that were added to form either the nonamer or dodecamer are shown in the same colours used in the top row. The electron density reconstruction, generated by negative staining electron microscopy analysis of the TIP48/TIP49 complex, is also shown. The modelled TIP49 dodecamer shown, as a red ribbon trace and EM reconstruction are overlaid to highlight their differences in structure. In the bottom row, the hexamer and electron microscopy models are viewed after a 90^{o} rotation in order to reveal the void at the middle of the hexameric axis of symmetry. Domains are indicated using roman numerals.

for self-association in the conditions of their elution (Lou et al., 2004). A slower disassociation rate for TIP48 oligomers may explain the observed 70 kDa elution peak for this when compared to that at 55 kDa for TIP49. Both the AUC and SEC data showed that TIP48 hexamer formation was induced by adenine nucleotides and Mg^{2+}, while the oligomeric state of TIP49 was not affected. These data firmly point to similarities in the physical properties of TIP48 and TIP49, despite the differences seen by the more qualitative SEC approach. This similarity is corroborated by sequence and secondary structure comparisons.

The AUC analyses show that in EDTA, TIP48/TIP49 complexes showed complex sedimentation profiles and peaks of molecular masses that were higher than hexamers observed for TIP48 or TIP49 individually. These data were collected using a high molecular mass fraction of the complex isolated from a SEC column, therefore the AUC profile shows the dissociation of the TIP48/TIP49 complex. The stability of the TIP48/TIP49 double hexamer was slightly reduced by incubation with ATP or ADP and Mg^{2+}, as there was a shift to hexameric protein. This may be interpreted as the complex falling apart into hexamers, or monomeric TIP48 hexamerising when bound to nucleotides; it is difficult to dissect to what degree these contribute to the change in the profiles in Figure 3.7.

As these recombinant proteins are being studied outside of a cellular environment, their stability under the conditions tested may not be optimal. It is probable that other cellular factors stabilise this complex *in vivo*. Indeed, the TIP48/TIP49 complex is typically a component of large multi-protein complexes, and it is most likely that this environment is required for the most favourable complex stability. However, the heterogeneity of the TIP48/TIP49 complex by AUC may be misleading, as the data were gathered at high centrifugal force over several hours. In contrast, the SEC data showed a more stable complex with a prominent dodecameric peak; this technique is less intense than the AUC employed.

Oligomers higher than a dodecamer were observed at high protein concentration by SEC and with all AUC analyses. This could be interpreted as self association of the complex, with progressive rings stacking on the double hexamer. This would suggest a head-to-tail orientation of the complex, and would allow further assembly of hexamers onto the dodecameric complex. Furthermore, in the dodecameric EM structure, the orientation of the two rings was also tentatively interpreted as being head-to-tail (Dr. Petra Wendler, personal communication)(Puri et al., 2007).

In comparison to our AUC data, a sedimentation equilibrium study of *S. cerevisiae* TIP48/TIP49 determined a mass of 313 kDa for the complex (Gribun et al., 2008). Together with EM analysis of the complex showing a hexameric ring, this result was used to propose that yTIP48 and yTIP49 formed a single mixed hexameric ring with no further oligomers. Since the yeast proteins appear to differ biochemically from the human TIP49 and TIP48, their quaternary organisation may also be different (Gribun et al., 2008). It should be noted, however, that only absorbance optics were used to study the yeast complex in the presence of ADP, and the observed intensities above 1.5 may be saturated, meaning that the molecular mass of 313 kDa may be underestimated (Cole et al., 2008). More recently, a double hexameric configuration for yTIP48/TIP49 was demonstrated by cryo-EM (Torreira et al., 2008). The conflicting data for the yeast homologues may suggest that different oligomeric forms of TIP48 and TIP49 exist in the cell, which may in part regulate their disparate functions. We observed a double hexamer of human TIP48/TIP48 with a small proportion of mixed single-hexamers, supporting this idea. It would be interesting to delineate which oligomers of TIP48 and TIP49 are associated with which functions, and how these are co-ordinated.

3.8.1 Assembly mechanisms of TIP48 and TIP49 oligomers

The clarification of oligomers and intermediates by AUC suggests an assembly pathway for the TIP48/TIP49 complex. Dimers, trimers and hexamers were the

prevalent intermediate species of the TIP48/TIP49 double hexamer. In addition to this, 14.7 S nonamers were detected in small amounts by AUC when these proteins were analysed individually. In contrast, unresolved intermediate species significantly lower than 14.7 S were detected when the TIP48/TIP49 complex was analysed (Figures 3.7, 3.8 and Table 3.1), although these were less resolved and there seemed to be several different intermediates. Compared with the 14.7 S putative nonamers, the TIP48/TIP49 complex intermediates had S values with an average of around 13 S. These intermediates could be consistent with octamers, where dimers are stacked on the hexameric ring. One could hypothesize that trimers are important building blocks for the individual hexamers, whereas dimers are important in assembling the double hexamer. One interpretation could be that TIP48 and TIP49 heterodimers are the first step in forming the dodecamer; alternatively, the small amounts of TIP48 hexamers could stabilise TIP49 hexamers by forming the dodecamer (Figure 3.11). The difference in assembling individual hexamers and the double hexamer could be an important way of regulating the assembly of the TIP48/TIP49 double hexamer, as hexamerisation of TIP48 in the presence of nucleotides could limit heterodimers, and therefore the formation of the TIP48/TIP49 complex. However, these interpretations are currently only speculative, as our AUC modelling analysis of the TIP48/TIP49 complex does not allow us to distinguish between models of the complex consisting of two homohexamers or two heterohexamers. Indeed, the composition of the rings of the TIP48/TIP49 double hexamer is something we are currently addressing.

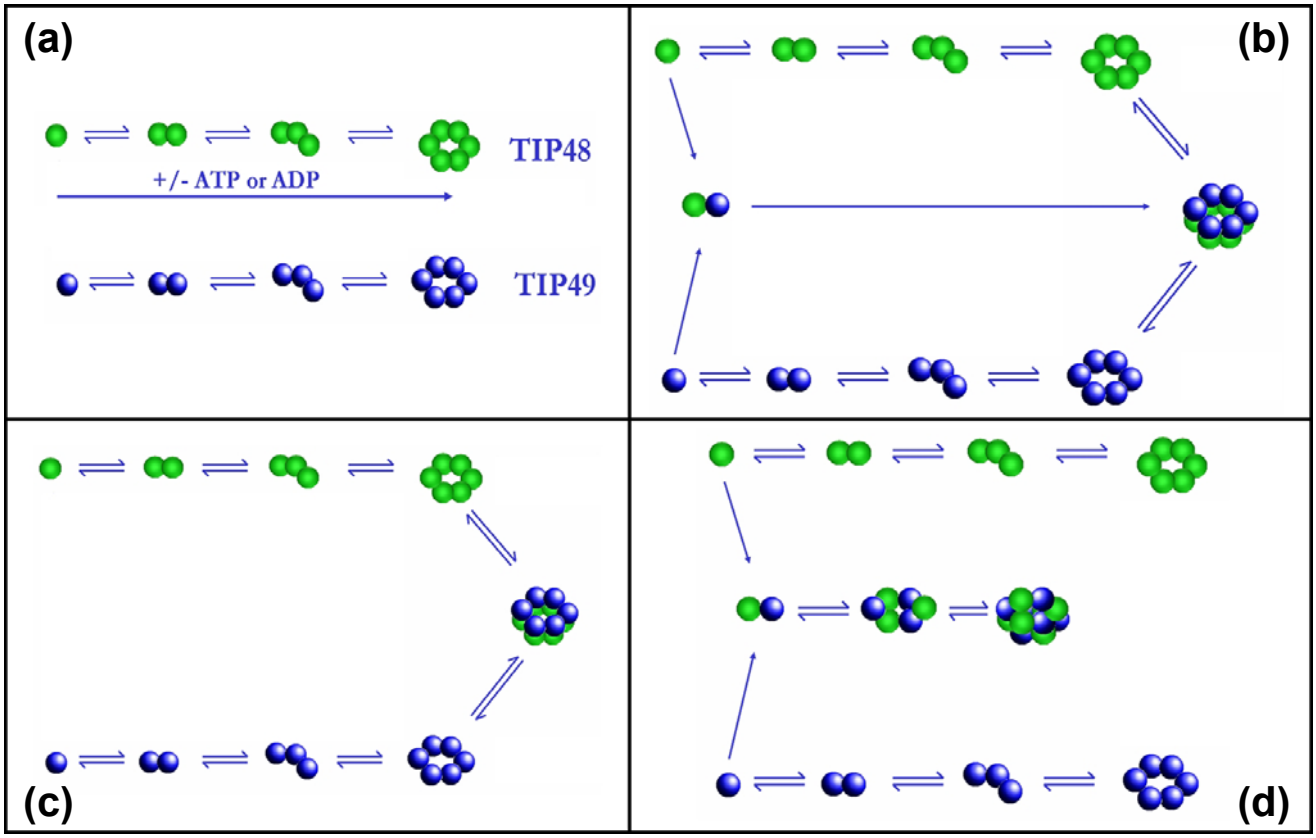

Figure 3.11. Hypothesised assembly mechanisms of TIP48 and TIP49 oligomers. TIP48 (green) and TIP49 (blue) form hexamers via dimer and trimer intermediates (a). TIP48 hexamers are nucleotide inducible, TIP49 hexamers are not. Heterodimers may drive the formation of the double hexamer (b); alternatively, homo-hexameric rings may bind each other to form the double hexamer (c). A mixed-ring hexamer may be formed from heterodimers (d).

Chapter 4

Exploring the Function of Domain II of TIP48 and TIP49 Using Mutants

4.1 Introduction

Since their initial identification, high sequence conservation for both TIP48 and TIP49 has been shown between all eukaryotic species (see Chapter 1.3.1). In archaea, there is evidence of a single homologue in all crenarchaeota, which indicates that TIP48 and TIP49 diverged from a common ancestor, and were inherited by all modern eukaryotes. The closest homologue of TIP48 and TIP49 in bacteria is RuvB: the AAA^+ motor protein that facilitates branch migration as part of the RuvABC system; however, to date, there is no evidence that TIP48 and TIP49 facilitate branch migration in eukaryotes, and the hypothesis that they act on DNA is controversial. Dispite the differences between these homologues, it is clear that they are linked by the fold of their ATPase domains, which are highly conserved between the eukaryotic, archaeal and bacterial homologues of TIP48 and TIP49. RuvB has a three domain structure, where Domains I and II are responsible for ATPase activity, and a DNA binding domain is present at the C-terminus; this DNA binding domain is not present in TIP48 or TIP49. Conversely, a novel domain of unknown function is present in TIP48 and TIP49 but not RuvB; this domain is inserted in Domain I between the Walker A and Walker B motifs, and is linked to Domain I by two anti-parallel β-strands (Figure 4.1).

It has been suggested that Domain II of TIP48 and TIP49 could be involved in DNA/RNA interactions, modulating protein-protein interactions or regulating ATPase activity and oligomerisation; however, no published experimental data has confirmed these hypotheses. To gain insight into the functions of Domain II, TIP48 and TIP49 mutants were expressed and purified based on the *liebeskummer* mutation (*lik*) of TIP48 and mutants lacking Domain II. The effects of these mutations on the oligomerisation, ATPase activity and protein interactions of TIP48 and TIP49 could give important insights into the functions of Domain II, as well as the full length proteins. As TIP48 and TIP49 are critical for

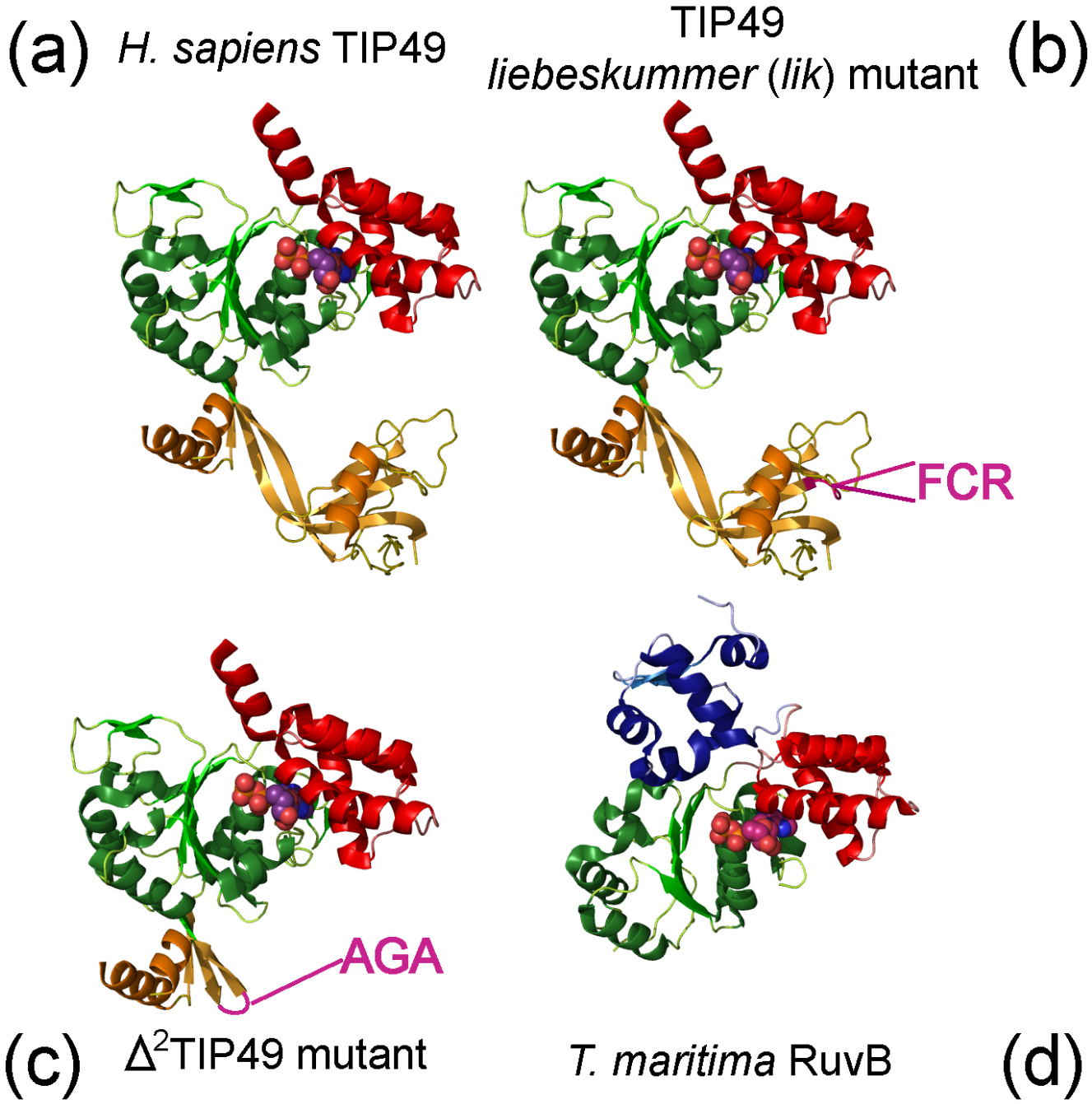

Figure 4.1. Putative structures of TIP49 Domain II mutants. Cartoons of the crystal structures of *Homo sapiens* TIP49 (Matias et. al, 2006) (a) and *Thermotoga maritima* RuvB (Putnam et. al., 2001) (d) are shown with equivalent domains in corresponding colours. TIP49 Domains I (Green) and III (Red) are equivalent to Domains I (Green) and III (Red) in RuvB. TIP49 Domain II (Gold) has no equivalent in RuvB; Domain III (Blue) in RuvB has no equivalent in TIP49. Mutations are highlighted in purple for the TIP49 *liebeskummer* (FCR: Phe-Cys-Arg) insertion (b) and truncation mutant,

oncogenic transformation in certain cancers, small molecule inhibitors could target this activity, possibly leading to novel cancer drugs. Individually, TIP48 and TIP49 have very low ATPase activity. This activity increases when the proteins assemble into a heteromeric complex; however, an activity of 1 mole of ATP hydrolysed per monomer per minute is still too low for high throughput screening of small molecule inhibitors of the ATPase activity of TIP48 and TIP49. If Domain II regulates ATPase activity, Domain II mutants of TIP48 and TIP49 may have increased ATPase activity. A more robust ATPase activity could potentially lead to more efficient screening of inhibitors of the ATPase activity of TIP48 and TIP49.

4.2 Construction of TIP48 and TIP49 Domain II mutants

4.2.1 Cloning of *lik*TIP48 and *lik*TIP49 mutants

The Zebrafish *liebeskummer* (*lik*) mutation confers a phenotype of heart hyperplasia (see chapter 1.4.3). The reason for this phenotype is mis-splicing of Zebrafish TIP48 mRNA, resulting in a three residue insertion after Glycine[191]. Further characterisation of *liebeskummer* mutants suggested that the product of the mutated gene - *lik*TIP48 - forms aberrant complexes and has de-regulated ATPase activity (Rottbauer et al., 2002). We wanted to test this hypothesis *in vitro*, as de-regulation of oligomerisation and ATPase activity could help elucidate the mechanism of TIP48 activity. The remarkable conservation between Zebrafish and human TIP48 encouraged us to attempt to express and purify the *H. sapiens* equivalent of *lik*TIP48, to study its biochemical properties. Moreover, the *lik* mutation occurs in a region conserved between TIP48 and TIP49, implying the three residue insertion could have the same effect on hTIP49 functions. Sequence alignment between Zebrafish and *Homo sapiens* TIP48 and TIP49 and the crystal structure of TIP49 led us to design *liebeskummer* mutants of TIP48 and TIP49 with the three amino acid (Phe; Cys; Arg) insertion after Gly^{190} in hTIP48 and Gly^{188} in hTIP49 (Figures 4.1b and 4.2). pET21b-TIP48-His_6 and pET15b-His_6-TIP49 were mutagenised using PCR to generate bacterial

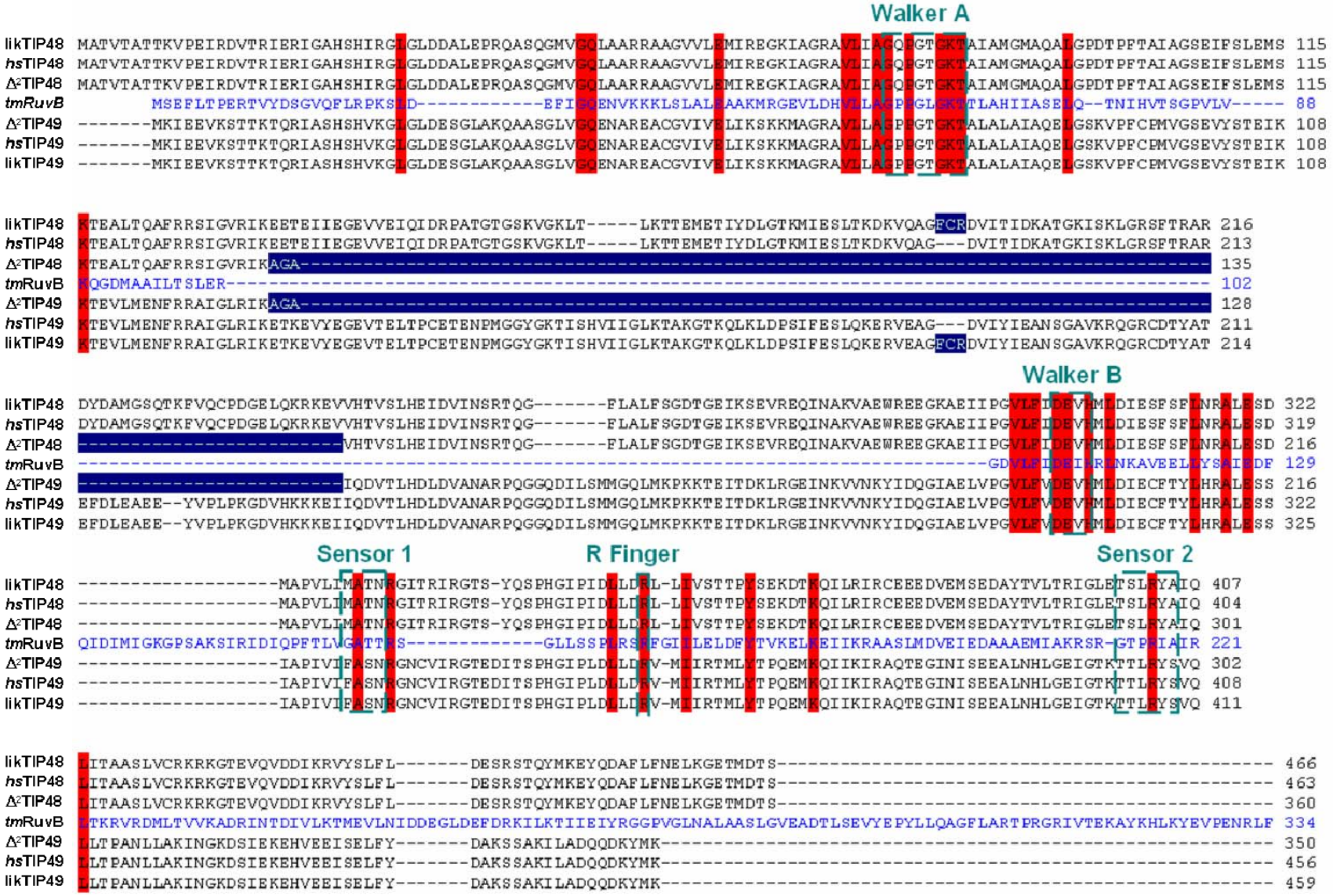

Figure 4.2. Amino acid sequence alignment of TIP48 and TIP49 domain II mutants. TIP48, TIP49, RuvB and the Domain II mutants *lik* and Δ^2 are shown, with mutated regions highlighted in dark blue. Residues conserved across the three wild type proteins (TIP48, TIP49 and RuvB) are shown in red. Important ATPase motifs are highlighted in cyan.

expression constructs for the over-expression of recombinant likTIP48 and likTIP49 (see Chapters 2.5.4 and 2.7.8).

4.2.2 Cloning of TIP48 and TIP49 Domain II deletion mutants

As demonstrated by the *liebeskummer* mutation, Domain II may be important for oligomerisation and the regulation of ATPase activity of TIP48 and TIP49. To test this further, we generated bacterial expression constructs of TIP48 and TIP49 with a truncated Domain II. pET21b-TIP48-His_6 and pET15b-His_6-TIP49 were mutagenised using PCR and constructs for the over-expression of TIP48 and TIP49 lacking a significant globular portion of Domain II were generated. Initially, truncations were based on the alignment of TIP48, TIP49 and RuvB carried out by (Putnam et al., 2001). This alignment was made before any structural data were published and was therefore inaccurate in predicting the interface between Domain I and Domain II in TIP48 and TIP49. Thus, Domain II deletion mutants were cloned: Δ^1TIP48, where Ile-147 to Ile-293 inclusive were deleted; and Δ^1TIP49, where Cys-141 to Pro-296 were deleted. When Δ^1TIP48 and Δ^1TIP49 were expressed in the BL21-Gold (DE3) cells, the resulting recombinant proteins were insoluble under all conditions tested (Figure 4.3). Re-folding of Δ^1TIP49 was attempted using 6 M urea; however, Δ^1TIP49 formed soluble aggregates under these conditions (not shown). Shortly after cloning Δ^1TIP48 and Δ^1TIP49, a crystal structure of hTIP49 was published (Matias et al., 2006), which allowed us to more accurately align TIP48, TIP49 and RuvB protein sequences and characterise their domain interfaces. Using these structures, we designed mutants of TIP48 and TIP49, where a significant portion of Domain II was truncated, but some of Domain II remained to aid proper protein folding and solubility. Bacterial plasmid expression constructs were generated and expression and solubility of the mutated proteins were tested (Figure 4.3). The best solubility was obtained with Δ^2TIP48, where Glu-133 to Val-238 were deleted and replaced with Ala-Gly-Ala; and Δ^2TIP49, where Glu-126 to Ile-234 were deleted and replaced with Ala-Gly-Ala: an unstructured linker to facilitate correct protein folding (Figures 4.1, 4.2 and 4.3).

Mutagenised Plasmid	Resulting Construct	Mutation	Soluble?
pET21b-TIP48-His_6	pET21b-Δ^1TIP48-His_6	Deleted I^{147} — I^{293}	NO
pET21b-TIP48-His_6	pET21b-Δ^2TIP48-His_6	Replaced E^{133} — V^{238} with AGA	YES
pET15b-His_6-TIP49	pET15b- His_6-Δ^1TIP49	Deleted C^{141} — P^{296}	NO
pET15b-His_6-TIP49	pET15b- His_6-Δ^2TIP49	Replaced E^{126} — I^{234} with AGA	YES
pET15b-His_6-TIP49	pET15b- His_6-Δ^3TIP49	Replaced E^{129} — I^{234} with AGA	YES
pET15b-His_6-TIP49	pET15b- His_6-Δ^4TIP49	Replaced E^{126} — K^{231} with AGA	YES
pET15b-His_6-TIP49	pET15b- His_6-Δ^5TIP49	Replaced E^{129} — K^{231} with AGA	YES

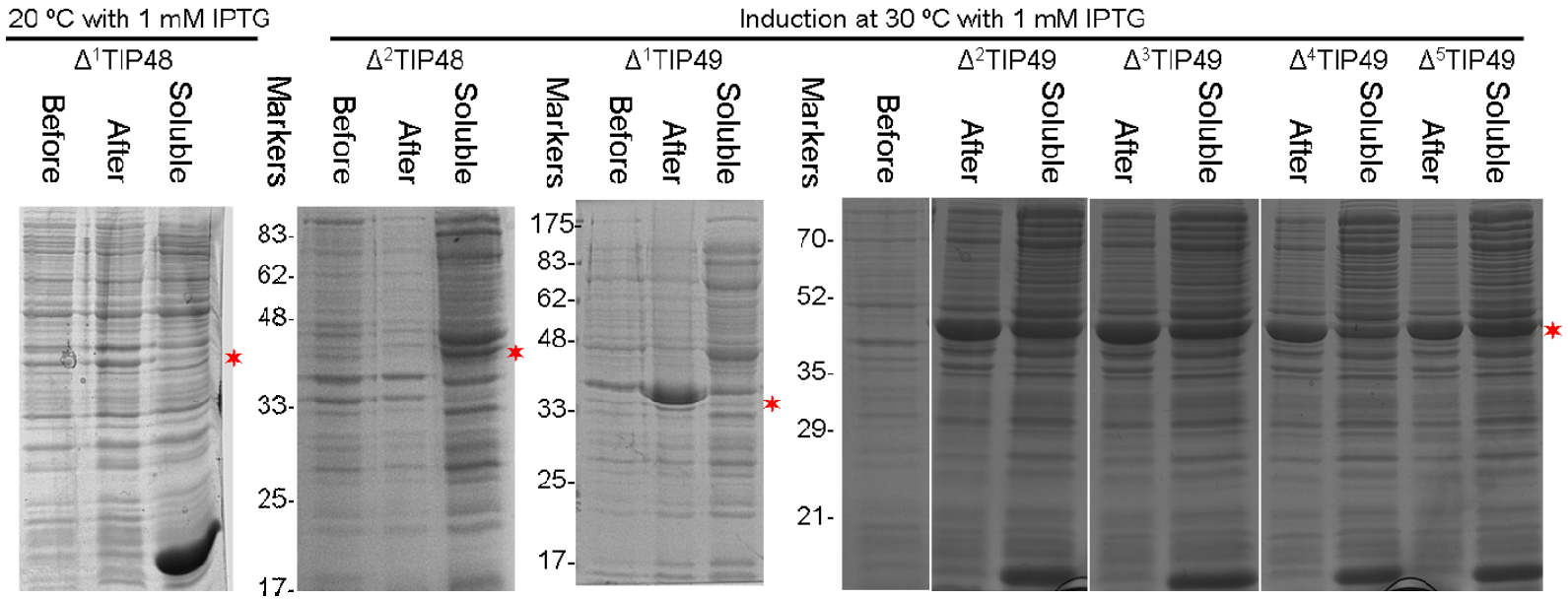

Figure 4.3. Expression constructs and solubility of TIP48 and TIP49 Domain II mutants. The table shows expression constructs generated by site directed mutagenesis. Below are 12 % polyacrylamide SDS PAGE analyses of solubility tests for recombinant proteins induced in *E. coli* BL21-Gold (DE3). Red stars indicate the locations of induced recombinant proteins. Molecular markers (in kDa) are shown beside the gels.

4.3 Expression and Purification of Domain II mutants of TIP48 and TIP49

4.3.1 The *lik* mutation in TIP48-His_6 encourages non-specific protein-protein interactions and mis-folding

The pET21b expression construct, for the expression of a C-terminal $Histidine_6$ tagged hTIP48 *liebeskummer* mutant, was transformed into Rosetta II (DE3) competent cells for the over-expression of *lik*TIP48-His_6 (referred to hereafter as *lik*TIP48). Induction using IPTG gave excellent over-expression of *lik*TIP48, although the majority of the protein was insoluble (Figure 4.4a). Bacterial cells over-expressing *lik*TIP48 were lysed and the soluble components were applied to a Talon column. *lik*TIP48 was eluted using a 10 – 500 mM imidazole gradient with the elution peak at around 100 mM imidazole. Unfortunately, the yield of soluble *lik*TIP48 purified from bacteria was quite low, and it co-purified with a large quantity of bacterial contaminants. To attempt separation of *lik*TIP48 and the contaminants, further purification using a MonoQ column was employed; however, this did not improve the concentration or purity of *lik*TIP48 (Figure 4.4a). As the sample was not pure enough for biochemical assays, further characterisation of *lik*TIP48 was not performed. It is clear that the three amino acid insertion in Domain II affects the structural integrity, solubility and non-specific interaction with other proteins, which may explain the phenotype presented in *liebeskummer* Zebrafish.

4.3.2 His_6-*lik*TIP49 forms aggregates under all native and re-folding conditions tested

For bacterial over-expression of *lik*TIP49, a pET15b expression construct which incorporated an N-terminal $Histidine_6$ tag was transformed into BL21-Gold (DE3) competent cells for the over-expression of His_6-*lik*TIP49. Bacterial lysis after over-expression of His_6-*lik*TIP49 (referred to hereafter as *lik*TIP49), using the

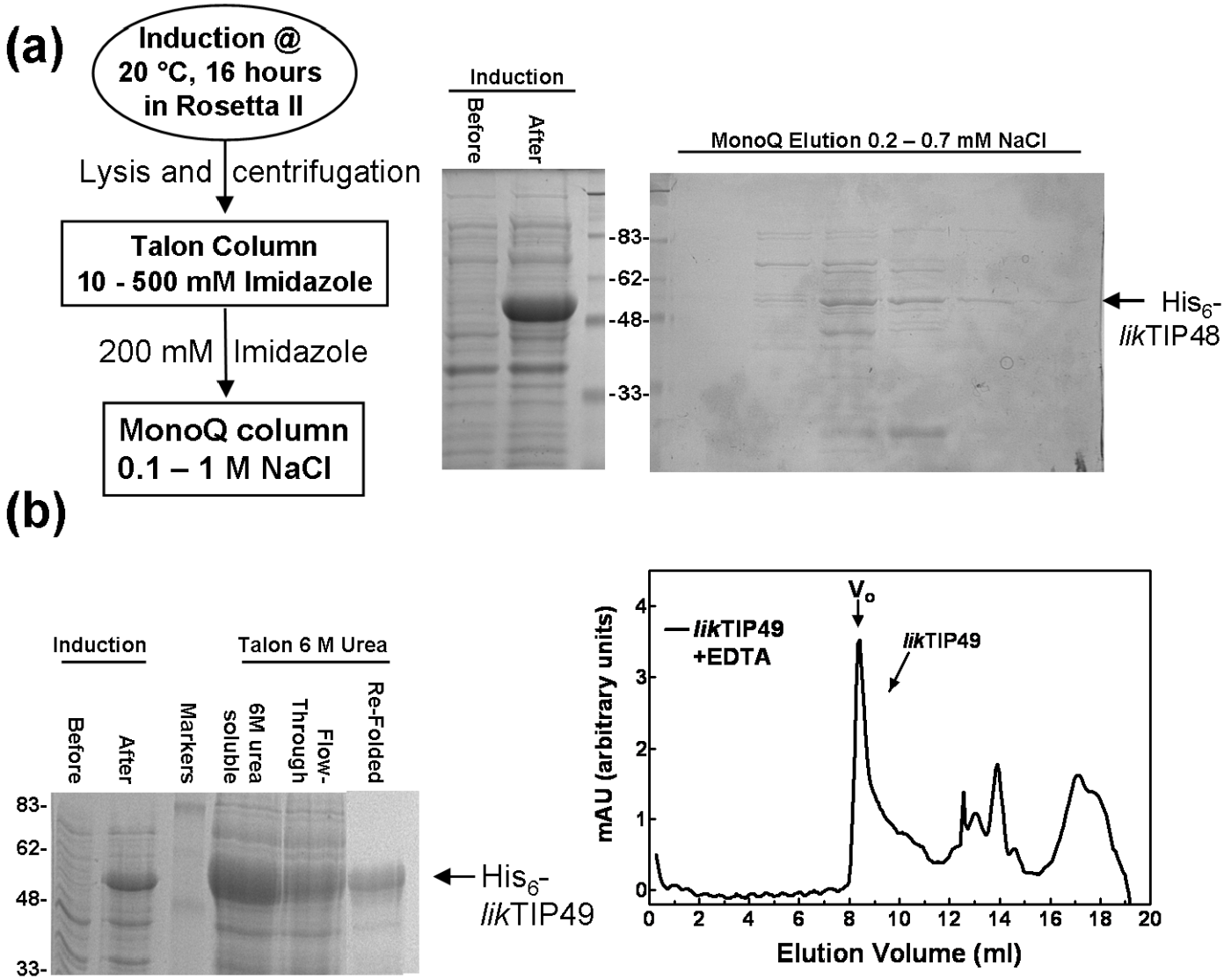

Figure 4.4. Purification of TIP48 and TIP49 *liebeskummer* mutants. (a) A schematic representation of *lik*TIP48-His_6 purification is shown on the left. On the right are 12 % polyacrylamide SDS PAGE analyses of TIP48-His_6 induction and purification by MonoQ anion exchange chromatography. (b) The left side shows 12 % polyacrylamide SDS PAGE of His_6-*lik*TIP49 induction and purification under denaturing conditions in 6 M urea. The right hand curve shows the elution profile of His_6-*lik*TIP49 purified under denaturing conditions; His_6-*lik*TIP49 eluted in the void volume of the Superdex 200 HR SEC column. Numbers beside gels refer to the sizes of molecular weight standards in kDa.

same procedure as for wild-type TIP49, resulted in all of the recombinant protein appearing in the insoluble portion of the lysate (Figure 4.4b). Induction of recombinant *lik*TIP49 at 20 ºC for longer periods of time did not improve the solubility of *lik*TIP49 (not shown).

As *lik*TIP49 was insoluble under native conditions, we attempted to use urea to purify *lik*TIP49 under denaturing conditions. Insoluble *lik*TIP49 from the bacterial cell lysate was denatured using 6 M urea. *lik*TIP49 was then applied to a Talon column, eluted in urea, then re-folded by step-wise removal of urea by dialysis. Soluble *lik*TIP49 was obtained under these conditions; however, when the oligomeric state of *lik*TIP49 was assessed using a Superdex 200 HR size exclusion chromatography column, *lik*TIP49 eluted mainly in the void volume. This observation indicated that *lik*TIP49 formed soluble aggregates under re-folding conditions (Figure 4.4b). In summary, the introduction of this three residue insertion in Domain II is likely to affect the stability and proper folding of recombinant *lik*TIP48 and *lik*TIP49.

4.3.3 Purification of Δ^2TIP48-His$_6$

pET21b-Δ^2TIP48-His$_6$ was transformed into BL21-Gold (DE3) competent cells for the over-expression of Δ^2TIP48-His$_6$. Bacterial cells were lysed and the soluble lysate was purified using a Talon column, and passed through an ssDNA column. Δ^2TIP48 was bound and eluted from a MonoQ column using a 0.1 – 1 M NaCl gradient with an elution peak of around 0.4 mM NaCl (Figure 4.5). The protocol resulted in Δ^2TIP48 of approximately 95 % purity.

4.3.4 Purification of His$_6$-Δ^2TIP49

A pET15b-His$_6$-Δ^2TIP49 plasmid was transformed into BL21-Gold (DE3) competent cells for the over-expression of His$_6$-Δ^2TIP49. Bacterial cells were lysed and the soluble lysate was purified on a Talon column as for Δ^2TIP48 above. Δ^2TIP49 was then purified on a hydroxylapatite column and eluted using

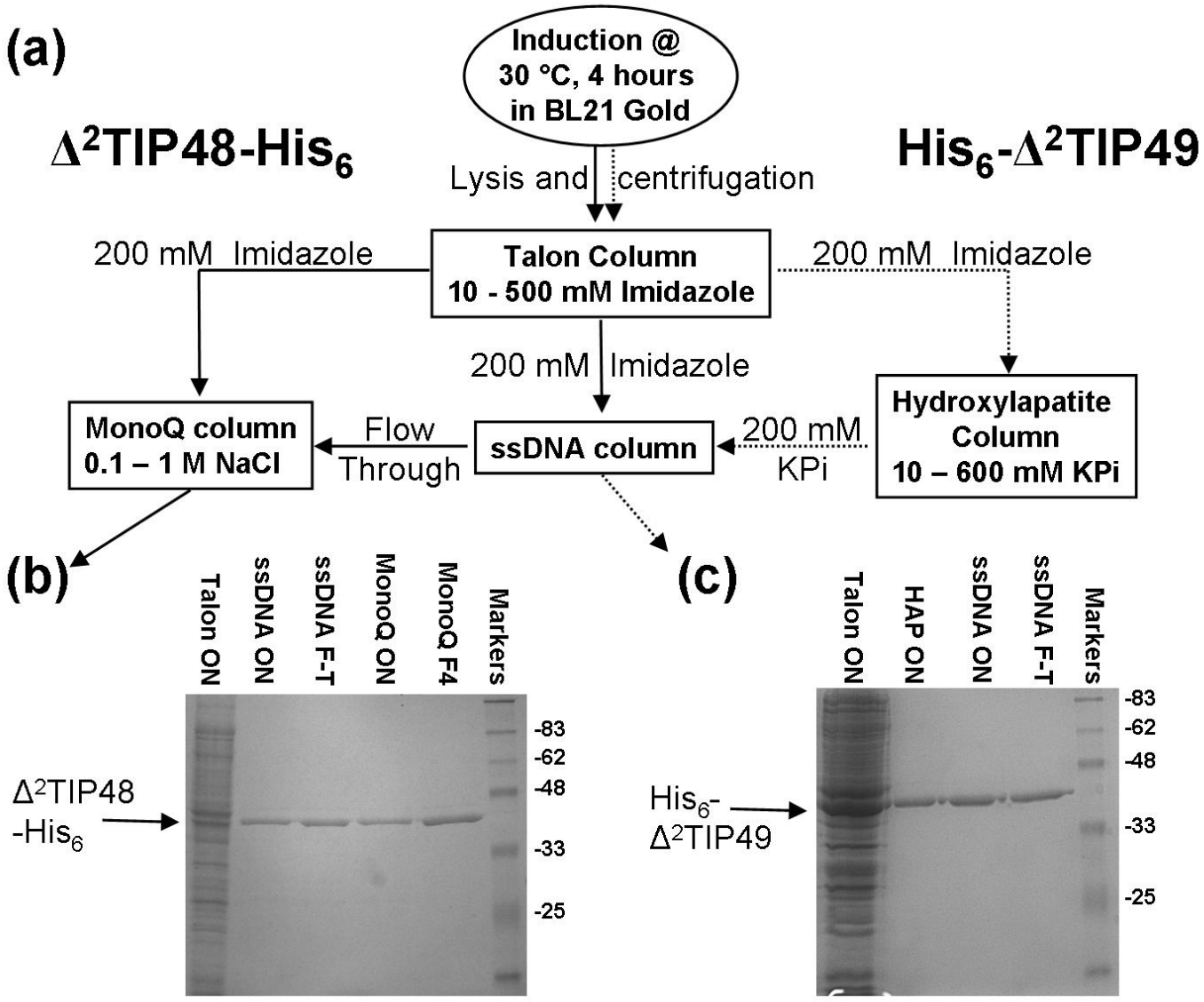

Figure 4.5. Purification of Δ^2TIP48-His_6 and His_6-Δ^2TIP49. A schematic representation of Δ^2TIP48-His_6 (solid lines) and His_6-Δ^2TIP49 (broken lines) purification are shown (a). 12 % SDS PAGE summary gels stained with Coomassie show the purification of Δ^2TIP48-His_6 (b) and His_6-Δ^2TIP49 (c). Numbers beside gels refer to the sizes of molecular weight standards in kDa.

a 10 – 600 mM KPi gradient. Δ^2TIP49 eluted around 200 mM KPi. Finally contaminants were removed by passing through a single stranded DNA cellulose column and collecting the flow-through (Figure 4.5).

4.4 Oligomerisation of TIP48 and TIP49 Domain II mutants by SEC

To assess the importance of Domain II in the oligomeric organisation of TIP48 and TIP49, and to confirm correct folding of the mutants, Δ^2TIP48 and Δ^2TIP49 were analysed by SEC. Δ^2TIP49 was analysed by SEC in EDTA, and eluted in a single peak corresponding to 40 kDa: a monomer (Figure 4.6d). When incubated with 1 mM ATP and 2 mM $MgCl_2$, Δ^2TIP49 also eluted at the position of a monomer. This is in agreement with the work carried out in Chapter 3, which showed that wild type TIP49 is exclusively monomeric by SEC.

When Δ^2TIP48 was analysed by SEC, two major species were observed in EDTA: a peak at 45 kDa corresponding to a monomer, and one at 220 KDa which was likely to be a hexamer (Figure 4.6b). The absorbance trace also indicated protein eluting up to the void volume of the column, although this was likely to be soluble aggregates included in that specific sample (Figure 4.6b). This elution profile is comparable to wild type TIP48 under similar conditions, although the peak corresponding to a ~ 240 kDa Δ^2TIP48 hexamer was more prominent. As illustrated in Chapter 3, TIP48 assembles into hexamers upon incubation with adenine nucleotides and divalent magnesium. To assess the oligomeric organisation of Δ^2TIP48 in the presence of nucleotide cofactors, SEC was performed after incubation of Δ^2TIP48 with 1 mM ATP and 2 mM $MgCl_2$. The resulting elution profile indicated that there was no significant change in the oligomeric state of Δ^2TIP48 when bound to nucleotide cofactors (Figure 4.6c).

As there were a number of oligomeric species of Δ^2TIP48 detected by SEC, we used different concentrations of Δ^2TIP48 to assess whether the species were in a

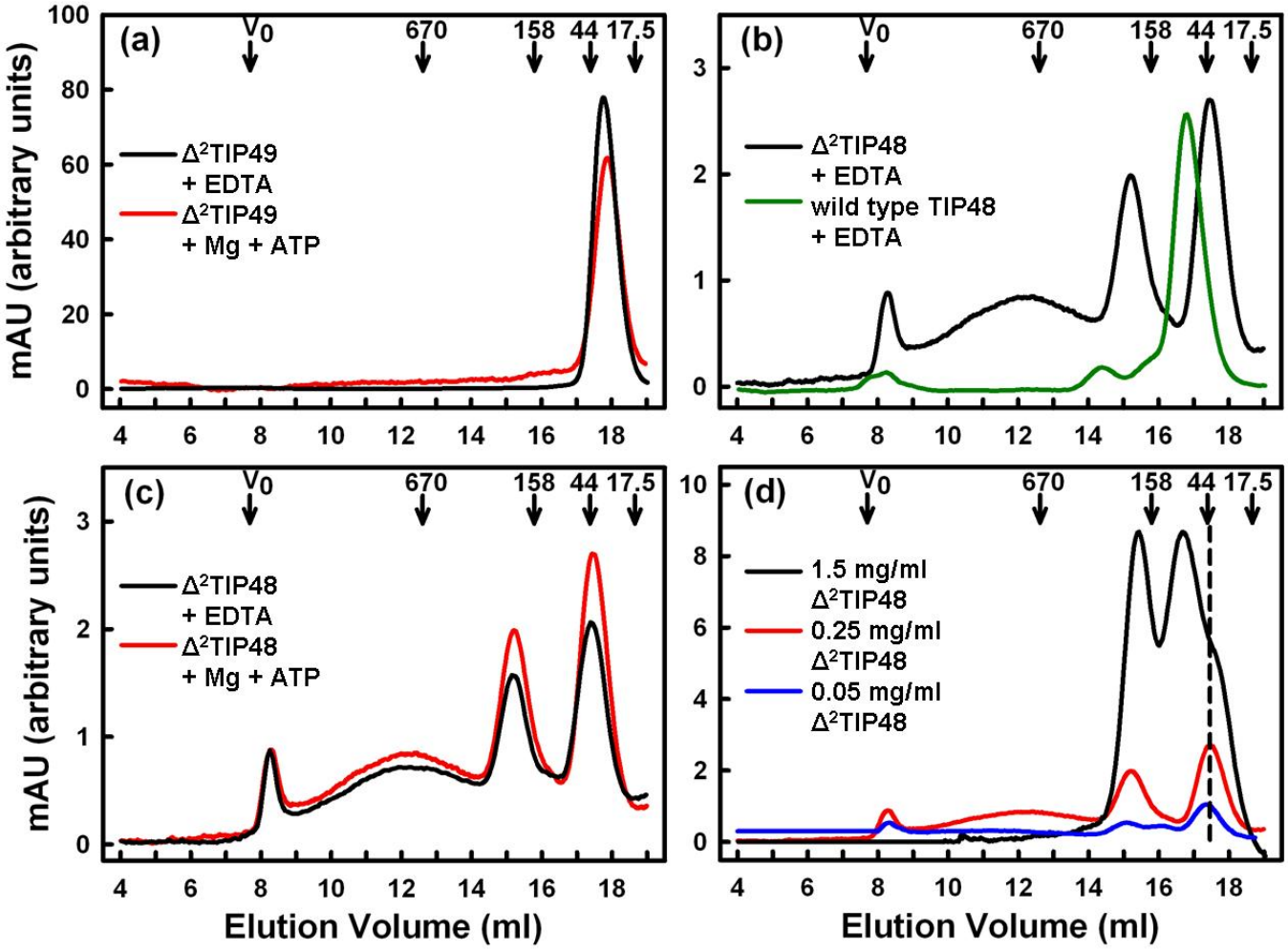

Figure 4.6. Size exclusion chromatography of Δ^2TIP48-His_6 and His_6-Δ^2TIP49. Samples were run on a Superose 6 HR SEC column. The UV_{280} absorbance profiles are shown for His_6-Δ^2TIP49 in EDTA (a); Δ^2TIP48-His_6 and wild type TIP48-His_6 (b); Δ^2TIP48-His_6 with EDTA or with ATP/$MgCl_2$ (c); and Δ^2TIP48-His_6 at three concentrations (d). The dotted line in (d) shows the expected elution volume of a monomer. The numbered arrows in each figure denote the elution volumes of four molecular mass standards in kDa and the void volume (V_o).

concentration dependent equilibrium. Δ^2TIP48 was analysed by SEC at monomer concentrations of 1.5, 0.25 and 0.05 mg/ml (Figure 4.6d). At the lowest concentrations tested, Δ^2TIP48 eluted predominantly as a monomer, with small amounts of hexamers and other unassigned intermediates. At high concentrations Δ^2TIP48 became hexameric, and the monomeric species was reduced in comparison - a new peak was also detected which corresponded to 90 kDa, which could correspond to a dimer of Δ^2TIP48 (Figure 4.6c).

These data suggest that Domain II of TIP48 is essential for controlling the nucleotide dependent oligomerisation of TIP48, and has a functional role in regulation of TIP48 activity. However, unlike for TIP48, Domain II in TIP49 is not important for regulating the oligomerisation of TIP49. The comparison with SEC profiles of wild type proteins also provide good evidence that both Δ^2TIP48-His_6 and His_6-Δ^2TIP49 are correctly folded.

4.5 ATPase activity of TIP48 and TIP49 Domain II mutants

TIP48 and TIP49 hydrolyse ATP *in vitro*. Individually their ATPase activities are low, although when TIP48 and TIP49 form a heteromeric complex their activities increase synergistically (Figure 4.7). To assess how the lack of Domain II in TIP48 and TIP49 affects their ATPase activity, the individual activities of Δ^2TIP48 and Δ^2TIP49 were tested. Δ^2TIP48 and Δ^2TIP49 both had activities which were comparable to wild type proteins (activities were calculated to be less than 1 mole of ATP hydrolysed per mole of monomer in 30 mins for wild type and mutant proteins).

Recombinant TIP48 and TIP49 were mixed *in vitro*, incubated on ice for 5 mins, then the ATPase activity was measured. After mixing the ATPase activity increased to over 10 moles of ATP hydrolysed per monomer of protein in 30 mins (Figure 4.7). This synergistic activity is in agreement with observations by

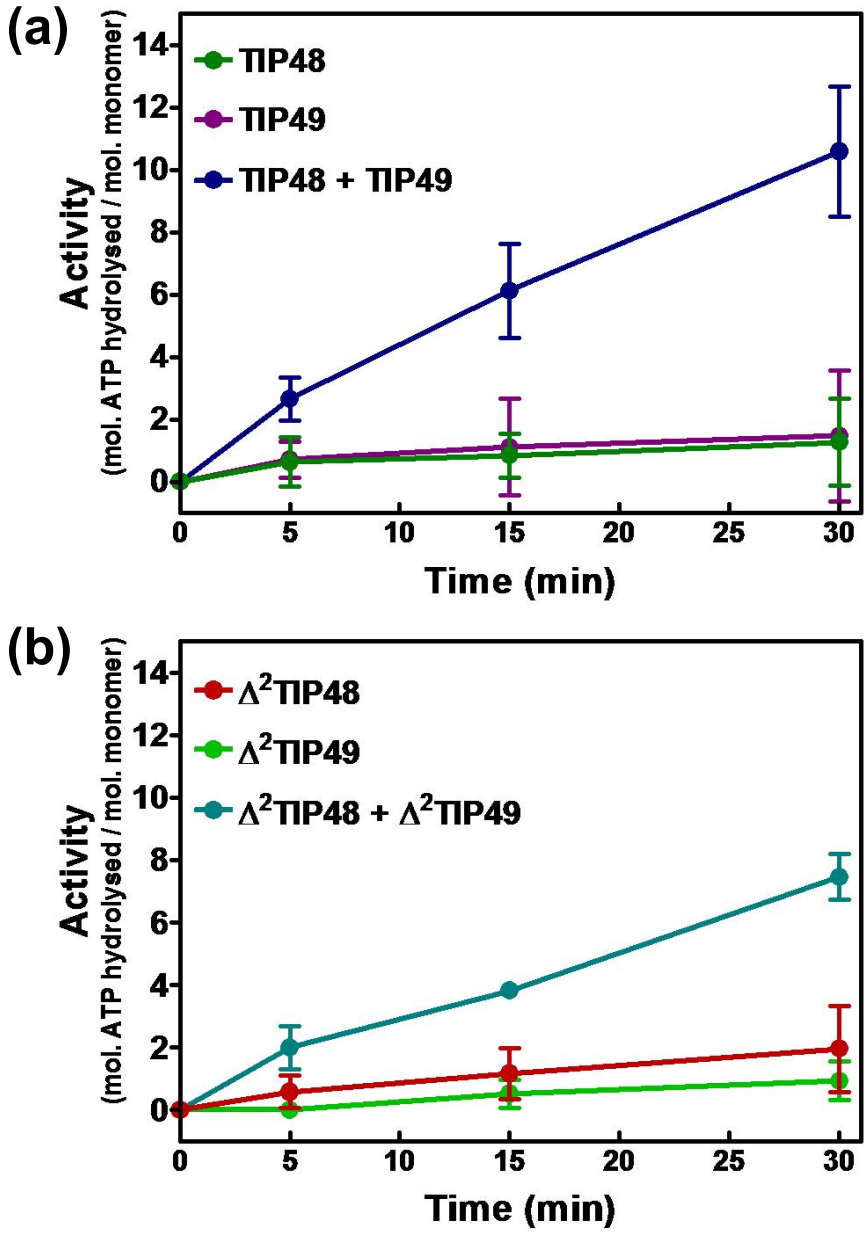

Figure 4.7. ATPase activity of TIP48, TIP49 and Domain II mutants. ATPase activity of 1 μM monomer of each protein was measured using a malachite green colourimetric assay that measures changes in inorganic phosphate (P_i) concentration. Activities for wild type TIP48 and TIP49 (a) and Δ^2 mutants (b) are shown. Proteins were individually assessed or mixed *in vitro* before the assay was initiated. Activity is measured in moles of ATP hydrolysed per mole of monomer at 4 different time points. Time points were normalised by subtracting the background P_i concentration from the 0 minute time point. The error bars denote standard deviation.

other groups and is direct evidence for a strong functional interaction of wild type TIP48 and TIP49 *in vitro*. To assess whether the lack of Domain II in TIP48 and TIP49 modulates the interactions or activity of the TIP48/TIP49 complex, Δ^2TIP48 and Δ^2TIP49 were mixed and incubated, then ATP hydrolysis was measured. As with wild type proteins, a synergistic increase of ATPase activity was observed when Δ^2TIP48 and Δ^2TIP49 were incubated, although the activity was around 75 % of the activity of wild type complex (7.5 moles ATP hydrolysed per mole protein in 30 mins). These data show that Domain II in TIP48 and TIP49 is not essential for the interaction or ATPase activity of TIP48 and TIP49.

4.6 Assembling Heteromeric Complexes of TIP48 and TIP49 Domain II mutants

The interaction of Δ^2TIP48 and Δ^2TIP49 was demonstrated in ATPase assays (Figure 4.7). To find out how removal of Domain II from TIP48/TIP49 complexes affects their activities *in vitro*, different plasmid constructs for bacterial expression of the TIP48/TIP49 complex were cloned. The following constructs were used:

- pET21b – TIP48 (no tag) – TIP49-His_6 (Chapter 3.3)
- pET21b – TIP48 (no tag) – Δ^2TIP49-His_6
- pET21b – Δ^2TIP48 (no tag) – TIP49-His_6
- pET21b – Δ^2TIP48 (no tag) – Δ^2TIP49-His_6

The wild type complex of TIP48/TIP49-His_6 described in Chapter 3.3 consisted of a dodecameric complex as shown by AUC and SEC. Moreover, the dodecameric complex showed a synergistic increase in ATPase activity compared to the individual monomers. To compare the wild type complex of TIP48 and TIP49 with complexes lacking TIP48 Domain II, TIP49 Domain II, or both, we expressed and purified the above complexes using the protocol carried out for wild type TIP48/TIP49-His_6 described in Chapter 3.3.

4.7 Characterisation of heteromeric complexes of TIP48 and TIP49 Domain II mutants

4.7.1 Δ^2TIP48/TIP49-His_6 complex

A complex of Δ^2TIP48/TIP49-His_6 was expressed in bacterial cells and purified as described for the wild type complex. Un-tagged Δ^2TIP48 co-purified with $histidine_6$ tagged TIP49, which demonstrates that the two proteins are in a stable complex, further confirming that the globular portion of Domain II of TIP48 is not required for heteromeric interactions (Figure 4.8a). As with the wild complex, TIP49 shifts from being predominantly monomeric to large multimers when bound to Δ^2TIP48. The elution profile of Δ^2TIP48/TIP49-His_6 was very similar to wild type complex: free TIP49 monomers eluted in fractions 17 and 18, while Δ^2TIP48/TIP49 complex eluted in a major peak at 13.7 ml, calculated as 452 kDa (Figure 4.8a and b, and Table 4.1). Although a Δ^2TIP48/TIP49 double hexamer has a predicted mass of 552.8 KDa, the SEC experiments suggested a slightly lower molecular mass. In contrast, the wild type complex, which has a mass of 617.3 KDa by SEC, correlated well with the predicted mass of 621.7 (Chapter 3.3, Table 4.1). This discrepancy most likely results from smaller oligomers eluting in an overlapping peak during SEC, which may contribute to a shifted elution volume for the double hexamer. The difference could also be due to large changes in shape between the wild type complex and Δ^2TIP48/TIP49, implying Domain II is exposed on the outside of the double hexamer. In agreement with observations of the wild type complex in Chapter 3, Δ^2TIP48/TIP49-His_6 shows a slight tendency to form oligomers higher than a double hexamer, demonstrated by complex eluting as far as the void volume of the column. These higher order oligomers indicate further stacking of hexamers on the double hexamer, suggesting that the configuration of the hexameric rings in this complex is head-to-tail.

Figure 4.8. Oligomerisation and activity of the Δ^2TIP48/TIP49-His$_6$ complex. Δ^2TIP48/TIP49-His$_6$ was purified and analysed by SEC. Separation of Δ^2TIP48/TIP49-His$_6$ oligomers by Superose 6 HR SEC column is shown as a $UV_{280\ nm}$ absorbance trace (a). 1 ml fractions were collected (fraction 1 is from 0.5 – 1.5 ml etc). Fractions were then analysed by 12 % polyacrylamide SDS PAGE stained with Coomassie (b). Protein content was measured by the method of Bradford; ATPase activity was measured by detecting P_i concentration using a colourimetric malachite green assay (c). ATPase activity is defined as the nmoles of ATP hydrolysed after 30 minutes incubation at 37 ºC in a 200 µl reaction. The numbered arrows in (a) denote the elution volumes of four molecular mass standards in kDa and the void volume (V_o).

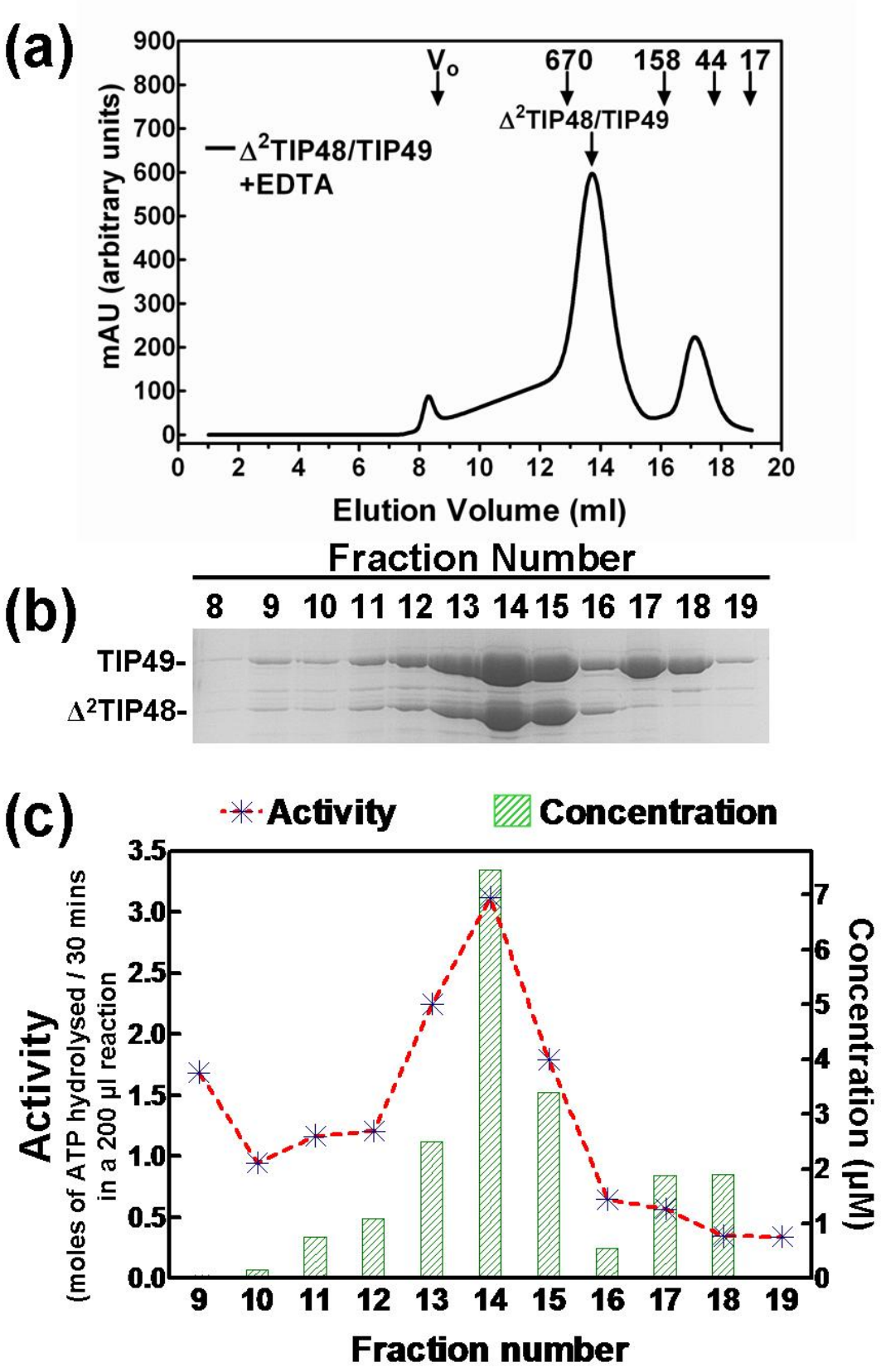
(a)
mAU (arbitrary units)
Elution Volume (ml)
Vo
670
158
44
17
Δ2TIP48/TIP49
Δ2TIP48/TIP49 +EDTA
(b)
Fraction Number
8 9 10 11 12 13 14 15 16 17 18 19
TIP49-
Δ2TIP48-
(c)
Activity
Concentration
Activity (moles of ATP hydrolysed / 30 mins in a 200 µl reaction
Concentration (µM)
Fraction number

The ATPase activity of each fraction was measured to investigate the activity of different oligomeric forms of the Δ^2TIP48/TIP49 complex (Figure 4.8b and c). The peak of activity was detected in fraction 14; this is the elution peak of the Δ^2TIP48/TIP49 complex. High molecular mass contaminants from *E. coli* are probably responsible for the ATPase activity seen in fractions 9, 10 and 11. Comparison between ATPase activity and protein concentration shows a striking difference between dodecameric Δ^2TIP48/TIP49 and TIP49 alone, which can be clearly seen in fractions 17 and 18. This shows that TIP49 interacts with TIP48 lacking Domain II, and that the complex efficiently hydrolyses ATP, with the dodecamer displaying maximal catalytic activity.

4.7.2 TIP48/Δ^2TIP49-His$_6$ complex

The experiments to characterise the Δ^2TIP48/TIP49 complex in chapter 4.7.1 were repeated with the TIP48/Δ^2TIP49 complex. Recombinant TIP48/Δ^2TIP49 was purified from BL21-Gold (DE3) as above. Untagged TIP48 eluted with histidine$_6$ tagged Δ^2TIP49 captured on a Talon column, demonstrating that Domain II of TIP49 is not required for interactions between TIP48 and TIP49. By SEC, the TIP48/Δ^2TIP49 complex eluted at high molecular mass, with a major peak at 13.6 ml, calculated to be approximately 480 kDa (Figure 4.9a and b, Table 4.1). The predicted molecular mass of the TIP48/Δ^2TIP49 complex is 553.1 KDa. As with Δ^2TIP48/TIP49, the difference between the observed and predicted mass may be due to several overlapping oligomers or a large difference in shape of the particles, indicating that Domain II of TIP49 may lie on the outer surface of the double hexameric ring complex. Interestingly, there was also an elution peak of TIP48/Δ^2TIP49 complex at 14.7 ml (Figure 4.9a), corresponding with ~ 270 kDa. Thus, it is likely that a proportion of TIP48/Δ^2TIP49 forms hexamers. This demonstrates an unstable interaction between the two rings of the dodecameric complex when TIP49 Domain II is not present, implying that Domain II of TIP49 supports, but is not required for, interactions between the top and bottom rings of the TIP48/TIP49 complex.

Figure 4.9. Oligomerisation and activity of the TIP48/Δ^2TIP49-His$_6$ complex. TIP48/Δ^2TIP49-His$_6$ was purified and analysed by SEC. Separation of TIP48/Δ^2TIP49-His$_6$ oligomers by Superose 6 HR SEC column is shown as a $UV_{280\ nm}$ absorbance trace (a). 1 ml fractions were collected (fraction 1 is from 0.5 – 1.5 ml etc). Fractions were then analysed by 12 % polyacrylamide SDS PAGE stained with Coomassie (b). Protein content was measured by the method of Bradford; ATPase activity was measured by detecting P_i concentration using a colourimetric malachite green assay (c). ATPase activity is defined as the nmoles of ATP hydrolysed after 30 minutes incubation at 37 ºC in a 200 µl reaction. The numbered arrows in (a) denote the elution volumes of four molecular mass standards in kDa and the void volume (V_o).

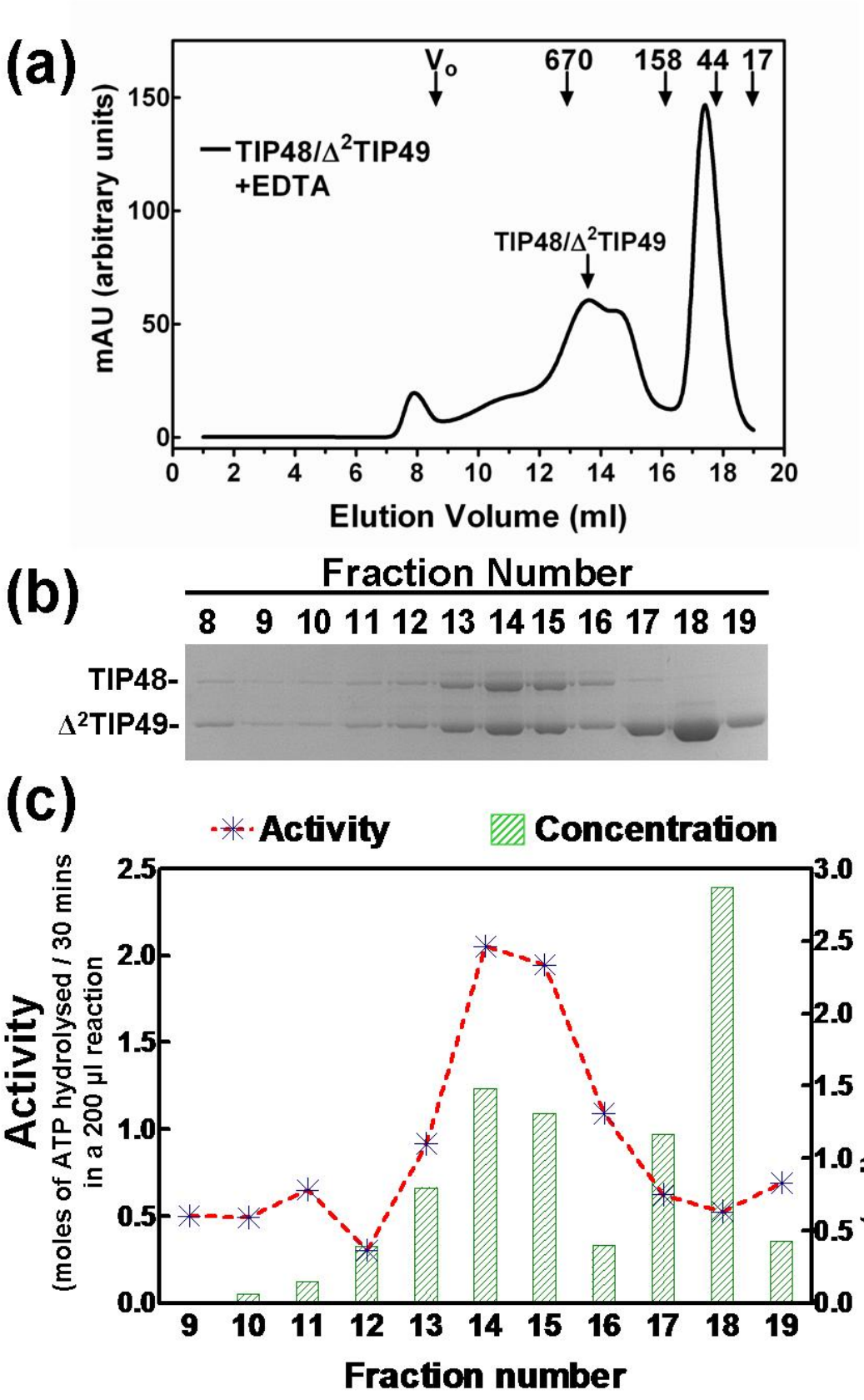
(a)
Vo
670
158
44
17
mAU (arbitrary units)
TIP48/Δ2TIP49
+EDTA
TIP48/Δ2TIP49
Elution Volume (ml)
(b)
Fraction Number
8 9 10 11 12 13 14 15 16 17 18 19
TIP48-
Δ2TIP49-
(c)
Activity
Concentration
Activity
(moles of ATP hydrolysed / 30 mins in a 200 µl reaction
Concentration (µM)
Fraction number

After the separation of the TIP48/Δ^2TIP49 complex by SEC, the ATPase activity was measured across the fractions collected (Figure 4.9b and c). The ATPase activity peaked in fraction 14, demonstrating that the dodecameric complex of TIP48/Δ^2TIP49 was the oligomer with the maximal catalytic activity. Monomeric Δ^2TIP49 in fraction 18 had much less activity than the heteromeric complex at the same protein concentration. These data demonstrate that Domain II of TIP49 is not required for interaction between TIP48 and TIP49, but may stabilise interactions between the top and bottom rings of the double hexamer.

4.7.3 Δ^2TIP48/Δ^2TIP49-His$_6$ complex

TIP48 and TIP49 both lacking Domain II were co-expressed as described above. The resulting Δ^2TIP48/Δ^2TIP49-His$_6$ complex was purified on a Talon column; untagged Δ^2TIP48 co-eluted with Δ^2TIP49-His$_6$ showing stable interaction of the two mutants. The Δ^2TIP48/Δ^2TIP49 complex was separated according to size and shape by SEC, and a high molecular mass complex of Δ^2TIP48/Δ^2TIP49 eluted at 13.9 ml, calculated to be ~ 411 KDa (Figure 4.10 a and b, Table 4.1). As with the TIP48/Δ^2TIP49 complex, there was a small peak lower than the dodecamer, which eluted at 15.1 ml, corresponding to ~ 215 kDa. Again, this species is likely to be a hexamer, confirming the observation that TIP49 Domain II may stabilise interactions between the top and bottom rings of the TIP48/TIP49 double hexamer. Excess monomeric Δ^2TIP49 eluted mainly in fractions 17 and 18.

The ATPase activity was measured across the SEC fractions and showed a peak in fraction 14 corresponding with the elution of the Δ^2TIP48/Δ^2TIP49 complex (Figure 4.10c). Monomeric Δ^2TIP49 eluting in fraction 17 and 18 had low ATPase activity compared with the complex. This demonstrates a functional interaction between TIP48 and TIP49, even when both lack Domain II, and further confirms the importance of oligomerisation for maximal ATP hydrolysis.

Figure 4.10. Oligomerisation and activity of the Δ^2TIP48/Δ^2TIP49-His$_6$ complex. Δ^2TIP48/Δ^2TIP49-His$_6$ was purified and analysed by SEC. Separation of Δ^2TIP48/Δ^2TIP49-His$_6$ oligomers by Superose 6 HR SEC column is shown as a $UV_{280\ nm}$ absorbance trace (a). 1 ml fractions were collected (fraction 1 is from 0.5 – 1.5 ml etc). Fractions were then analysed by 12 % polyacrylamide SDS PAGE stained with Coomassie (b). Protein content was measured by the method of Bradford; ATPase activity was measured by detecting P_i concentration using a colourimetric malachite green assay (c). ATPase activity is defined as the nmoles of ATP hydrolysed after 30 minutes incubation at 37 ºC in a 200 µl reaction. The numbered arrows in (a) denote the elution volumes of four molecular mass standards in kDa and the void volume (V_o).

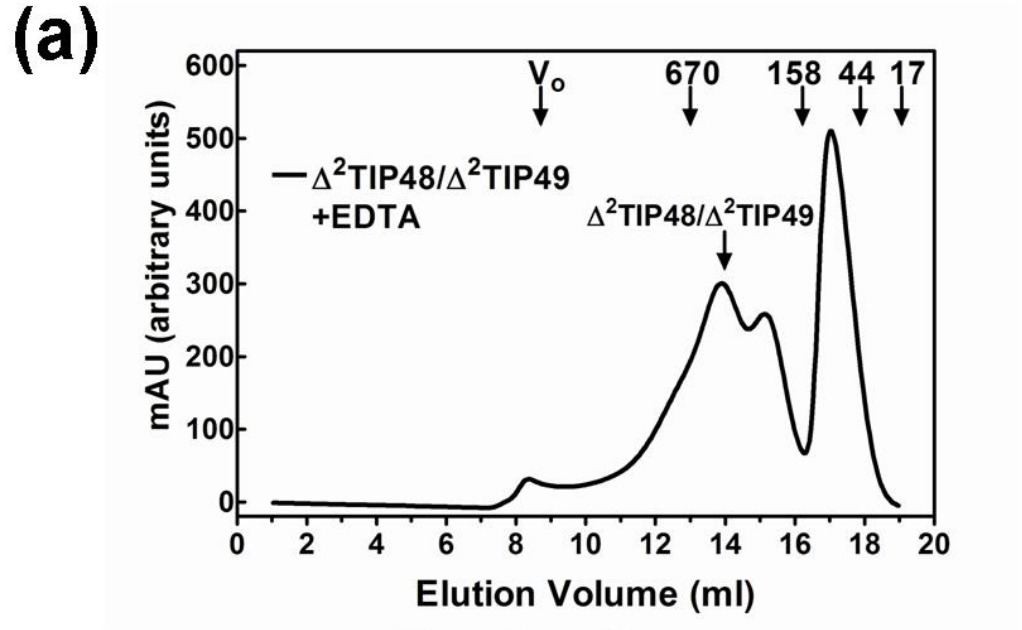
(a)
mAU (arbitrary units)
Elution Volume (ml)
Vo
670
158
44
17
Δ2TIP48/Δ2TIP49 +EDTA
Δ2TIP48/Δ2TIP49

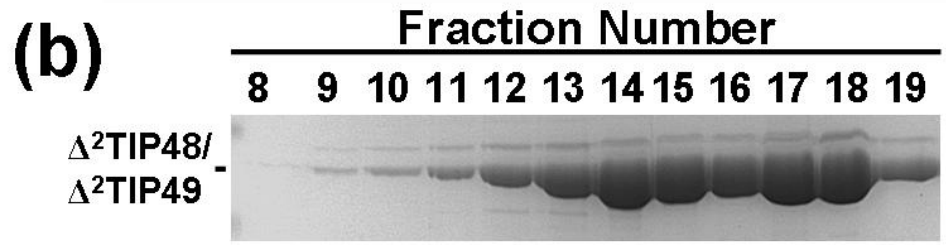
(b)
Fraction Number
8 9 10 11 12 13 14 15 16 17 18 19
Δ2TIP48/
Δ2TIP49

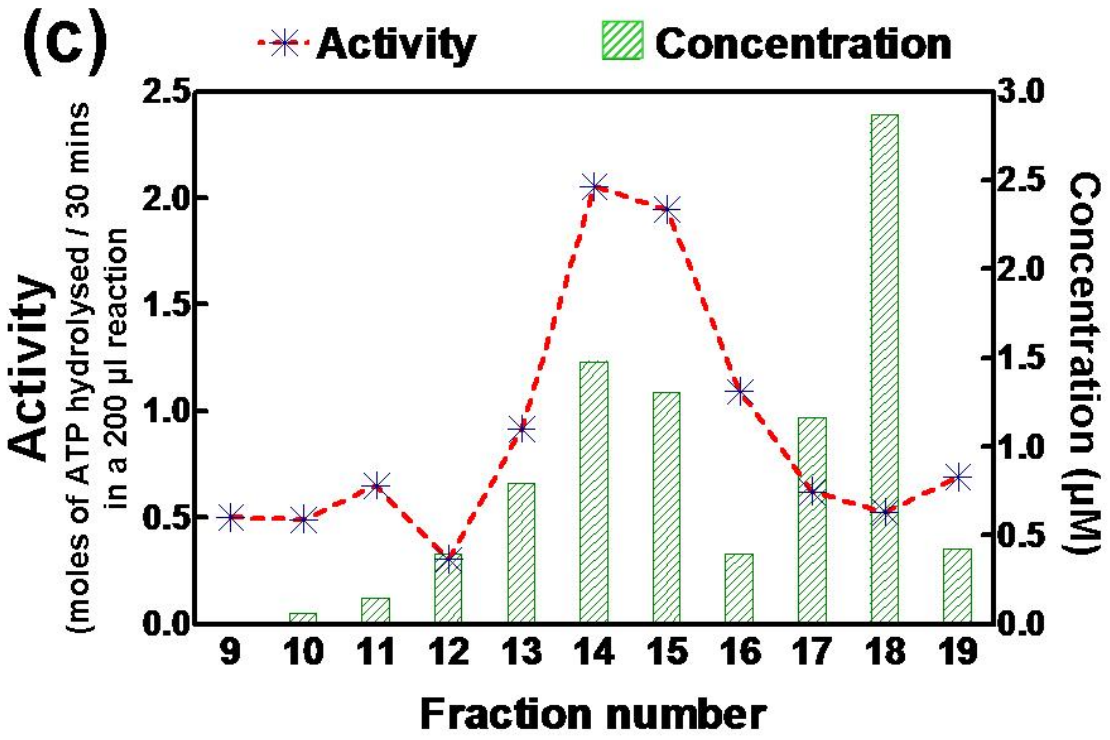
(c)
Activity
Concentration
Activity
(moles of ATP hydrolysed / 30 mins in a 200 µl reaction
Concentration (µM)
Fraction number

4.8 Comparison of the ATPase activities of TIP48 and TIP49 Domain II mutant complexes

The dodecameric complex of TIP48/TIP49 is expected to elute from a Superose 6 SEC column in fractions 13 and 14 (12.5 to 14.5 ml). For direct comparison between wild type and mutant complexes, fractions 13 and 14 were diluted to final monomer concentrations of 1 µM and the ATPase activity measured using a malachite-green colorimetric assay (Figure 4.11, Table 4.1). All complexes demonstrated ATPase activity that was comparable to wild type TIP48/TIP49. Δ^2TIP48/TIP49 demonstrated activity equivalent to that of the wild type complex. TIP48/Δ^2TIP49 showed 20 % higher activity than wild type dodecamers whereas when both deletion mutants were in a complex, the activity was 60 % higher than the wild type complex.

4.9 Discussion

In this chapter we have generated several recombinant mutants of human TIP48 and TIP49. The motivation behind these mutations was to characterise the function of Domain II, which is not present in the closest prokaryotic homologue RuvB. In addition, Domain II has been shown to interact with many binding partners of TIP48 and TIP49, including Hint1 (see chapter 5). We have found that removal of a significant globular portion of Domain II does not modify the ATPase activity of TIP48 or TIP49 individually, although a synergistic increase in ATPase activity occurs when the TIP48 and TIP49 mutants interact. Moreover, the removal of Domain II from TIP49 disrupts interactions between the individual rings of the double hexamer complex, and increases the ATPase activity of the complex. We also showed that TIP48 Domain II is important for regulating the oligomerisation of TIP48.

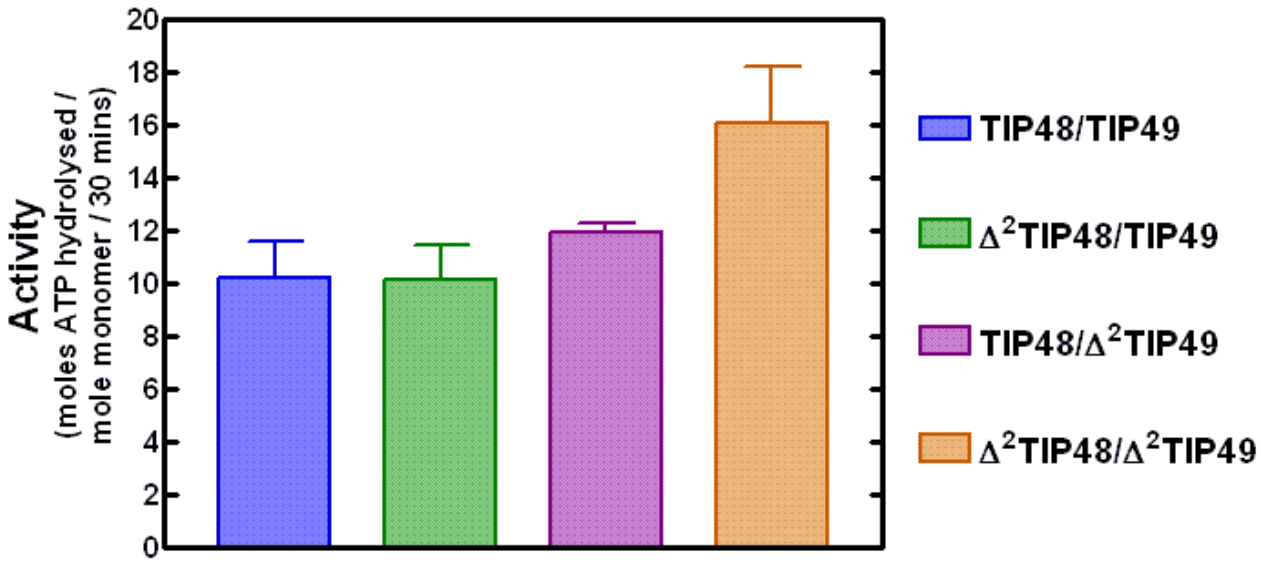

Figure 4.11. ATPase activity of TIP48/TIP49 complexes lacking Domain II. The ATPase activity of 1 μM monomer was measured using a malachite green colorimetric assay, which measures changes in P_i concentration. Activity is defined as the moles of ATP hydrolysed per mole of monomer at 37 °C after 30 mins.

Dodecameric Complex	Predicted Mass (kDa)	Elution Volume (ml)	Observed Mass (KDa)	ATPase activity	Relative activity
TIP48/TIP49-His_6	621.7	13.1	617.3	10.2 ± 1.4	1 ± 0.14
Δ^2TIP48/TIP49-His_6	552.8	13.7	452.0	10.1 ± 1.3	1 ± 0.13
TIP48/Δ^2TIP49-His_6	553.1	13.6	480.1	12.0 ± 0.4	1.2 ± 0.04
Δ^2TIP48/Δ^2TIP49-His_6	484.2	13.9	411.1	16.1 ± 2.1	1.6 ± 0.21

Table 4.1. Summary of SEC and ATPase activities of TIP48/TIP49 complexes. Elution volumes of TIP48/TIP49 complexes are those from Figures 3.2, 4.8, 4.9 and 4.10. Activities are those shown in Figure 4.11. Relative activity is defined as the activity of 1 μM wild type TIP48/TIP49 complex = 1.

Using the published Zebrafish mutation as a guide, we generated recombinant *liebeskummer* mutants of TIP48 and TIP49. *lik*TIP48 displayed low solubility when purified from bacterial hosts, and had a propensity for non-specific protein-protein interactions. *lik*TIP49 did not fold correctly under native conditions and formed soluble aggregates when re-folded after de-naturation with urea. The fact that a 3 amino acid insertion in Domain II of TIP48 and TIP49 affected their stability so drastically implies that this region has an important structural role. Moreover, the residues surrounding this region are conserved between TIP48 and TIP49 in higher eukaryotes, suggesting their importance, and implying a conserved function of Domain II between TIP48 and TIP49. The mutation occurs between α-helix 5 and β-strand 7 in Domain II, both of which are on the surface of the protein (Figure 4.1). The insertion may change the position of the alpha helix and disrupt the protein fold. Furthermore, Phenylalanine is hydrophobic, while Arginine is positively charged. The introduction of a positive or hydrophobic group on the surface of Domain II clearly has negative implications for the overall structure of TIP48 and TIP49. Taking this into consideration, it is likely that this region of Domain II is critical for protein folding and protein-protein interactions. The *liebeskummer* mutation in Zebrafish was thought to be a gain of function of TIP48 activity (Rottbauer et al., 2002). Using recombinant *liebeskummer* mutants of human TIP48 and TIP49, we demonstrated that the protein folding and interactions of *liebeskummer* mutants are compromised. Thus, we find it more likely that the *lik*TIP48 mutation constitutes a loss of function of TIP48 in Zebrafish. This may have important implications for the interpretation of findings in that report, although further investigation is required to confirm our findings in the Zebrafish system.

From the SEC data, it can be concluded that Domain II of TIP48 is important for the regulation of hexamerisation. Δ^2TIP48 forms concentration dependent hexamers independent of ATP; in contrast, wild type TIP48 forms hexamers in the presence adenine nucleotides. This gives appealing insights into the structural role of Domain II. In the crystal structure of TIP49, Domain II is shown

to be extended away from the hexameric ring, and does not seem to have close contact with Domains I or III. This is comparable to our biochemical data for TIP48. The data presented in this chapter suggest that a conformational change occurs when TIP48 binds and hydrolyses ATP, which allows Domain II to contact and stabilise the hexameric ring. Alternatively, Domain II may block hexamerisation in the apo-form of TIP48, then Domain II moves when ATP is bound, allowing hexamerisation (Figure 4.12). This observation is supported by the unequivalent shapes of the top and bottom rings of the double hexamer in the EM reconstruction (Puri et al., 2007). Furthermore, the authors had difficulty fitting the crystal structure of TIP49 into the EM reconstruction (Puri et al., 2007). The EM reconstruction was generated from a complex purified in EDTA, whereas the crystal structure was of TIP49 with ADP bound. These structural differences are likely to be nucleotide induced conformations of Domain II, or changes in Domain II due to interactions between TIP48 and TIP49 in the complex. The low turnover of ATP hydrolysis due to tight binding of ADP is the likely reason for the stability of TIP48 hexamers observed by SEC and AUC in Chapter 3. These conformational changes and subsequent movement of Domain II are likely to be important for the mechanism of action of TIP48, and interactions with other proteins *in vivo*. Indeed, movement of Domain II may facilitate the modulation of protein interactions by bringing together or separating proteins.

The increase in ATPase activity of the TIP48/TIP49 complex when Domain II is removed from TIP49, but not TIP48, implies different roles for the ATPase activity of TIP48 and TIP49 within the complex. TIP49 is likely to have a regulatory role in the complex, such as binding to other proteins and structures and transducing this information to TIP48. Conversely, TIP48 is likely to convert the chemical energy of ATP hydrolysis into mechanical force, through movements in Domain II. This may explain the implication of the TIP48/TIP49 in restructuring protein complexes and modulating protein-protein interactions, such as in the telomerase complex or in snoRNP maturation.

Figure 4.12. Schematic representation of the hypothetical architecture of the TIP48/TIP49 dodecamer. Domain II (red) of TIP48 protrudes from a core hexamer of Domains I and III (blue). TIP48 hexamers are unstable in EDTA; ATP binding and hydrolysis may move the position of Domain II promoting hexamerisation (a). The TIP48/TIP49 complex is composed of a ring of TIP49 bound to a ring of TIP48 (b). Domain II of TIP49 (orange) protrudes from Domains I and III (green), and supports the interactions between the top and bottom rings. This allows TIP48 to undergo multiple rounds of ATP hydrolysis and promotes Domain II movement. This model is consistent with the un-equivalent top and bottom rings of the EM reconstruction.

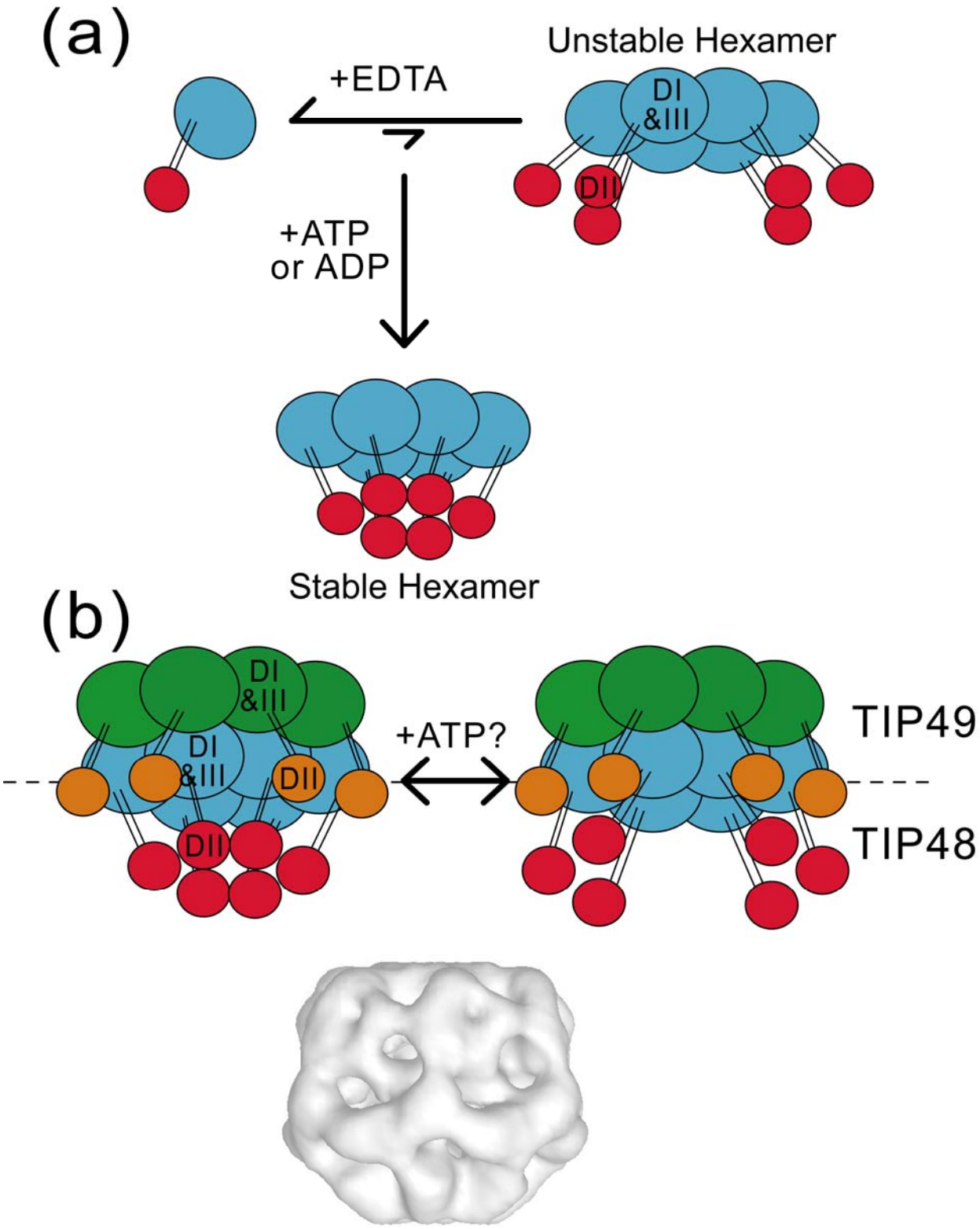
(a)
Unstable Hexamer
+EDTA
DI
&III
DII
+ATP
or ADP
Stable Hexamer
(b)
DI
&III
DI
&III
DII
DII
+ATP?
TIP49
TIP48

The finding that TIP48 and TIP49 assemble into a dodecameric complex, even when a significant portion of Domain II is absent, can help to elucidate the structure of TIP48/TIP49 complexes. It is evident that Domain II of TIP48 is not responsible for interactions of proteins within the hexameric ring of the dodecamer, and does not mediate interactions between the two rings. This indicates that Domain II of TIP48 is extended from a core of a double hexamer of Domains I and III. In contrast, Domain II of TIP49 does affect the stability of the dodecameric complex by facilitating interactions between the top and bottom rings. TIP49 Domain II may also regulate the assembly of different forms of the TIP48/TIP49 complex, as an increase in putative hetero-hexamers was observed when Domain II was deleted. The work carried out in Chapter 3 suggested a head-to-tail configuration of the two rings, to allow oligomers higher than a double hexamer to form. This was also suggested by the authors of the EM reconstruction of the human TIP48/TIP49 double hexamer (Dr. Petra Wendler, personal communication) (Puri et al., 2007). Assuming this model is correct, it is likely that Domain II of TIP49 extends away from the core hexamer of Domains I and III, and interacts with the ring of TIP48 below it (Figure 4.12).

Our structural and biochemical data for the human TIP48/TIP49 complex are in conflict with studies of the yeast complex (Gribun et al., 2008; Torreira et al., 2008). One study showed a hexameric complex made up of three yTIP48 and three yTIP49 monomers (Gribun et al., 2008). These authors also observed concentration dependent hexamerisation of both TIP48 and TIP49 (Gribun et al., 2008). This shows a clear difference between the yeast and human proteins; while we did observe a small proportion of TIP48/TIP49 single hetero-hexamers in Chapter 3, the oligomerisation of individual yTIP48 and yTIP49 were regulated differently. In a separate study, a yeast TIP48/TIP49 double hexamer was demonstrated by cryo-EM (Torreira et al., 2008). Using antibodies targeted against Myc-tagged yTIP49, it was demonstrated that the rings were composed of homo-hexamers, corroborating our observations. However, the shape of the yeast TIP48/TIP49 EM reconstruction was significantly different to the human

TIP48/TIP49 reconstruction (Figure 1.5). Indeed, interpretation of the yeast Cryo-EM reconstruction using the hTIP49 crystal structure was used to propose that contacts between the top and bottom rings of the double hexamer are mediated by Domain II. In this chapter, we demonstrate that Domain II is not required for hexamer-hexamer interactions. This was also supported by a low resolution crystallographic analysis of a complex of human TIP48/TIP49 where the globular portion of Domain II was deleted from both proteins (Gorynia et al., 2008); the complex was similar to the Δ^2TIP48/Δ^2TIP49 complex used in this chapter, and gave a dodecameric configuration (Gorynia et al., 2008).

Thus, we propose a genuine difference between the yeast and human TIP48/TIP49 double hexamer structure, which is supported by the observation that human TIP48 cannot rescue a yeast TIP48-knockout mutant (Lim et al., 2000). This difference in structure may suggest different functions of the TIP48/TIP49 complex in yeast and vertebrates. Indeed, many complexes have a modified composition in multicellular organisms. This is demonstrated by the TIP60 complex. The human TIP60 complex contains TIP48 and TIP49, while the yeast TIP60 complex does not. The human TIP60 complex corresponds to a fusion of yeast TIP60 and Swr1 complexes (See chapter 1.5.5). Clearly, the modification of TIP60 from yeast to humans resulted in the acquisition of new functions, which may also be the case for TIP48 and TIP49.

Chapter 5

Investigating interactions of TIP48 and TIP49 with cellular factors

5.1 Introduction

TIP48 and TIP49 have individually essential roles within cells, as demonstrated by the lethality of individual knockouts (King et al., 2001; Lim et al., 2000; Qiu et al., 1998). This essential role may be attributed to the presence of TIP48 and TIP49 in large multi-subunit nuclear complexes, such as in INO80 and TIP60. Clearly, the intricate assembly of these complexes must be coordinated by specific protein-protein interactions to build up the correct oligomers, in the correct order, for their designated roles. As TIP48 and TIP49 interact with a multitude of proteins within these complexes, we focused on common or core interactions, to identify how the oligomerisation or activity of TIP48 and TIP49 are modulated upon interactions with these factors. In our initial studies, we focused on BAF53, β-catenin and Hint1, and in addition, attempted to verify the putative interactions of TIP48 and TIP49 with DNA. BAF53 is commonly associated with TIP48 and TIP49 in chromatin remodelling complexes, and forms a core complex with TIP48, TIP49 and actin (Gallant, 2007). TIP48 and TIP49 form complexes with β-catenin to antagonistically regulate expression of genes downstream of Wnt signalling (Bauer et al., 2000). Moreover, the ATPase activities of TIP48, TIP49 and their complex were shown to be slightly inhibited by the presence of β-catenin (Puri, 2006). Hint1 putatively disrupts interactions between TIP48 and TIP49 in order to regulate Wnt dependent regulation of genes through β-catenin (Weiske and Huber, 2005). Thus, BAF53, β-catenin and Hint1 were selected, due to their reported interactions with TIP48 and TIP49.

We attempted to purify the three human recombinant proteins. BAF53 was insoluble and formed aggregates upon refolding. β-catenin formed dimers by gel filtration in contrast with reports from the literature, where β-catenin was exclusively monomeric (Daniels and Weis, 2002). Recombinant Hint1 formed stable homodimers in solution after purification, in agreement with the published structure (Lima et al., 1996). We then used SEC and ATPase assays to observe the biochemical effects of Hint1 on TIP48, TIP49 and their complex.

5.2 Recombinant human BAF53 is insoluble and forms aggregates upon re-solubilisation

In order to study the effects of BAF53 on the biochemical activity and oligomerisation of TIP48, TIP49 and their complex, we proceeded to express and purify recombinant human BAF53 using a bacterial expression system. A pET21-BAF53-His_6 expression plasmid was provided by Dr. Tsaneva. This plasmid was transformed into *E. coli* BL21-Gold (DE3) cells; expression of BAF53-His_6 and cell lysis was carried out as detailed in the materials and methods (Chapter 2.7.9). Expression and solubilisation was attempted under various conditions; however, BAF53-His_6 was present exclusively in the insoluble fraction after cell lysis under all conditions tested (Figure 5.1a).

A report in the literature showed that a yeast BAF53 homologue, Arp4, binds ATP *in vitro*. The authors in that study produced recombinant Arp4, which was insoluble; however, re-folding was performed after denaturation in 8 M urea (Sunada et al., 2005). We explored the possibility that human recombinant BAF53 could be refolded under similar conditions. BAF53-His_6 was expressed in bacteria, then the cells were lysed; the insoluble fraction after bacterial cell lysis was resuspended in buffer containing 8 M urea. Two renaturation protocols were then utilized to obtain soluble BAF53: 1) urea was removed by stepwise dialysis against buffers with decreasing concentrations of urea, followed by Talon metal affinity chromatography under native conditions; 2) BAF53 was loaded onto a Talon metal affinity column in 8 M urea, then the bound protein was washed in buffers containing decreasing concentrations of urea before elution under native conditions. Both approaches resulted in re-solubilised BAF53-His_6; however, when analysed by SEC under native conditions, BAF53 eluted exclusively in the void volume, where aggregates are expected to elute (Figure 5.1b). These data confirm previous observations that bacterially expressed recombinant BAF53 is not soluble (Puri, 2006); moreover, denaturation in urea, followed by re-solubilisation, does not promote correct folding of BAF53.

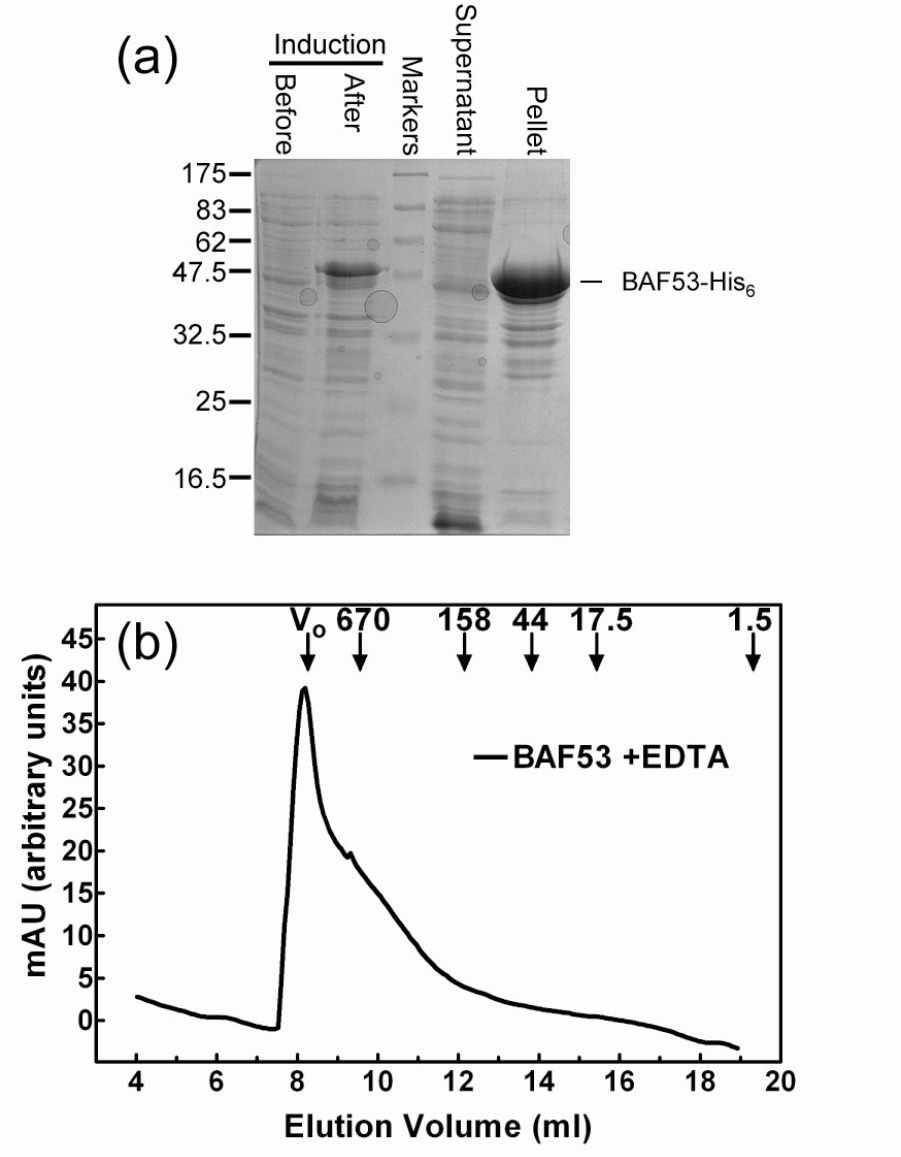

Figure 5.1. Purification of BAF53-His$_6$ under denaturing conditions. (a) BAF53-His$_6$ was induced in BL21-Gold (DE3) *E. coli*; the protein was in the insoluble pellet after cell lysis and solubilisation of proteins. (b) Re-solubilised BAF53-His$_6$ was analysed by SEC using a Superose 6 HR column; the protein eluted in the void volume indicating that it formed soluble aggregates. The arrows indicate the elution volumes of five molecular weight standards and the void volume of the column (V_0).

5.3 Expression and purification of recombinant human β-catenin

To investigate the effects of β-catenin on the oligomerisation of TIP48 and TIP49, recombinant human β-catenin was purified using a bacterial expression system. A pET30-His_6-β-catenin expression plasmid was kindly provided by Prof. Laurence Pearl. β-catenin was expressed and purified following the procedures for purification of TIP48-His_6 (see Chapter 2.7.10).

5.4 SEC of TIP48, TIP49 and β-catenin

Previously, β-catenin was shown to slightly inhibit the ATPase activities of TIP48, TIP49 and their complex *in vitro* (Puri, 2006). In light of these data, and the reported interactions of TIP48, TIP49 and β-catenin *in vivo*, we used recombinant proteins coupled with SEC to observe changes in oligomerisation of TIP48 and TIP49 in the presence of β-catenin.

TIP48 was mixed with β-catenin (equi-molar concentrations) under various conditions and protein complexes were analysed by SEC (Figure 5.2a). TIP48 and β-catenin did not form a stable complex, both in EDTA or in ATP with magnesium, as judged by SEC followed by SDS PAGE analysis of the eluted fractions (Figure 5.2a, SDS PAGE not shown). TIP48 was incubated with ATP and $MgCl_2$ in the presence of β-catenin. Only a small proportion of hexamers were detected in both cases, although TIP48 hexamers reduced by approximately half when mixed with β-catenin. Similarly, TIP49 and β-catenin did not form a complex by SEC in EDTA, and the oligomerisation of TIP49 was not affected (Figure 5.2b). Furthermore, SDS PAGE analysis of the eluted fractions did not demonstrate complexes of TIP49 and β-catenin (data not shown).

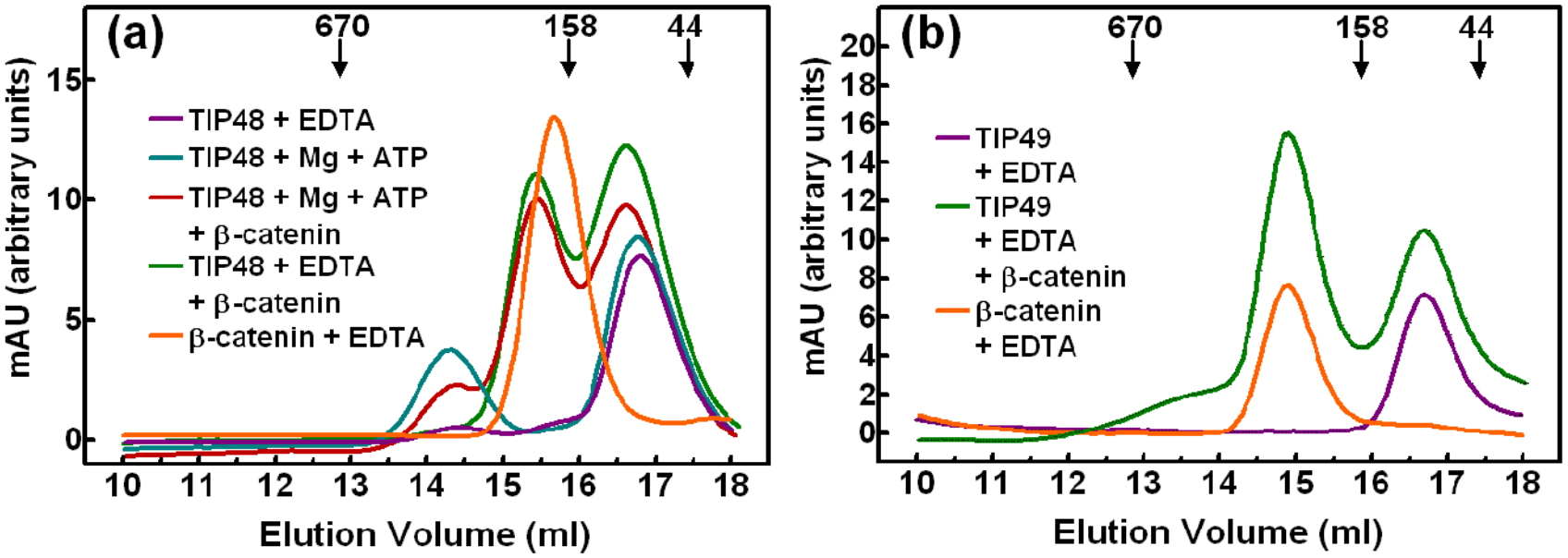

Figure 5.2. Size Exclusion Chromatography of TIP48, TIP49 and β-catenin. TIP48 with EDTA or ATP/Mg was incubated with β-catenin and analysed on a Superose 6 HR SEC column (a). TIP49 was incubated with β-catenin in EDTA and analysed by SEC (b). Arrows indicate the elution volumes of three molecular weight standards in kDa.

Strikingly, β-catenin eluted as a single species at ~ 14.9 ml, which equates to 247 kDa. The molecular mass of human β-catenin is 85.5 kDa; this implies that the species observed by SEC is a dimer or trimer of β-catenin. A previous analysis of a truncated mouse β-catenin (β-cat ARM-CT: residues 118–781) using SEC clearly showed that β-catenin eluted as a monomer (Daniels and Weis, 2002). This discrepancy may be explained by the elongated coiled-coil shape of β-catenin, giving rise to the increased estimated molecular mass of β-catenin by our method (Xing et al., 2008); however, there may also be inappropriate oligomerisation of β-catenin in our study. For this reason, further analysis using this construct of β-catenin was not performed, pending further investigation of the solution structure of recombinant β-catenin.

5.5 Expression and purification of recombinant human Hint1

Evidence has recently come to light that Hint1, a human cancer suppressor protein, plays a role in regulating the Wnt signalling pathway by modulating β-catenin activity. It was suggested that Hint1 may be involved in regulation of the Wnt pathway by disrupting interactions between TIP48 and TIP49 oligomers (Weiske and Huber, 2005). This in turn may affect the catalytic activity of TIP48, TIP49 or their complex in the presence of Hint1. To address these hypotheses, we generated recombinant human Hint1-His_6 using a bacterial expression system.

The Hint1 CDS was amplified from a cDNA library derived from human testes tissue. The PCR product was then cloned into pGEM and the Hint1 CDS was sequenced. Finally, Hint1 was sub-cloned into pET21b and pET15b expression vectors in order to express recombinant Hint1 (no tag) and His_6-Hint1 respectively. pET21-Hint1 and pET15-His_6-Hint1 were transformed into BL21-Gold (DE3) *E. coli*; induction of protein production and cell lysis was carried out

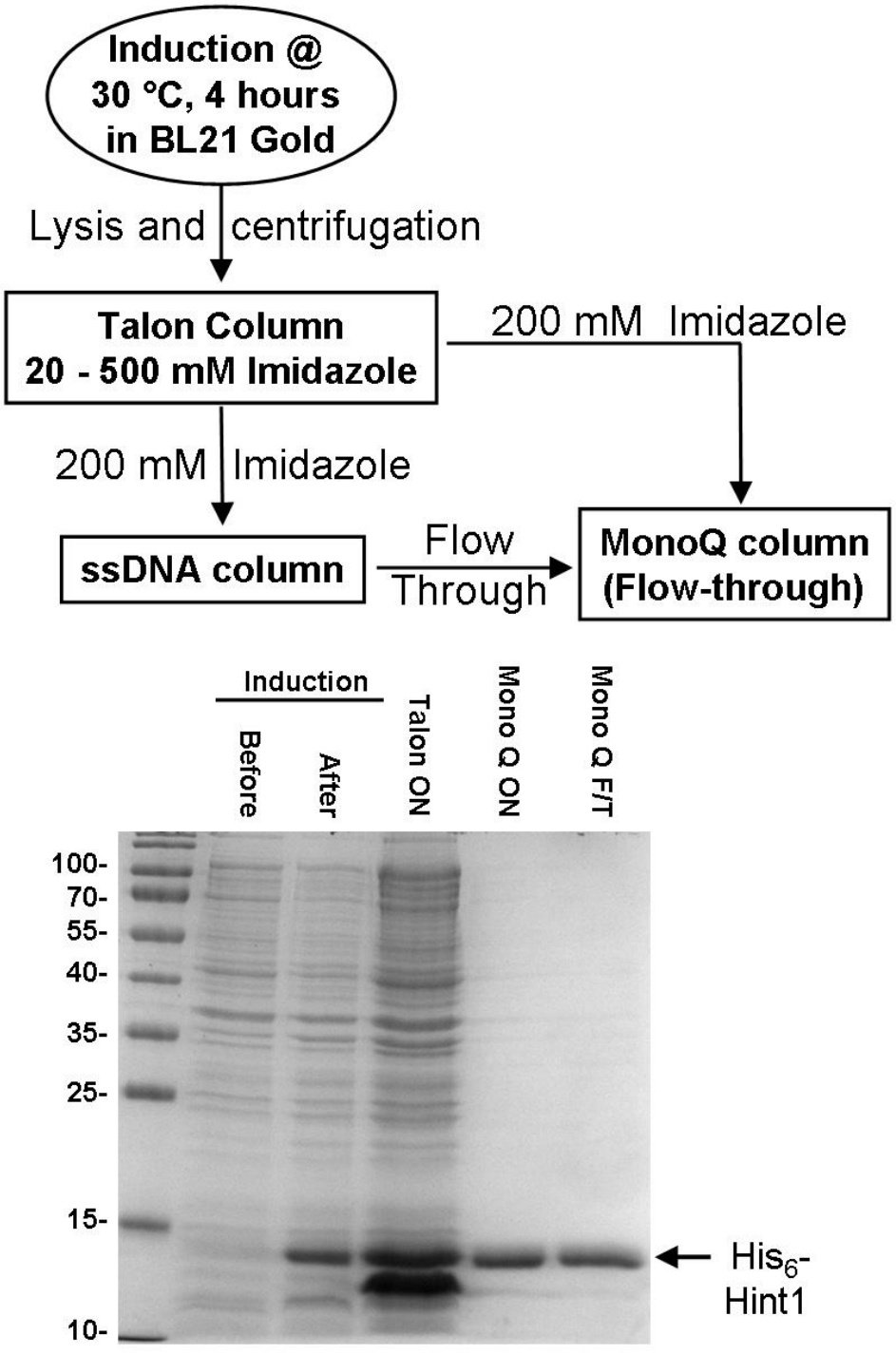

Figure 5.3. Purification of His_6-Hint1. A schematic representation of His_6-Hint1 purification is shown above. Below, a 12 % polyacrylamide SDS PAGE summary gel stained with Coomassie depicts the stages of Hint1 purification. Numbers beside gels refer to the sizes of molecular weight standards in kDa. F/T - Flowthrough

as outlined in Chapter 2.7.11. Both Hint1 and His_6-Hint1 were predominantly in the soluble fraction after cell lysis and ultracentrifugation (Figure 5.3).

Surprisingly, untagged Hint1 did not bind to any columns tested (data not shown - see materials and methods 2.7.11). As the hexa-Histidine tag did not affect the expression or solubility of the recombinant protein, His_6-Hint1 was expressed and purified using a Talon metal affinity column. His_6-Hint1 was thus used for all further biochemical characterization. His_6-Hint1 was expressed in BL21-Gold (DE3) *E.coli* and harvested. The bacterial lysate was applied to a Talon column, then eluted Hint1 was passed through a MonoQ column (Figure 5.3).

5.6 Hint1 does not affect the oligomeric state of TIP48, TIP49 or their complex

The oligomeric state of recombinant human His_6-Hint1 (hereafter referred to as Hint1) was analysed by SEC using a Superose 6 HR SEC column. Hint1 eluted at approximately 18.3 ml, calculated to be equivalent to 28 kDa (Figure 5.4a); this is consistent with a dimer of Hint1 which would have a molecular mass of 27.4 kDa. Our data are in agreement with other groups, who demonstrated that Hint1 forms a dimer in solution (Weiske and Huber, 2005); Hint1 was also dimeric in crystallographic analyses (Lima et al., 1996). Incubation of Hint1 with ATP in magnesium chloride did not affect this dimer of Hint1 (Figure 5.4a).

Having established that magnesium and ATP do not modulate the oligomerisation of Hint1, we tested the effect of Hint1 on the oligomerisation of TIP48 and TIP49. TIP48, which is monomeric in EDTA, forms hexamers when incubated with adenine nucleotides and divalent magnesium (Chapter 3.3). Furthermore, TIP48 is predominantly hexameric if purified from bacteria in buffer containing divalent magnesium (Chapter 3.3). TIP48 was incubated with $MgCl_2$ or $MgCl_2$ and ATP, then oligomers were analysed by SEC (Figure 5.4b). As seen previously, a large proportion of TIP48 forms hexamers when incubated with ATP, seen by increase in the 14.6 ml (hexamer) peak and proportionate decrease in

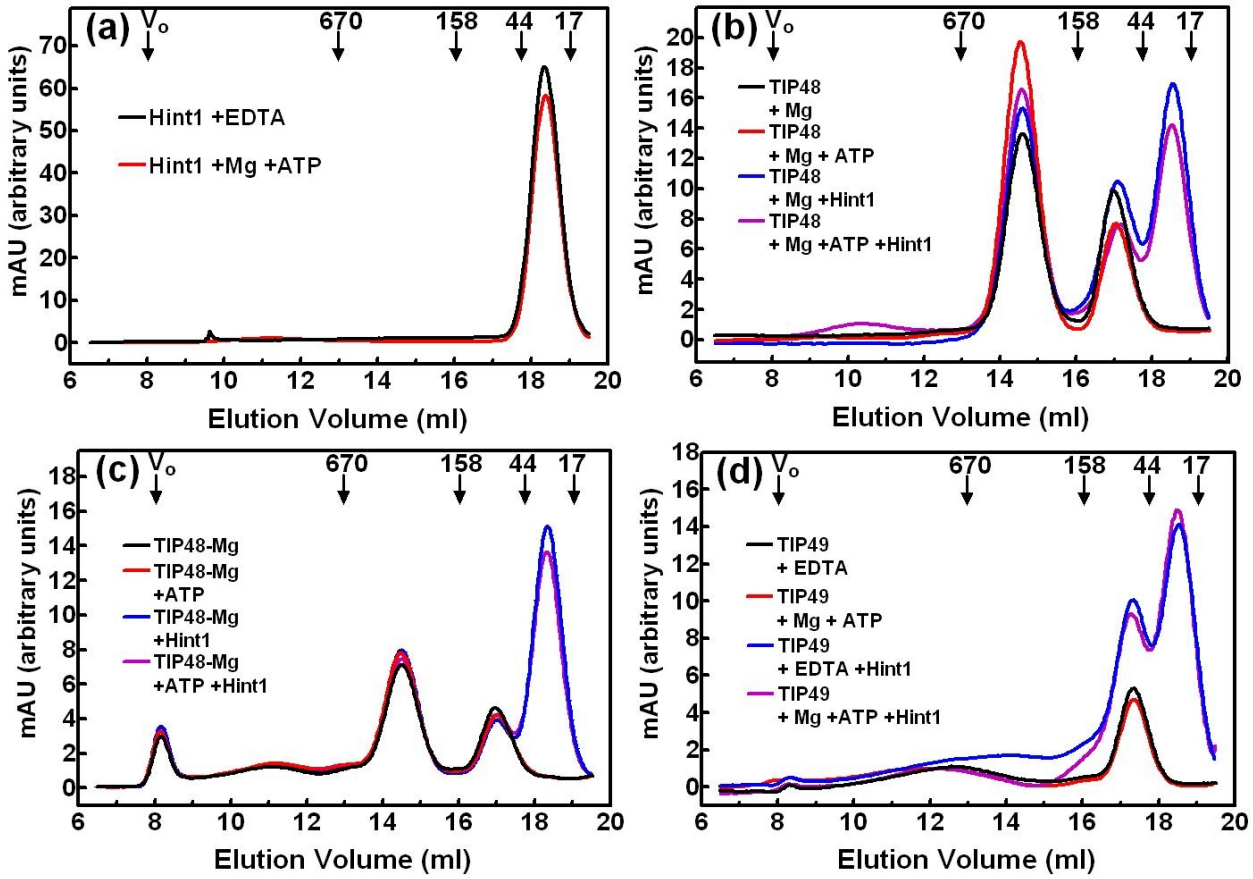

Figure 5.4. Size exclusion chromatography of TIP48-His_6, His_6-TIP49 and His_6-Hint1. The UV_{280} absorbance profiles for samples analysed using a Superose 6 HR SEC column. Hint1-His_6 was incubated with EDTA or Mg/ATP (a). TIP48 and was incubated in $MgCl_2$ buffer for 10 mins at 37 °C with or without Hint1 and/or ATP (b). Hexameric TIP48 purified in $MgCl_2$ buffer was incubated for 10 mins at 37 °C with or without Hint1 and/or ATP (c). TIP49 was incubated in $MgCl_2$ buffer for 10 mins at 37 °C with or without Hint1 and/or ATP (d). The numbered arrows in each figure denote the elution volumes of four molecular mass standards in kDa and the void volume (V_o).

the 17.1 ml (monomer) peak. TIP48 was mixed with Hint1, with or without ATP and the samples were incubated for 10 mins at 37 °C. SEC analysis of these samples indicated no substantial effect of Hint1 on the nucleotide dependent hexamerisation of TIP48 (Figure 5.4b). Next, Hint1 was incubated with TIP48 purified in $MgCl_2$, which is mainly hexameric. There was no significant difference between the proportions of TIP48 hexamers and monomers in the sample when incubated with Hint1 with or without nucleotides (Figure 5.4c). By SEC, TIP49 forms monomers in EDTA, with no change in oligomerisation upon incubation with nucleotides (Chapter 3.2). TIP49 was incubated with Hint1, with or without ATP and the samples were incubated for 10 mins at 37 °C. TIP49 remained exclusively monomeric, both in EDTA and with ATP in magnesium (Figure 5.4d). In all cases, complexes between Hint1 and TIP48 or TIP49 were not detected after SDS PAGE analysis of SEC fractions (data not shown). These data indicate that Hint1 does not stably interact with TIP48 or TIP49 as detected by SEC, and that Hint1 does not affect homo-typic interactions of TIP48 and TIP49.

We then used SEC to explore the effects of Hint1 upon TIP48/TIP49 complexes. As detailed in Chapter 3, two stable TIP48/TIP49 complexes can be separated by SEC: a double hexamer and a single hexamer. We initially incubated the single hexamer, which elutes in fraction 15 from a Superose 6 SEC column, with and without ATP in magnesium. We saw an enrichment of hexamers in the presence of nucleotides, which may be attributed to hexamerisation of free TIP48 or destabilization of double hexameric species (Figure 5.5a). In the presence of Hint1, there was no difference in the proportions of these species in EDTA or nucleotides, indicating that Hint1 does not affect the single hexamer of TIP48/TIP49. The predominant form of the TIP48/TIP49 complex, purified from bacterial expression strains, is a double hexamer, and elutes in fractions 13 and 14 from a Superose 6 SEC column. We assessed the effect of Hint1 upon this double hexameric complex in buffer containing either EDTA or ATP with magnesium chloride (Figure 5.5b). Hint1 did not have a significant effect on the double hexameric complex by this method (Figure 5.5b). Moreover, no stable

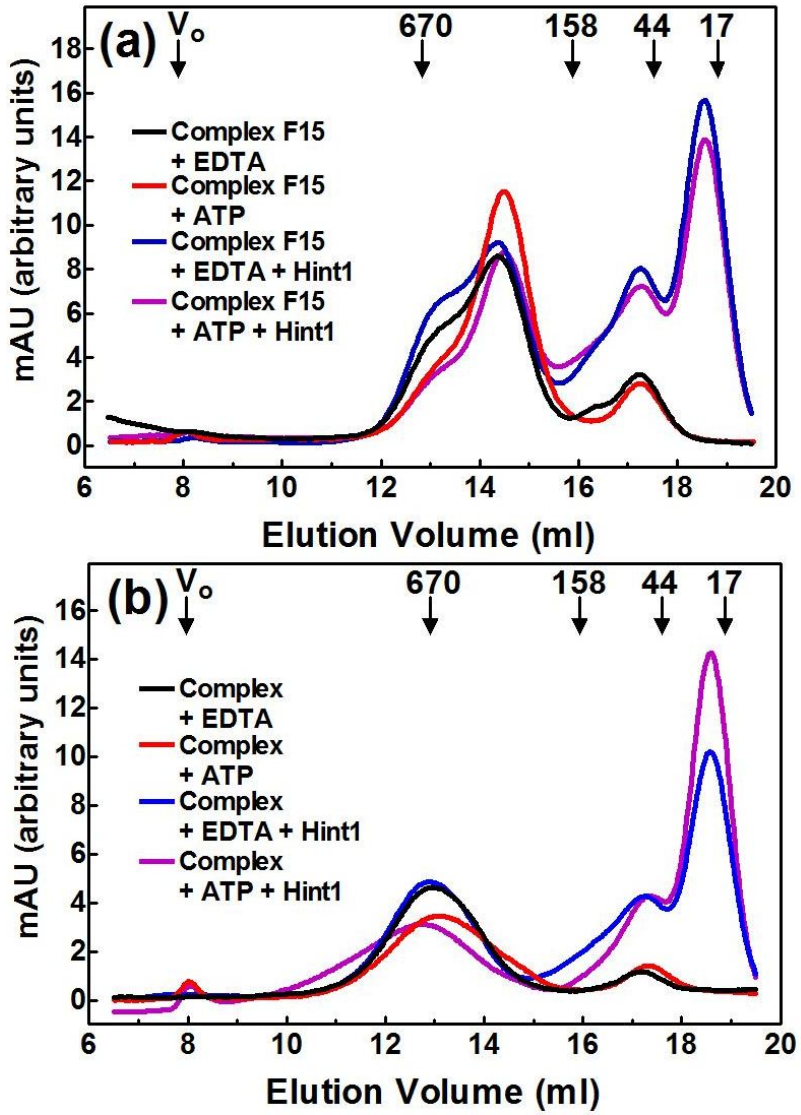

Figure 5.5. Size exclusion chromatography of TIP48/TIP49-His$_6$ complexes and His$_6$-Hint1. The UV_{280} absorbance profiles for samples analysed using a Superose 6 HR SEC column. Putative hexamers of TIP48/TIP49-His$_6$ (isolated from fraction 15 of a Superose 6 column) were incubated in $MgCl_2$ buffer for 10 mins at 37 °C with or without Hint1 and/or ATP (a). Double hexameric TIP48/TIP49-His$_6$ was incubated for 10 mins at 37 °C with or without Hint1 and/or ATP (b). The numbered arrows in each figure denote the elution volumes of four molecular mass standards in kDa and the void volume (V_o).

complexes of TIP48/TIP49/Hint1 were detected by SEC followed by SDS PAGE analysis for the single or double hexamers (data not shown). Our SEC data suggest that Hint1 does not noticeably disrupt pre-assembled TIP48/TIP49 complexes.

No stable interactions of Hint1 and TIP48 or TIP49 were detected by SEC. In order to assess if interactions between Hint1 and TIP49 were evident, we cross-linked proteins by incubating with 1 mg/ml Dimethyl suberimidate in 20 mM Tris pH8, followed by SDS PAGE. TIP48 was not used due to the large number of stable oligomers it forms in solution, compared with TIP49. After cross linking and SDS PAGE analysis, Hint1 ran mainly as a 14 kDa monomeric species; a higher species of approximantely 30 kDa was clearly visible (Figure 5.6). The proportion of Hint1 monomers:dimers appears to be around 3:1, indicating that the cross linking reaction promotes covalently linked dimers, although with limited efficiency. Consistent with AUC profiles in Chapter 3.4, several species of TIP49 were detected after cross linking (Figure 5.6). Although the majority of TIP49 ran as 50 kDa monomers, a proportion was also observed at 70 kDa, 120 kDa and over 200 kDa; dimers, trimers and hexamers would account for these observed species. Next, TIP49 and Hint1 were mixed and crosslinked. The SDS PAGE analysis was similar to the individual proteins, and no novel species were detected (Figure 5.6). This suggests that there is no stable interaction between TIP49 and Hint1, although a weak or transient interaction may exist *in vitro*.

We also analysed species present when Hint1 was incubated with Δ^2TIP49. After crosslinking, Δ^2TIP49 was mainly monomeric (40 kDa) and minor species were detected at approximately 50 kDa, 80 kDa and 200 kDa (Figure 5.6). Again, these could be attributed to dimers, trimers and hexamers of Δ^2TIP49; we did not see any novel species when Hint1 and Δ^2TIP49 were mixed and cross linked (Figure 5.6). This again implies that Hint1 does not stably interact with TIP49. This is consistent with reports that Domain II of TIP49 is responsible for interaction with Hint1, although we cannot rule out a weak or transient interaction.

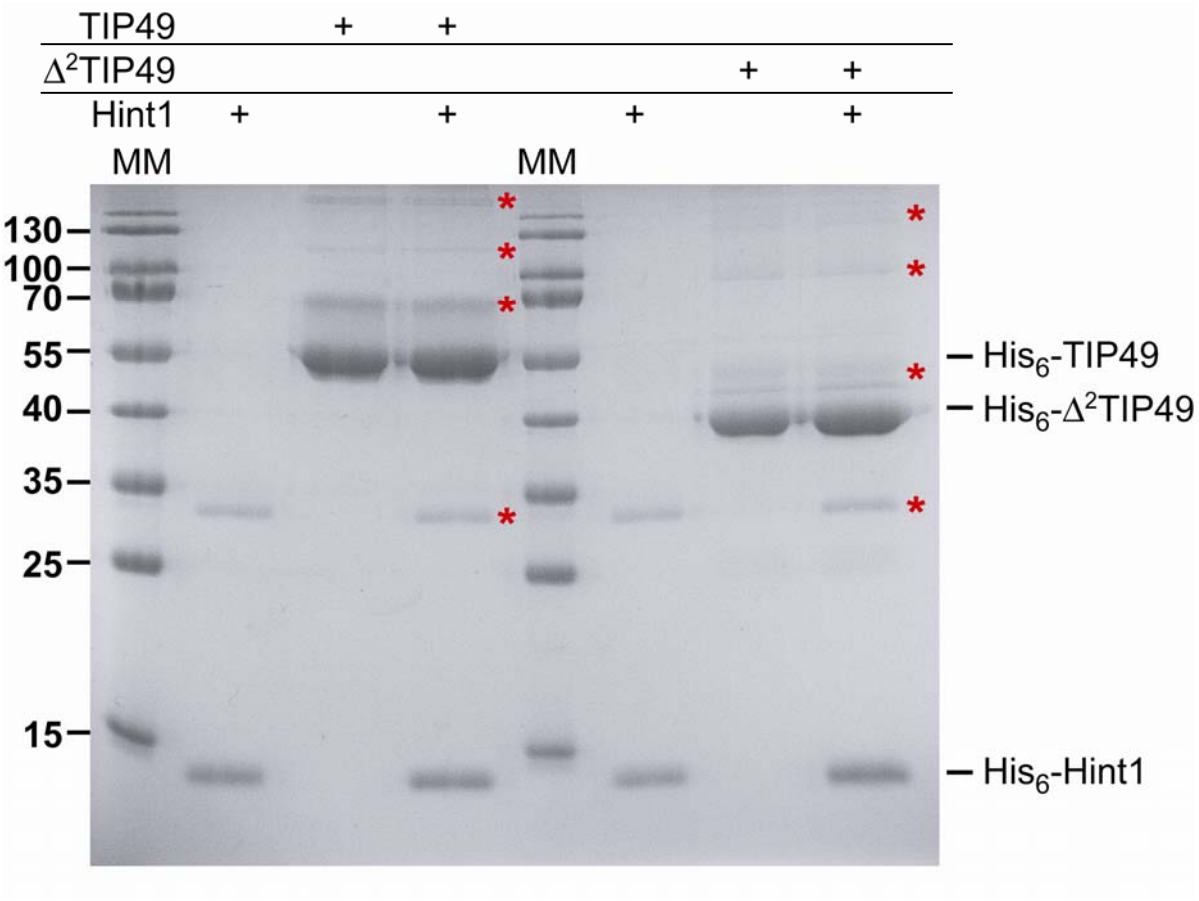

Figure 5.6. Covalent cross-linking of TIP49, Δ^2TIP49 and Hint1 complexes. Proteins were incubated with 1mg/ml dimethyl suberimidate for 3 hours at room temperature, then analysed by 12 % polyacrylamide SDS PAGE. Red stars indicate putative cross linked species. Molecular markers (MM) are indicated with the molecular weights shown in kDa.

5.7 The effect of Hint1 on the activity of TIP48, TIP49 and their complex

Although Hint1 did not have a dramatic effect upon the oligomeric state of TIP48, TIP49 or their complex, it may be the case that Hint1 affects their ATPase activity without modulating tertiary structure. ATPase assays were carried out using P_i Colour Lock colourimetric assay (Innova biosciences) to measure release of P_i upon ATP hydrolysis. TIP48 and TIP49 have individually low ATPase activities: less than 2 moles of ATP were hydrolysed per mole of monomer in 30 mins (Figures 5.7a and 5.7b). The Hint1 preparation displayed basal ATPase activity; activity was likely due to bacterial contaminants. 1 μM TIP48 or TIP49 were incubated with increasing concentrations of Hint1 (1, 3 and 6 μM) and ATP hydrolysis was monitored. The activities of TIP48 and TIP49 were individually unaffected by Hint1 at all concentrations tested (Figures 5.7a and 5.7b), suggesting Hint1 does not modulate the activities of TIP48 or TIP49 *in vitro*.

Next, we tested the ATPase activity of the pre-formed TIP48/TIP49 complex in the presence of Hint1. Hint1 displayed very low ATPase activity, while the activity of the complex was around 10 moles of ATP hydrolysed per mole of monomer in 30 mins (Figure 5.7c). This activity is consistent with previous reports and confirms the synergistic increase in activity when TIP48 and TIP49 form a complex (Puri et al., 2007). Interestingly, when Hint1 was incubated with the complex and the activity measured, the activity decreased in a concentration dependent manner. In the presence of 1, 3 and 6 μM of Hint1, the TIP48/TIP49 complex hydrolysed 10, 9 and 8 moles of ATP respectively, per mole of monomer in 30 mins (Figure 5.7c). This indicates that weak or transient interactions with Hint1 may modulate the ATPase activity of the TIP48/TIP49 double hexamer complex.

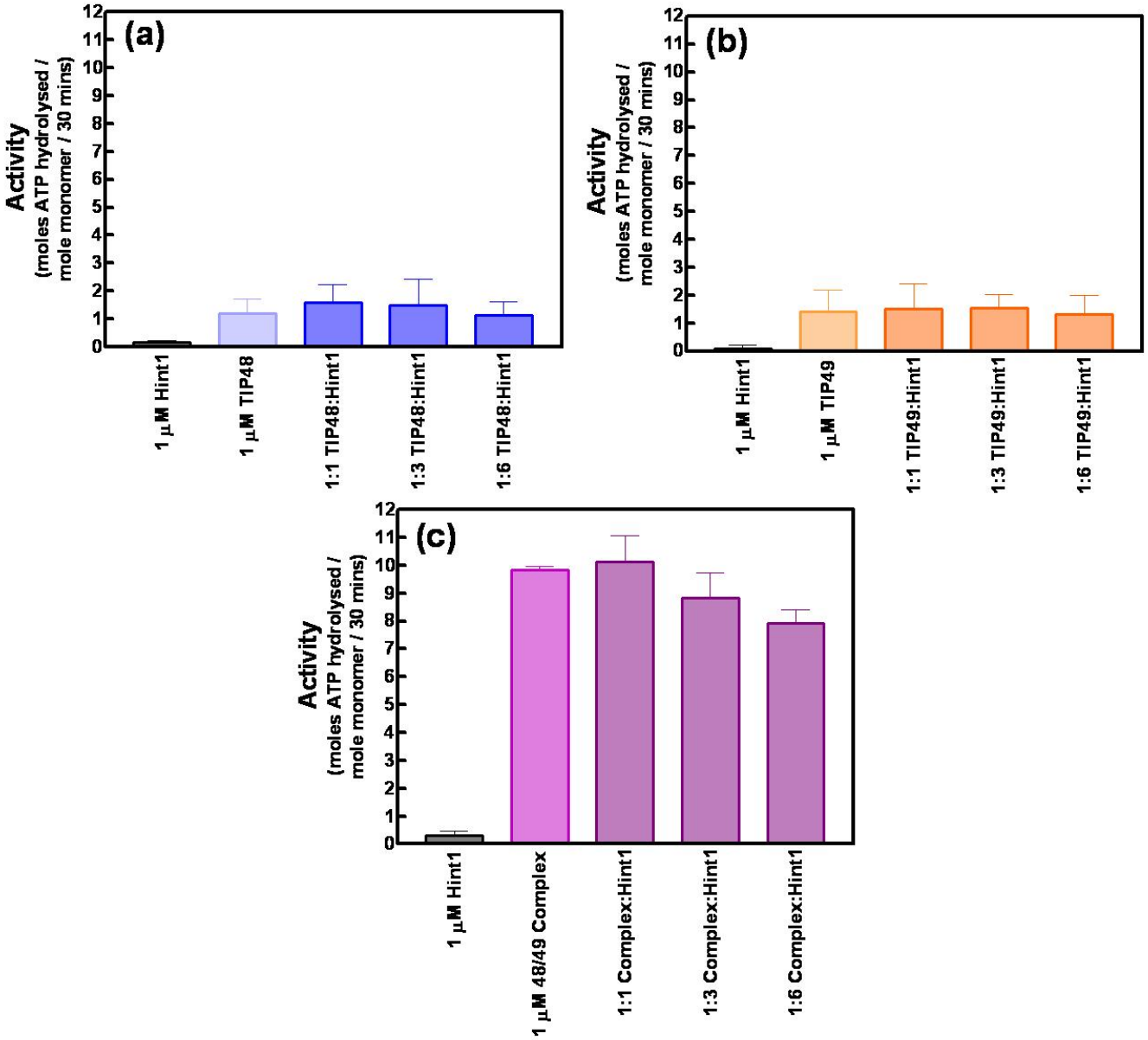

Figure 5.7. The effect of Hint1 on the ATPase activities of TIP48, TIP49 and their complex. The ATPase activities of 1 μM (monomer concentration) of TIP48-His_6 (a); His_6-TIP49 (b); and the TIP48/TIP49-His_6 complex (c) were measured using a malachite green colorimetric assay. 1, 3 or 6 μM Hint1 was incubated with the proteins on ice prior to activity measurement. Activity is defined as the moles of ATP hydrolysed per mole of monomer at 37 °C after 30 mins.

5.8 TIP48, TIP49 and their complex do not display helicase activity

While the work in this thesis was being carried out, a report in the literature rekindled the controversy surrounding the helicase activities of TIP48, TIP49 and their complex. The report in question demonstrated ATP dependent helicase activity for yTIP48, yTIP49 and their complex (Gribun et al., 2008). Since TIP48 and TIP49 are remarkably conserved between eukaryotic species, one would expect that the activities between yeast and mammals would also be conserved; however, no helicase activity has been demonstrated for *Homo sapiens* TIP48 and TIP49. Moreover, it was suggested from the crystal structure that Domain II is the putative DNA binding domain, although that group detected no helicase activity with recombinant proteins (Matias et al., 2006). The helicase activity with the yeast proteins was on a short duplex substrate (15 bp), so these differences may be due to the length of duplex DNA on the helicase substrates tested. In order to substantiate this, helicase substrates were constructed which had 16 and 30 bp duplex regions. Neither TIP48, TIP49 nor their complex were capable of disrupting the duplex DNA in an ATP dependent manner; additionally no activity was seen when TIP48 and TIP49 were mixed and incubated in the presence of substrate (Figure 5.8 for 16 bp; 30 bp not shown). A small proportion of product was seen in some lanes, although these did not contain ATP, so the activity is most likely due to contaminants (Figure 5.8). Although it is still possible that hTIP48 and hTIP49 do act on DNA, we could not detect any helicase activity under these conditions, in agreement with other observations in the literature (Ikura et al., 2000; Matias et al., 2006; Puri et al., 2007; Puri, 2006). Furthermore, we did not test the helicase activities of Δ^2TIP48 or Δ^2TIP49, as these proteins lack Domain II, which is hypothesised to be the domain responsible for interacting with DNA.

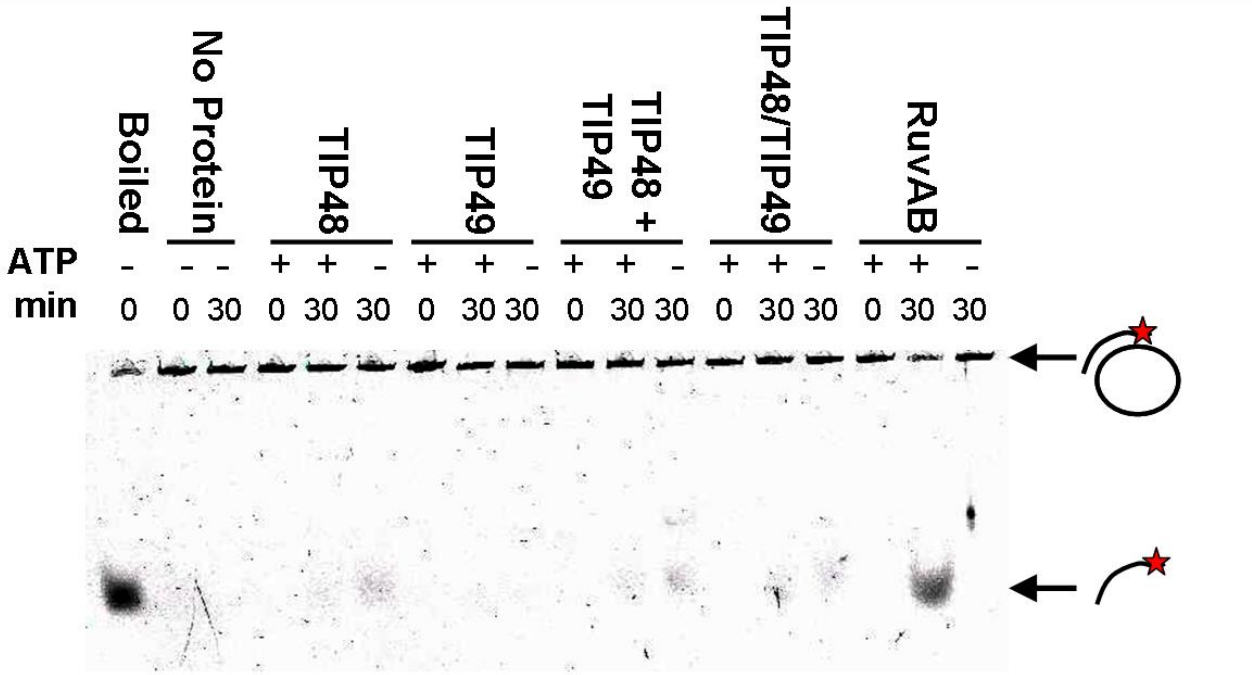

Figure 5.8. TIP48, TIP49 and their complex do not display helicase activity. A 16 nucleotide ssDNA oligomer with a fluorescent tag (red star) annealed to ΦX174 virion ssDNA was used as a helicase substrate. 1 μM (monomer concentration) of TIP48, TIP49 and their complex were incubated with or without 1 mM ATP and the helicase substrate for 30 minutes at 37 ºC. RuvA and RuvB (at 0.2 μM and 1 μM respectively) were used as a positive control. The products of the reaction were analysed by 6 % polyacrylamide TAE (40 mM Tris, 20 mM glacial acetic acid, 1 mM EDTA) PAGE and visualised on the Li-Cor Odyssey imaging system.

5.9 Discussion

In this chapter, we attempted to purify and characterise several putative interacting proteins of TIP48 and TIP49. Unfortunately, BAF53 purified from a bacterial expression system did not form natively folded soluble protein under any conditions tested. This could be explained by BAF53 being an integral component of several nuclear complexes, and presumably, would normally reside in a hydrophobic environment. BAF53 frequently purifies from human nuclei in a complex with actin, which is also a component of the same nuclear complexes as BAF53. Co-expression of BAF53 and actin in bacterial expression systems could aid in the correct folding of BAF53. Likewise, BAF53 is found in nuclear complexes with TIP48 and TIP49. We attempted co-expression of TIP49 and BAF53 in bacteria; however, this did not alter the solubility of BAF53 when purified from bacterial cells (data not shown). It would be interesting to attempt this approach with TIP48, TIP49, actin and BAF53, although co-expression of four proteins is technically challenging. Alternatively, BAF53 could be re-folded in the presence of TIP48/TIP49 complex, as the double hexamer of TIP48/TIP49 has been shown to efficiently re-fold from urea (Puri, 2006).

In addition to its role in controlling the transcriptional response to cell adhesion, β-catenin is a pivotal transcriptional regulator in the Wnt signalling pathway. We expressed and purified human recombinant β-catenin using bacteria. In contrast to previously published work, we observed β-catenin as a dimer or trimer by gel filtration. This could be explained by the elongated shape of β-catenin in solution (Xing et al., 2008), giving rise to a monomer that elutes at the position of a dimer from a Superose 6 SEC column. However, previous studies showed a monomer of β-catenin by SEC (Daniels and Weis, 2002). Thus, dimerisation could have been due to the hexa-histidine tag. As we did not have time to investigate this possibility further, we did not use β-catenin for further studies, and will try to clarify this issue in future experiments.

Hint1 was shown to disrupt homo- and hetero-typic interactions of TIP48 and TIP49 (Weiske and Huber, 2005). These observations were used to speculate that Hint1 disrupts TIP48/TIP49 complexes to regulate β-catenin dependent transcription. We purified recombinant Hint1 using a bacterial expression system. However, we did not detect any disruption of TIP48/TIP49 complexes in the presence of Hint1 by SEC, nor did we see disruption of TIP48 hexamers. Interestingly, (Weiske and Huber, 2005) reported disruption of TIP49 oligomers by Hint1, however, by SEC and AUC we observed TIP49 as predominantly monomeric, with only a small proportion of oligomers. In their study, GST-TIP49 was mixed with TIP49-His_6, then this complex was bound to GSH-agarose. When Hint1-His_6 was mixed with the bound protein, TIP49-His_6 was detected in the supernatant in a concentration dependent manner. The authors concluded that Hint1 disrupts TIP49 oligomers by competitive binding. It is possible that these observations were due to the tags, as we did not detect any stable interactions between Hint1 and TIP49. Moreover, antibodies were used to detect proteins in their assay, meaning quantification may have been in-accurate. (Weiske and Huber, 2005) also purported similar disruption of GST-TIP48/TIP48-His_6 and GST-TIP49/TIP48-His_6 complexes, but did not show the data in their publication. Again, we did not see disruption of these oligomers in SEC experiments, which could be due to the experimental techniques used.

Although no disruption of TIP48 or TIP49 oligomers was seen in our studies, we did observe a moderate decrease in ATPase activity of the TIP48/TIP49 complex by Hint1. This could indicate a weak interaction of Hint1 and TIP48/TIP49, although the functional significance of this is difficult to deduce without further experiments. Indeed an interaction between tagged, ectopically expressed TIP48/TIP49 and Hint1 was demonstrated by co-immunoprecipitation from HEK293 cells (Weiske and Huber, 2005), supporting the possibility of a weak binding, or that other cellular factors facilitate this interaction.

Finally we employed helicase assays using substrates with short duplex regions to confirm if hTIP48 or hTIP49 are *bona fide* helicases. Several groups have not

detected helicase activity for human recombinant TIP48, TIP49 or the TIP48/TIP49 complex (Ikura et al., 2000; Matias et al., 2006; Puri et al., 2007), while helicase activity for the equivalent yeast proteins has been reported (Gribun et al., 2008). One important difference was the length of duplex region for the helicase substrate. For this reason, we assayed the activity of the human proteins with a helicase substrate with a 16 bp duplex region. In agreement with other published data, we saw no helicase activity for the human proteins. Conversely, a group that studied the yeast proteins reported robust ATP dependent helicase activity, with substrate processed to completion by the yTIP48/TIP49 complex after 30 mins (Gribun et al., 2008). This difference may be due to a genuine disparity between the catalytic activities of the yeast and human proteins. However, in the yeast study, the TIP48/TIP49 complex purified was a single hexamer. In chapter 3, we also detected a small proportion of TIP48/TIP49 hexamers, although they did not display activity equivalent to the double hexamer of TIP48/TIP49. We find it unlikely that TIP48/TIP49 are genuine helicases in yeast and are not in mammals; we instead suggest either that human TIP48/TIP49 require other co-factors for helicase activity *in vitro*, or that the yeast proteins co-purified with bacterial helicase contaminants. Although we demonstrated structural differences between yeast and human TIP48/TIP49 complexes in Chapter 4, we favour the latter possibility for several reasons: 1) The highly conserved protein sequences of TIP48 and TIP49 in all eukaryotes makes it unlikely that they would be active helicases in some species, but not others. 2) The TIP60 complex has helicase activity *in vitro*; however, TIP60, but not TIP48 or TIP49, is the catalytic subunit responsible for this activity (Ikura et al., 2000). 3) TIP48 and TIP49 seem to have DNA-independent roles in several processes, including telomerase assembly, snoRNP maturation and mitotic spindle dynamics. Further characterisation of the yeast and human proteins *in vitro* will begin to address these issues, and may give insights into their differences and will clarify their molecular mechanisms *in vivo*.

Chapter 6

Sub-cellular Localisation and Post-translational modification of TIP48 and TIP49

6.1 Introduction

TIP48 and TIP49 are regularly found in the same nuclear complexes. Interestingly, TIP48 and TIP49 also have several seemingly unrelated roles in eukaryotic cells. Examples of these distinct roles include the interactions of TIP48 with ATF2 and the *Drosophila* PcG complex; in both complexes, TIP49 was not detected (Cho et al., 2001; Diop et al., 2008).

It has been reported that TIP48 and TIP49 both localise at the mitotic spindle during mitosis (Gartner et al., 2003; Sigala et al., 2005). Moreover, both were implicated in the correct assembly of the mitotic spindle (Ducat et al., 2008). Interestingly, TIP48, but not TIP49, was detected at the midbody and midzone during cytokinesis (Sigala et al., 2005). This difference between the sub-cellular localisation of TIP48 and TIP49 during the cell cycle may reflect a genuine difference in their roles. Alternatively, the methods used to study the localisation of TIP49 during mitosis may not have been appropriate to detect TIP49 at the midbody and midzone. To investigate these possibilities, we used a CDK1 (Cyclin dependent kinase 1) inhibitor, RO-3306, to enrich the population of cells in mitosis. We also ectopically expressed a TIP49-GFP fusion protein in combination with the RO-3306 mediated mitotic synchronisation.

TIP48 and TIP49 were reportedly SUMOylated in metastatic cell lines (Kim et al., 2006; Kim et al., 2007). Acetylation and phosphorylation of TIP48 and TIP49 has also been reported as part of large scale proteomics studies (Chapter 1.7.7). To begin to delineate the PTMs (Post translational modifications) of TIP48 and TIP49, we analysed HeLa cell extracts using 2-D PAGE. The identification and dynamics of specific PTMs could give valuable insights into the co-ordination of the different functions of TIP48 and TIP49.

6.2 Generation of antibodies against recombinant human TIP48 and TIP49

Polyclonal antibodies against recombinant hTIP48 and hTIP49 were raised in rabbits. Antibodies were then affinity purified using recombinant hTIP48-His_6 and His_6-hTIP49 bound to HiTrap NHS activated columns (Chapter 2.8).

Recombinant TIP48 was used as an epitope for raising antibodies in rabbit. Two separate affinity purifications of the resulting polyclonal anti-hTIP48 antibodies from the same rabbit were performed. The first was carried out by previous members of Dr. Tsaneva's group (TIP48-PC1) (Figure 6.1a), the other was performed as part of the work for this thesis (TIP48-PC2) (Figure 6.1b). The rabbit anti-TIP48 antibodies were characterised by testing their affinity for purified recombinant TIP48-His_6 as well as endogenous TIP48 in HeLa cells. Cross reactivity with His_6-TIP49 was also tested. TIP48-His_6, His_6-TIP49 and HeLa cell WCE (whole cell extracts) were analysed by 12 % polyacrylamide SDS PAGE followed by Western blotting using anti-TIP48 antibodies (Figure 6.1). Both TIP48-PC1 and TIP48-PC2 antibodies reacted strongly with 0.1 and 0.5 µg of TIP48-His_6. TIP48-PC1 and TIP48-PC2 antibodies also reacted with His_6-TIP49 indicating a degree of cross reactivity, although TIP48-PC1 antibodies cross reacted with TIP49 slightly less than TIP48-PC2 antibodies (Figures 6.1a and b). The affinities of the anti-TIP48 antibodies for TIP48 or TIP49 were compared by measurement of the signal density of each band. In both cases, the antibodies detected TIP48 over 100 fold more strongly than the same amount of TIP49 (Figure 6.1a and b). A prominent band of ~ 55 kDa was consistently detected in HeLa WCEs, and is most likely to be endogenous TIP48. Although there seemed to be some non-specific binding to proteins in the HeLa WCE, there was a band consistently detected at around 65 kDa, which could be a modified form of TIP48 (Figures 6.1a and b). Bands which were below 50 kDa could correspond to partially degraded TIP48 in the extracts. The putative modified form(s) of TIP48 was further investigated using 2-D PAGE (see Chapter 6.6).

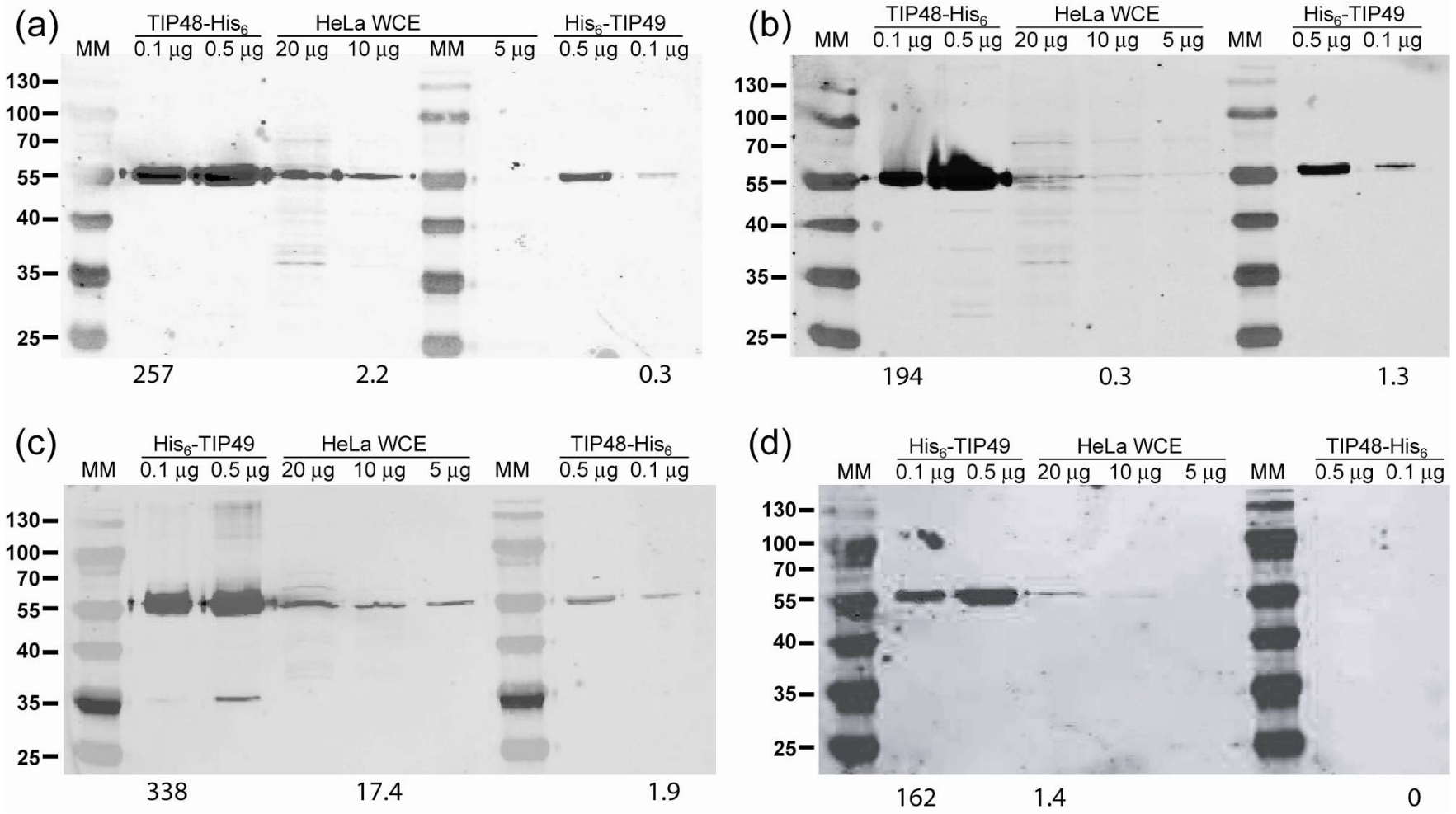

Figure 6.1. Characterisation of anti-TIP48 and anti-TIP49 antibodies. 0.1 µg and 0.5 µg of recombinant TIP48 and TIP49, and 20, 10 and 5 µg of HeLa extracts were loaded onto 12 % polyacrylamide SDS gels. Western blotting was then performed using (a) rabbit polyclonal anti-TIP48-PC1, (b) rabbit polyclonal anti-TIP48-PC2, (c) rabbit polyclonal anti-TIP49, or (d) mouse monoclonal anti-TIP49. The numbers below each gel refer to the quantification of the intensity of signal densities (0.1 µg of recombinant protein, 10 µg of HeLa extract for polyclonal antibodies and 20 µg of HeLa extract for monoclonal antibodies were quantified). Molecular markers (MM) are shown in kDa on the left of each gel.

Polyclonal rabbit antibodies against human His_6-TIP49 were raised, and affinity purified using His_6-TIP49. The properties of the antibodies were assessed by Western blotting (Figure 6.1c). TIP49 polyclonal antibodies reacted very strongly with recombinant His_6-TIP49 at 0.5 µg and 0.1 µg. In comparison, the antibodies weakly bound to recombinant TIP48-His_6; the affinity of the TIP49 polyclonal antibodies for TIP48 was judged to be over 150 fold weaker than TIP49 by comparing the density of the bands. A prominent band was seen at ~ 55 kDa in Western blots of HeLa WCEs, which is most likely to be endogenous TIP49. Faint bands of higher mass than TIP49 were also detected in HeLa WCEs at around 60 and 70 kDa (Figure 6.1c). This could be post translationally modified forms of TIP49, and will be further investigated using 2-D PAGE (see Chapter 6.6).

Mouse monoclonal antibodies raised against an N-terminal peptide of TIP49 (A^{35} ASGLVGQENAR^{46}) were kindly provided by Dr. Wagner (Gartner et al., 2003). Growth medium containing monoclonal antibodies was passed through a HiTrap Protein A column and TIP49 monoclonal antibodies were eluted using 1 M Sodium Citrate, pH3. The specificity of the TIP49 monoclonal antibodies was tested using Western blotting (Figure 6.1d). TIP49 monoclonal antibodies strongly reacted with 0.5 µg and 0.1 µg of recombinant His_6-TIP49 and a single band was seen in HeLa WCEs (Figure 6.1d); however, the band was only detected at 20 µg of HeLa extract. As expected, the monoclonal antibodies did not react with 0.5 µg TIP48-His_6, demonstrating strong specificity. Thus, the monoclonal TIP49 antibodies are more specific than the polyclonal antibodies. However the monoclonal antibodies reacted more weakly with TIP49 in HeLa extracts than the polyclonal antibodies (compare Figures 6.1c and d).

6.3 TIP48 localises at the midbody during cytokinesis in HeLa cells after synchronisation with RO-3306

Using a double thymidine block, TIP48 was previously shown to localise at the mitotic spindle, and at the midzone and midbody during cytokinesis (Sigala et al., 2005). RO-3306 is a recently discovered compound which blocks cells at G2/M by inhibiting CDK1 (Vassilev et al., 2006). In order to confirm a difference between the localisation of TIP48 and TIP49 in late mitosis, we wanted to use a TIP49-GFP fusion protein in conjunction with RO-3306 to directly visualise TIP49 in HeLa cells during mitosis. Initially, we synchronised cells with RO-3306 and released into mitosis, then used anti-TIP48 antibodies to demonstrate the sub-cellular localisation of TIP48. HeLa cells were incubated in growth medium supplemented with 9 μM RO-3306 for 20 hrs. Cells were released from the G2/M by removing RO-3306 and were grown for a further 30 - 120 mins. Treatment of the cells with RO-3306 and subsequent release substantially enriched the mitotic population of HeLa cells. Immunostaining of the cells with polyclonal antibodies against TIP48 and monoclonal antibodies against Tubulin confirmed that TIP48 localised at the mitotic spindle (Figure 3.2). TIP48 was also detected at the midbody and midzone during cytokinesis (Figure 3.2).

TIP49 has been shown to localise at the mitotic spindle, but unlike TIP48, has not been detected at the midbody or midzone (Gartner et al., 2003; Sigala et al., 2005). This may have been due to the mitotic enrichment, detection method or antibodies used. Indeed, a limitation of immunofluorescence is the possibility that epitopes are hidden, which may have resulted in the apparent absence of TIP49 at the midbody with the previous antibodies (Sigala et al. 2005). In order to confirm this disparity, we used new polyclonal TIP49 antibodies that were generated using a fresh immunisation of rabbit with full length TIP49, and synchronised cells in mitosis using RO-3306. Although TIP49 localised at the spindle, no TIP49 was seen at the midbody or midzone using this method, substantiating previous observations (data not shown).

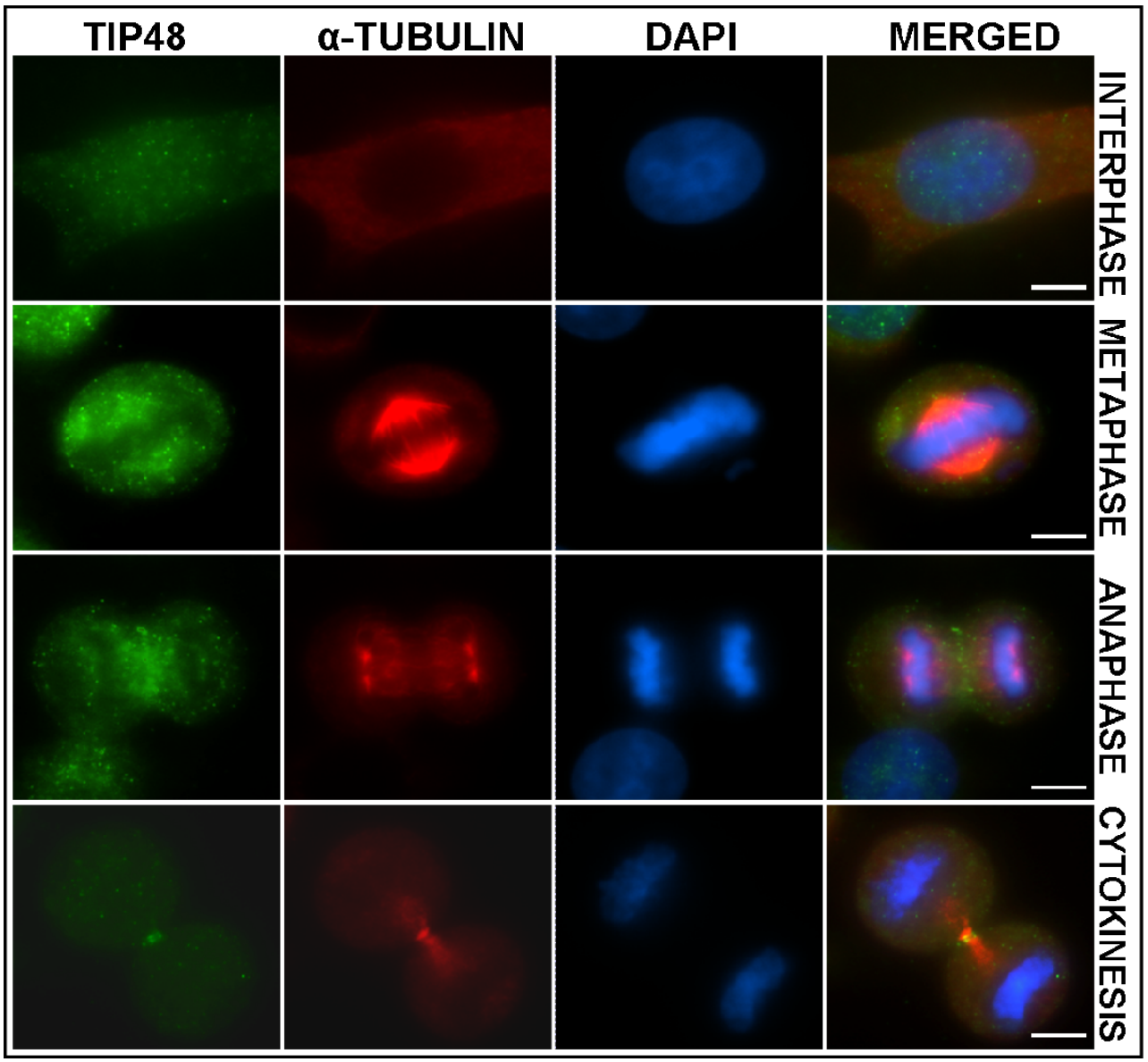

Figure 6.2. Mitotic localisation of TIP48 in HeLa cells. HeLa cells were blocked in G2/M using RO-3306, then released into mitosis. The localisation of TIP48 was assessed using immunofluorescence with rabbit TIP48-PC2 polyclonal antibodies (green), mouse polyclonal anti Tubulin antibodies (red) and DAPI (blue). Representative cells were selected to show interphase, metaphase, anaphase and cytokinetic cells. The scale bars denote 10 μm.

6.4 GFP tagged TIP49 localises at the mitotic spindle in HeLa cells

To further characterise the localisation of TIP49 during mitosis, a pEGFP-TIP49-GFP plasmid (constructed in Dr. Tsaneva's laboratory) was used to ectopically express TIP49-GFP fusion protein in HeLa cells. Cells were initially transfected with the pEGFP-TIP49-GFP plasmid, then blocked in G2/M by adding 9 μM RO-3306 to the growth medium for 20 hours. Cells were then released into mitosis by removal of RO-3306 and addition of fresh growth medium for 30 - 120 mins. Direct visualisation of TIP49-GFP revealed that TIP49 associated with the mitotic spindle (Figure 6.3), confirming previous observations (Gartner et al., 2003). Unfortunately, the population of mitotic cells was severely reduced compared with untransfected controls (data not shown), and the percentage of cells expressing TIP49-GFP was lower than cells expressing GFP only, after transfection with an empty pEGFP plasmid (Figure 6.3). Moreover, we did not identify any cells in telophase or cytokinesis. These observations may have been due to a dominant negative effect of TIP49-GFP, causing transfected cells to undergo apoptosis or detach from cover slips. In addition, it was recently purported that N- or C-terminal GFP-tags affected localisation of TIP49 in HeLa cells (Cvackova et al., 2008), which may also affect the localisation of endogenous TIP49. Thus, using GFP to directly visualise TIP49 during mitosis is not an effective method of confirming distinct localisation of TIP48 and TIP49.

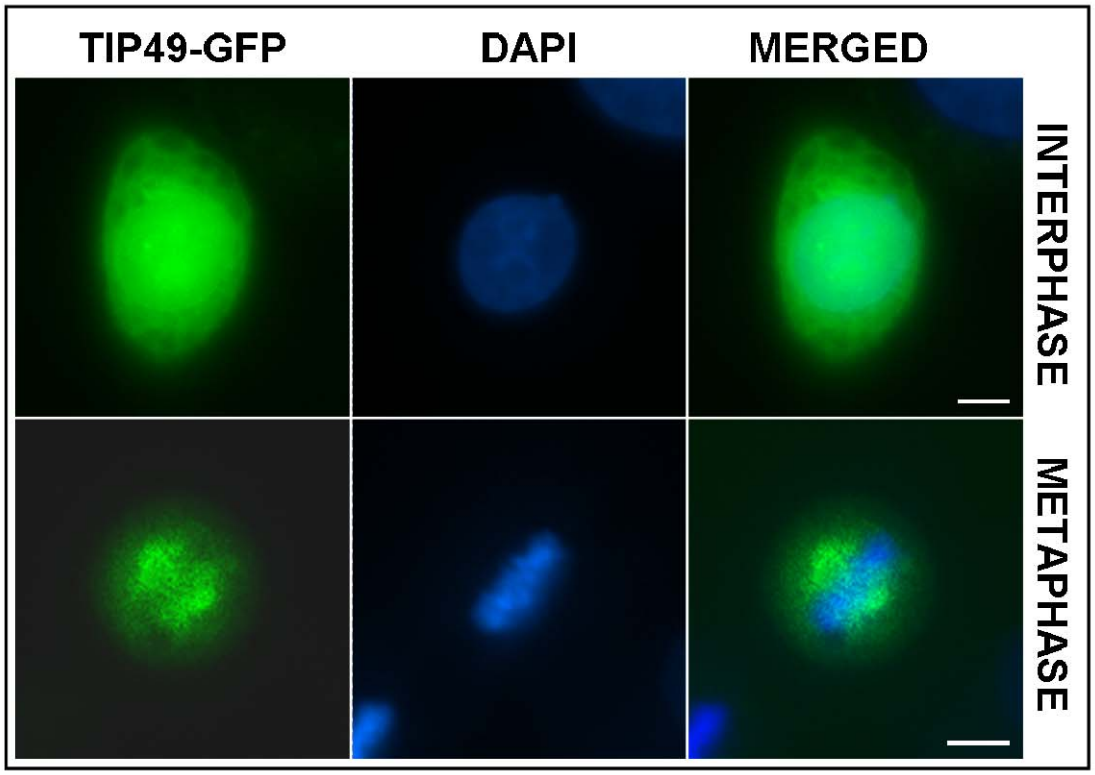

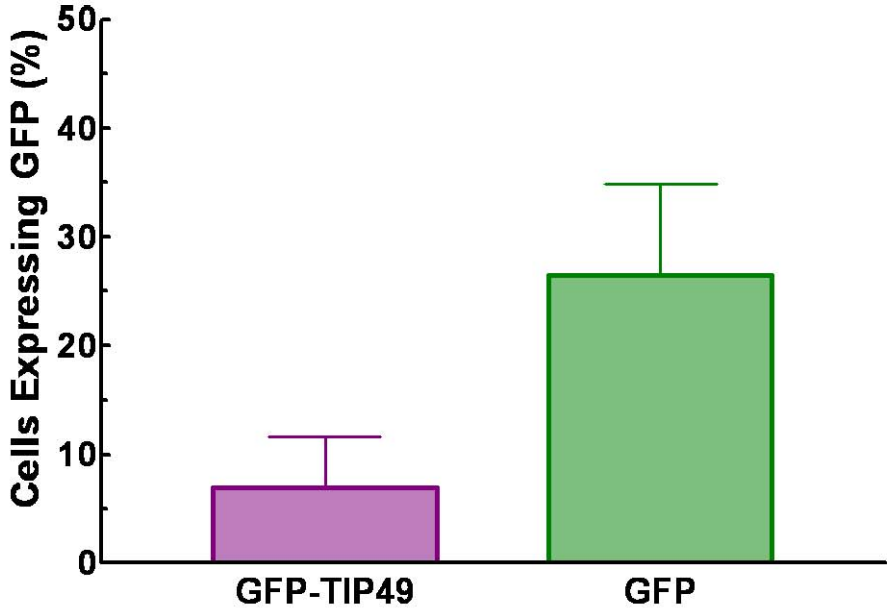

Figure 6.3. Direct visualisation of TIP49-GFP in HeLa cells. HeLa cells were transfected with pEGFP-TIP49, blocked in G2/M using RO-3306, then released into mitosis. The localisation of TIP49 was monitored by direct visualisation of TIP49-GFP (green) and DAPI (blue) at interphase and metaphase (top). The scale bars denote 10 μm. No cells beyond metaphase were detected. After transfection with pEGFP-TIP49 or an empty pEGFP plasmid, cells were synchronised in mitosis. The number of cells expressing TIP49-GFP or GFP is shown as a percentage (bottom). Error bars denote standard deviation.

6.5 Nuclear and cytoplasmic localization of TIP48 and TIP49

Immunofluorescence, and direct visualisation of TIP49 by GFP tagging, showed both nuclear and cytoplasmic localisation of TIP48 and TIP49. Furthermore, immunodetection of TIP48 and TIP49 in HeLa cell lysates showed several species, which could account for modified forms of TIP48 and TIP49. We wanted to further explore the distribution of TIP48 and TIP49 in HeLa nuclei and cytoplasm, and to identify if the distinct putative forms of TIP48 and TIP49 associate with the nucleus or cytoplasm. We performed nuclear-cytoplasmic fractionation of HeLa cells using a commercially available kit (Proteo-JET from Fermentas).

HeLa cell nuclear (Nuc.), cytoplasmic (Cyt.) and whole cell (WCE) extracts were separated using 12 % polyacrylamide SDS PAGE and analysed by Western Blotting (Figure 6.4). When anti-TIP48 antibodies (TIP48-PC1 and TIP48-PC2) were used to characterise endogenous TIP48, several bands were detected, which were not consistent between several experiments (data not shown). This was most likely due to the antibodies used, and could not be resolved due to time constraints. In future, these experiments will be repeated after fresh purification of antibodies and cell extracts. More successful results were obtained with the 2-D PAGE experiments, and these give more detailed insights into putative PTMs of TIP48 (Chapter 6.6).

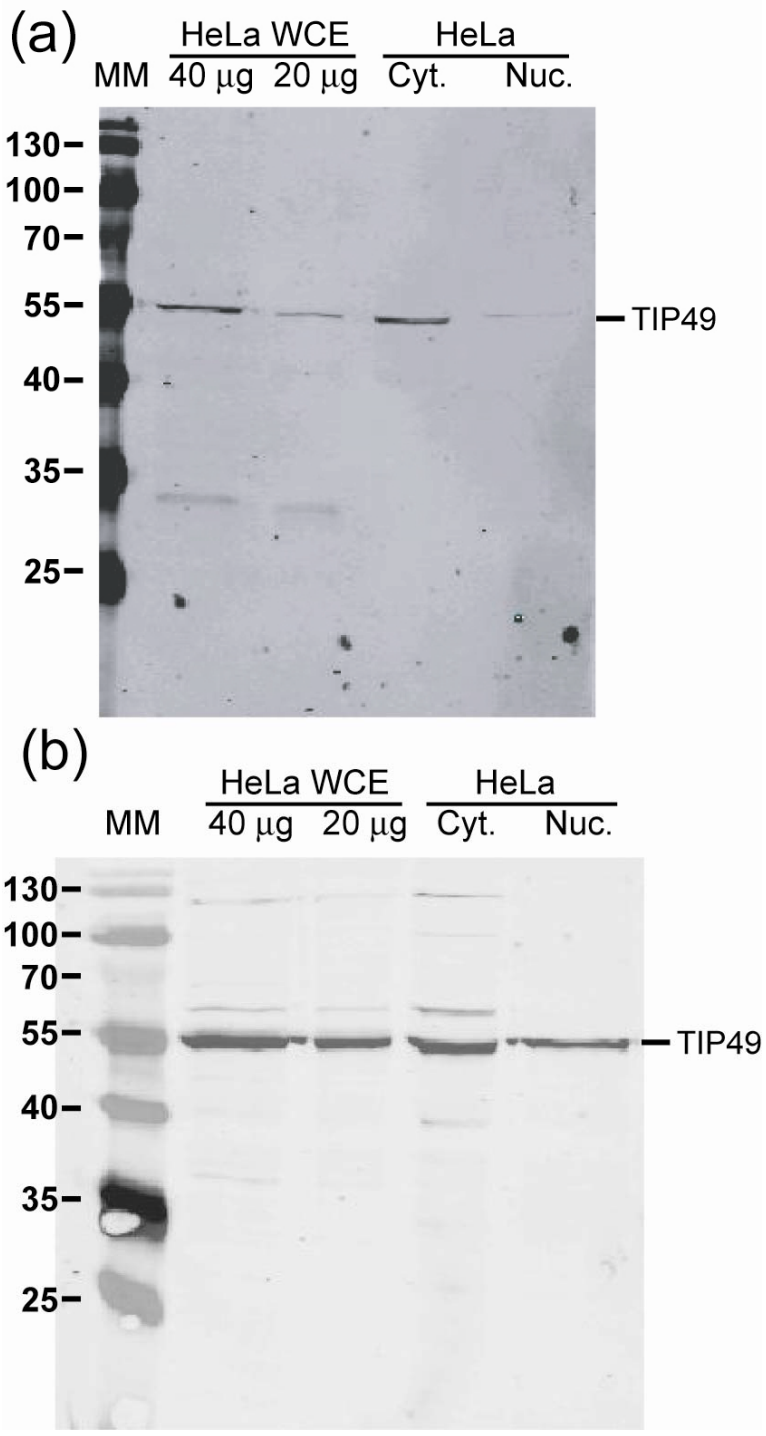

Figure 6.4. Nuclear and cytoplasmic localisation of TIP49. HeLa cells extracts were separated into nuclear (Nuc.) and cytoplasmic (Cyt.) fractions. These fractions, along with whole cell extracts (WCE) were analysed by Western blotting using (a) mouse monoclonal anti-TIP49, or (b) rabbit polyclonal anti-TIP49 antibodies. Molecular markers (MM) are shown in kDa beside each gel.

Analysis of HeLa cell fractions with the TIP49 monoclonal and polyclonal antibodies was also performed (Figure 6.4). Monoclonal antibodies detected a single band of approximately 55 kDa in HeLa cell WCE. Due to the high specificity of these antibodies, this band is most likely to be TIP49. The 55 kDa band was present in cytoplasmic extracts and was faintly detected in nuclear fractions (Figure 6.4a). As seen previously (Chapter 6.2), the anti-TIP49 polyclonal antibodies react more strongly with TIP49 compared with the monoclonal antibodies (Figure 6.1). When the HeLa cell fractions were analysed by immunostaining with TIP49 polyclonal antibodies, the prominent band at 55 kDa was again detected (Figure 6.4b). Although more of this species (likely to be un-modified TIP49) was detected in the cytoplasmic fraction, a significant amount was present in the nucleus, with a ratio of around 3:1 cytoplasmic to nuclear (Figure 6.4b). In addition to this band, several higher bands were observed at approximately 60, 70 and 90 kDa, with the 60 kDa being the most prominent, followed by the 90 kDa band. All of the immunoreactive species above 55 kDa were exclusively observed in cytoplasmic fractions, with none detected in the nucleus (Figure 6.4b). The lower reactivity of the monoclonal antibodies with TIP49 could have been insufficient to detect the species above 55 kDa, or the epitope could have been hidden by the modifications. Alternatively, these forms may not have been detected by monoclonal antibodies as they may not be TIP49 species. Further analysis, including mass spectrometry, would shed light on these discrepancies.

6.6 Putative post-translational modification of TIP48 and TIP49 detected by 2-D PAGE

The species of TIP48 and TIP49 detected in Western blot analysis were further characterised by utilizing 2-D PAGE, which separates species according to both mass and isoelectric point (pI). HeLa cells were lysed in urea containing buffer to obtain the total protein content, then the samples were analysed by 2-D PAGE followed by Western blotting using the antibodies characterised in Chapter 6.2.

Next, nuclear and cytoplasmic fractions of HeLa cells were obtained (as described in Chapter 2.12.4). These samples were analysed by 2-D PAGE and Western blotting.

6.6.1 2-D PAGE of TIP48

Consistent with 1-D SDS PAGE analysis of TIP48 in HeLa extracts, we observed several species of TIP48 by 2-D PAGE analysis followed by Western blotting (Figure 6.5a). TIP48 has an apparent molecular mass of around 55 kDa by SDS PAGE. We observed at least six distinct species, all with a pI of around pH 5 to 6, which is consistent with the theoretical pI of TIP48 of 5.49 based on the primary sequence (http://www.expasy.ch/tools/protparam.html). There are four species with a mass of around 55 kDa. These species have approximately the same intensity; however, the species with the lowest pI, also seemed to have a slightly smaller molecular mass compared with the others, leading us to hypothesise that this is the unmodified form of TIP48. Two other immunoreactive species were observed at approximately 60 and 80 kDa, with a pI of approximately 5 to 6 (Figure 6.5a). These could be further modified forms of TIP48. The unresolved species at very low pI, and those below 50 kDa are likely to be artefacts or degraded forms of TIP48.

We isolated cytoplasmic and nuclear fractions of HeLa cells, then analysed them by 2-D PAGE and Western blotting. Several species of TIP48 were observed in the cytoplasmic fraction of HeLa cells (Figure 6.5b). The most intense species was the 80 kDa protein, also seen in HeLa whole cell extracts. Three 55 kDa spots were also detected, and correlate well with similar species observed in whole cell extracts. Interestingly, only three of the four 55 kDa species detected in WCEs were observed in cytoplasmic extracts; the 55 kDa species with the highest pI was not detected (Figure 6.5b). In addition, a 60 kDa species was also seen in HeLa cytoplasmic extracts (Figure 6.5b). These data suggest that specific forms of TIP48 may localise in the cytoplasm.

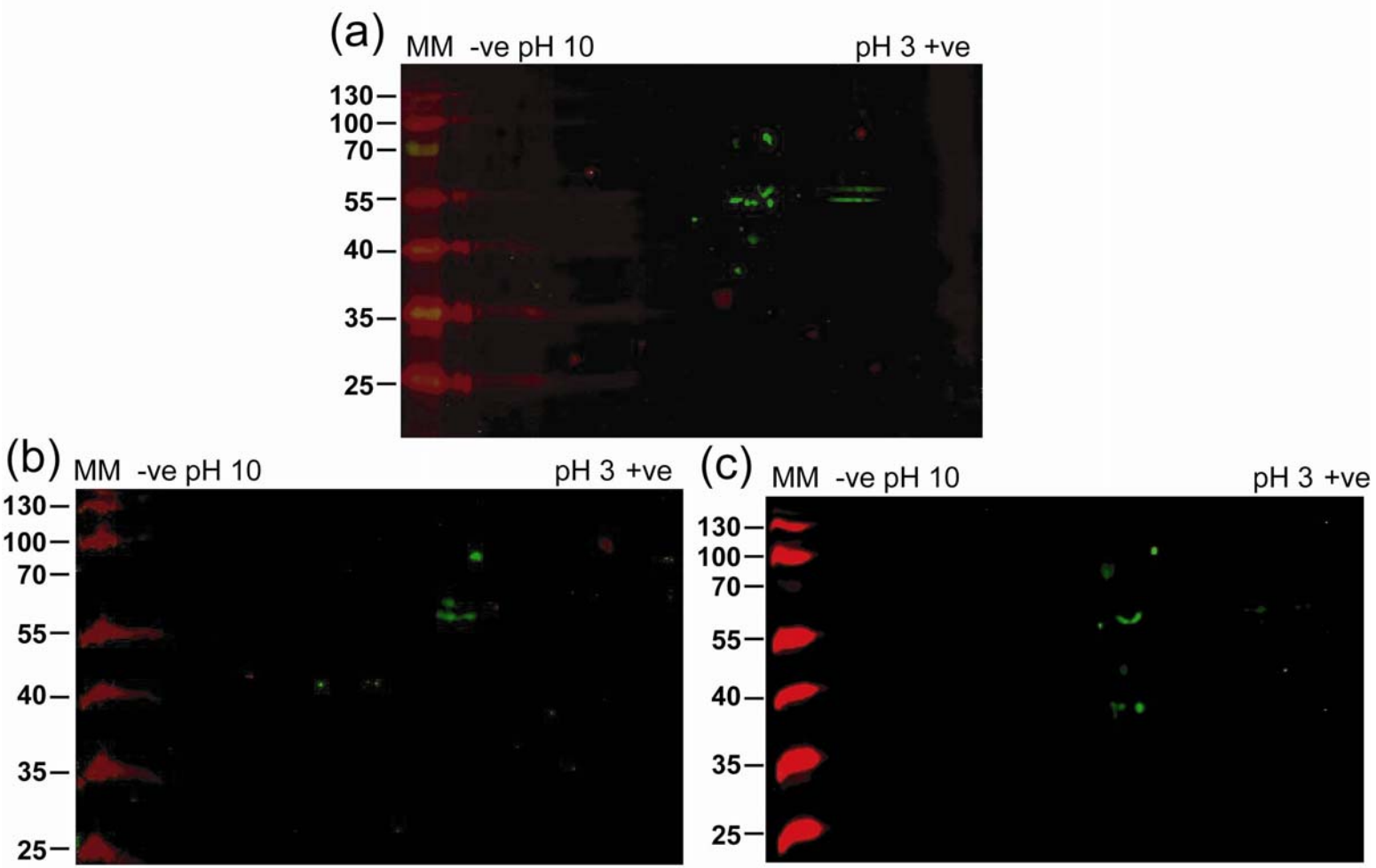

Figure 6.5. 2-D PAGE analysis of TIP48. HeLa cells were lysed in urea buffer (a), or subjected to cytoplasmic (b) and nuclear (c) fractionation, then analysed by 2-D SDS PAGE followed by Western blotting with TIP48-PC2 polyclonal antibodies. Molecular markers are shown on the left of each blot in kDa. The isoelectric point decreases linearly from pH 10 to pH 3 from the left to right of the blot.

Several species of TIP48 were detected in HeLa nuclear fractions (Figure 6.5c). In contrast with HeLa whole cell and cytoplasmic extracts, only a single 55 kDa species was detected (Figure 6.5c); this is the form of TIP48 which was not detected in cytoplasmic extracts. This species may be a modified form of TIP48, as it has a slightly larger mass than the other species in whole cell extracts. Additionally, prominent species were detected at approximately 60 and 80 kDa, with a pI of around pH 5 or 6. These are consistent with similar species of TIP48 seen in whole cell extracts, which are putative modified forms of TIP48. Specific modified forms of TIP48 may be predominantly nuclear, and it could be that only modified TIP48 localises in the nucleus. Further characterisation of the immunoreactive species would confirm that they are modified forms of TIP48.

6.6.2 2-D PAGE of TIP49

Improving on 1-D SDS PAGE analysis of TIP49 in HeLa extracts, 2-D PAGE of HeLa extracts followed by Western blotting with anti-TIP49 antibodies allowed us to resolve several species of TIP49 (Figure 6.6). Using mouse monoclonal antibodies against TIP49, at least three species with apparent molecular masses of around 55 kDa and pI values of approximately pH 6 were detected (Figure 6.6a). The theoretical pI of TIP49 is 6.02 based on its primary sequence (http://www.expasy.ch/tools/protparam.html). The species with the highest pI was most intense, followed by the centre species, then the species with the lowest pI (Figure 6.6a). It is plausible that the most abundant species is the unmodified form of TIP49. As the monoclonal antibodies are very specific, it is highly probable that these are genuine modified forms of TIP49. The polyclonal antibodies exhibit reactivity with TIP48; however, they react more strongly with TIP49 than the monoclonal antibodies. When HeLa extracts were separated by 2-D SDS PAGE, followed by immunoblotting with the polyclonal TIP49 antibodies, the three 55 kDa species were detected in the same proportions as with the monoclonal antibodies (Figure 6.6b). Strikingly, three species were also observed

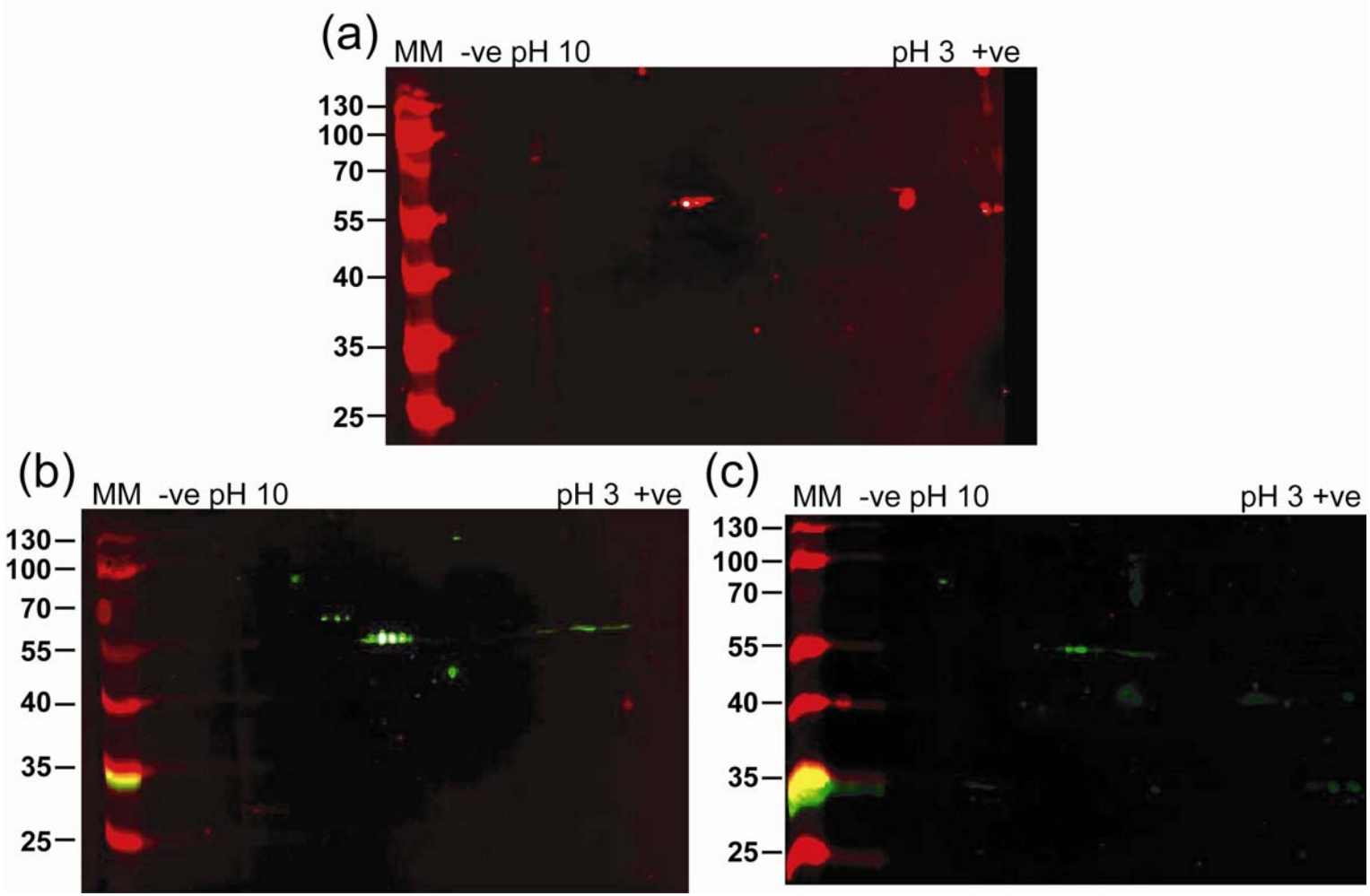

Figure 6.6. 2-D PAGE analysis of TIP49. HeLa cells were lysed in urea buffer (a and b), or subjected to nuclear fractionation (c), then analysed by 2-D SDS PAGE followed by Western blotting. Monoclonal anti-TIP49 antibodies (red) were used in (a), while polyclonal antibodies (green) were used in (b and c). Molecular markers are shown on the left of each blot in kDa. The isoelectric point decreases linearly from pH 10 to pH 3 from the left to right of the blot.

at approximately 70 kDa, with a shift in pI to around pH 7. As the distance between the spots mirrored the triplet seen at 55 kDa, it is credible that these are genuine modified forms of TIP49 with the same modification resulting in a 15 kDa increase in mass. One further immunoreactive species was observed at 90 kDa, with a pI of around pH 8, although this could be too large to be a distinct modification of TIP49 and could be non-specific. The unresolved species at very low pI, and those below 50 kDa are likely to be gel artefacts or proteolysed TIP49.

After isolation of cytoplasmic and nuclear fractions of HeLa cells, 2-D PAGE and Western blotting were used to analyse TIP49 species. Unfortunately, several attempts to analyse cytoplasmic fractionations of HeLa extracts by 2-D PAGE and Western blotting gave rise to unresolved species, which could not be analysed (data not shown). This may have been due to the lysis conditions, or the buffer used for isoelectric focusing. However, analysis of HeLa nuclear fractions was more successful.

Compared with whole cell extracts, only a small number of TIP49 species were detected in nuclear extracts (Figure 6.6c). While a clear triplet was seen in whole cell extracts, only a doublet was seen at 55 kDa in nuclear extracts (Figure 6.6c). Furthermore, the intensity of the species was also different: the 55 kDa species with the lowest pI was most abundant in nuclear extracts, while the 55 kDa species with the highest pI was slightly more abundant in whole cell extracts (Figure 6.6b and c). The triplet at 70 kDa seen in whole cell extracts was not observed in nuclear extracts, although the 90 kDa species with a pI of around 8, was detected (Figure 6.6c). This is in agreement with 1-D PAGE analysis of TIP49, whereby some immunoreactive species detected in the cytoplasm were not detected in the nucleus (Figure 6.4b). These data imply that there are distinct putative modified forms of TIP49 associated with the nucleus and cytoplasm.

6.7 Discussion

In this chapter, we used cell culture coupled with immunodetection techniques to study of the *in vivo* properties of TIP48 and TIP49. We initially purified and characterised several antibodies for use in these experiments.

We purified rabbit antibodies raised against full length TIP48. Two affinity purified batches of anti-TIP48 antibodies, TIP48-PC1 and TIP48-PC2, reacted well with TIP48, but also cross reacted with TIP49 (Figure 6.1). Furthermore, there was some non-specific binding to other components of HeLa cell extracts. Although this made immunostaining assays more difficult to interpret, we feel the antibodies are of sufficient specificity to answer basic questions about the *in vivo* properties of TIP48. For instance, our HeLa cell immunofluorescence data using these antibodies agree well with those previously published with a different polyclonal anti-TIP48 antibody (Puri, 2006; Sigala et al., 2005).

The TIP49 antibodies were of consistently good quality in our experiments. We obtained mouse monoclonal antibodies raised against an N-terminal peptide of TIP49, for comparison with the rabbit polyclonal antibodies against full length TIP49. We found that the mouse monoclonal anti-TIP49 antibodies were highly specific, and generally detected a single discrete band in 1-D SDS PAGE followed by Western blotting (Figure 6.1). In contrast, the rabbit polyclonal anti-TIP49 antibodies displayed some cross reactivity with TIP48, and may have detected non-specific products; however, the polyclonal antibodies reacted with TIP49 more strongly than the polyclonal antibodies. For this reason, the polyclonal antibodies were better at detecting less abundant species, such as the extra spots seen with 2-D PAGE of HeLa extracts (Figure 6.6b). Thus, using both polyclonal and monoclonal antibodies in tandem gives a broader and more objective analysis than using them individually.

Previous studies of the sub-cellular localisation of TIP48 and TIP49 revealed differences between the proteins during late mitosis (Gartner et al., 2003; Puri,

2006; Sigala et al., 2005). This difference is critical in the understanding of TIP48 and TIP49; in some pathways TIP48 and TIP49 function as a complex, while in late mitosis, the proteins seem to localise independently. This may imply different oligomeric forms of TIP48 and TIP49 carry out different roles at specific stages of the cell cycle. To confirm the difference in localisation, a different approach to the previously published data was used. We transiently expressed a TIP49-GFP fusion protein in HeLa cells, then monitored the localisation of TIP49-GFP during mitosis by synchronising cells with RO-3306. We observed nuclear localisation of TIP49 as well as association with the mitotic spindle (Gartner et al., 2003). Unfortunately, the TIP49-GFP fusion protein affected the viability of HeLa cells, as demonstrated by the low number of cells expressing TIP49-GFP after splitting the cells and seeding them on coverslips. This observation is supported by reports that correct localisation of TIP49 is disrupted by addition of a GFP-tag in HeLa cells (Cvackova et al., 2008). It may be the case that GFP tagged TIP49 is a dominant negative form of the protein; the localisation experiments could be repeated using a construct which does not express the TIP49-GFP protein to such a high level, or by using stably transfected HeLa cells. Alternatively, if TIP49-GFP is dominant negative, this could allow us to characterise TIP49 *in vivo* by expressing the fusion protein and seeing how pathways such as Wnt/β-catenin signalling or chromatin remodelling are affected.

1- and 2-D SDS PAGE analysis of HeLa cell extracts gave key insights into the possibility of post translational modifications of TIP48 and TIP49, and whether they associate with specific compartments. Interestingly, we detected at least six species of TIP48 and seven species of TIP49 in 2-D PAGE analysis of whole cell extracts. Due to the specificity of the TIP49 monoclonal antibodies and the similarity of the two triplets with TIP49 polyclonal antibodies, we are confident that these are genuine modified forms of TIP49. In comparison, the TIP48 antibodies displayed cross reactivity, and were non-specific, meaning assignment of modified forms of TIP48 should be tentative. However, we feel that these data are a good starting point for further investigation of TIP48 and TIP49 modifications, and how they relate to ATPase activity, oligomerisation, and sub-

cellular localisation. Interestingly, we observed clear differences in the modified forms of TIP48 and TIP49 associated with the nucleus and cytoplasm, hinting that modifications of TIP48 and TIP49 may regulate the plethora of functions in which they are implicated (Figures 6.4, 6.5 and 6.6).

Very little is currently known about PTMs of TIP48 and TIP49. One group has suggested that SUMOylation of both TIP48 and TIP49 accounts in part for their nuclear localisation in metastatic LNCaP cells (Kim et al., 2006; Kim et al., 2007). Other groups have commented that since less than 5 % of endogenous TIP48 and TIP49 is SUMOylated, other mechanisms must also promote their nuclear localisation (Gallant, 2007; Huber et al., 2008). The 80 kDa species of TIP48 in Figure 6.6 may indeed be a SUMOylated form of TIP48, as a SUMO group would decrease the pI of wild type TIP48 and increase its mass by at least 11 kDa; however, we detected this form of TIP48 in both the nuclear and cytoplasmic fractions. In contrast, the modified forms of TIP49 all had increased pI, suggesting these modifications are not SUMOylation (Figure 6.5).

As part of large scale proteomic analyses, acetylation and phosphorylation of TIP48 and TIP49 have been reported (Matsuoka et al., 2007) (see Chapter 1.7.7). Both acetylation and phosphorylation would not visibly increase the molecular masses of TIP48 and TIP49 by PAGE, but would decrease their isoelectric points. It is quite possible that several of the observed species are acetylated or phosphorylated forms of TIP48 and TIP49, such as the triplet of TIP49 seen in Figure 6.6. Mass spectrometric analysis could allow us to confirm that the species observed by 2-D PAGE from HeLa extracts are genuine, and would allow us to identify the modifications that account for the shift in mass and pI. This would provide fundamental insights into the temporal and contextual regulation of the functions of TIP48 and TIP49 by PTM.

Chapter 7

General Discussion

7.1 Summary of research and its relation to the field

In this thesis, we have used recombinant TIP48 and TIP49 to better understand their structures and ATPase activities *in vitro*. We also generated mutants and interacting proteins to analyse their effects on these properties of TIP48 and TIP49. Finally, we looked at the sub-cellular distribution of TIP48 and TIP49 and how this is related to post translational modification.

Initially we utilised analytical ultracentrifugation and size exclusion chromatography to understand the oligomeric properties and assembly of TIP48 and TIP49 complexes. Both TIP48 and TIP49 formed monomers as the predominant species in the absence of co-factors, with dimers, trimers and hexamers as minor species. The presence of dimers, trimers and hexamers of TIP49 in solution was surprising, as TIP49 was exclusively monomeric by SEC (Puri et al., 2007). However, the detection of these oligomers by AUC is strengthened by the cross linking analyses of TIP49 in Chapter 5.6, which showed several distinct oligomers higher than 50 kDa. The presence of trimers as intermediates in hexamer formation, as well as putative nonamers in the samples analysed by AUC, suggest that trimers form stable building blocks in oligomer assembly. One could speculate that TIP48 and TIP49 are assembled into a hexameric ring which acts as a catalytic 'dimer-of-trimers', whereby one trimeric subunit contains one ATP bound monomer, one ADP bound monomer and a nucleotide free monomer. Although definitive evidence for the 'dimer-of-trimers' model has not been reported, several AAA^+ proteins assemble into hexameric rings where different subunits have different affinities for nucleotides, including ClpX (Hersch et al., 2005), p97 (Zalk and Shoshan-Barmatz, 2003) and RuvB (Hishida et al., 2004; Putnam et al., 2001). Within the hexameric rings, the conserved arginine finger contacts the adjacent subunit and is thought to allosterically modulate its affinity for nucleotides (Ogura et al., 2004). This leads to concerted binding of ATP, hydrolysis, then subsequent release of ADP, and may allow subunits within the hexameric ring to adopt different conformations.

Indeed, RuvB, the closest prokaryotic homologue of TIP48 and TIP49, was suggested to hydrolyse ATP as a 'dimer-of-trimers', allowing efficient branch migration. One study used RuvB mutants, $RuvB^{R174A}$ and $RuvB^{K68A}$, which have mutations it their arginine finger and Walker A motifs respectively (Hishida et al., 2004). $RuvB^{R174A}$ and $RuvB^{K68A}$ could not hydrolyse ATP *in vitro*, which was also the case for the $RuvB^{R174A\ /\ K68A}$ double mutant. Significantly, mixing $RuvB^{R174A}$ and $RuvB^{K68A}$ in a 1:1 ratio partially restored ATPase activity, arguing that the subunits in the homo-hexamer are not equivalent (Hishida et al., 2004). In a separate study, structural and mutational analysis of RuvB indicated that ATP is an allosteric effector, so that ATP binding drives ATP hydrolysis in the adjacent subunit, possibly by movement of the arginine finger (Putnam et al., 2001). Taken together with more recent theoretical data of the molecular mechanism of RuvB (Xie, 2007), it is likely that the subunits in the RuvB hexamer hydrolyse ATP as a dimer-of-trimers. The conserved tertiary structure of TIP48, TIP49 and RuvB, particularly in Domain I (which incorporates ATP hydrolysis motifs), points to a conserved mechanism of ATPase activity. How this relates to a mechanistic function of TIP48 and TIP49 is currently unknown, but confirming this model would give valuable information into the molecular mechanisms of TIP48 and TIP49, as well as general AAA^{+} proteins.

We also confirmed that TIP48 has low ATPase activity in isolation, compared with the ATPase activity of the TIP48/TIP49 complex (Ikura et al., 2000; Puri et al., 2007). Biochemical studies demonstrated that TIP48 binds ADP with higher affinity than ATP, and so the rate limiting step is the release of bound ADP (Puri et al., 2007). An analogy can be drawn with the TIP49 crystal structure, as ADP was trapped between the subunit interfaces, and the authors noted that ADP release, and thus, ATP turnover, would be limiting (Matias et al., 2006). Individually, only a small proportion of TIP48 and TIP49 are hexameric in solution, and only TIP48 hexamers are promoted by adenine nucleotides. Interactions between TIP48 and TIP49 promote hexamer formation by driving both proteins into the stable TIP48/TIP49 double hexamer. More importantly, these interactions seem to provide a mechanism for more efficient ATPase activity than the

individual proteins, arguing that structural changes occur within the TIP48/TIP49 double hexamer to allow ADP release and more efficient ATP hydrolysis. Indeed, structural changes upon nucleotide binding have also been reported for RuvB (Putnam et al., 2001). Furthermore, many AAA+ proteins assemble into double hexamers; either with two individual rings, e.g. TIP48/TIP49 (Puri et al., 2007; Torreira et al., 2008), or two ATPase rings made from different domains of the same protein, e.g. p97 (Zhang et al., 2000). Communication between the top and bottom rings may allow for concerted hydrolysis of ATP (Briggs et al., 2008).

The TIP48/TIP49 complex remained a stable double hexamer by size exclusion chromatography, with minimal dissociation in the presence of co-factors. Conversely, TIP48, but not TIP49, formed hexamers with ATP. These results signify important differences between the roles of TIP48 and TIP49 within the heteromeric complex. We demonstrated that Domain II of TIP48 does not contribute to interactions within the double hexamer, while TIP49 Domain II is important, but not essential, for stabilising interactions between the top and bottom rings. This argues that TIP49 has more of a structural role, and may drive the assembly of TIP48 into different oligomeric forms: homo-hexamers in the absence of TIP49, hetero-single or double hexamers in the presence of TIP49. This may explain the various and often distinct roles which are attributed to TIP48 and TIP49, supported by several converging lines of research that claim the ratio of TIP48 and TIP49 in the cell is functionally important (Bauer et al., 2000; Diop et al., 2008; Rottbauer et al., 2002). Although it is possible that TIP49 acts purely in a structural or regulatory manner, this is at odds with the fact that TIP49 ATPase activity is required for efficient activity of the TIP48/TIP49 complex (Puri, 2006). Moreover, both TIP48 and TIP49 were shown to hydrolyse ATP within the double hexamer (Puri, 2006). The ATPase activity of TIP49 could simply be required for efficient ADP release and subsequent hydrolysis by TIP48, alternatively, the activity of TIP49 could have a direct catalytic role.

It may also be possible that the ATPase activities of TIP48 or TIP49 have become redundant for some of their functions. It is clear that the ATPase

activities of TIP48 and TIP49 in eukaryotes are essential for correct development and growth, as demonstrated by the lethality of mutations in conserved ATPase motifs in TIP48 and TIP49 (Jonsson et al., 2001; King et al., 2001; Lim et al., 2000; Wood et al., 2000). Intriguingly, some functions of TIP48 and TIP49 did not require ATP hydrolysis. A Walker B mutation in yeast TIP48 (which could bind, but not hydrolyse, ATP) did not affect its ability to recruit yeast Arp5 into the INO80 in conjunction with wild type yeast TIP49 (Jonsson et al., 2004). In addition, a Walker B mutant of TIP48 was able to interact with ATF2 (Cho et al., 2001). Nevertheless, the vast majority of studies have established that ATP hydrolysis is critical for the correct functions of TIP48 and TIP49, including telomerase complex assembly (Venteicher et al., 2008) and TIP60 dependent histone acetylation (Feng et al., 2003). Since only one study to date has confidently calculated a 6:1 ratio of both TIP48 and TIP49 to other components of the multi-subunit complex (Shen et al., 2000), different TIP48 and TIP49 oligomers may be required in different processes. Indeed, data we presented in Chapters 3.3 and 4.7 corroborated the argument that various forms of the TIP48/TIP49 complex exist, including single and double hexamers (Gribun et al., 2008; Torreira et al., 2008). In addition, TIP48 can form hexamers independently of TIP49 and seems to have some distinct roles. Using these observations, we can postulate that individually, or as a complex, TIP48 and TIP49 may have more than one mechanism; in some instances, they may act as scaffold subunits with limited requirement for ATP hydrolysis, while having a direct catalytic role in others. Mechanistically, catalytically competent TIP48 and TIP49 were both needed for progressive rounds of ATP hydrolysis within the double hexamer; however, a single round of ATP hydrolysis by the individual proteins would be possible (Puri 2006). Further research into these possibilities would have enormous impact on the understanding of TIP48 and TIP49.

Based on our work detailed in Chapters 3 and 4, we have proposed a model whereby a TIP49 hexamer is bound to a TIP48 hexamer, allowing multiple rounds of ATP hydrolysis (Figure 4.12). Support for this model came from several observations of the recombinant proteins: 1) A head-to-tail arrangement is

supported by progressive stacking of rings by AUC in Chapter 3.5, as well as unpublished observation regarding the EM structure (Puri et al., 2007). 2) The unequivalent top and bottom rings in the human TIP48/TIP49 EM structure suggest homo-hexamers, and immunolabelling of the yeast cryo-EM TIP48/TIP49 complex also pointed to homo-hexamers (Torreira et al., 2008). 3) Instability of TIP48/TIP49 double hexamers when TIP49 Domain II is removed, compared with TIP48 Domain II, suggests TIP48 and TIP49 have a different orientation and functions within the complex. 4) The difficulty in fitting the crystal structure of TIP49 into either ring of the EM reconstruction of the TIP48/TIP49 complex suggests large conformational changes take place.

Our hypothesised architecture of the TIP48/TIP49 double hexamer may explain how multiple round of ATP hydrolysis occur without the need for assembly and disassembly of hexameric rings. It also provides clues as to how ATP hydrolysis translates to mechanical function. Many AAA^+ proteins use the chemical energy of ATP hydrolysis to drive conformational changes in distant domains, for instance, ATP hydrolysis in p97 leads to the movement of its N-terminal domain relative to the core ATPase domains (DeLaBarre and Brunger, 2005). Similar movement in Domain II may provide a means by which TIP48 and TIP49 carry out their functions, which may include modulating protein-protein or protein-nucleic acid interactions.

The composition of the TIP48/TIP49 complex currently remains unanswered. In conjunction with the authors of the yeast TIP48/TIP49 EM structure (Torreira et al., 2008), we prefer the hypothesis that the TIP48/TIP49 complex comprises of stacked homo-hexamers of TIP48 and TIP49. However, the possibility of mixed double hexameric rings is still justifiable, and our work in chapter 3.2 supports single hetero-hexamers (Gribun et al., 2008). It may in fact be the case that several complexes exist and each has a specialised function. Heterogeneity of samples containing distinct complexes could explain the difficulty in obtaining high resolution structures of the TIP48/TIP49 complex (Gorynia et al., 2008).

As well as acting in a complex, several reports have proposed that TIP48 and TIP49 have separate functions (Cho et al., 2001; Diop et al., 2008; Kim et al., 2005). The transaction between different TIP48 and TIP49 oligomers will help to understand how these functions are coordinated. Indeed, if TIP48/TIP49 hetero-hexamers are present *in vivo*, these would need to be completely disassembled in order to form TIP48 homo-hexamers. As interchange between these different oligomers would be difficult, the distinct oligomers would be more tightly regulated. Conversely, homo-hexamers of TIP48 and TIP49 within the complex would allow for more dynamic regulation, as the double hexamer could separate into functional homo-hexamers. Identifying which TIP48 and TIP49 oligomers exist in cells, as well as the dynamics between them, should be one of the primary goals for the field.

In vivo, we demonstrated that the sub-cellular localisation of TIP48 and TIP49 during the late stages of mitosis is distinct. Both TIP48 and TIP49 clearly function as a complex to promote correct spindle assembly (Ducat et al., 2008). In addition, TIP48 may have a separate role in cytokinesis, as TIP48, but not TIP49, was detected at the midbody and midzone. This strengthens the hypothesis that TIP48 and TIP49 may have independent roles in some cases, such as their antagonistic regulation of β-catenin dependent transcription (Kim et al., 2005), antagonistic HOX gene control (Diop et al., 2008) and only TIP48 affecting ATF2 dependent transcription (Cho et al., 2001). One possible explanation of these observations is that TIP48 has functions independent of TIP49, while TIP49 can only function as part of the TIP48/TIP49 complex. This would account for the relative levels of TIP48 and TIP49 affecting certain processes, as this would influence which form of TIP48 is present. This is supported by observations that TIP48 has well described roles independent of TIP49, including the recruitment of HDAC1 to the KAI1 promoter (Kim et al., 2005), localisation of TIP48 at the midbody during cytokinesis and the regulation of ATF2 by TIP48 (Cho et al., 2001). In contrast, the putative roles of TIP49 independent of TIP48 are poorly defined, and may in fact be carried out by complexes in which both TIP48 and TIP49 are both present (Diop et al., 2008; Gallant, 2007; Kim et al., 2005). More

research into the molecular roles of TIP48 independent of TIP49, including its functions in late mitosis, would contribute greatly to our understanding of this system.

Using 2-D PAGE analysis of HeLa cell extracts, we identified species of TIP48 and TIP49 which may be post-translationally modified. Interestingly, some of these species are specific to either nuclear or cytoplasmic fractions of HeLa cells; thus, PTMs are a plausible method of regulating sub-cellular localisation of TIP48 and TIP49. As our data are currently still preliminary, it is difficult to conclude whether these observed species of TIP48 and TIP49 are genuine, and the specific modification associated with each spot. SUMOylation, phosphorylation and acetylation have been reported for TIP48 and TIP49 (Kim et al., 2006; Kim et al., 2007; Matsuoka et al., 2007). Of particular interest is that TIP48 is phosphorylated by ATM/ATR in response to DNA damage (Matsuoka et al., 2007). Indeed, testing for these modifications would provide a good starting point for further experiments. Given the abundance of activities ascribed to TIP48 and TIP49, it is not surprising that several modified forms exist *in vivo*. Indeed, we have observed several oligomeric forms of TIP48 and TIP49 *in vitro*, including single and double rings. PTM could be one way of promoting specific complexes of TIP48 and TIP49. Deducing how the post translational modification of TIP48 and TIP49 affects their localisation, ATPase activity and oligomerisation would begin to shed light on their complicated regulation *in vivo*.

'What are the molecular functions of TIP48 and TIP49 in eukaryotes?' This question remains the predominant quandary within the field. Our experimental research has contributed towards the understanding of TIP48 and TIP49, but has also generated new questions that need to be addressed. One significant finding is the possibility that the yeast and human TIP48/TIP49 complexes are structurally different. Indeed, biochemical differences between the yeast and human homologues have already been reported (Gribun et al. 2008). If this structural difference is indeed the case, then TIP48 and TIP49 may have acquired different functions after the divergence of lower and higher eukaryotes.

The yeast proteins displayed helicase activity *in vitro*, while helicase activity of human TIP48/TIP49 complex has, to date, never been published, and the helicase activity of the rat proteins is controversial. Although it is unlikely that TIP48 and TIP49 act on DNA in yeast, but not mammals, it is possible that TIP48 and TIP49 have gained a different function in higher eukaryotes. Indeed, higher eukaryotic organisms contain proteins such as c-Myc and β-catenin, which are intimately linked to the functions of TIP48 and TIP49 in metazoans, but are not present in yeast.

The biochemical and structural properties of TIP48 and TIP49 differ slightly between yeast and humans; nevertheless, a further possibility is that TIP48 and TIP49 have the same function in yeast and higher eukaryotes. The breadth of interacting proteins and processes in which TIP48 and TIP49 are involved makes it more likely that they have a transient role, such as a chaperone activity. In light of research carried out during this thesis, and published studies by other groups, we propose that TIP48 and TIP49 modulate protein-protein, or protein-nucleic acid interactions in a context specific fashion. Future research will no doubt deduce the molecular mechanisms of TIP48 and TIP49, and highlight their importance throughout the eukaryotic domain.

7.2 Future Directions

Subunit Composition of TIP48/TIP49 complexes

One of the most critical (but to date quite elusive) problems regarding TIP48 and TIP49 is the molecular architecture of their complex. Several structural studies of yeast and human TIP48/TIP49 complexes did not conclusively identify the composition the double hexameric rings (Gorynia et al., 2008; Puri et al., 2007; Torreira et al., 2008). Although both mixed- and homo-rings have been suggested, deducing which (or if indeed both) forms comprise the TIP48/TIP49 complex would give valuable insight into their function. As part of this work, we have generated tools to help answer this problem. The mutants of TIP48 and

TIP49 could be coupled with EM analysis to assign missing electron densities upon removal of Domain II. This would indicate both where Domain II is positioned within the double hexamer, and also, whether the rings are homo- or hetero-hexamers.

High resolution structures of TIP48/TIP49 complexes

Further structural analysis could be carried out using crystallisation and X-ray diffraction analysis of the TIP48/TIP49 complex. A high resolution structure would give a detailed description of composition, molecular architecture and interactions within the TIP48/TIP49 complex. In light of this, we have initiated collaboration with Dr. Tracey Barrett (Birkbeck, School of Crystallography) to generate crystals for X-ray diffraction analysis. Full length TIP48/TIP49-His_6 did not yield any crystals during initial screening, possibly due to the heterogeneity of the sample (as seen by AUC). However, we have some preliminary diffraction data for Δ^2TIP48 crystals, as well as small crystals of the Δ^2TIP48/TIP49-His_6 complex. Hence, high resolution structures of these proteins in the near future are a strong possibility.

Architecture and interactions within multi-subunit complexes

An important future area for investigation is the role of TIP48 and TIP49 within large multisubunit complexes, particularly chromatin remodelling complexes. Structural analysis of INO80, TIP60 and SWR complexes would provide information about the composition and protein-protein interactions within these essential complexes. It is likely that association within these complexes is transient and dynamic. Immunoprecipitation studies under different conditions could provide clues regarding functions. Further discerning the conditions under which TIP48 and TIP49 associate with BAF53, β-catenin and Hint1 would also be a great benefit. Indeed, it is possible that BAF53, along with actin, TIP48 and TIP49, form a sub-complex. It would be interesting to co-express and purify these proteins, and subsequently, test the biochemical properties of this complex.

Differences between yeast and human TIP48/TIP49 complexes

One possibility that was highlighted by our study is the structural difference between the yeast and human TIP48/TIP49 complex. Cryo-EM of the human TIP48/TIP49 complex would provide a higher resolution structure, and allow direct comparison with the recently published yeast cryo-EM reconstruction. Purifying Δ^2TIP48 and Δ^2TIP49 complexes of the yeast proteins would also allow direct comparison of the biochemical properties of the human proteins lacking Domain II. These experiments would give critical insights into possible structural and biochemical differences between yeast and human TIP48/TIP49, allowing further understanding of their functions and evolution.

Characterise the different TIP48/TIP49 complexes

Several lines of evidence, including characterisation of recombinant proteins in this study, have implicated distinct complexes of TIP48 and TIP49. Discerning the significance and function of these complexes, such as double and single hetero-hexamers, will give important information about the regulation and activities of TIP48/TIP49 complexes. Structural analysis, including native mass spectrometry and electron microscopy, coupled with *in vivo* work could begin to address these problems. As seen in Chapter 5, the TIP48/Δ^2TIP49 complex may favour assembling into a single ring, rather than a double hexamer. Expression of Δ^2TIP49 in cell lines may give insights into the functions and properties of the putative TIP48/TIP49 hexamer.

Identify PTM of TIP48 and TIP49 and their relation to mitosis and DNA damage repair

The PTMs of TIP48 and TIP49 could be characterised using a combination of immunoprecipitation, 2-D SDS PAGE and mass spectrometry. Once the specific modifications have been identified, further analysis of HeLa and other cell lines would focus on how the PTMs affect the localisation of TIP48 and TIP49 to different cellular compartments or their separation during mitosis. The

contribution of these modifications to facilitating the roles of TIP48 and TIP49 in DNA damage repair and chromatin remodelling could also be explored. *In vitro* analysis of modified forms of TIP48 and TIP49 could provide information about how PTM affect the interactions between TIP48 and TIP49 and their ATPase activity.

7.3 Broader Challenges

The dynamics of TIP48/TIP49 interactions with other factors

One of the most characteristic features of TIP48 and TIP49 is their interaction with a plethora of seemingly unrelated cellular factors. At least in yeast, it would be highly unlikely that every TIP49 monomer is associated with every single putative interacting partner at the same time, and even less likely as a hexamer. Thus it is probable that the association of TIP48 and TIP49 with other cellular factors is a tightly controlled temporal and contextual event. Picking apart the nature and conditions governing these interactions remains an important research objective within the field. Characterising novel interactions and broader comprehension of alleged interactions will greatly progress the fundamental understanding of TIP48 and TIP49.

The nature of the catalytic activity of TIP48/TIP49 and identifying substrates

Delineating which roles of TIP48 and TIP49 require ATP, how these are linked to different forms or complexes, and whether ATPase activity of TIP48 or TIP49 has become redundant in some instances, would be a significant step towards understanding their activities. Furthermore, high resolution structures of the TIP48/TIP49 in several transition states during ATP hydrolysis will give invaluable insights into structure-function relationships, although this approach may prove to be quite demanding. Most importantly, identifying the specific substrates of TIP48 and TIP49 is an imperative problem, and could resolve many issues and controversies within the field, yet the identification of direct substrates remains a

significant challenge. It would be important to identify substrates of TIP48 and TIP49 in the context of specific macromolecular complexes.

Bibliography

Allard, S., Utley, R. T., Savard, J., Clarke, A., Grant, P., Brandl, C. J., Pillus, L., Workman, J. L., and Cote, J. (1999). NuA4, an essential transcription adaptor/histone H4 acetyltransferase complex containing Esa1p and the ATM-related cofactor Tra1p. Embo J *18*, 5108-5119.

Amati, B., Frank, S. R., Donjerkovic, D., and Taubert, S. (2001). Function of the c-Myc oncoprotein in chromatin remodeling and transcription. Biochim Biophys Acta *1471*, M135-145.

Arents, G., and Moudrianakis, E. N. (1993). Topography of the histone octamer surface: repeating structural motifs utilized in the docking of nucleosomal DNA. Proc Natl Acad Sci U S A *90*, 10489-10493.

Auger, A., Galarneau, L., Altaf, M., Nourani, A., Doyon, Y., Utley, R. T., Cronier, D., Allard, S., and Cote, J. (2008). Eaf1 is the platform for NuA4 molecular assembly that evolutionarily links chromatin acetylation to ATP-dependent exchange of histone H2A variants. Mol Cell Biol *28*, 2257-2270.

Baek, S. H. (2008). When ATPases pontin and reptin met telomerase. Dev Cell *14*, 459-461.

Baek, S. H., Ohgi, K. A., Rose, D. W., Koo, E. H., Glass, C. K., and Rosenfeld, M. G. (2002). Exchange of N-CoR corepressor and Tip60 coactivator complexes links gene expression by NF-kappaB and beta-amyloid precursor protein. Cell *110*, 55-67.

Baharoglu, Z., Bradley, A. S., Le Masson, M., Tsaneva, I., and Michel, B. (2008). ruvA Mutants that resolve Holliday junctions but do not reverse replication forks. PLoS Genet *4*, e1000012.

Bauer, A., Chauvet, S., Huber, O., Usseglio, F., Rothbacher, U., Aragnol, D., Kemler, R., and Pradel, J. (2000). Pontin52 and reptin52 function as antagonistic regulators of beta-catenin signalling activity. Embo J *19*, 6121-6130.

Bauer, A., Huber, O., and Kemler, R. (1998). Pontin52, an interaction partner of beta-catenin, binds to the TATA box binding protein. Proc Natl Acad Sci U S A *95*, 14787-14792.

Bellosta, P., Hulf, T., Balla Diop, S., Usseglio, F., Pradel, J., Aragnol, D., and Gallant, P. (2005). Myc interacts genetically with Tip48/Reptin and Tip49/Pontin to control growth and proliferation during *Drosophila* development. Proc Natl Acad Sci U S A *102*, 11799-11804.

Bird, A. W., Yu, D. Y., Pray-Grant, M. G., Qiu, Q., Harmon, K. E., Megee, P. C., Grant, P. A., Smith, M. M., and Christman, M. F. (2002). Acetylation of histone H4 by Esa1 is required for DNA double-strand break repair. Nature *419*, 411-415.

Blanc, J. F., Lalanne, C., Plomion, C., Schmitter, J. M., Bathany, K., Gion, J. M., Bioulac-Sage, P., Balabaud, C., Bonneu, M., and Rosenbaum, J. (2005). Proteomic analysis of differentially expressed proteins in hepatocellular carcinoma developed in patients with chronic viral hepatitis C. Proteomics *5*, 3778-3789.

Boudreault, A. A., Cronier, D., Selleck, W., Lacoste, N., Utley, R. T., Allard, S., Savard, J., Lane, W. S., Tan, S., and Cote, J. (2003). Yeast enhancer of polycomb defines global Esa1-dependent acetylation of chromatin. Genes Dev *17*, 1415-1428.

Bradley, A. S. (2009) Insights into the Molecular Mechanism of Replication Fork Rescue by RuvAB and the putative role of the bacterial RuvB-like protein RarA and its human homologue WRNIP1, UCL.

Brembeck, F. H., Rosario, M., and Birchmeier, W. (2006). Balancing cell adhesion and Wnt signaling, the key role of beta-catenin. Curr Opin Genet Dev *16*, 51-59.

Briggs, L. C., Baldwin, G. S., Miyata, N., Kondo, H., Zhang, X., and Freemont, P. S. (2008). Analysis of nucleotide binding to P97 reveals the properties of a tandem AAA hexameric ATPase. J Biol Chem *283*, 13745-13752.

Bruce, K., Myers, F. A., Mantouvalou, E., Lefevre, P., Greaves, I., Bonifer, C., Tremethick, D. J., Thorne, A. W., and Crane-Robinson, C. (2005). The replacement histone H2A.Z in a hyperacetylated form is a feature of active genes in the chicken. Nucleic Acids Res *33*, 5633-5639.

Burgess, S. A., Walker, M. L., Sakakibara, H., Knight, P. J., and Oiwa, K. (2003). Dynein structure and power stroke. Nature *421*, 715-718.

Cai, Y., Jin, J., Florens, L., Swanson, S. K., Kusch, T., Li, B., Workman, J. L., Washburn, M. P., Conaway, R. C., and Conaway, J. W. (2005). The mammalian YL1 protein is a shared subunit of the TRRAP/TIP60 histone acetyltransferase and SRCAP complexes. J Biol Chem *280*, 13665-13670.

Cai, Y., Jin, J., Tomomori-Sato, C., Sato, S., Sorokina, I., Parmely, T. J., Conaway, R. C., and Conaway, J. W. (2003). Identification of new subunits of the multiprotein mammalian TRRAP/TIP60-containing histone acetyltransferase complex. J Biol Chem *278*, 42733-42736.

Cai, Y., Jin, J., Yao, T., Gottschalk, A. J., Swanson, S. K., Wu, S., Shi, Y., Washburn, M. P., Florens, L., Conaway, R. C., and Conaway, J. W. (2007). YY1 functions with INO80 to activate transcription. Nat Struct Mol Biol *14*, 872-874.

Cann, K. L., and Hicks, G. G. (2007). Regulation of the cellular DNA double-strand break response. Biochem Cell Biol *85*, 663-674.

Carlson, M. L., Wilson, E. T., and Prescott, S. M. (2003). Regulation of COX-2 transcription in a colon cancer cell line by Pontin52/TIP49a. Mol Cancer *2*, 42.

Cen, B., Li, H., and Weinstein, I. B. (2009). Histidine Triad Nucleotide-binding Protein 1 Up-regulates Cellular Levels of p27KIP1 by Targeting ScfSKP2 Ubiquitin Ligase and Src. J Biol Chem *284*, 5265-5276.

Cheng, Z., Ke, Y., Ding, X., Wang, F., Wang, H., Wang, W., Ahmed, K., Liu, Z., Xu, Y., Aikhionbare, F.*, et al.* (2008). Functional characterization of TIP60 sumoylation in UV-irradiated DNA damage response. Oncogene *27*, 931-941.

Cho, S. G., Bhoumik, A., Broday, L., Ivanov, V., Rosenstein, B., and Ronai, Z. (2001). TIP49b, a regulator of activating transcription factor 2 response to stress and DNA damage. Mol Cell Biol *21*, 8398-8413.

Chong, J. P., Hayashi, M. K., Simon, M. N., Xu, R. M., and Stillman, B. (2000). A double-hexamer archaeal minichromosome maintenance protein is an ATP-dependent DNA helicase. Proc Natl Acad Sci U S A *97*, 1530-1535.

Clarke, A. S., Lowell, J. E., Jacobson, S. J., and Pillus, L. (1999). Esa1p is an essential histone acetyltransferase required for cell cycle progression. Mol Cell Biol *19*, 2515-2526.

Cole, J. L., Lary, J. W., T, P. M., and Laue, T. M. (2008). Analytical ultracentrifugation: sedimentation velocity and sedimentation equilibrium. Methods Cell Biol *84*, 143-179.

Connolly, B., Parsons, C. A., Benson, F. E., Dunderdale, H. J., Sharples, G. J., Lloyd, R. G., and West, S. C. (1991). Resolution of Holliday junctions in vitro requires the Escherichia coli ruvC gene product. Proc Natl Acad Sci U S A *88*, 6063-6067.

Cvackova, Z., Albring, K. F., Koberna, K., Ligasova, A., Huber, O., Raska, I., and Stanek, D. (2008). Pontin is localized in nucleolar fibrillar centers. Chromosoma *117*, 487-497.

Daniels, D. L., and Weis, W. I. (2002). ICAT inhibits beta-catenin binding to Tcf/Lef-family transcription factors and the general coactivator p300 using independent structural modules. Mol Cell *10*, 573-584.

Dehan, E., Ben-Dor, A., Liao, W., Lipson, D., Frimer, H., Rienstein, S., Simansky, D., Krupsky, M., Yaron, P., Friedman, E.*, et al.* (2007). Chromosomal aberrations and gene expression profiles in non-small cell lung cancer. Lung Cancer *56*, 175-184.

DeLaBarre, B., and Brunger, A. T. (2005). Nucleotide dependent motion and mechanism of action of p97/VCP. J Mol Biol *347*, 437-452.

Diop, S. B., Bertaux, K., Vasanthi, D., Sarkeshik, A., Goirand, B., Aragnol, D., Tolwinski, N. S., Cole, M. D., Pradel, J., Yates, J. R., 3rd*, et al.* (2008). Reptin and Pontin function antagonistically with PcG and TrxG complexes to mediate Hox gene control. EMBO Rep *9*, 260-266.

Dobreva, I., Fielding, A., Foster, L. J., and Dedhar, S. (2008). Mapping the integrin-linked kinase interactome using SILAC. J Proteome Res *7*, 1740-1749.

Downs, J. A., Allard, S., Jobin-Robitaille, O., Javaheri, A., Auger, A., Bouchard, N., Kron, S. J., Jackson, S. P., and Cote, J. (2004). Binding of chromatin-modifying activities to phosphorylated histone H2A at DNA damage sites. Mol Cell *16*, 979-990.

Downs, J. A., Lowndes, N. F., and Jackson, S. P. (2000). A role for Saccharomyces cerevisiae histone H2A in DNA repair. Nature *408*, 1001-1004.

Doyon, Y., and Cote, J. (2004). The highly conserved and multifunctional NuA4 HAT complex. Curr Opin Genet Dev *14*, 147-154.

Doyon, Y., Selleck, W., Lane, W. S., Tan, S., and Cote, J. (2004). Structural and functional conservation of the NuA4 histone acetyltransferase complex from yeast to humans. Mol Cell Biol *24*, 1884-1896.

Ducat, D., Kawaguchi, S., Liu, H., Yates, J. R., 3rd, and Zheng, Y. (2008). Regulation of microtubule assembly and organization in mitosis by the AAA+ ATPase Pontin. Mol Biol Cell *19*, 3097-3110.

Dugan, K. A., Wood, M. A., and Cole, M. D. (2002). TIP49, but not TRRAP, modulates c-Myc and E2F1 dependent apoptosis. Oncogene *21*, 5835-5843.

Ebbert, R., Birkmann, A., and Schuller, H. J. (1999). The product of the SNF2/SWI2 paralogue INO80 of Saccharomyces cerevisiae required for efficient expression of various

yeast structural genes is part of a high-molecular-weight protein complex. Mol Microbiol *32*, 741-751.

Etard, C., Gradl, D., Kunz, M., Eilers, M., and Wedlich, D. (2005). Pontin and Reptin regulate cell proliferation in early Xenopus embryos in collaboration with c-Myc and Miz-1. Mech Dev *122*, 545-556.

Etard, C., Wedlich, D., Bauer, A., Huber, O., and Kuhl, M. (2000). Expression of Xenopus homologs of the beta-catenin binding protein pontin52. Mech Dev *94*, 219-222.

Faast, R., Thonglairoam, V., Schulz, T. C., Beall, J., Wells, J. R., Taylor, H., Matthaei, K., Rathjen, P. D., Tremethick, D. J., and Lyons, I. (2001). Histone variant H2A.Z is required for early mammalian development. Curr Biol *11*, 1183-1187.

Feng, Y., Lee, N., and Fearon, E. R. (2003). TIP49 regulates beta-catenin-mediated neoplastic transformation and T-cell factor target gene induction via effects on chromatin remodeling. Cancer Res *63*, 8726-8734.

Fernandez, P. C., Frank, S. R., Wang, L., Schroeder, M., Liu, S., Greene, J., Cocito, A., and Amati, B. (2003). Genomic targets of the human c-Myc protein. Genes Dev *17*, 1115-1129.

Fielding, A. B., Dobreva, I., McDonald, P. C., Foster, L. J., and Dedhar, S. (2008). Integrin-linked kinase localizes to the centrosome and regulates mitotic spindle organization. J Cell Biol *180*, 681-689.

Frank, S. R., Parisi, T., Taubert, S., Fernandez, P., Fuchs, M., Chan, H. M., Livingston, D. M., and Amati, B. (2003). MYC recruits the TIP60 histone acetyltransferase complex to chromatin. EMBO Rep *4*, 575-580.

Frank, S. R., Schroeder, M., Fernandez, P., Taubert, S., and Amati, B. (2001). Binding of c-Myc to chromatin mediates mitogen-induced acetylation of histone H4 and gene activation. Genes Dev *15*, 2069-2082.

Fritsch, O., Benvenuto, G., Bowler, C., Molinier, J., and Hohn, B. (2004). The INO80 protein controls homologous recombination in Arabidopsis thaliana. Mol Cell *16*, 479-485.

Fuchs, M., Gerber, J., Drapkin, R., Sif, S., Ikura, T., Ogryzko, V., Lane, W. S., Nakatani, Y., and Livingston, D. M. (2001). The p400 complex is an essential E1A transformation target. Cell *106*, 297-307.

Galarneau, L., Nourani, A., Boudreault, A. A., Zhang, Y., Heliot, L., Allard, S., Savard, J., Lane, W. S., Stillman, D. J., and Cote, J. (2000). Multiple links between the NuA4 histone acetyltransferase complex and epigenetic control of transcription. Mol Cell *5*, 927-937.

Gallant, P. (2007). Control of transcription by Pontin and Reptin. Trends Cell Biol *17*, 187-192.

Garcia De La Torre, J., Huertas, M. L., and Carrasco, B. (2000). Calculation of hydrodynamic properties of globular proteins from their atomic-level structure. Biophys J *78*, 719-730.

Garcia de la Torre, J., Llorca, O., Carrascosa, J. L., and Valpuesta, J. M. (2001). HYDROMIC: prediction of hydrodynamic properties of rigid macromolecular structures obtained from electron microscopy images. Eur Biophys J *30*, 457-462.

Gartner, W., Rossbacher, J., Zierhut, B., Daneva, T., Base, W., Weissel, M., Waldhausl, W., Pasternack, M. S., and Wagner, L. (2003). The ATP-dependent helicase RUVBL1/TIP49a associates with tubulin during mitosis. Cell Motil Cytoskeleton *56*, 79-93.

Ghaemmaghami, S., Huh, W. K., Bower, K., Howson, R. W., Belle, A., Dephoure, N., O'Shea, E. K., and Weissman, J. S. (2003). Global analysis of protein expression in yeast. Nature *425*, 737-741.

Giorgio, G., Alfieri, M., Prattichizzo, C., Zullo, A., Cairo, S., and Franco, B. (2007). Functional Characterization of the OFD1 Protein Reveals a Nuclear Localization and Physical Interaction with Subunits of a Chromatin Remodeling Complex. Mol Biol Cell *18*, 4397-4404.

Glover, J. R., and Lindquist, S. (1998). Hsp104, Hsp70, and Hsp40: a novel chaperone system that rescues previously aggregated proteins. Cell *94*, 73-82.

Gohshi, T., Shimada, M., Kawahire, S., Imai, N., Ichimura, T., Omata, S., and Horigome, T. (1999). Molecular cloning of mouse p47, a second group mammalian RuvB DNA helicase-like protein: homology with those from human and Saccharomyces cerevisiae. J Biochem *125*, 939-946.

Gorrini, C., Squatrito, M., Luise, C., Syed, N., Perna, D., Wark, L., Martinato, F., Sardella, D., Verrecchia, A., Bennett, S.*, et al.* (2007). Tip60 is a haplo-insufficient tumour suppressor required for an oncogene-induced DNA damage response. Nature *448*, 1063-1067.

Gorynia, S., Matias, P. M., Bandeiras, T. M., Donner, P., and Carrondo, M. A. (2008). Cloning, expression, purification, crystallization and preliminary X-ray analysis of the human RuvBL1-RuvBL2 complex. Acta Crystallogr Sect F Struct Biol Cryst Commun *64*, 840-846.

Gorynia, S., Matias, P. M., Goncalves, S., Coelho, R., Lopes, G., Thomaz, M., Huber, M., Haendler, B., Donner, P., and Carrondo, M. A. (2006). Expression, purification, crystallization and preliminary X-ray analysis of the human RuvB-like protein RuvBL1. Acta Crystallograph Sect F Struct Biol Cryst Commun *62*, 61-66.

Gospodinov, A., Tsaneva, I., and Anachkova, B. (2009). RAD51 foci formation in response to DNA damage is modulated by TIP49. Int J Biochem Cell Biol *41*, 925-933.

Granneman, S., and Baserga, S. J. (2004). Ribosome biogenesis: of knobs and RNA processing. Exp Cell Res *296*, 43-50.

Gribun, A., Cheung, K. L., Huen, J., Ortega, J., and Houry, W. A. (2008). Yeast Rvb1 and Rvb2 are ATP-Dependent DNA Helicases that Form a Heterohexameric Complex. J Mol Biol *376*, 1320-1333.

Gstaiger, M., Luke, B., Hess, D., Oakeley, E. J., Wirbelauer, C., Blondel, M., Vigneron, M., Peter, M., and Krek, W. (2003). Control of nutrient-sensitive transcription programs by the unconventional prefoldin URI. Science *302*, 1208-1212.

Hanson, P. I., and Whiteheart, S. W. (2005). AAA+ proteins: have engine, will work. Nat Rev Mol Cell Biol *6*, 519-529.

Harata, M., Oma, Y., Mizuno, S., Jiang, Y. W., Stillman, D. J., and Wintersberger, U. (1999). The nuclear actin-related protein of Saccharomyces cerevisiae, Act3p/Arp4, interacts with core histones. Mol Biol Cell *10*, 2595-2605.

Henriksson, M., and Luscher, B. (1996). Proteins of the Myc network: essential regulators of cell growth and differentiation. Adv Cancer Res *68*, 109-182.

Hersch, G. L., Burton, R. E., Bolon, D. N., Baker, T. A., and Sauer, R. T. (2005). Asymmetric interactions of ATP with the AAA+ ClpX6 unfoldase: allosteric control of a protein machine. Cell *121*, 1017-1027.

Hiom, K., and West, S. C. (1995). Branch migration during homologous recombination: assembly of a RuvAB-Holliday junction complex in vitro. Cell *80*, 787-793.

Hishida, T., Han, Y. W., Fujimoto, S., Iwasaki, H., and Shinagawa, H. (2004). Direct evidence that a conserved arginine in RuvB AAA+ ATPase acts as an allosteric effector for the ATPase activity of the adjacent subunit in a hexamer. Proc Natl Acad Sci U S A *101*, 9573-9577.

Holzmann, K., Gerner, C., Korosec, T., Poltl, A., Grimm, R., and Sauermann, G. (1998). Identification and characterization of the ubiquitously occurring nuclear matrix protein NMP 238. Biochem Biophys Res Commun *252*, 39-45.

Huang, H., and He, X. (2008). Wnt/beta-catenin signaling: new (and old) players and new insights. Curr Opin Cell Biol *20*, 119-125.

Huber, O., Menard, L., Haurie, V., Nicou, A., Taras, D., and Rosenbaum, J. (2008). Pontin and reptin, two related ATPases with multiple roles in cancer. Cancer Res *68*, 6873-6876.

Ikura, T., Ogryzko, V. V., Grigoriev, M., Groisman, R., Wang, J., Horikoshi, M., Scully, R., Qin, J., and Nakatani, Y. (2000). Involvement of the TIP60 histone acetylase complex in DNA repair and apoptosis. Cell *102*, 463-473.

Ikura, T., Tashiro, S., Kakino, A., Shima, H., Jacob, N., Amunugama, R., Yoder, K., Izumi, S., Kuraoka, I., Tanaka, K.*, et al.* (2007). DNA damage-dependent acetylation and ubiquitination of H2AX enhances chromatin dynamics. Mol Cell Biol *27*, 7028-7040.

Iouzalen, N., Moreau, J., and Mechali, M. (1996). H2A.ZI, a new variant histone expressed during Xenopus early development exhibits several distinct features from the core histone H2A. Nucleic Acids Res *24*, 3947-3952.

Ishikawa, T., Beuron, F., Kessel, M., Wickner, S., Maurizi, M. R., and Steven, A. C. (2001). Translocation pathway of protein substrates in ClpAP protease. Proc Natl Acad Sci U S A *98*, 4328-4333.

Jackson, J. D., and Gorovsky, M. A. (2000). Histone H2A.Z has a conserved function that is distinct from that of the major H2A sequence variants. Nucleic Acids Res *28*, 3811-3816.

Jeronimo, C., Forget, D., Bouchard, A., Li, Q., Chua, G., Poitras, C., Therien, C., Bergeron, D., Bourassa, S., Greenblatt, J.*, et al.* (2007). Systematic analysis of the protein interaction network for the human transcription machinery reveals the identity of the 7SK capping enzyme. Mol Cell *27*, 262-274.

Jha, S., Shibata, E., and Dutta, A. (2008). Human Rvb1/Tip49 is required for the histone acetyltransferase activity of Tip60/NuA4 and for the downregulation of phosphorylation on H2AX after DNA damage. Mol Cell Biol *28*, 2690-2700.

Jonsson, Z. O., Dhar, S. K., Narlikar, G. J., Auty, R., Wagle, N., Pellman, D., Pratt, R. E., Kingston, R., and Dutta, A. (2001). Rvb1p and Rvb2p are essential components of a

chromatin remodeling complex that regulates transcription of over 5% of yeast genes. J Biol Chem *276*, 16279-16288.

Jonsson, Z. O., Jha, S., Wohlschlegel, J. A., and Dutta, A. (2004). Rvb1p/Rvb2p recruit Arp5p and assemble a functional Ino80 chromatin remodeling complex. Mol Cell *16*, 465-477.

Kanemaki, M., Kurokawa, Y., Matsu-ura, T., Makino, Y., Masani, A., Okazaki, K., Morishita, T., and Tamura, T. A. (1999). TIP49b, a new RuvB-like DNA helicase, is included in a complex together with another RuvB-like DNA helicase, TIP49a. J Biol Chem *274*, 22437-22444.

Kanemaki, M., Makino, Y., Yoshida, T., Kishimoto, T., Koga, A., Yamamoto, K., Yamamoto, M., Moncollin, V., Egly, J. M., Muramatsu, M., and Tamura, T. (1997). Molecular cloning of a rat 49-kDa TBP-interacting protein (TIP49) that is highly homologous to the bacterial RuvB. Biochem Biophys Res Commun *235*, 64-68.

Kawasaki, H., Schiltz, L., Chiu, R., Itakura, K., Taira, K., Nakatani, Y., and Yokoyama, K. K. (2000). ATF-2 has intrinsic histone acetyltransferase activity which is modulated by phosphorylation. Nature *405*, 195-200.

Kikuchi, N., Gohshi, T., Kawahire, S., Tachibana, T., Yoneda, Y., Isobe, T., Lim, C. R., Kohno, K., Ichimura, T., Omata, S., and Horigome, T. (1999). Molecular shape and ATP binding activity of rat p50, a putative mammalian homologue of RuvB DNA helicase. J Biochem *125*, 487-494.

Kim, J. H., Choi, H. J., Kim, B., Kim, M. H., Lee, J. M., Kim, I. S., Lee, M. H., Choi, S. J., Kim, K. I., Kim, S. I., *et al.* (2006). Roles of sumoylation of a reptin chromatin-remodelling complex in cancer metastasis. Nat Cell Biol *8*, 631-639.

Kim, J. H., Kim, B., Cai, L., Choi, H. J., Ohgi, K. A., Tran, C., Chen, C., Chung, C. H., Huber, O., Rose, D. W., *et al.* (2005). Transcriptional regulation of a metastasis suppressor gene by Tip60 and beta-catenin complexes. Nature *434*, 921-926.

Kim, J. H., Lee, J. M., Nam, H. J., Choi, H. J., Yang, J. W., Lee, J. S., Kim, M. H., Kim, S. I., Chung, C. H., Kim, K. I., and Baek, S. H. (2007). SUMOylation of pontin chromatin-remodeling complex reveals a signal integration code in prostate cancer cells. Proc Natl Acad Sci U S A *104*, 20793-20798.

Kimura, A., and Horikoshi, M. (1998). Tip60 acetylates six lysines of a specific class in core histones in vitro. Genes Cells *3*, 789-800.

King, T. H., Decatur, W. A., Bertrand, E., Maxwell, E. S., and Fournier, M. J. (2001). A well-connected and conserved nucleoplasmic helicase is required for production of box C/D and H/ACA snoRNAs and localization of snoRNP proteins. Mol Cell Biol *21*, 7731-7746.

Kirchner, J., Vissi, E., Gross, S., Szoor, B., Rudenko, A., Alphey, L., and White-Cooper, H. (2008). *Drosophila* Uri, a PP1alpha binding protein, is essential for viability, maintenance of DNA integrity and normal transcriptional activity. BMC Mol Biol *9*, 36.

Kobor, M. S., Venkatasubrahmanyam, S., Meneghini, M. D., Gin, J. W., Jennings, J. L., Link, A. J., Madhani, H. D., and Rine, J. (2004). A protein complex containing the conserved Swi2/Snf2-related ATPase Swr1p deposits histone variant H2A.Z into euchromatin. PLoS Biol *2*, E131.

Krogan, N. J., Keogh, M. C., Datta, N., Sawa, C., Ryan, O. W., Ding, H., Haw, R. A., Pootoolal, J., Tong, A., Canadien, V.*, et al.* (2003). A Snf2 family ATPase complex required for recruitment of the histone H2A variant Htz1. Mol Cell *12*, 1565-1576.

Kurokawa, Y., Kanemaki, M., Makino, Y., and Tamura, T. A. (1999). A notable example of an evolutionary conserved gene: studies on a putative DNA helicase TIP49. DNA Seq *10*, 37-42.

Kusch, T., Florens, L., Macdonald, W. H., Swanson, S. K., Glaser, R. L., Yates, J. R., 3rd, Abmayr, S. M., Washburn, M. P., and Workman, J. L. (2004). Acetylation by Tip60 is required for selective histone variant exchange at DNA lesions. Science *306*, 2084-2087.

Laue, T. M., Shah, B. D., Ridgeway, T. M., and Pelletier, S. L. (1992). Computer-aided interpretation of analytical sedimentation data for proteins. Analytical Ultracentrifugation in Biochemistry and Polymer Science, 90-125.

Lauscher, J. C., Loddenkemper, C., Kosel, L., Grone, J., Buhr, H. J., and Huber, O. (2007). Increased pontin expression in human colorectal cancer tissue. Hum Pathol *38*, 978-985.

Legube, G., Linares, L. K., Tyteca, S., Caron, C., Scheffner, M., Chevillard-Briet, M., and Trouche, D. (2004). Role of the histone acetyl transferase Tip60 in the p53 pathway. J Biol Chem *279*, 44825-44833.

Lenzen, C. U., Steinmann, D., Whiteheart, S. W., and Weis, W. I. (1998). Crystal structure of the hexamerization domain of N-ethylmaleimide-sensitive fusion protein. Cell *94*, 525-536.

Leone, G., Sears, R., Huang, E., Rempel, R., Nuckolls, F., Park, C. H., Giangrande, P., Wu, L., Saavedra, H. I., Field, S. J.*, et al.* (2001). Myc requires distinct E2F activities to induce S phase and apoptosis. Mol Cell *8*, 105-113.

Leung, A. K., Trinkle-Mulcahy, L., Lam, Y. W., Andersen, J. S., Mann, M., and Lamond, A. I. (2006). NOPdb: Nucleolar Proteome Database. Nucleic Acids Res *34*, D218-220.

Li, H., Balajee, A. S., Su, T., Cen, B., Hei, T. K., and Weinstein, I. B. (2008). The HINT1 tumor suppressor regulates both gamma-H2AX and ATM in response to DNA damage. J Cell Biol *183*, 253-265.

Li, H., Zhang, Y., Su, T., Santella, R. M., and Weinstein, I. B. (2006). Hint1 is a haplo-insufficient tumor suppressor in mice. Oncogene *25*, 713-721.

Lim, C. R., Kimata, Y., Ohdate, H., Kokubo, T., Kikuchi, N., Horigome, T., and Kohno, K. (2000). The Saccharomyces cerevisiae RuvB-like protein, Tih2p, is required for cell cycle progression and RNA polymerase II-directed transcription. J Biol Chem *275*, 22409-22417.

Lima, C. D., Klein, M. G., Weinstein, I. B., and Hendrickson, W. A. (1996). Three-dimensional structure of human protein kinase C interacting protein 1, a member of the HIT family of proteins. Proc Natl Acad Sci U S A *93*, 5357-5362.

Liu, Q., Tan, G., Levenkova, N., Li, T., Pugh, E. N., Jr., Rux, J. J., Speicher, D. W., and Pierce, E. A. (2007). The proteome of the mouse photoreceptor sensory cilium complex. Mol Cell Proteomics *6*, 1299-1317.

Lou, X., Zhu, Q., Lei, Z., van Dongen, J. L., and Meijer, E. W. (2004). Simulation of size exclusion chromatography for characterization of supramolecular complex: a theoretical study. J Chromatogr A *1029*, 67-75.

Lupas, A. N., and Martin, J. (2002). AAA proteins. Curr Opin Struct Biol *12*, 746-753.

Makino, Y., Kanemaki, M., Koga, A., Osano, K., Matsu-Ura, T., Kurokawa, Y., Kishimoto, T., and Tamura, T. (2000). Chromosome mapping and expression of human tip49 family genes. DNA Seq *11*, 145-148.

Makino, Y., Kanemaki, M., Kurokawa, Y., Koji, T., and Tamura, T. (1999). A rat RuvB-like protein, TIP49a, is a germ cell-enriched novel DNA helicase. J Biol Chem *274*, 15329-15335.

Martinato, F., Cesaroni, M., Amati, B., and Guccione, E. (2008). Analysis of Myc-induced histone modifications on target chromatin. PLoS ONE *3*, e3650.

Matias, P. M., Gorynia, S., Donner, P., and Carrondo, M. A. (2006). Crystal structure of the human AAA+ protein RuvBL1. J Biol Chem *281*, 38918-38929.

Matsuoka, S., Ballif, B. A., Smogorzewska, A., McDonald, E. R., 3rd, Hurov, K. E., Luo, J., Bakalarski, C. E., Zhao, Z., Solimini, N., Lerenthal, Y.*, et al.* (2007). ATM and ATR substrate analysis reveals extensive protein networks responsive to DNA damage. Science *316*, 1160-1166.

McKeegan, K. S., Debieux, C. M., Boulon, S., Bertrand, E., and Watkins, N. J. (2007). A dynamic scaffold of pre-snoRNP factors facilitates human box C/D snoRNP assembly. Mol Cell Biol *27*, 6782-6793.

McMahon, S. B., Van Buskirk, H. A., Dugan, K. A., Copeland, T. D., and Cole, M. D. (1998). The novel ATM-related protein TRRAP is an essential cofactor for the c-Myc and E2F oncoproteins. Cell *94*, 363-374.

McMahon, S. B., Wood, M. A., and Cole, M. D. (2000). The essential cofactor TRRAP recruits the histone acetyltransferase hGCN5 to c-Myc. Mol Cell Biol *20*, 556-562.

McRorie, D. K., and Voelker, P. J. (1993). Self-Associating Systems in the Analytical Ultracentrifuge (Fullerton, California, USA: Beckman Instruments).

Meneghini, M. D., Wu, M., and Madhani, H. D. (2003). Conserved histone variant H2A.Z protects euchromatin from the ectopic spread of silent heterochromatin. Cell *112*, 725-736.

Mezard, C., Davies, A. A., Stasiak, A., and West, S. C. (1997). Biochemical properties of RuvBD113N: a mutation in helicase motif II of the RuvB hexamer affects DNA binding and ATPase activities. J Mol Biol *271*, 704-717.

Mizuguchi, G., Shen, X., Landry, J., Wu, W. H., Sen, S., and Wu, C. (2004). ATP-driven exchange of histone H2AZ variant catalyzed by SWR1 chromatin remodeling complex. Science *303*, 343-348.

Moran, E. (1993). Interaction of adenoviral proteins with pRB and p53. Faseb J *7*, 880-885.

Morrison, A. J., Highland, J., Krogan, N. J., Arbel-Eden, A., Greenblatt, J. F., Haber, J. E., and Shen, X. (2004). INO80 and gamma-H2AX interaction links ATP-dependent chromatin remodeling to DNA damage repair. Cell *119*, 767-775.

Morrison, A. J., Kim, J. A., Person, M. D., Highland, J., Xiao, J., Wehr, T. S., Hensley, S., Bao, Y., Shen, J., Collins, S. R.*, et al.* (2007). Mec1/Tel1 phosphorylation of the INO80 chromatin remodeling complex influences DNA damage checkpoint responses. Cell *130*, 499-511.

Newman, D. R., Kuhn, J. F., Shanab, G. M., and Maxwell, E. S. (2000). Box C/D snoRNA-associated proteins: two pairs of evolutionarily ancient proteins and possible links to replication and transcription. Rna *6*, 861-879.

Ni, L., Saeki, M., Xu, L., Nakahara, H., Saijo, M., Tanaka, K., and Kamisaki, Y. (2009). RPAP3 interacts with Reptin to regulate UV-induced phosphorylation of H2AX and DNA damage. J Cell Biochem.

Ogura, T., Whiteheart, S. W., and Wilkinson, A. J. (2004). Conserved arginine residues implicated in ATP hydrolysis, nucleotide-sensing, and inter-subunit interactions in AAA and AAA+ ATPases. J Struct Biol *146*, 106-112.

Ohdate, H., Lim, C. R., Kokubo, T., Matsubara, K., Kimata, Y., and Kohno, K. (2003). Impairment of the DNA binding activity of the TATA-binding protein renders the transcriptional function of Rvb2p/Tih2p, the yeast RuvB-like protein, essential for cell growth. J Biol Chem *278*, 14647-14656.

Okorokov, A. L., Sherman, M. B., Plisson, C., Grinkevich, V., Sigmundsson, K., Selivanova, G., Milner, J., and Orlova, E. V. (2006). The structure of p53 tumour suppressor protein reveals the basis for its functional plasticity. Embo J *25*, 5191-5200.

Omer, A. D., Lowe, T. M., Russell, A. G., Ebhardt, H., Eddy, S. R., and Dennis, P. P. (2000). Homologs of small nucleolar RNAs in Archaea. Science *288*, 517-522.

Parfait, B., Giovangrandi, Y., Asheuer, M., Laurendeau, I., Olivi, M., Vodovar, N., Vidaud, D., Vidaud, M., and Bieche, I. (2000). Human TIP49b/RUVBL2 gene: genomic structure, expression pattern, physical link to the human CGB/LHB gene cluster on chromosome 19q13.3. Ann Genet *43*, 69-74.

Park, J., Kunjibettu, S., McMahon, S. B., and Cole, M. D. (2001). The ATM-related domain of TRRAP is required for histone acetyltransferase recruitment and Myc-dependent oncogenesis. Genes Dev *15*, 1619-1624.

Park, J., Wood, M. A., and Cole, M. D. (2002). BAF53 forms distinct nuclear complexes and functions as a critical c-Myc-interacting nuclear cofactor for oncogenic transformation. Mol Cell Biol *22*, 1307-1316.

Parusel, C. T., Kritikou, E. A., Hengartner, M. O., Krek, W., and Gotta, M. (2006). URI-1 is required for DNA stability in C. elegans. Development *133*, 621-629.

Pazour, G. J., and Witman, G. B. (2003). The vertebrate primary cilium is a sensory organelle. Curr Opin Cell Biol *15*, 105-110.

Philo, J. S. (2006). Improved methods for fitting sedimentation coefficient distributions derived by time-derivative techniques. Anal Biochem *354*, 238-246.

Polakis, P. (2007). The many ways of Wnt in cancer. Curr Opin Genet Dev *17*, 45-51.

Puri, T., Wendler, P., Sigala, B., Saibil, H., and Tsaneva, I. R. (2007). Dodecameric structure and ATPase activity of the human TIP48/TIP49 complex. J Mol Biol *366*, 179-192.

Puri, T. S. (2006) Characterisation of the human TIP48 and TIP49 AAA+ proteins and their complex, UCL.

Putnam, C. D., Clancy, S. B., Tsuruta, H., Gonzalez, S., Wetmur, J. G., and Tainer, J. A. (2001). Structure and mechanism of the RuvB Holliday junction branch migration motor. J Mol Biol *311*, 297-310.

Qi, D., Jin, H., Lilja, T., and Mannervik, M. (2006). *Drosophila* Reptin and other TIP60 complex components promote generation of silent chromatin. Genetics *174*, 241-251.

Qian, Y., Zhong, X., Flynn, D. C., Zheng, J. Z., Qiao, M., Wu, C., Dedhar, S., Shi, X., and Jiang, B. H. (2005). ILK mediates actin filament rearrangements and cell migration and invasion through PI3K/Akt/Rac1 signaling. Oncogene *24*, 3154-3165.

Qiu, X. B., Lin, Y. L., Thome, K. C., Pian, P., Schlegel, B. P., Weremowicz, S., Parvin, J. D., and Dutta, A. (1998). An eukaryotic RuvB-like protein (RUVBL1) essential for growth. J Biol Chem *273*, 27786-27793.

Radovic, S., Rapisarda, V. A., Tosato, V., and Bruschi, C. V. (2007). Functional and comparative characterization of Saccharomyces cerevisiae RVB1 and RVB2 genes with bacterial Ruv homologues. FEMS Yeast Res *7*, 527-539.

Rafferty, J. B., Sedelnikova, S. E., Hargreaves, D., Artymiuk, P. J., Baker, P. J., Sharples, G. J., Mahdi, A. A., Lloyd, R. G., and Rice, D. W. (1996). Crystal structure of DNA recombination protein RuvA and a model for its binding to the Holliday junction. Science *274*, 415-421.

Reid, J. L., Iyer, V. R., Brown, P. O., and Struhl, K. (2000). Coordinate regulation of yeast ribosomal protein genes is associated with targeted recruitment of Esa1 histone acetylase. Mol Cell *6*, 1297-1307.

Ringrose, L., and Paro, R. (2004). Epigenetic regulation of cellular memory by the Polycomb and Trithorax group proteins. Annu Rev Genet *38*, 413-443.

Rottbauer, W., Saurin, A. J., Lickert, H., Shen, X., Burns, C. G., Wo, Z. G., Kemler, R., Kingston, R., Wu, C., and Fishman, M. (2002). Reptin and pontin antagonistically regulate heart growth in zebrafish embryos. Cell *111*, 661-672.

Rousseau, B., Menard, L., Haurie, V., Taras, D., Blanc, J. F., Moreau-Gaudry, F., Metzler, P., Hugues, M., Boyault, S., Lemiere, S.*, et al.* (2007). Overexpression and role of the ATPase and putative DNA helicase RuvB-like 2 in human hepatocellular carcinoma. Hepatology *46*, 1108-1118.

Rowe, A., Weiske, J., Kramer, T. S., Huber, O., and Jackson, P. (2008). Phorbol ester enhances KAI1 transcription by recruiting Tip60/Pontin complexes. Neoplasia *10*, 1421-1432, following 1432.

Ruhl, D. D., Jin, J., Cai, Y., Swanson, S., Florens, L., Washburn, M. P., Conaway, R. C., Conaway, J. W., and Chrivia, J. C. (2006). Purification of a human SRCAP complex that remodels chromatin by incorporating the histone variant H2A.Z into nucleosomes. Biochemistry *45*, 5671-5677.

Rynditch, A., Pekarsky, Y., Schnittger, S., and Gardiner, K. (1997). Leukemia breakpoint region in 3q21 is gene rich. Gene *193*, 49-57.

Salzer, U., Kubicek, M., and Prohaska, R. (1999). Isolation, molecular characterization, and tissue-specific expression of ECP-51 and ECP-54 (TIP49), two homologous, interacting erythroid cytosolic proteins. Biochim Biophys Acta *1446*, 365-370.

Sardiu, M. E., Cai, Y., Jin, J., Swanson, S. K., Conaway, R. C., Conaway, J. W., Florens, L., and Washburn, M. P. (2008). Probabilistic assembly of human protein interaction networks from label-free quantitative proteomics. Proc Natl Acad Sci U S A *105*, 1454-1459.

Saurin, A. J., Shao, Z., Erdjument-Bromage, H., Tempst, P., and Kingston, R. E. (2001). A *Drosophila* Polycomb group complex includes Zeste and dTAFII proteins. Nature *412*, 655-660.

Schones, D. E., Cui, K., Cuddapah, S., Roh, T. Y., Barski, A., Wang, Z., Wei, G., and Zhao, K. (2008). Dynamic regulation of nucleosome positioning in the human genome. Cell *132*, 887-898.

Schuck, P. (2000). Size-distribution analysis of macromolecules by sedimentation velocity ultracentrifugation and lamm equation modeling. Biophys J *78*, 1606-1619.

Schuck, P. (2003). On the analysis of protein self-association by sedimentation velocity analytical ultracentrifugation. Anal Biochem *320*, 104-124.

Shen, X., Mizuguchi, G., Hamiche, A., and Wu, C. (2000). A chromatin remodelling complex involved in transcription and DNA processing. Nature *406*, 541-544.

Shen, X., Ranallo, R., Choi, E., and Wu, C. (2003). Involvement of actin-related proteins in ATP-dependent chromatin remodeling. Mol Cell *12*, 147-155.

Siegert, R., Leroux, M. R., Scheufler, C., Hartl, F. U., and Moarefi, I. (2000). Structure of the molecular chaperone prefoldin: unique interaction of multiple coiled coil tentacles with unfolded proteins. Cell *103*, 621-632.

Sigala, B., Edwards, M., Puri, T., and Tsaneva, I. R. (2005). Relocalization of human chromatin remodeling cofactor TIP48 in mitosis. Exp Cell Res *310*, 357-369.

Simon, J. A., and Tamkun, J. W. (2002). Programming off and on states in chromatin: mechanisms of Polycomb and trithorax group complexes. Curr Opin Genet Dev *12*, 210-218.

Staller, P., Peukert, K., Kiermaier, A., Seoane, J., Lukas, J., Karsunky, H., Moroy, T., Bartek, J., Massague, J., Hanel, F., and Eilers, M. (2001). Repression of p15INK4b expression by Myc through association with Miz-1. Nat Cell Biol *3*, 392-399.

Stolc, V., Samanta, M. P., Tongprasit, W., and Marshall, W. F. (2005). Genome-wide transcriptional analysis of flagellar regeneration in Chlamydomonas reinhardtii identifies orthologs of ciliary disease genes. Proc Natl Acad Sci U S A *102*, 3703-3707.

Sun, Y., Jiang, X., Chen, S., Fernandes, N., and Price, B. D. (2005). A role for the Tip60 histone acetyltransferase in the acetylation and activation of ATM. Proc Natl Acad Sci U S A *102*, 13182-13187.

Sun, Y., Xu, Y., Roy, K., and Price, B. D. (2007). DNA damage-induced acetylation of lysine 3016 of ATM activates ATM kinase activity. Mol Cell Biol *27*, 8502-8509.

Sun, Z., Amsterdam, A., Pazour, G. J., Cole, D. G., Miller, M. S., and Hopkins, N. (2004). A genetic screen in zebrafish identifies cilia genes as a principal cause of cystic kidney. Development *131*, 4085-4093.

Sunada, R., Gorzer, I., Oma, Y., Yoshida, T., Suka, N., Wintersberger, U., and Harata, M. (2005). The nuclear actin-related protein Act3p/Arp4p is involved in the dynamics of chromatin-modulating complexes. Yeast *22*, 753-768.

Sykes, S. M., Mellert, H. S., Holbert, M. A., Li, K., Marmorstein, R., Lane, W. S., and McMahon, S. B. (2006). Acetylation of the p53 DNA-binding domain regulates apoptosis induction. Mol Cell *24*, 841-851.

Takahashi, K., Tanabe, K., Ohnuki, M., Narita, M., Ichisaka, T., Tomoda, K., and Yamanaka, S. (2007). Induction of pluripotent stem cells from adult human fibroblasts by defined factors. Cell *131*, 861-872.

Takahashi, K., and Yamanaka, S. (2006). Induction of pluripotent stem cells from mouse embryonic and adult fibroblast cultures by defined factors. Cell *126*, 663-676.

Tang, Y., Luo, J., Zhang, W., and Gu, W. (2006). Tip60-dependent acetylation of p53 modulates the decision between cell-cycle arrest and apoptosis. Mol Cell *24*, 827-839.

Taubert, S., Gorrini, C., Frank, S. R., Parisi, T., Fuchs, M., Chan, H. M., Livingston, D. M., and Amati, B. (2004). E2F-dependent histone acetylation and recruitment of the Tip60 acetyltransferase complex to chromatin in late G1. Mol Cell Biol *24*, 4546-4556.

Torreira, E., Jha, S., Lopez-Blanco, J. R., Arias-Palomo, E., Chacon, P., Canas, C., Ayora, S., Dutta, A., and Llorca, O. (2008). Architecture of the pontin/reptin complex, essential in the assembly of several macromolecular complexes. Structure *16*, 1511-1520.

Tsaneva, I. R., Muller, B., and West, S. C. (1992). ATP-dependent branch migration of Holliday junctions promoted by the RuvA and RuvB proteins of E. coli. Cell *69*, 1171-1180.

Tyteca, S., Vandromme, M., Legube, G., Chevillard-Briet, M., and Trouche, D. (2006). Tip60 and p400 are both required for UV-induced apoptosis but play antagonistic roles in cell cycle progression. Embo J *25*, 1680-1689.

Vainberg, I. E., Lewis, S. A., Rommelaere, H., Ampe, C., Vandekerckhove, J., Klein, H. L., and Cowan, N. J. (1998). Prefoldin, a chaperone that delivers unfolded proteins to cytosolic chaperonin. Cell *93*, 863-873.

van Attikum, H., Fritsch, O., and Gasser, S. M. (2007). Distinct roles for SWR1 and INO80 chromatin remodeling complexes at chromosomal double-strand breaks. Embo J *26*, 4113-4125.

van Attikum, H., Fritsch, O., Hohn, B., and Gasser, S. M. (2004). Recruitment of the INO80 complex by H2A phosphorylation links ATP-dependent chromatin remodeling with DNA double-strand break repair. Cell *119*, 777-788.

Vassilev, L. T., Tovar, C., Chen, S., Knezevic, D., Zhao, X., Sun, H., Heimbrook, D. C., and Chen, L. (2006). Selective small-molecule inhibitor reveals critical mitotic functions of human CDK1. Proc Natl Acad Sci U S A *103*, 10660-10665.

Venteicher, A. S., Meng, Z., Mason, P. J., Veenstra, T. D., and Artandi, S. E. (2008). Identification of ATPases pontin and reptin as telomerase components essential for holoenzyme assembly. Cell *132*, 945-957.

Wang, L., Li, H., Zhang, Y., Santella, R. M., and Weinstein, I. B. (2009). HINT1 inhibits beta-catenin/TCF4, USF2 and NFkappaB activity in human hepatoma cells. Int J Cancer *124*, 1526-1534.

Watkins, N. J., Dickmanns, A., and Luhrmann, R. (2002). Conserved stem II of the box C/D motif is essential for nucleolar localization and is required, along with the 15.5K protein, for the hierarchical assembly of the box C/D snoRNP. Mol Cell Biol *22*, 8342-8352.

Watkins, N. J., Lemm, I., Ingelfinger, D., Schneider, C., Hossbach, M., Urlaub, H., and Luhrmann, R. (2004). Assembly and maturation of the U3 snoRNP in the nucleoplasm in a large dynamic multiprotein complex. Mol Cell *16*, 789-798.

Watkins, N. J., Newman, D. R., Kuhn, J. F., and Maxwell, E. S. (1998). In vitro assembly of the mouse U14 snoRNP core complex and identification of a 65-kDa box C/D-binding protein. Rna *4*, 582-593.

Weiske, J., and Huber, O. (2005). The histidine triad protein Hint1 interacts with Pontin and Reptin and inhibits TCF-beta-catenin-mediated transcription. J Cell Sci *118*, 3117-3129.

Weiske, J., and Huber, O. (2006). The histidine triad protein Hint1 triggers apoptosis independent of its enzymatic activity. J Biol Chem *281*, 27356-27366.

West, S. C. (1997). Processing of recombination intermediates by the RuvABC proteins. Annu Rev Genet *31*, 213-244.

White, S. R., and Lauring, B. (2007). AAA+ ATPases: achieving diversity of function with conserved machinery. Traffic *8*, 1657-1667.

Wong, M. M., Cox, L. K., and Chrivia, J. C. (2007). The chromatin remodeling protein, SRCAP, is critical for deposition of the histone variant H2A.Z at promoters. J Biol Chem *282*, 26132-26139.

Wood, M. A., McMahon, S. B., and Cole, M. D. (2000). An ATPase/helicase complex is an essential cofactor for oncogenic transformation by c-Myc. Mol Cell *5*, 321-330.

Woychik, N. A., Liao, S. M., Kolodziej, P. A., and Young, R. A. (1990). Subunits shared by eukaryotic nuclear RNA polymerases. Genes Dev *4*, 313-323.

Wu, L., Timmers, C., Maiti, B., Saavedra, H. I., Sang, L., Chong, G. T., Nuckolls, F., Giangrande, P., Wright, F. A., Field, S. J., *et al.* (2001). The E2F1-3 transcription factors are essential for cellular proliferation. Nature *414*, 457-462.

Wu, S., Shi, Y., Mulligan, P., Gay, F., Landry, J., Liu, H., Lu, J., Qi, H. H., Wang, W., Nickoloff, J. A., *et al.* (2007). A YY1-INO80 complex regulates genomic stability through homologous recombination-based repair. Nat Struct Mol Biol *14*, 1165-1172.

Xie, P. (2007). Model for RuvAB-mediated branch migration of Holliday junctions. J Theor Biol *249*, 566-573.

Xing, Y., Takemaru, K., Liu, J., Berndt, J. D., Zheng, J. J., Moon, R. T., and Xu, W. (2008). Crystal structure of a full-length beta-catenin. Structure *16*, 478-487.

Yamada, K., Miyata, T., Tsuchiya, D., Oyama, T., Fujiwara, Y., Ohnishi, T., Iwasaki, H., Shinagawa, H., Ariyoshi, M., Mayanagi, K., and Morikawa, K. (2002). Crystal structure of the

RuvA-RuvB complex: a structural basis for the Holliday junction migrating motor machinery. Mol Cell *10*, 671-681.

Yamamoto, T., and Horikoshi, M. (1997). Novel substrate specificity of the histone acetyltransferase activity of HIV-1-Tat interactive protein Tip60. J Biol Chem *272*, 30595-30598.

Zalk, R., and Shoshan-Barmatz, V. (2003). ATP-binding sites in brain p97/VCP (valosin-containing protein), a multifunctional AAA ATPase. Biochem J *374*, 473-480.

Zhang, X., Shaw, A., Bates, P. A., Newman, R. H., Gowen, B., Orlova, E., Gorman, M. A., Kondo, H., Dokurno, P., Lally, J., *et al.* (2000). Structure of the AAA ATPase p97. Mol Cell *6*, 1473-1484.

Zhang, Y. J., Li, H., Wu, H. C., Shen, J., Wang, L., Yu, M. W., Lee, P. H., Bernard Weinstein, I., and Santella, R. M. (2009). Silencing of Hint1, a novel tumor suppressor gene, by promoter hypermethylation in hepatocellular carcinoma. Cancer Lett *275*, 277-284.

Zlatanova, J., and Thakar, A. (2008). H2A.Z: view from the top. Structure *16*, 166-179.

Appendix

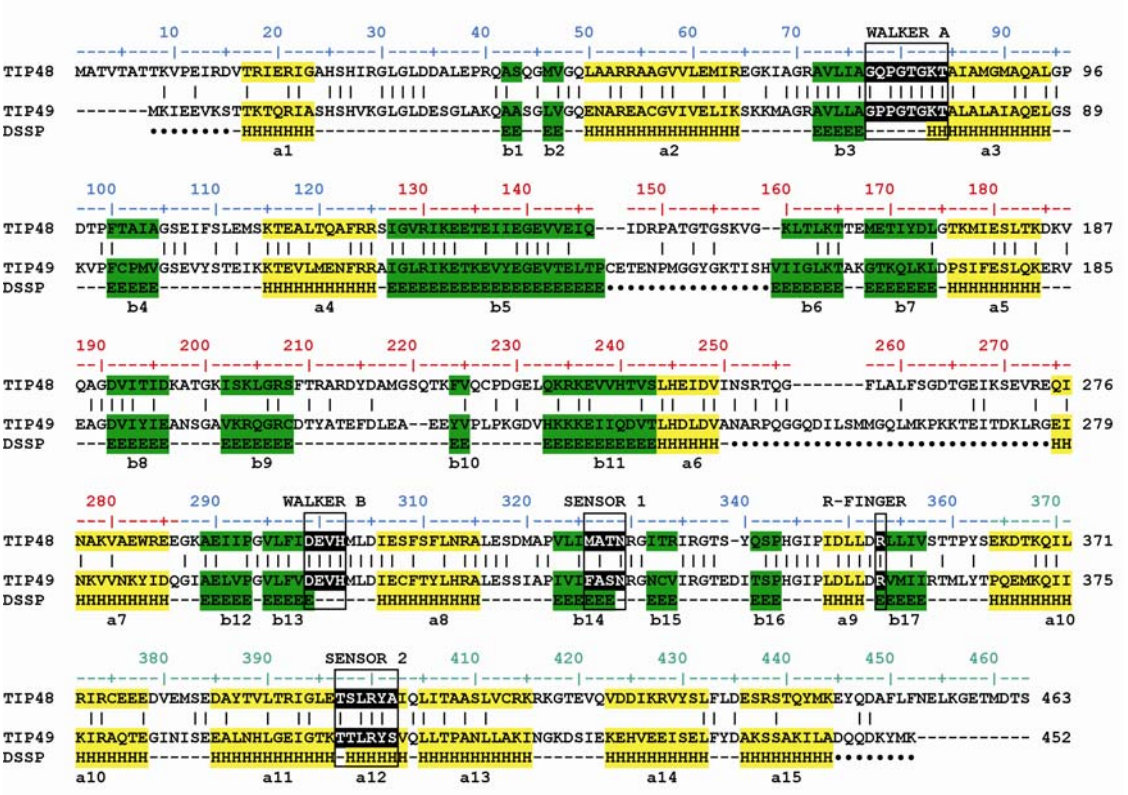

Appendix Figure A1. Sequence alignment of human TIP48 and TIP49. The two sequences were aligned using ClustalW. The residue numbering for TIP48 is shown above the alignment, and coloured as blue for Domain I (two segments), red for Domain II and green for Domain III. Identical residue pairs are indicated by vertical strokes (|). The Dictionary of protein Secondary Structure Pattern (DSSP) analysis of Molecule A in the TIP49 crystal structure identified the secondary structure of TIP49 (H, α-helix, yellow; E, β-strand, green) below the alignment. Residues missing from the TIP49 crystal structure (•) are shown below the alignment. The conserved sequence motifs for the AAA+ ATPase Walker A and B motifs, the Sensor 1 and 2 motifs and the (arginine) R-Finger are shown within boxes.